MCEER
EARTHQUAKE ENGINEERING TO EXTREME EVENTS

ISSN 1520-295X

Experimental Seismic Performance Evaluation of Isolation/Restraint Systems for Mechanical Equipment

Part 2: Light Equipment Study

by
Saeed Fathali and André Filiatrault

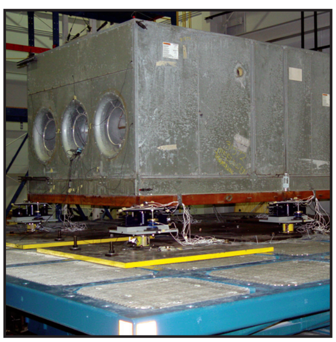
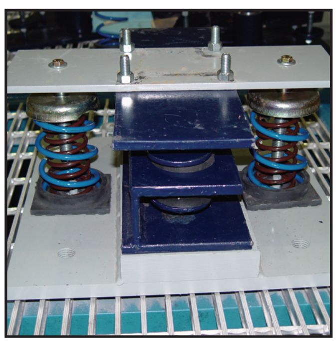

Technical Report MCEER-07-0022

December 13, 2007

This research was conducted at the University at Buffalo, State University of New York and was supported primarily by the Earthquake Engineering Research Centers Program of the National Science Foundation under award number EEC 9701471 and the American Society of Heating, Refrigerating and Air Conditioning Engineers project number 1323-RP.

NOTICE

Experimental Seismic Performance Evaluation of Isolation/Restraint Systems for Mechanical Equipment
Part 2: Light Equipment Study

by

Saeed Fathali[1] and Andre Filiatrault[2]

Publication Date: December 13, 2007
Submittal Date: December 5, 2007

Technical Report MCEER-07-0022

Task Number 9.2.1

NSF Master Contract Number EEC 9701471
and
ASHRAE Project Number 1323-RP-Static/Dynamic
Equipment Testing and Certification

1 Graduate Student, Department of Civil, Structural and Environmental Engineering, University at Buffalo, State University of New York
2 Professor, Department of Civil, Structural and Environmental Engineering, University at Buffalo, State University of New York

MCEER
University at Buffalo, The State University of New York
Red Jacket Quadrangle, Buffalo, NY 14261
Phone: (716) 645-3391; Fax (716) 645-3399
E-mail: *mceer@buffalo.edu*; WWW Site: *http://mceer.buffalo.edu*

Preface

The Multidisciplinary Center for Earthquake Engineering Research (MCEER) is a national center of excellence in advanced technology applications that is dedicated to the reduction of earthquake losses nationwide. Headquartered at the University at Buffalo, State University of New York, the Center was originally established by the National Science Foundation in 1986, as the National Center for Earthquake Engineering Research (NCEER).

Comprising a consortium of researchers from numerous disciplines and institutions throughout the United States, the Center's mission is to reduce earthquake losses through research and the application of advanced technologies that improve engineering, pre-earthquake planning and post-earthquake recovery strategies. Toward this end, the Center coordinates a nationwide program of multidisciplinary team research, education and outreach activities.

MCEER's research is conducted under the sponsorship of two major federal agencies: the National Science Foundation (NSF) and the Federal Highway Administration (FHWA), and the State of New York. Significant support is derived from the Federal Emergency Management Agency (FEMA), other state governments, academic institutions, foreign governments and private industry.

MCEER's NSF-sponsored research objectives are twofold: to increase resilience by developing seismic evaluation and rehabilitation strategies for the post-disaster facilities and systems (hospitals, electrical and water lifelines, and bridges and highways) that society expects to be operational following an earthquake; and to further enhance resilience by developing improved emergency management capabilities to ensure an effective response and recovery following the earthquake (see the figure below).

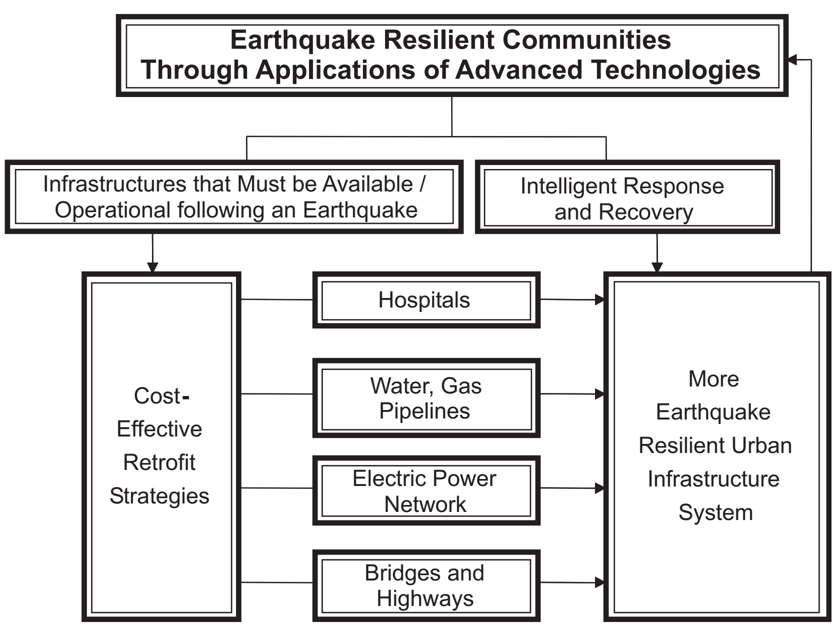

A cross-program activity focuses on the establishment of an effective experimental and analytical network to facilitate the exchange of information between researchers located in various institutions across the country. These are complemented by, and integrated with, other MCEER activities in education, outreach, technology transfer, and industry partnerships.

This report describes experimental research aimed at evaluating the seismic performance of an isolation/restraint system, typical of the systems designed by the ASHRAE members, supporting light mechanical equipment. Shake table experiments were conducted on an air-handling unit in two different conditions: supported by six isolation/restraint systems and rigidly-mounted. The test plan included seismic and system-identification tests, and incorporated different input-motion amplitudes and different isolation/restraint system properties. Experimental results showed that limiting the displacement of the equipment by the restraint components of the isolation/restraint systems resulted in amplification of the equipment acceleration responses. Based on these results, reducing the gap size is recommended to improve the seismic performance of these systems in areas of high seismicity. The test results also showed that higher amplification of acceleration responses should be expected for light and flexible equipment than for rugged and heavy equipment. This is the second report by the authors on isolation/restraint systems for mechanical equipment. The first report, MCEER-07-0007, focused on heavy mechanical equipment.

ABSTRACT

The experimental study described in this report is aimed at evaluating the seismic-performance of Isolation/Restraint (I/R) systems for light mechanical equipment. Earthquake-simulator experiments were conducted on an air-handling unit in two different conditions: supported by six I/R systems and rigidly-mounted. The test plan included seismic and system-identification tests, and incorporated different input-motion amplitudes and different I/R system properties. The test results showed that limiting the displacement of the equipment by the restraint components of the I/R systems resulted in amplification of the equipment acceleration-responses. Dynamic forces induced into the I/R systems were considerably larger than the forces predicted by the static approach. Based on the test results, reducing the gap size is the first recommendation to improve the seismic-performance of I/R systems in areas of high seismicity. Increasing the thickness of rubber snubbers is a solution to reduce the dynamic forces induced into the I/R systems, however it might result in higher acceleration and displacement responses of the equipment. Reducing hardness of rubber snubbers is not recommended as it can degrade the overall seismic performance of the I/R systems. The test results showed that higher amplification of acceleration responses should be expected for light and flexible equipment than for rugged and heavy equipment.

ACKNOWLEDGEMENTS

This project was supported by the American Society of Heating, Refrigerating, and Air-Conditioning Engineers (ASHRAE), and by the Earthquake Engineering Research Centers Program of the National Science Foundation (NSF) under Award Number EEC-9701471 to the Multidisciplinary Center for Earthquake Engineering Research (MCEER). The air-handling unit used as a test specimen, and the isolation and restraint components of the I/R systems tested in this study were generously provided by Trane Corporations, Kinetics Noise Control, and Mason Industries, respectively.

The authors gratefully acknowledge the guidance received by the members of the ASHRAE Technical Committee 2.7 during the project. Accomplishment of the presented experimental study is indebted to the hard work and expertise of the technical staff of the Structural Engineering and Earthquake Simulation Laboratory (SEESL) of Department of Civil, Structural, and Environmental Engineering at University at Buffalo, the State University of New York.

Any opinions, findings, conclusions, and recommendations presented in this reports are those of the authors, and do not necessarily reflect the views of the sponsors.

TABLE OF CONTENTS

TABLE OF CONTENTS (cont'd)

LIST OF ILLUSTRATIONS

LIST OF ILLUSTRATIONS (cont'd)

LIST OF ILLUSTRATIONS (cont'd)

LIST OF ILLUSTRATIONS (cont'd)

LIST OF ILLUSTRATIONS (cont'd)

LIST OF TABLES

LIST OF TABLES (cont'd)

SECTION 1

INTRODUCTION

Elastomeric snubbers are the most popular restraint devices used for the seismic protection of vibration-isolated mechanical equipment items. To prevent vibration isolators from short-circuiting during the normal operation of the equipment, a practical air gap separates the snubbers and the equipment. If the relative displacement of the equipment in response to a seismic excitation exceeds the gap size, the equipment hits the snubber and bounces back to move within the range of displacements that prevent failure of the equipment-supports and secure the associated service connections. To prevent a potential destructive impact between two hard surfaces, snubbers are typically made of elastomeric materials such as neoprene or natural rubber. Using impact mechanisms, elastomeric snubbers are supposed to protect the equipment by limiting its displacement responses rather than by dissipating the seismic input energy. Elastomeric snubbers can be installed around the equipment, separate from the vibration-isolator supports, or they can be integrated with the vibration-isolator supports and form isolation/restraint (I/R) systems.

The experimental research presented in this report is aimed at evaluating the seismic performance of an I/R system typical of commercially available systems for seismic application. The relatively light mechanical equipment used as the test specimen in this study was an air-handling unit. The experimental study included two phases of earthquake-simulator tests. In the first phase of the experiments, the test specimen was mounted on six I/R systems. Throughout 11 test series, the test plan of this phase of the experiments incorporated 11 different combinations of the restraint component properties. In addition to seismic tests with a triaxial input motion scaled to different amplitudes, each of the 11 test series included pulse-type system-identification tests. The triaxial input motion used in the seismic tests was generated to match the AC156 (ICC-ES, 2004) Required Response Spectra (RRS) for the roof level of a building in an area of high seismicity. During the seismic tests of this phase, the dynamic forces induced into the I/R systems, the triaxial displacement responses on the housing of the test specimen, and the triaxial acceleration responses near the center of mass, on the housing, and at the support locations of the test specimen were measured.

In order to establish the modal properties of the test specimen and to compare the seismic responses of the isolated and rigidly mounted test specimen, the second phase of the experiments were conducted with the test specimen rigidly mounted on the earthquake simulator. The test plan of the second phase of the experiments included system-identification and seismic tests with the triaxial input motion scaled to different amplitudes. During the seismic tests of this phase, the dynamic forces experienced at the support locations of the test specimen, the triaxial displacement responses on the housing of the test specimen, and the triaxial acceleration responses near the center of mass and on the housing of the test specimen were measured.

After analyses of the test specimen responses during the system-identification and seismic tests, the modal properties of the isolated and rigidly mounted test specimen, and variations of the peak response quantities with the input motion amplitude for different sets of the restraint component properties were established. The peak response quantities considered for the analyses of the seismic performance of the I/R systems included the amplification of the acceleration responses near the center of mass, on the housing and at the support locations of the test specimen, the peak relative displacement responses on the housing of the test specimen, and peak dynamic forces induced into the I/R systems. The sensitivity of the seismic performance of the I/R systems to variations of the restraint component properties were investigated and seismic responses of the isolated and rigidly mounted test specimen were compared to each other.

1.1 Research Motivation and Past Studies

Mechanical equipment items, such as Heating, Ventilation, and Air-Conditioning (HVAC) units, form an important category of nonstructural components inside buildings. Compared to the structural components or other categories of nonstructural components, the direct loss associated to the damage to this category of nonstructural components might be insignificant. However, the indirect loss resulting from the damage to these components particularly in the critical facilities can be devastating. Even a short interruption in operation of HVAC-type mechanical equipment in critical facilities (such as hospitals) endangers the continued functionality required by the public from such facilities during and after an earthquake (Myrtle et al., 2005).

Most of HVAC-type mechanical equipment items have rotating components. Therefore, when rigidly mounted to the floor, they can be sources of mechanical vibrations and noise. Mechanical vibrations and noise are certainly annoying for occupants and detrimental for objects sensitive to vibrations. The obvious solution for this problem is to install mechanical equipment items outside buildings and away from occupied spaces. However, this solution strongly contradicts the energy-conservation concepts. In fact, from the energy-conservation point of view, it is always preferred to install mechanical equipment items on the roof or intermediate levels of buildings. Therefore, a better solution is to install mechanical equipment inside buildings (just adjacent or above occupied areas), and to prevent the transmission of mechanical vibrations by introducing resilient interfaces between the mechanical equipment and the building. Flexible supports such as coil springs reduce the transmission of noise, shock, and vibration produced by the equipment into the building structure or into other sensitive equipment items inside the building (ASHRAE, 2003).

A proper selection of mechanical properties of vibration isolators to satisfy noise-control requirements usually results in low natural frequencies for the isolated equipment. If the natural frequencies of the isolated equipment match the seismic response frequencies of the building during an earthquake, a quasi-resonance will happen and the equipment will experience large displacement responses. Typical vibration-isolator supports are not capable of accommodating large displacement responses. Due to excessive displacement responses of the equipment relative to the floor, the vibration-isolator supports might buckle or break. After losing its supports during an earthquake, a piece of mechanical equipment will move freely like a massive projectile, and will be a hazard. Moreover, if the service connections attached to the equipment cannot accommodate the excessive displacement responses they will break and cause serious problems such as flooding (Ayres and Phillips, 1998).

Seismic vulnerability of vibration-isolated equipment items was observed for the first time after the 1964 Alaska earthquake (Ayres et al., 1973). However, observations and recommendations about the vibration-isolated equipment prepared by Ayres et al. were published nine years later, after the 1971 San Fernando earthquake in California. The dramatic damage to vibration-isolated equipment items during the 1971 San Fernando earthquake (Ayres and Sun, 1973) convinced engineers that a serious conflict existed between vibration isolation and seismic protection of mechanical equipment items. Solving this conflict was complicated since the nature of the excitation and the expected performance during an earthquake were completely different from those during normal operation condition. The desirable characteristics of equipment supports to achieve vibration isolation were substantially different from those needed to secure seismic protection. Therefore, engineers started to develop equipment-supports, capable of exhibiting two-phase characteristics. This effort resulted in two types of seismic restraints: lockout devices, which functioned like seat belts, and elastomeric snubbers. However, elastomeric snubbers were soon proven much more economical, reliable, and practical than the lockout devices (Mason Industries Inc., 2004). Consequently, installation of elastomeric snubbers became the predominant method of seismic protection of vibration-isolated equipment.

During the earthquakes of the past three decades and particularly during the 1994 Northridge earthquake in California, vibration-isolated equipment items protected by elastomeric snubbers fared far better than unrestrained ones (Gates and McGavin, 1998). However, the overall performance of elastomeric snubbers during these three decades of application has not been consistent. In many cases on the roof or upper level of buildings, the elastomeric snubbers protecting mechanical equipment items were broken or their anchor bolts were shaken off (Reitherman and Sabol, 1995; Naeim and Lobo, 1998). Construction errors as well as lack of true assessment of the dynamic forces induced into the snubbers have been blamed for the repeated damage to the vibration-isolated equipment protected by rubber snubbers (Filiatrault et al., 2002).

Despite the repeated damage pattern to vibration-isolated equipment in recent earthquakes resulting mainly from the failure of snubbers, the basic research work in this area has remained sparse, and the available codes and guidelines are mainly based on experiences, engineering judgment, and intuition rather than on systematic experimental and analytical results.

In one of the few analytical studies about the seismic responses of vibration-isolated equipment protected by rubber snubber, Iwan (1978) showed that for the practical range of snubber properties, the translational acceleration response at the center of mass of the equipment can be up to four times the peak input acceleration.

Prior to the study presented in this report, another experimental study was conducted by Fathali and Filiatrault (2007) on the seismic performance of the I/R systems supporting a heavy centrifugal liquid chiller. The results of several series of seismic earthquake-simulator tests with various input motion amplitudes conducted in that study showed that the peak acceleration response at the center of mass of the chiller was amplified between 1.8 and 4.5 times in the horizontal direction and between 2.2 and 4.5 times in the vertical direction. The amplification of the peak acceleration response at the center of mass of the chiller reduced with an increase of the peak input acceleration. Regardless of the I/R system properties, with high-amplitude input motions, the acceleration amplification factor at the center of mass of the chiller varied only between 2.0 and 3.0. Throughout the experiments, the I/R systems experienced dynamic forces much higher than their static design capacity. The restraint component properties, particularly the gap size, were proven influential on the seismic performance of the I/R systems. Among different combinations of the restraint component properties considered in that study, the configuration with the smallest gap size resulted in the best overall seismic performance.

1.2 Report Organization

The introduction section of this report is followed by Section 2, which presents details and information about the test specimen. The properties and details about the configuration of the I/R systems considered in the experimental investigation are described in Section 3. The laboratory equipment and instrumentation used to conduct the experiments are presented in Section 4. The input motions, plan, and setup for the earthquake-simulator tests are explained in Section 5. Section 6 includes the system-identification and seismic tests results. The test results presented in Section 6 are the dynamic properties of the isolated and rigidly mounted test specimen (established based on the results of the system-identification tests), the selected response envelopes during the seismic tests, and the damage observation throughout the experiments. The seismic test results are analyzed and discussed in Section 7. Effects of variations of the restraint component properties on the seismic performance of the I/R systems are studied in Section 7. The conclusions drawn from the test results are provided in Section 8. The key and general findings from conducting two experimental studies on the seismic performance of the I/R systems (with light and heavy mechanical equipment) are summarized in Section 9. Section 10 lists the references used in the text of the report.

SECTION 2

TEST SPECIMEN

2.1 General Description of Test Specimen

The light mechanical equipment used in this study is an Air-Handling Unit (AHU) provided by the Trane Corporation. AHUs are important components of Heating, Ventilation, and Air-Conditioning (HVAC) systems inside buildings. For energy conservation, AHUs are often mounted on the roof of buildings. Typically, AHUs are sheet metal boxes containing modules and components to execute a three-stage procedure: 1) to bring in outdoor air, 2) to condition the air, and 3) to distribute the conditioned air to occupied spaces inside the building through duct systems. Each module is responsible to perform one of the three stages. Depending on the target function and location of an AHU, different modules can be arranged to function in parallel or in series.

Regardless of the outdoor temperature, an AHU should be able to bring sufficient conditioned air to achieve and maintain a comfortable and healthy climate within the building. Generally, the air-conditioning includes control of the moisture and temperature, and removing particulate and gaseous contaminants.

Figure 2-1 shows a photograph of the test specimen mounted on the earthquake simulator in the Structural Engineering and Earthquake Simulation Laboratory (SEESL) of the Department of Civil, Structural, and Environmental Engineering at University at Buffalo, the State University of New York.

Figure 2-1 Test Specimen: Air-Handling Unit

2.2 Test Specimen Components

The AHU used in this study consists of four modules functioning in series: an air-mixing module, two coil modules, and a fan module. With the coil modules placed upstream of the fan module, the test specimen is classified as a draw-through AHU. The overall view of the AHU and close-up photos of the AHU modules are shown in Figure 2-2.

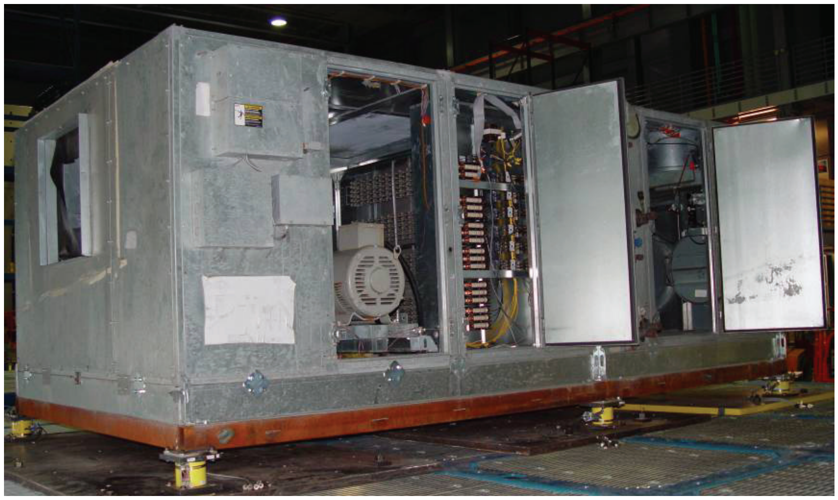

(a) Overall View

(b) Fan Module

(c) Electric Heat Coil Module

(d) Air-Mixing Module

Figure 2-2 Test Specimen Components

The incoming outdoor air and return air collected from the occupied spaces are combined in the air-mixing module. The dampers on the side and top of the air-mixing module control the volume of the ventilation air entering the system in response to specific operating conditions.

Coil modules condition the passing air stream by dehumidifying and heating it. Dehumidification is accomplished inside the coil module adjacent to the air-mixing module by condensing the water vapor on cooling coils. When air is passed through the cooling coils, water condenses out on the surfaces of the coils. Collection pans installed below the cooling coils collect the condensed water and stream it out through drainpipes. The dehumidification procedure by cooling the air might result in overcooling the air provided to the building. This problem is solved by the electric heat coil module between the cooling coil and the fan module.

The fan module delivers the conditioned air to occupied spaces inside the building. A centrifugal fan belt-driven by a motor inside the fan module blows the conditioned air into a duct system connected to the AHU. As shown in Figure 2-3, the centrifugal fan and motor are mounted on a framework of steel channels. Four restrained vibration isolators interface the AHU housing and the supporting frame. Each vibration isolator consists of two nested coil springs. The vibration isolators at four corners of the supporting frame can be deactivated by the leveling bolts passing through the coil springs. The deactivated vibration isolators act like rigid links between the supporting frame and the AHU housing. A framework of steel angles encases the centrifugal fan and is connected to the AHU housing with two vibration isolators. The vibration isolators interfacing the fan module components and AHU housing are shown in Figure 2-4.

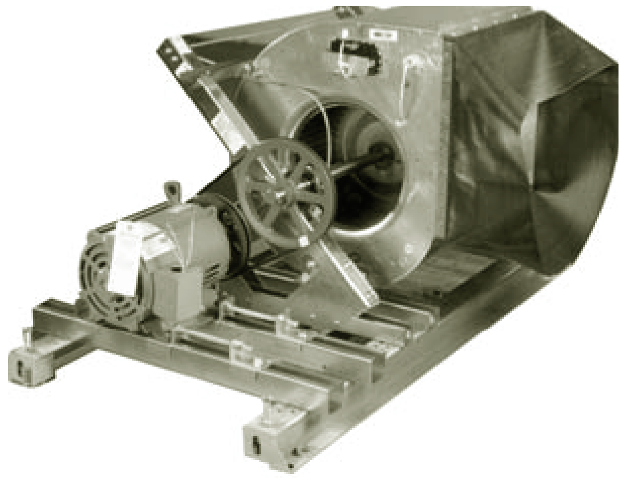

Figure 2-3 Fan Module Components (Trane Co., 2007)

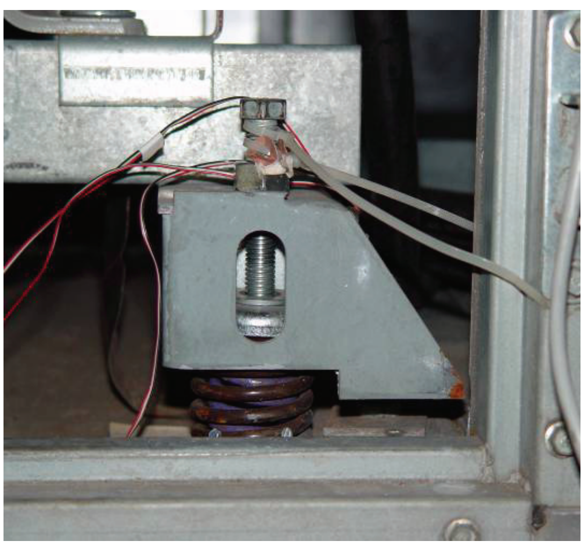

(a) Restrained Vibration Isolator Supporting Fan and Motor inside Fan Module

(b) Unrestrained Vibration Isolator between Fan Case and AHU Housing (Circled with Dotted Line)

Figure 2-4 Internal Vibration Isolators Interfacing Fan Module Components and AHU Housing

The AHU housing is formed by double-wall sheet metal welded to a framework of steel angles and channels. Double-wall sheet metal is used for the housing to promote the air quality and noise control. The AHU housing is heat insulated to prevent condensation on its surfaces. The AHU housing doors provide easy access to all areas inside the AHU for inspection, service, and cleaning. A steel base rail is bolted under the four modules. The isometric drawing of the base rail is shown in Figure 2-5. A steel-tube frame bolted under the base rail provides the proper contact surface for installation of the AHU.

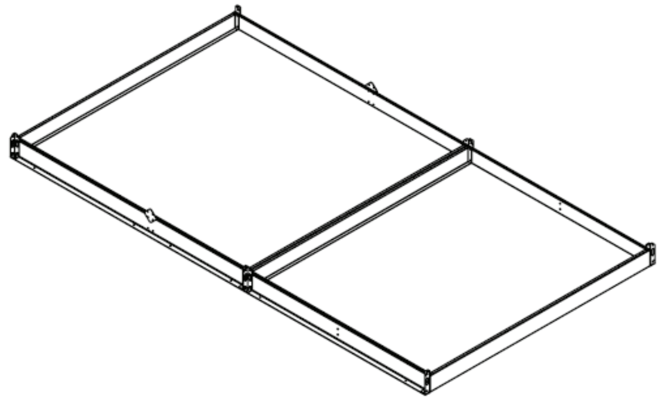

Figure 2-5 Base Rail Under AHU Modules

2.3 Test Specimen Dimensions and Mass

The test specimen overall dimensions are 4.37 x 2.31 x 1.69 *m* (172 x 91 x 66.5 *in.*). The overall 1.69 *m* (66.5 *in.*) height of the test specimen includes the 1.44 *m* (56.5 *in.*) height of the modules, 0.15 *m* (6 *in.*) height of the base rail and 0.10 *m* (4 *in.*) height of the steel-tube frame. The AHU overall and component dimensions are presented in Figure 2-6.

According to the data provided by the AHU manufacturer and the data obtained from the measurement in the laboratory, the total mass of the test specimen was 1971 *kg* (4345 *lbs*). Table 2-1 lists the mass of the test specimen components. Table 2-2 presents the coordinates of the center of mass of the AHU with respect to the coordinate system defined in Figure 2-6(a). The longitudinal, transverse, and vertical directions of the test specimen are associated with the x, y, and z axis, respectively. Table 2-3 lists the triaxial eccentricities between the center of mass of the AHU and the geometric center of the AHU in the longitudinal, transverse, and vertical directions.

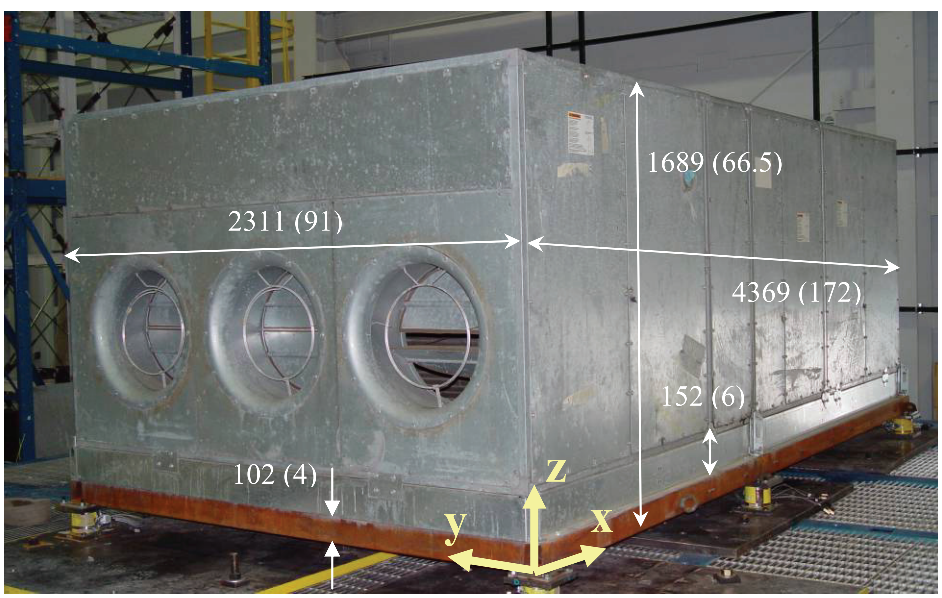

(a) Overall Dimensions

Figure 2-6 Test Specimen Dimensions, (unit: *mm* (*in.*))

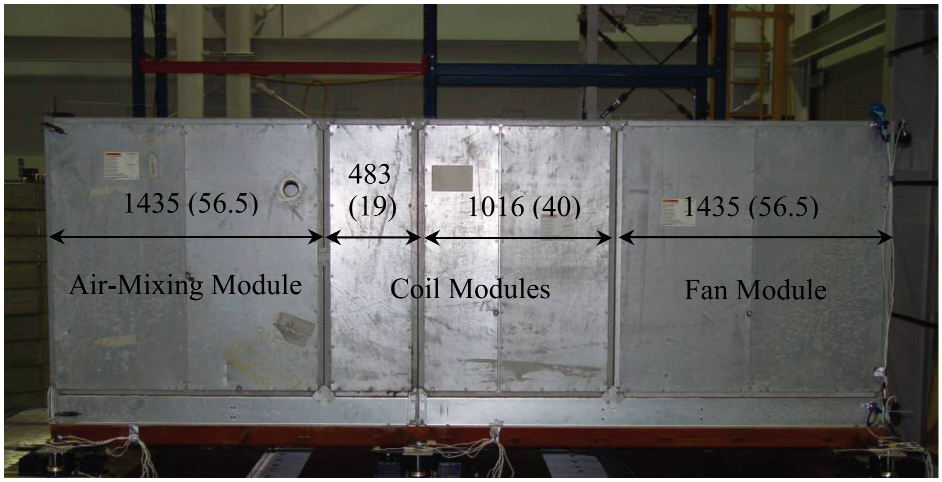

(b) Module Dimensions

Figure 2-6 (cont'd) Test Specimen Dimensions, (unit: *mm* (*in.*))

Table 2-1 Test Specimen Components Mass

Component	**Mass, *kg (lbs)***
Air-Mixing Module	307 (676)
Cooling Coil Module	293 (646)
Electric Heat Module	379 (836)
Fan Module	670 (1476)
Base Rail and Connections	158 (349)
Steel Tube Fixture	164 (362)
Total	1971 (4345)

Table 2-2 Coordinates of Center of Mass of Test Specimen, *m (in.)*

x : Longitudinal	y : Transverse	z : Vertical
2.42 (95.3)	1.31 (51.6)	0.76 (30.0)

Table 2-3 Eccentricities of Center of Mass with Respect to Geometric Center of Test Specimen, *mm (in.)*

x : Longitudinal	y : Transverse	z : Vertical
235 (9.3)	155 (6.1)	83 (3.3)

SECTION 3

ISOLATION/RESTRAINT SYSTEM

3.1 General Description of Isolation/Restraint System

For energy conservation, mechanical machinery such as HVAC equipment are often installed on the roof or intermediate level of buildings just adjacent or above occupied areas. Mechanical equipment rigidly mounted to a building structure can be a source of mechanical vibration and noise. The mechanical noise and vibration inside a building cause discomfort for the occupants, damage the sensitive equipment inside the building, and over a long period can be detrimental to the structural system.

The transmission of noise, shock, and vibration produced by a piece of mechanical equipment into the building occupied areas is reduced by mounting the equipment on vibration isolators. Vibration isolators are flexible supports, which interface the equipment and the building. Among different types of vibration isolators, steel coil springs are the most popular. Figure 3-1 shows photographs of steel coil-spring vibration isolators supporting the housekeeping pad of a mechanical equipment item.

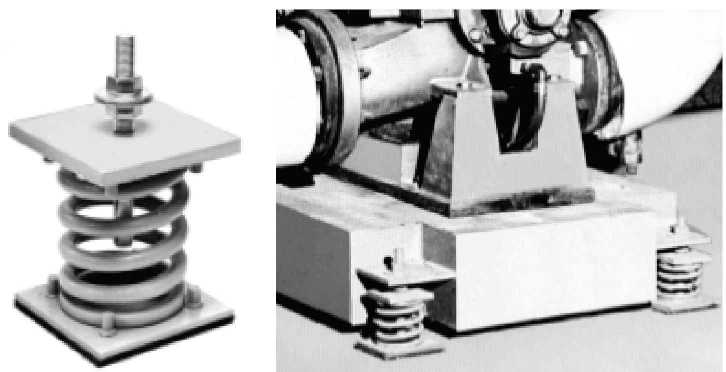

Figure 3-1 Coil-Spring Vibration Isolators Supporting Mechanical Equipment (Kinetics Noise Control, 2007)

While vibration isolators are perfectly capable of reducing the mechanical vibrations, their performance during a seismic event can be problematic. A piece of rugged mechanical equipment supported by flexible vibration isolators will have low natural frequencies. If the natural frequencies of the mounted equipment match the response frequencies of the building during an earthquake, quasi-resonance occurs, and the equipment will experience displacements much larger than the vibration isolator capacity. Consequently, the equipment will be shaken off its supports and move unrestrainedly. Large mechanical equipment moving without restraint during an earthquake will be threatening to both life and property. Furthermore, the excessive relative displacement response of the equipment can result in breakage of the ducts, pipes, and electrical wirings connected to it. Figure 3-2 shows an example of failed vibration isolators during the 1994 Northridge earthquake, which have resulted in rupture of the connected pipes (Lloyd, 2003).

The displacement response of an isolated equipment item can be limited by using snubbers. Snubbers (or bumpers) are installed with a practical clearance (air gap) from the equipment to limit the displacement responses within the range that ensures safety of the equipment and its associated ducts, pipe, and wires. The air gap is necessary to keep the snubbers out of contact during the normal operation of the equipment. When the equipment displacement response exceeds the gap size, an impact occurs between the equipment and the snubber, and the equipment bounces back to move within the accepted range of displacement.

Figure 3-2 Pipe Rupture Resulting from Vibration-Isolator Supports Failure during Northridge Earthquake (Lloyd, 2003)

Intensity of the impact between the equipment and snubber is reduced by making the snubber contact surface from a flexible material such as neoprene or natural rubber. The resilient contact surface of the snubber prevents the potential destructive impact between two hard surfaces but adds little to the energy dissipation capability of the snubber. Essentially, snubbers control the displacement response of vibration-isolated equipment by changing the stiffness of the support rather than by dissipating energy.

Some snubbers such as those shown in Figure 3-3 are designed to provide restraint in only one direction. Since earthquake direction is not predictable, sets of unidirectional snubber should be installed around the vibration-isolated equipment to ensure sufficient restraining forces in all directions.

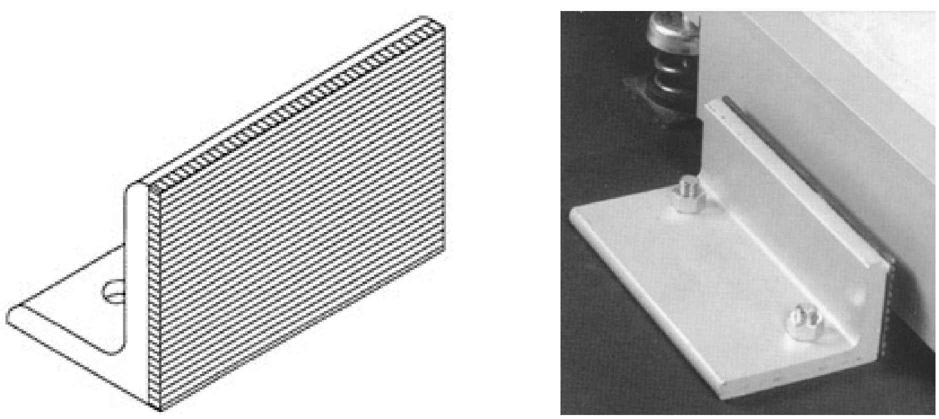

Figure 3-3 Unidirectional Seismic Snubber (Kinetics Noise Control, 2007)

Throughout the four decades of application of snubbers, the unidirectional snubbers have evolved into all-directional integrated isolation/restraint (I/R) systems. The integrated I/R systems do not require a supplemental support base. Therefore, they are ideal for the rugged point-loaded equipment such as chillers and fans. From the vibration-isolation point of view and especially for the heavy equipment with horizontal eccentricities between the center of support locations and the center of mass, installation of unidirectional snubbers separate from isolation springs are preferable. However, from the seismic-protection point of view, integrated I/R systems are superior. During the 1994 Northridge earthquake the integrated I/R systems fared much better than the other unidirectional snubbers (Lama, 1994).

The integrated I/R system used for this experimental study is typical of the systems designed and approved by the ASHRAE members. The isolation and restraint components of this I/R system are oriented orthogonally with respect to each other. The two components are integrated into an I/R system unit by bolting the top and bottom plate of the restraint component to the top and bottom plate of the isolation component. The assembled I/R system is about 84 *kg* (185 *lb*), 292 *mm* (8.5 *in.*) tall, and 445 x 445 *mm* (17.5 x 17.5 *in.*) in plan. Figure 3-4 shows photographs of the I/R system before and after mounting the test specimen.

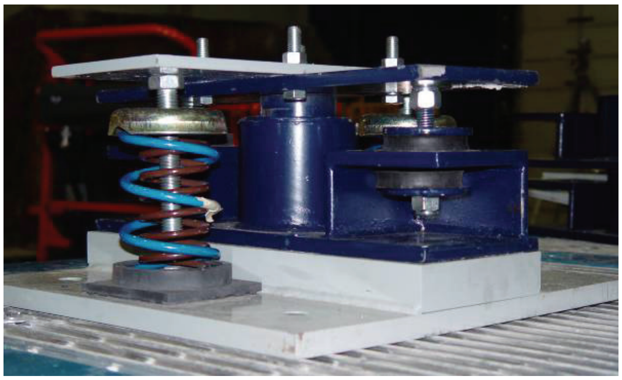

(a) Before Mounting Test Specimen

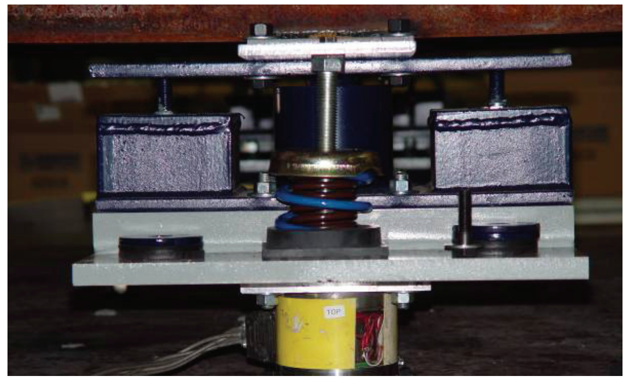

(b) After Mounting Test Specimen

Figure 3-4 Assembled Isolation/Restraint System

Six I/R systems were installed under the test specimen: under the four corners and the two ends of the joint between the coil modules. The I/R systems supporting the test specimen are numbered from 1 to 6, as shown in Figure 3-5.

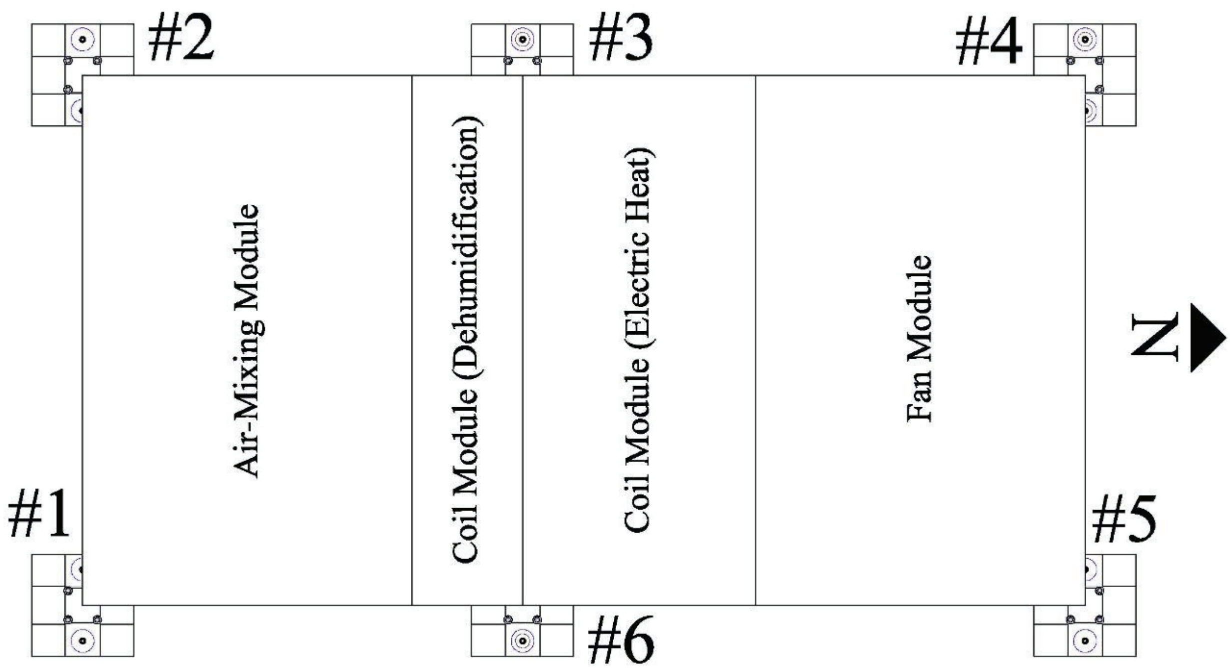

Figure 3-5 Arrangement of Six I/R Systems under Test Specimen

3.2 Isolation Component of Isolation/Restraint System

The isolation component of the I/R system used in this study consists of two single or nested steel coil springs embedded between two parallel rectangular steel plates. Dimensions and details of the isolation component of the I/R system are shown in Figure 3-6. For the I/R systems supporting large tributary mass of the test specimen, nested coil springs with different geometry and stiffness were used to limit the vertical deflection of the isolation component to 76 *mm* (3 *in.*). Figure 3-7 shows photographs of the single and nested coil springs.

The 210 *mm* (8.25 *in.*)-wide horizontal clearance between the two coil springs is provided for installation of the restraint component of the I/R system. The vertical distance left between the top and bottom plate after mounting the equipment (when the springs are compressed) is important because the restraint component should fit and function properly between the two plates. The required distance between the top and bottom plate is adjusted by the two leveling bolts that pass through the load plates on top of the springs.

Coil springs are typically designed and constructed for a required axial stiffness or a target vertical deflection. The required axial stiffness (or target vertical deflection) is selected based on the weight and the operation-induced forces of the equipment without any seismic considerations. After selecting the coil spring for a required axial stiffness (or a target deflection), the lateral (horizontal) stiffness of the spring can be calculated. The lateral stiffness of a coil spring is a function of several parameters including its axial stiffness, geometry, uncompressed and compressed length, and end conditions (Harris and Crede, 1961; Yao and Lien, 1998).

Table 3-1 lists the information about the type (single or nested), axial stiffness, estimated lateral stiffness, and vertical deflection for the isolation component of each of the I/R systems supporting the test specimen. The values for the axial and lateral stiffness of the isolation components of the I/R systems were provided by their manufacturer. However, the values of the vertical deflection were measured in the laboratory after mounting the test specimen on the I/R systems. The vertical deflections of the isolation components under the test specimen showed that the I/R system #4 carries the largest tributary mass.

When the restraint component of the I/R system is not engaged, applied loads are carried only by the isolation component, and therefore, the total stiffness of the I/R system is equal to the stiffness of the isolation component.

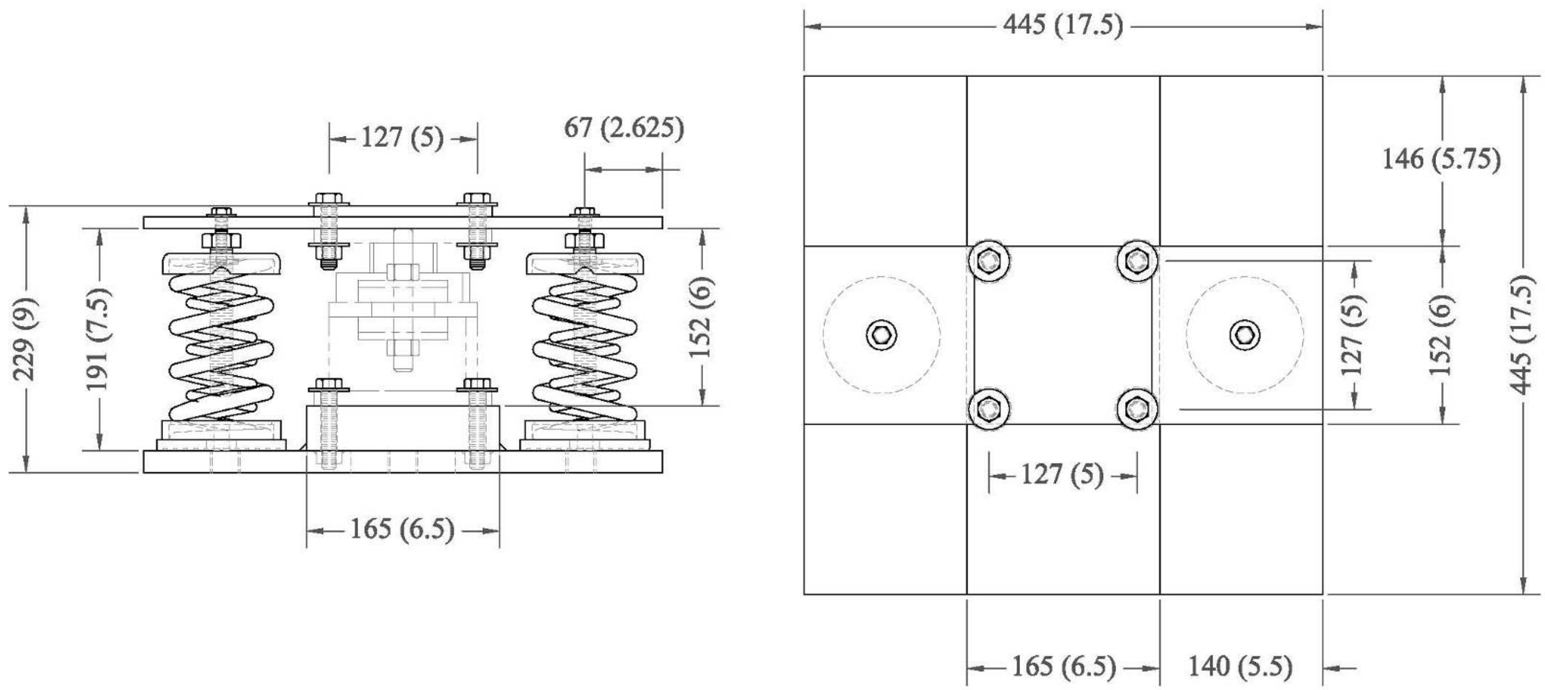

Figure 3-6 Dimensions and Details of Isolation Component of I/R System (unit: *mm* (*in.*))

Figure 3-7 Single and Nested Coil Springs Used for Isolation Component of I/R System

Table 3-1 Estimated Stiffness and Measured Vertical Deflection of Isolation Component of Six I/R Systems Supporting Test Specimen

I/R System No.	Coil Spring Type	Isolation Component Stiffness, *N/mm (lb/in.)*		Vertical Deflection, *mm (in.)*
		Axial	Lateral	
1	Single	43.8 (250)	22.8 (130)	49 (2.1250)
2	Single	43.8 (250)	22.8 (130)	51 (2.1250)
3	Nested	65.7 (375)	33.3 (190)	60 (2.5000)
4	Nested	65.7 (375)	40.3 (230)	75 (3.000)
5	Single	43.8 (250)	24.5 (140)	60 (2.5625)
6	Nested	65.7 (375)	31.5 (180)	56 (2.3125)

3.3 Restraint Component of Isolation/Restraint System

3.3.1 Configuration Details

Details and dimensions of the restraint component of the I/R system are shown in Figure 3-8 and are listed in Table 3-2. The restraint component consists of a top and a bottom thick rectangular steel plate. A piece of steel pipe is welded to the center of each plate. When the pipes are aligned coaxially, their different diameters allow the top pipe go through the bottom pipe with a 25 *mm* (1 *in.*) thick cylindrical air gap. Part of the cylindrical air gap is filled by a rubber tube fitted inside the bottom pipe. Two threaded rods are welded to the sides of the top plate. Each rod has a pair of nuts. Two pieces of 13 *mm* (0.5 *in.*) thick steel angle are welded to the sides of the bottom plate. A 13 *mm* (0.5 *in.*) thick plate with a hole in its center is welded on top of each of the two angles. A rubber washer is fitted into the hole of each plate. When the top and bottom pipes are aligned coaxially, the rods of the top plate of the restraint component pass through the center of the hole on the plates. The rubber washer fitted into the hole prevents impacts between the steel rod and the plate. On each side of the plate, there is a rubber washer and a steel washer. The steel washer interfaces the nut and rubber washer surface. Figures 3-9 and 3-10 present photographs of the top and bottom part of the restraint component of the I/R system, respectively.

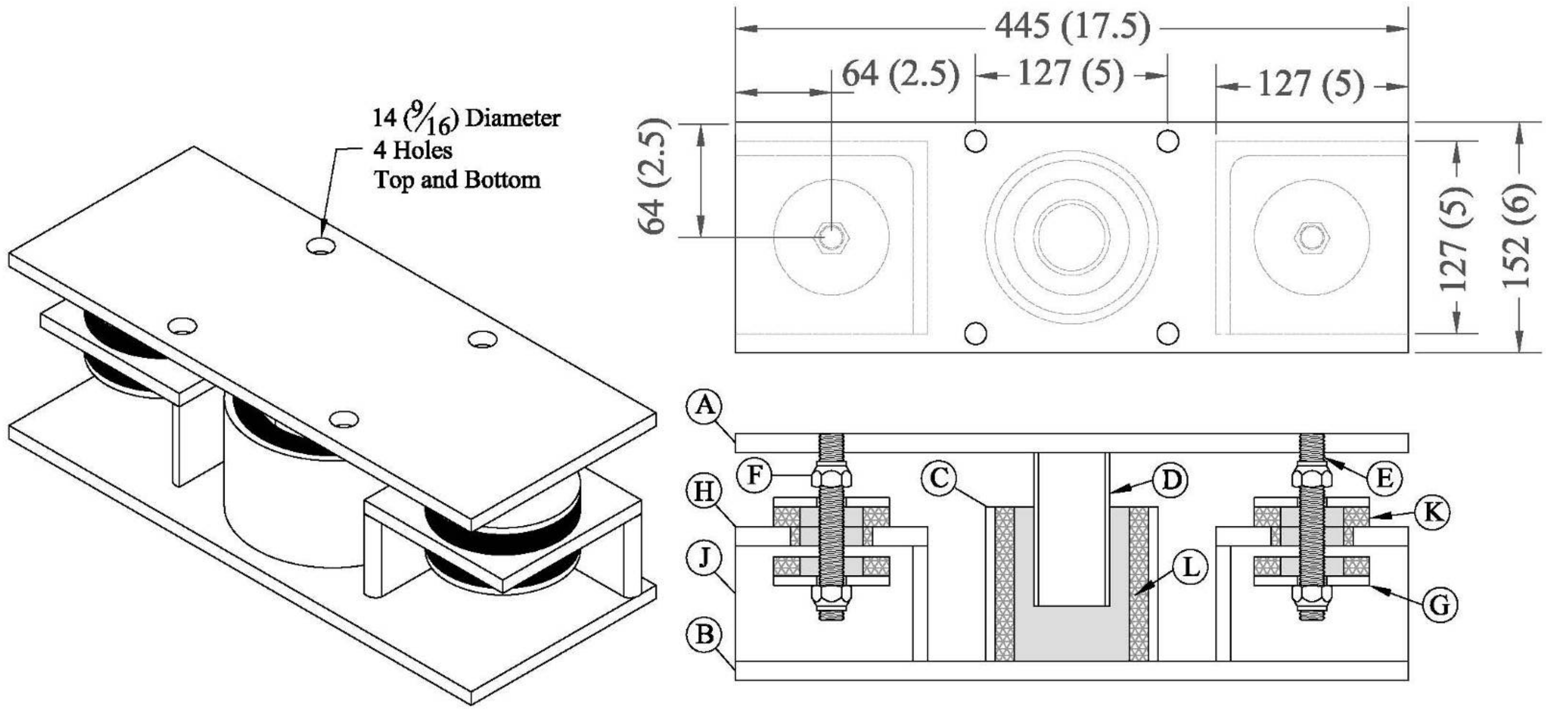

Figure 3-8 Dimensions and Details of Restraint Component of I/R System (unit: *mm* (*in.*))

Table 3-2 Details of Restraint Component of I/R System

Part[1]	Quantity	Description	Size[2]
A	1	Top Steel Plate	13 x 152 x 445 *mm* (0.5 x 6.0 x 17.5 *in.*)
B	1	Bottom Steel Plate	13 x 152 x 445 *mm* (0.5 x 6.0 x 17.5 *in.*)
C	1	Bottom Steel Pipe	102 *mm* (4 *in.*) Pipe / 102 *mm* (4 *in.*) long
D	1	Top Steel Pipe	51 *mm* (2 *in.*) Pipe / 102 *mm* (4 *in.*) long
E	2	Threaded Rod	16 *mm* (0.625 *in.*) - 11 UNC / 108 *mm* (4.25 *in.*) long
F	4	UNC Torque Hexagonal Nut	16 *mm* (0.625 *in.*) - 11 UNC
G	4	Steel Washer	76 *mm* (3 *in.*) O.D. / 19 *mm* (0.75 *in.*) I.D. / 6 *mm* (0.25 *in.*) Thick.
H	2	Steel Plate with Hole	13 x 127 x 127 *mm* (0.5 x 5.0 x 5.0 *in.*) / 54 *mm* (2.125 *in.*) Hole
J	2	Steel Angle	127 x 127 x 13 *mm* (5.0 x 5.0 x 0.5 *in.*) / 76 *mm* (3 *in.*) long
K	4	Rubber Washer	54 *mm* (2.125 *in.*) O.D. / 51 *mm* (2.0 *in.*) I.D. / 13 *mm* (0.5 *in.*) Thick.
L	1	Rubber Tube	Variable / See Table 3-3
M	2	Rubber Washer	Variable / See Table 3-3

1. See Figure 3-8
2. UNC: Uniform Coarse Thread, O.D.: Outside Diameter, I.D.: Inside Diameter

(a) Rubber Tubes

(b) Rubber Washers

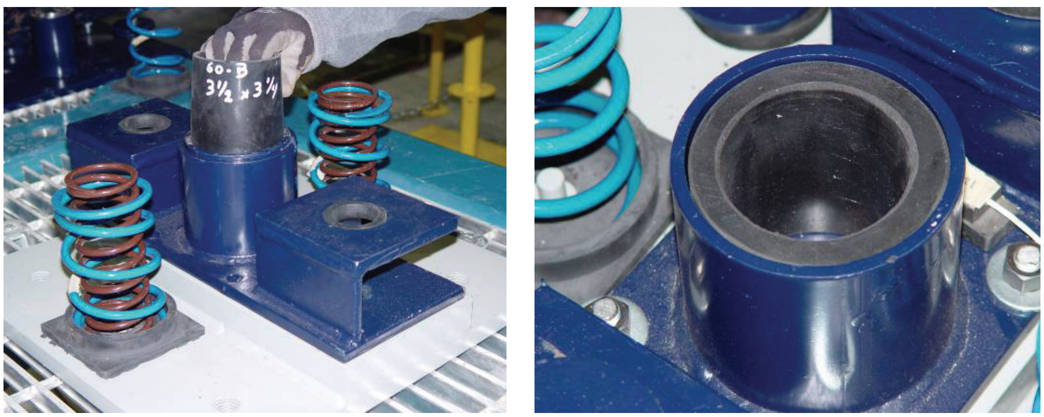

(c) Placing Rubber Tube inside the Bottom Pipe

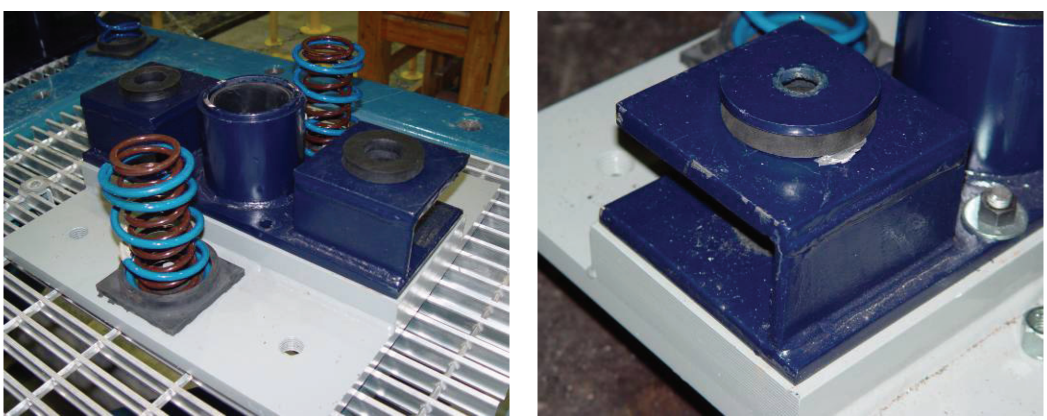

(d) Placement of Rubber Washers

Figure 3-9 Restraint Component of I/R System, Bottom Part

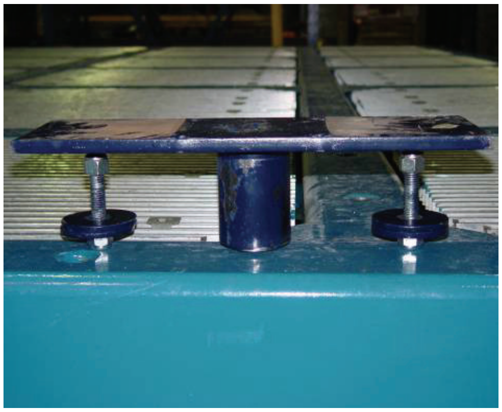

(a) Top Pipe and Threaded Rods

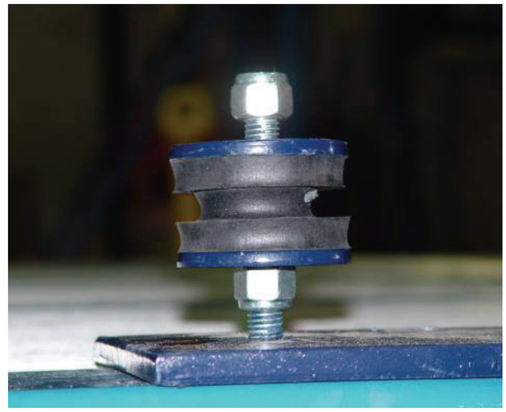

(b) Steel and Rubber Washers between Two Nuts

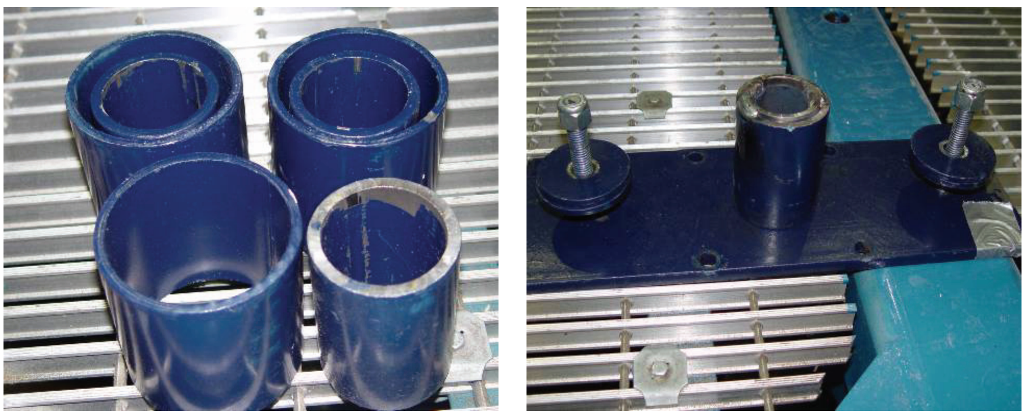

(c) Steel Bushing around Top Pipe to Adjust Horizontal Gap Size

Figure 3-10 Restraint Component of I/R System, Top Part

3.3.2 Restraining Mechanism

In the horizontal direction, the top and bottom parts of the restraint component can move freely relative to each other within the cylindrical air gap left between the top pipe and the rubber tube inside the bottom pipe. The restraining mechanism in the horizontal direction is triggered when the top pipe makes contact with the rubber tube inside the bottom pipe. The expanding contact surface between the top pipe and the rubber results in gradual engagement of the snubber in the horizontal direction and introduces a geometric nonlinearity.

Subtracting the total thickness of the two rubber washers, two steel washers, and steel plate (with a hole in the center) from the distance left between the two nuts on the threaded rod gives the peak-to-peak vertical gap of the restraint component. The restraining mechanism in the vertical direction is activated when at least one of the nuts on the rods starts to press the steel washer onto the rubber washer. The snubber in the vertical direction is fully engaged at once, and the contact surface between the steel washer and the rubber stays constant as long as the snubber is engaged.

The restraining mechanism resulting from the impact between two steel objects has been proven destructive and should be strictly avoided (Lama, 1998). Therefore, locations of the nuts on the rods should be adjusted such that the free end of the rods and top pipe are prevented from touching the bottom plate of the restraint component.

During the temporary engagement of the restraint component, the stiffness of the snubbers significantly increase the total horizontal and vertical stiffness of the I/R system. According to the manufacturer of the I/R systems, static engagement of the horizontal restraint would multiply the total horizontal stiffness of the I/R system by a factor larger than 20 (depending on the rubber tube properties) and engagement of the vertical restraint would increase the total vertical stiffness of the I/R system by a factor of factor 15 (depending on the rubber washer properties).

3.3.3 Variable Properties

The thickness and hardness of the rubber tube and rubber washer as well as the horizontal and vertical gaps are the configuration variables of the restraint component that can affect the seismic performance of the I/R system. Table 3-3 lists the variations of each of the configuration variables considered in this study.

Table 3-3 Variations of Restraint Component Properties

Restraint Component Property	Nominal Values
Gap Size, *mm (in.)*	6, 13 (0.25, 0.50)
Rubber Tube Thickness, *mm (in.)*	3, 6, 13, 19 (0.125, 0.25, 0.50, 0.75)
Rubber Washer Thickness, *mm (in.)*	6, 13, 19 (0.25, 0.50, 0.75)
Rubber Tube and Rubber Washer Hardness, *Duro*	50, 60

The vertical gap, which was always nominally equal to the horizontal gap, was adjusted by moving the nuts along the threaded rods. The horizontal gap was adjusted by inserting steel bushings around the top pipe (see figure 3-10(c)).

Ideally, as shown in Figure 3-11(a), the horizontal gap is uniform around the top pipe. However, after mounting the test specimen on top of the I/R systems, the horizontal gaps in the restraint components of the I/R systems were not always uniform. In the I/R systems with small nominal gap size, the offset between the axes of the rubber tube and the top pipe was sometimes larger than the nominal gap size and therefore, the top pipe was in contact with the rubber tube, as illustrated in Figure 3-11(b). In some cases throughout the test series, as the result of the severe shaking and impacts, the position of test specimen on top of the I/R systems were slightly readjusted and the contact inside the restraint component was decreased or even eliminated as shown in Figure 3-11(c).

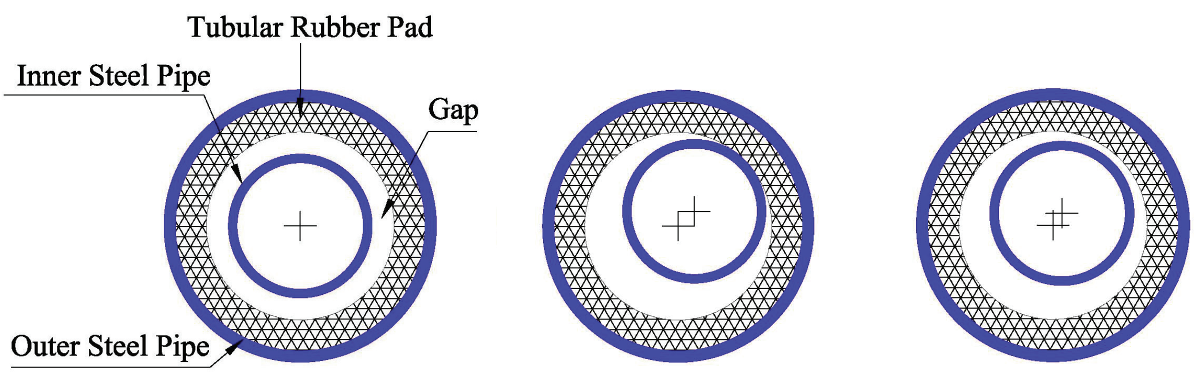

(a) Ideal Configuration (Uniform Gap) (b) Practical Configuration (Offset with Contact) (c) Practical Configuration (Offset without Contact)

Figure 3-11 Horizontal Gap in At-Rest Condition after Installation (Top View)

3.3.4 Static Design Capacity

The restraint component of I/R systems should be designed for the supplemental dynamic loads resulting from the impacts between the equipment and the restraint component during a seismic event. The maximum dynamic load induced into the restraint component of an I/R system is estimated by an equivalent static load, which is equal to the mass carried by the I/R system multiplied by a design peak acceleration (Meisel, 2001). The restraint component should be capable of withstanding the equivalent static load applied in any given direction.

The restraint component of the I/R system used in this study was designed for 3.0 g peak acceleration. In other words, the restraint component was designed to withstand static loads as large as three times the tributary supported weight. Assuming during the design that the central I/R systems would support almost one quarter of the test specimen mass, the restraint component of the I/R system was designed and manufactured for the static design capacity of 15 *kN* (3.4 *kips*).

SECTION 4

LABORATORY EQUIPMENT

4.1 Earthquake Simulator

The six-degree-of-freedom earthquake simulator utilized in this series of experiments is located in the Structural Engineering and Earthquake Simulation Laboratory (SEESL) of the Department of Civil, Structural, and Environmental Engineering at University at Buffalo, the State University of New York. The earthquake simulator is capable of the nominal performances listed in Table 4-1. The performance data is based on the continuous uniaxial sinusoidal motion of the earthquake simulator with a 20 *mton* (44 *kips*) rigid specimen installed on it. Performance levels are reduced with payloads larger than this nominal value. Figure 4-1 shows photographs of the earthquake simulator with and without its extension. The plan dimensions of the earthquake simulator extension, a welded steel truss with the approximate mass of 9.8 *mton* (22 *kips*), are shown in Figure 4-2. More details on the earthquake simulator characteristics can be found at http://nees.buffalo.edu/Facilities/Major_Equipment/.

Table 4-1 Nominal Performances of Six-Degree-of-Freedom Earthquake Simulator

Earthquake Simulator Size without Extension Platform	3.6 *m* x 3.6 *m* (12 *ft* x 12 *ft*)		
Earthquake Simulator Size with Extension Platform in Place	7.0 *m* x 7.0 *m* (23 *ft* x 23 *ft*)		
Maximum Specimen Mass without Extension Platform	50 *mton* maximum / 20 *mton* nominal (110 *kips* maximum / 44 *kips* nominal)		
Maximum Specimen Mass with Extension Platform in Place	40 *mton* maximum (88 *kips* maximum)		
Maximum Overturning Moment	46 *ton-m* (333 *kip-ft*)		
Maximum off-Center Loading Moment	15 *ton-m* (108 *kip-ft*)		
Frequency of Operation	0.1~50 *Hz* nominal / 100 *Hz* maximum		
Nominal Performance	X axis	Y axis	Z axis
Stroke	± 0.15 *m* (± 6 *in.*)	± 0.15 *m* (± 6 *in.*)	± 0.075 *m* (± 3 *in.*)
Velocity	1250 *mm/sec* (49.2 *in./sec*)	1250 *mm/sec* (49.2 *in./sec*)	500 *mm/sec* (19.7 *in./sec*)
Acceleration (with 20 *mton* Specimen)	$\pm 1.15 g$	$\pm 1.15 g$	$\pm 1.15 g$[1]

1. g is the acceleration due to gravity

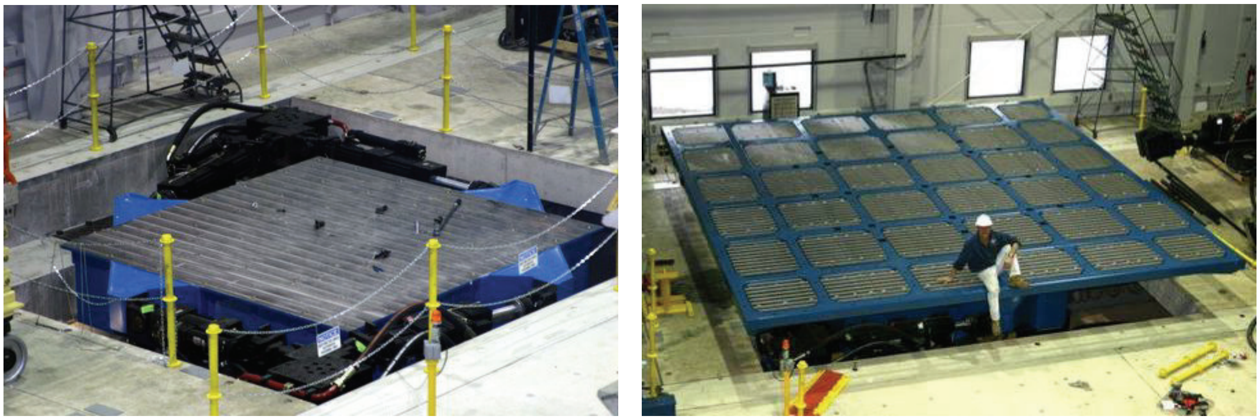

(a) without Table Extension (b) with Table Extension

Figure 4-1 Six-Degree-of-Freedom Earthquake Simulator

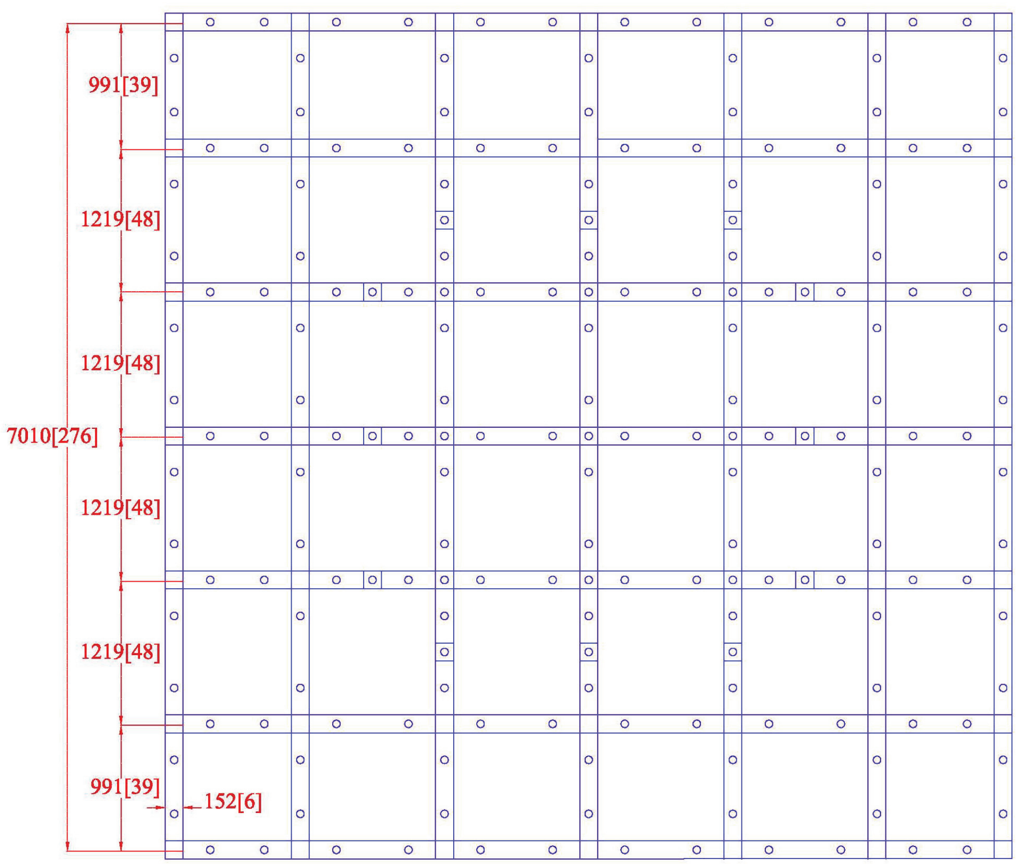

Figure 4-2 Plan Dimension of Earthquake Simulator Extension (units: mm[in])

4.2 Instrumentation

Measurements of the triaxial acceleration and displacement responses of the test specimen, and the dynamic forces induced into the I/R systems are required to evaluate the seismic performance of the I/R systems. The following sections describe the instrumentations used for the two phases of experiment conducted in this study: Phase I with the test specimen mounted on six I/R systems, and Phase II with the rigidly mounted test specimen.

4.2.1 Phase I: Isolated Test Specimen

A total of 79 accelerometers, 14 Light Emitting Diodes (LEDs) detected by a coordinate measurement machine, and 6 load cells were used to measure the triaxial acceleration and displacement responses of the test specimen, and the dynamic forces introduced into the I/R systems. To measure the potential deformation of the test specimen housing during the experiments, eight string displacement transducers were installed along diagonals of four faces of the test specimen. All the accelerometers, displacement transducers, and load cell signals were sampled at 256 *Hz*. The triaxial displacement responses at the LED locations were detected by the coordinate measurement machine at 125 *Hz.* An anti-aliasing filter with a corner frequency of 50 *Hz* was applied to all of the channels during the data acquisition.

The top of the motor inside the fan module was the closest location to the center of mass of the test specimen to which a set of triaxial accelerometers could be attached. Therefore, a set of triaxial accelerometers were installed on top of the motor. The acceleration responses at the support locations were measured by seven accelerometers installed on top level of each I/R system: two accelerometers in each of the transverse and longitudinal direction and three accelerometers in the vertical direction. Six accelerometers attached to the west face and four accelerometers attached to the north face of the test specimen measured the acceleration response of the test specimen housing in the transverse and longitudinal direction, respectively. The earthquake simulator performance was verified by comparison of the desired motion inputted to the earthquake simulator and the motion achieved at the bottom level of the I/R systems. For this purpose, arrays of three orthogonal accelerometers were installed at the center of the earthquake simulator, at the center of the extension platform, and on top level of each load cell (bottom level of the I/R systems). Table 4-2 lists information about the location and direction of the 79 accelerometers used for Phase I of the experiments. Figures 4-3 through 4-6, associated with Table 4-2, show locations of the accelerometers.

The dynamic forces induced in the I/R systems (particularly the axial and shear forces) were measured by the load cells installed under each of the six I/R systems. Each load cell could measure five different force components: the normal (vertical) force, horizontal shear forces in the two orthogonal directions (transverse and longitudinal), and moments around the transverse and longitudinal axes. The capacity of each load cell is 178 *kN* (40 *kips*) for pure axial force, 4.5 *kN-m* (40 *kips-in.*) for pure moment, and 22.5 *kN* (5 *kips*) for pure shear force. Information about the location and direction of the load cell channels are listed in Table 4-3 and are shown in Figure 4-7.

A coordinate measurement machine recorded the triaxial displacement response at nine points on the south face of the test specimen, four points on the bottom level of I/R systems #1 and #2, and one point on the earthquake simulator extension. The eight string displacement transducers were installed along diagonals of the west, north, east, and top faces of the test specimen. Figures 4-8 to 4-10, associated with Table 4-4, show the location of the LEDs and displacement transducers.

Table 4-2 Instrumentation List, Accelerometers, Phase I: Isolated Test Specimen

Channel #	Quantity	Type	Symbol	Direction	Location
1-3	3	Accelerometer	—	Triaxial	Center of Earthquake Simulator
4-6	3	Accelerometer	—	Triaxial	Center of Earthquake Simulator Extension
7-9	3	Accelerometer	—	Triaxial	Top of Motor inside AHU
10	1	Accelerometer	▶ (red)	Transverse	Top of Load Cell No.1 (South East Corner)
11	1	Accelerometer	▶	Longitudinal	
12	1	Accelerometer	◉	Vertical	
13	1	Accelerometer	▶ (red)	Transverse	Top of Load Cell No.2 (South West Corner)
14	1	Accelerometer	▶	Longitudinal	
15	1	Accelerometer	◉	Vertical	
16	1	Accelerometer	▶ (red)	Transverse	Top of Load Cell No.3 (Mid West Support)
17	1	Accelerometer	▶	Longitudinal	
18	1	Accelerometer	◉	Vertical	
19	1	Accelerometer	▶ (red)	Transverse	Top of Load Cell No.4 (North West Corner)
20	1	Accelerometer	▶	Longitudinal	
21	1	Accelerometer	◉	Vertical	
22	1	Accelerometer	▶ (red)	Transverse	Top of Load Cell No.5 (North East Corner)
23	1	Accelerometer	▶	Longitudinal	
24	1	Accelerometer	◉	Vertical	
25	1	Accelerometer	▶ (red)	Transverse	Top of Load Cell No.6 (Mid East Support)
26	1	Accelerometer	▶	Longitudinal	
27	1	Accelerometer	◉	Vertical	
28-29	2	Accelerometer	▶ (red)	Transverse	Top of I/R System No.1 (South East Corner)
30-31	2	Accelerometer	▶	Longitudinal	
32-34	3	Accelerometer	◉	Vertical	
35-36	2	Accelerometer	▶ (red)	Transverse	Top of I/R System No.2 (South West Corner)
37-38	2	Accelerometer	▶	Longitudinal	
39-41	3	Accelerometer	◉	Vertical	

Table 4-2 (cont'd) Instrumentation List, Accelerometers, Phase I: Isolated Test Specimen

Channel #	Quantity	Type	Symbol	Direction	Location
42-43	2	Accelerometer	▶ (red)	Transverse	Top of I/R System No.3 (Mid West Support)
44-45	2	Accelerometer	▶	Longitudinal	
46-48	3	Accelerometer	⦿	Vertical	
49-50	2	Accelerometer	▶ (red)	Transverse	Top of I/R System No.4 (North East Corner)
51-52	2	Accelerometer	▶	Longitudinal	
53-55	3	Accelerometer	⦿	Vertical	
56-57	2	Accelerometer	▶ (red)	Transverse	Top of I/R System No.5 (North West Corner)
58-59	2	Accelerometer	▶	Longitudinal	
60-62	3	Accelerometer	⦿	Vertical	
63-64	2	Accelerometer	▶ (red)	Transverse	Top of I/R System No.6 (Mid East Point)
65-66	2	Accelerometer	▶	Longitudinal	
67-69	3	Accelerometer	⦿	Vertical	
70-75	6	Accelerometer	▶ (red)	Transverse	AHU West Face
76-79	4	Accelerometer	▶	Longitudinal	AHU North Face

Figure 4-3 Triaxial Accelerometers Installed Close to Center of Mass of Test Specimen, Top of Motor inside Fan Module

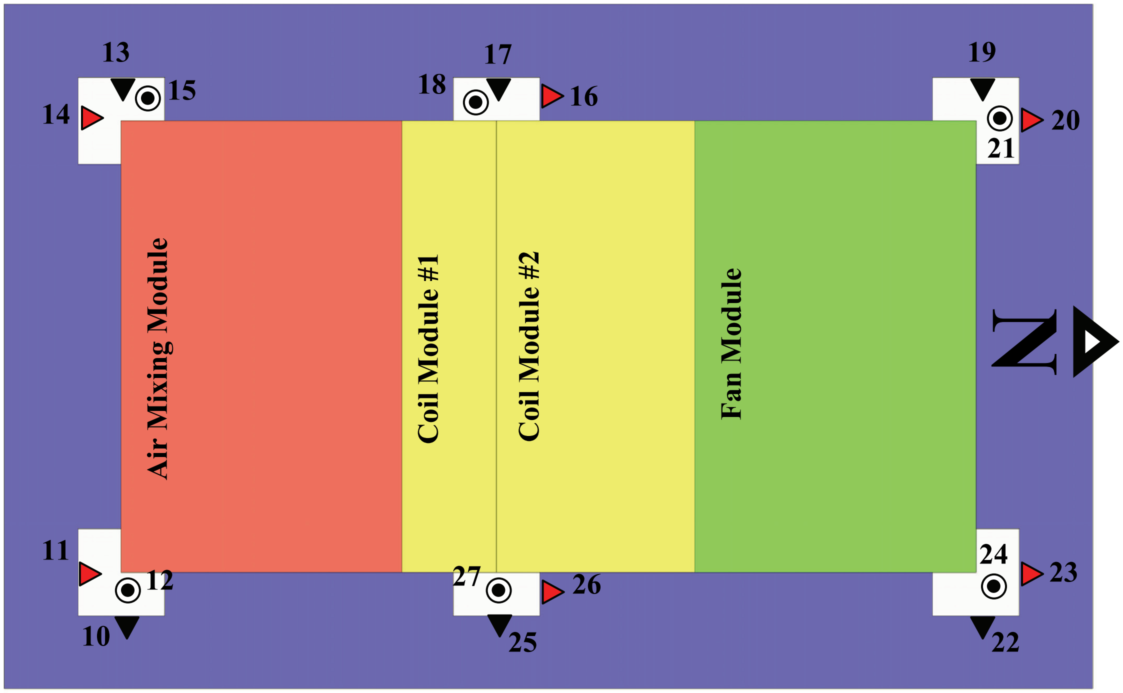

Figure 4-4 Arrangement of Accelerometers at Top Level of Load Cells, Channels #10 to #27

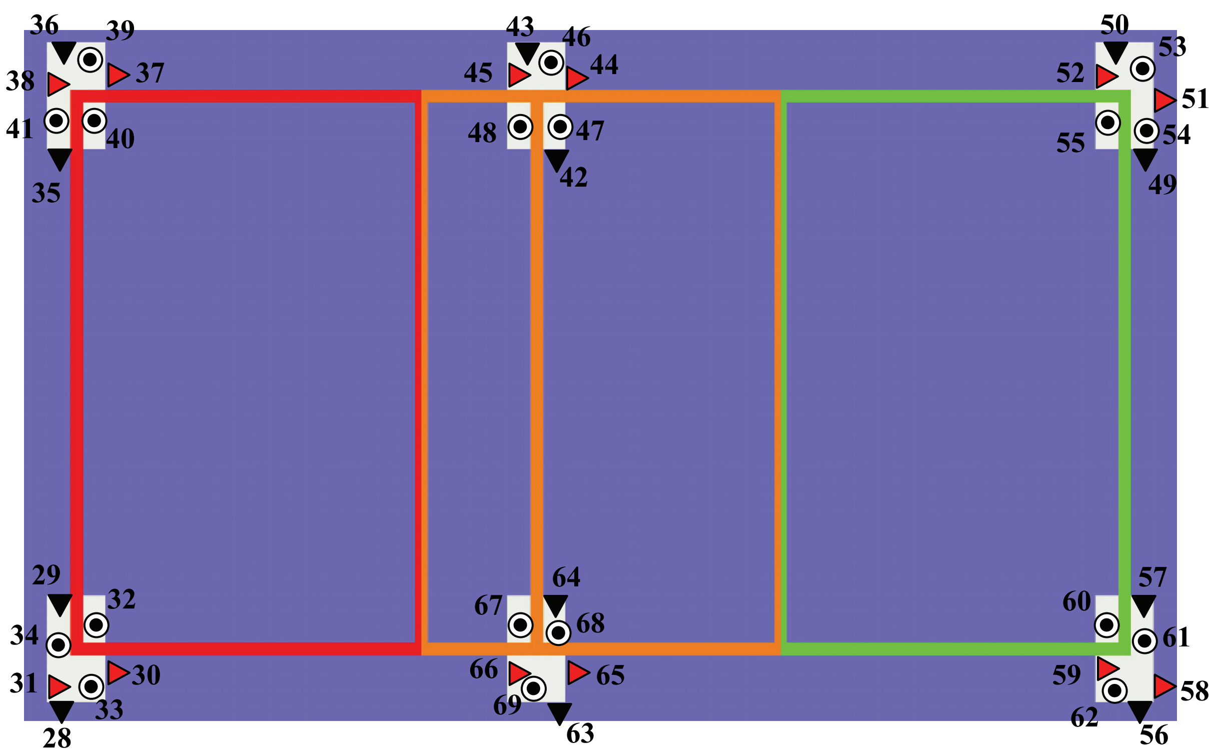

Figure 4-5 Arrangement of Accelerometers at Top Level of I/R Systems, Channels #28 to #69

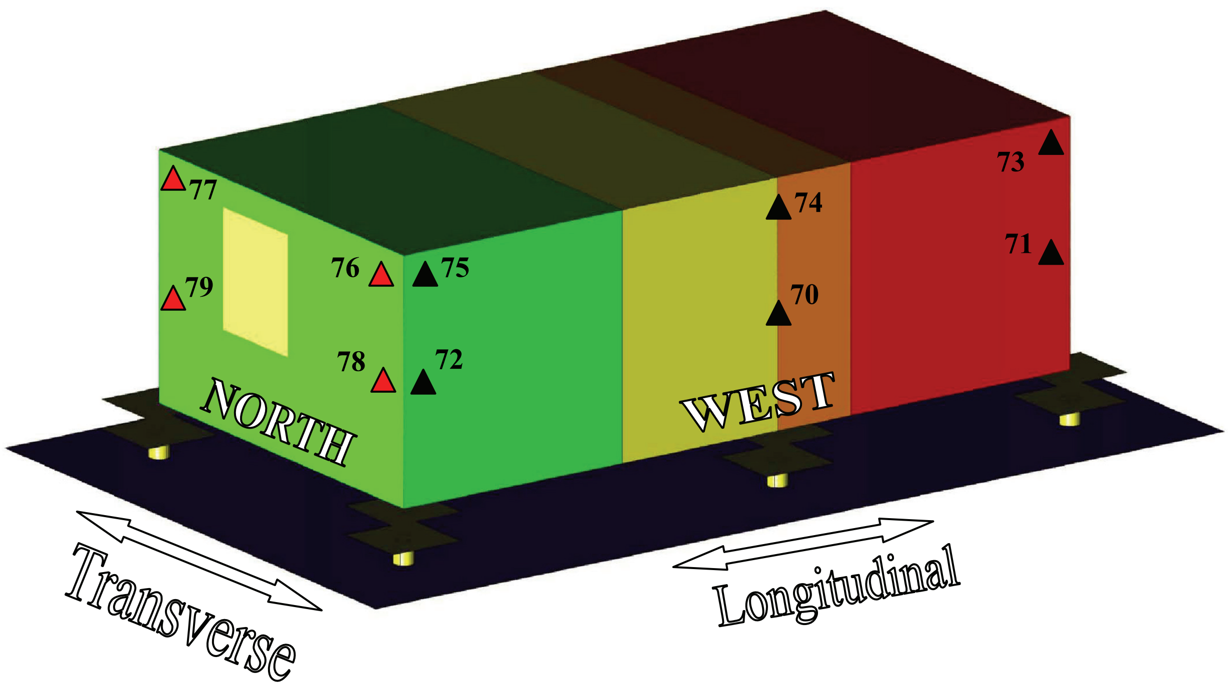

Figure 4-6 Arrangement of Accelerometers on Test Specimen Housing, Channels #70 to #79, Phase I: Isolated Test Specimen

Table 4-3 Instrumentation List, Load Cells, Phase I: Isolated Test Specimen

Channel #	Qty.	Type	Symbol	Direction	Location
80	1	Load Cell	☆	Transverse Shear	South East Corner (Load Cell No.1)
81	1	Load Cell		Longitudinal Shear	
82	1	Load Cell		Normal Force	
83	1	Load Cell		Moment around Transverse Axis	
84	1	Load Cell		Moment around Longitudinal Axis	
85	1	Load Cell	☆	Transverse Shear	South West Corner (Load Cell No.2)
86	1	Load Cell		Longitudinal Shear	
87	1	Load Cell		Normal Force	
88	1	Load Cell		Moment around Transverse Axis	
89	1	Load Cell		Moment around Longitudinal Axis	
90	1	Load Cell	☆	Transverse Shear	Mid West Support (Load Cell No.3)
91	1	Load Cell		Longitudinal Shear	
92	1	Load Cell		Normal Force	
93	1	Load Cell		Moment around Transverse Axis	
94	1	Load Cell		Moment around Longitudinal Axis	
95	1	Load Cell	☆	Transverse Shear	North West Corner (Load Cell No.4)
96	1	Load Cell		Longitudinal Shear	
97	1	Load Cell		Normal Force	
98	1	Load Cell		Moment around Transverse Axis	
99	1	Load Cell		Moment around Longitudinal Axis	
100	1	Load Cell	☆	Transverse Shear	North East Corner (Load Cell No.5)
101	1	Load Cell		Longitudinal Shear	
102	1	Load Cell		Normal Force	
103	1	Load Cell		Moment around Transverse Axis	
104	1	Load Cell		Moment around Longitudinal Axis	
105	1	Load Cell	☆	Transverse Shear	Mid East Support (Load Cell No.6)
106	1	Load Cell		Longitudinal Shear	
107	1	Load Cell		Normal Force	
108	1	Load Cell		Moment around Transverse Axis	
109	1	Load Cell		Moment around Longitudinal Axis	

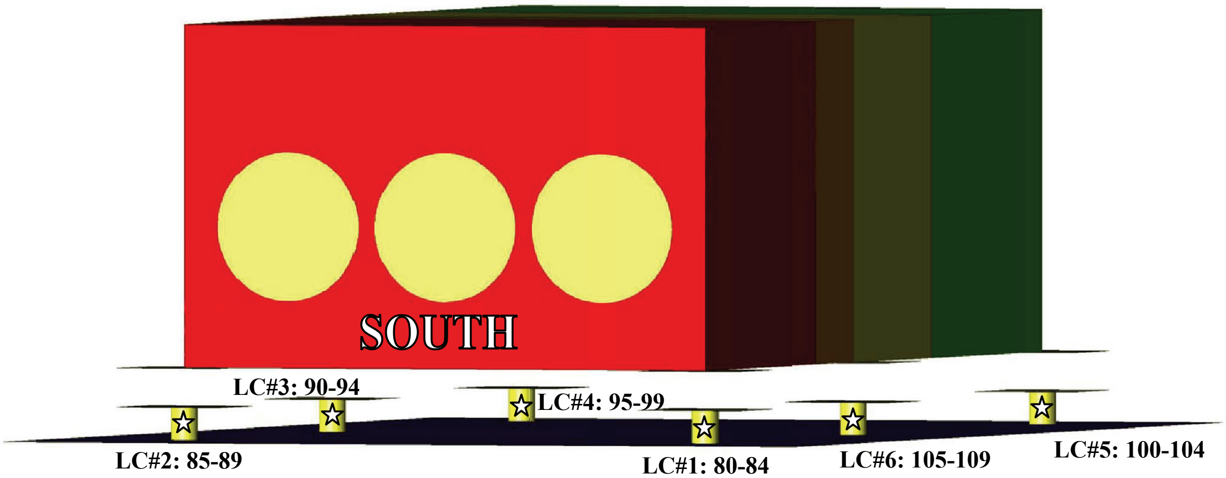

Figure 4-7 Arrangement of Six Load Cells under Test Specimen, Channels #80 to #109, Phase I: Isolated Test Specimen

Table 4-4 Instrumentation List, Coordinate Measurement Machine LEDs, and Displacement Transducers, Phase I: Isolated Test Specimen

Channel #	Qty.	Type	Symbol	Direction	Location
110-111	2	Displacement Transducer		Diagonal	AHU Top Surface
112-113	2	Displacement Transducer		Diagonal	AHU West Face
114-115	2	Displacement Transducer		Diagonal	AHU North Face
116-117	2	Displacement Transducer		Diagonal	AHU East Face
118-126	9	KRYPTON LED		Triaxial	AHU South Face
127-128	2	KRYPTON LED		Triaxial	Top of Load Cell No.1
129-130	2	KRYPTON LED		Triaxial	Top of Load Cell No.2
131	1	KRYPTON LED		Triaxial	Extension South Edge

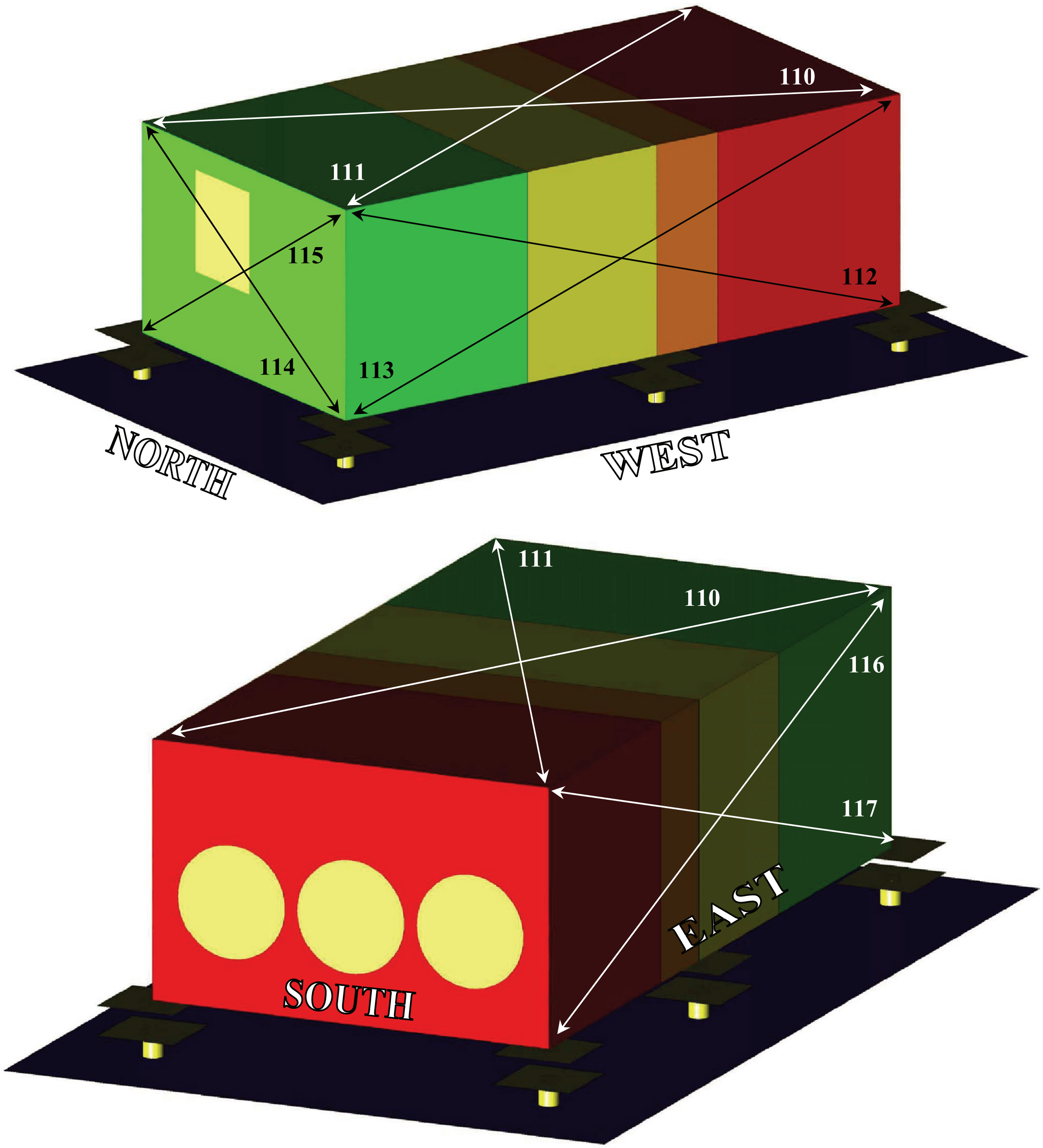

Figure 4-8 Arrangement of Displacement Transducers on Test Specimen Housing, Channels #110 to #117, Phase I: Isolated Test Specimen

Figure 4-9 Displacement Transducers on West Face of Test Specimen, Channel#113, Phase I: Isolated Test Specimen

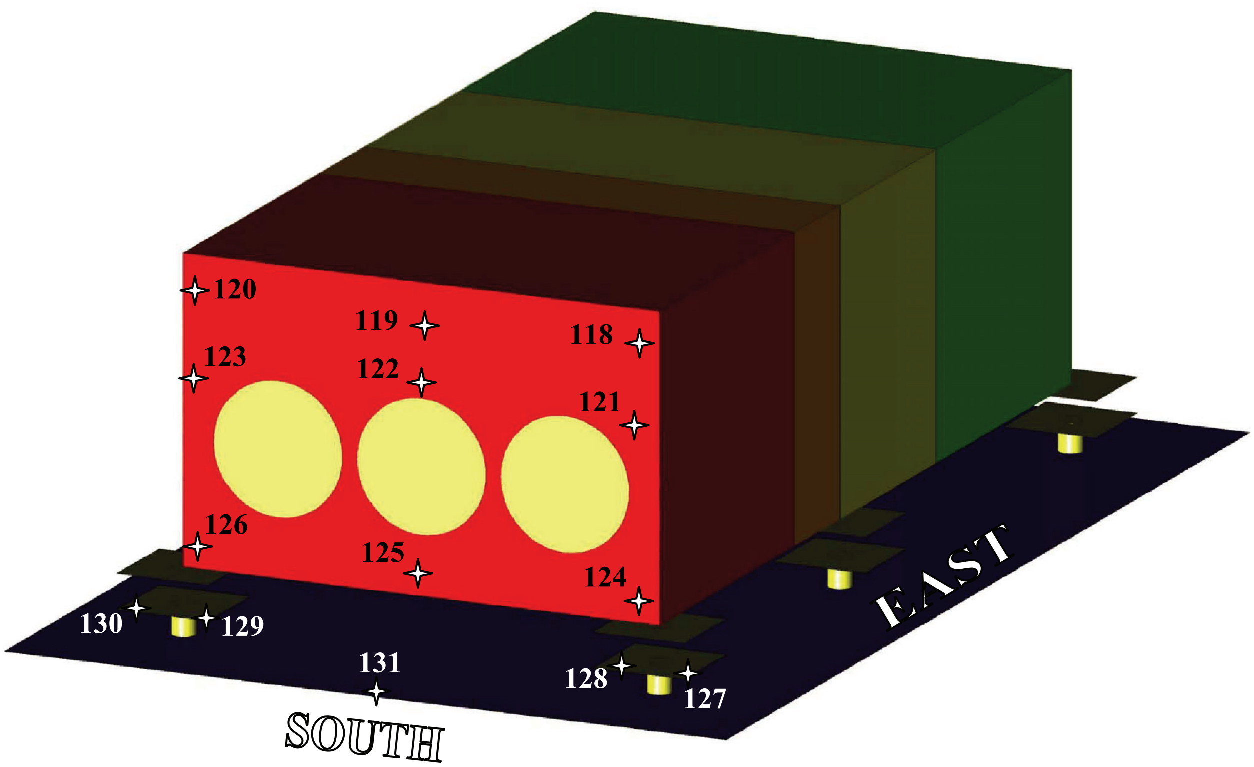

Figure 4-10 Arrangement of KRYPTON LEDs on Test Specimen Housing, on Top Level of Load Cells, and on Earthquake Simulator Extension, Channels #118 to #131, Phase I: Isolated Test Specimen

4.2.2 Phase II: Rigidly Mounted Test Specimen

The instrumentation plan of the Phase II of the experiments (rigidly mounted test specimen) was similar to that of the Phase I but without the instrumentation on the top level of the I/R systems and with 16 additional accelerometers attached to the test specimen housing. The instrumentations used for Phase II of the experiments are listed in Tables 4-5 through 4-7. Figures 4-11 through 4-15 show the locations of the instrumentation for this phase of the experiments.

Table 4-5 Instrumentation List, Accelerometers, Phase II: Rigidly Mounted Test Specimen

Channel #	Quantity	Type	Symbol	Direction	Location
1-3	3	Accelerometer	—	Triaxial	Center of Earthquake Simulator
4-6	3	Accelerometer	—	Triaxial	Center of Earthquake Simulator Extension
7-9	3	Accelerometer	—	Triaxial	AHU Center of Gravity
10	1	Accelerometer	▶	Transverse	
11	1	Accelerometer	▶	Longitudinal	Top of Load Cell No.1 (South East Corner)
12	1	Accelerometer	◉	Vertical	
13	1	Accelerometer	▶	Transverse	
14	1	Accelerometer	▶	Longitudinal	Top of Load Cell No.2 (South West Corner)
15	1	Accelerometer	◉	Vertical	
16	1	Accelerometer	▶	Transverse	
17	1	Accelerometer	▶	Longitudinal	Top of Load Cell No.3 (Mid West Support)
18	1	Accelerometer	◉	Vertical	
19	1	Accelerometer	▶	Transverse	
20	1	Accelerometer	▶	Longitudinal	Top of Load Cell No.4 (North West Corner)
21	1	Accelerometer	◉	Vertical	
22	1	Accelerometer	▶	Transverse	
23	1	Accelerometer	▶	Longitudinal	Top of Load Cell No.5 (North East Corner)
24	1	Accelerometer	◉	Vertical	
25	1	Accelerometer	▶	Transverse	
26	1	Accelerometer	▶	Longitudinal	Top of Load Cell No.6 (Mid East Support)
27	1	Accelerometer	◉	Vertical	
28-33	6	Accelerometer	▶	Transverse	AHU West Face
34-37	4	Accelerometer	▶	Longitudinal	AHU North Face
38-43	6	Accelerometer	▶	Transverse	AHU East Face
44-47	4	Accelerometer	▶	Longitudinal	AHU South Face
48-53	6	Accelerometer	◉	Vertical	AHU Top Surface

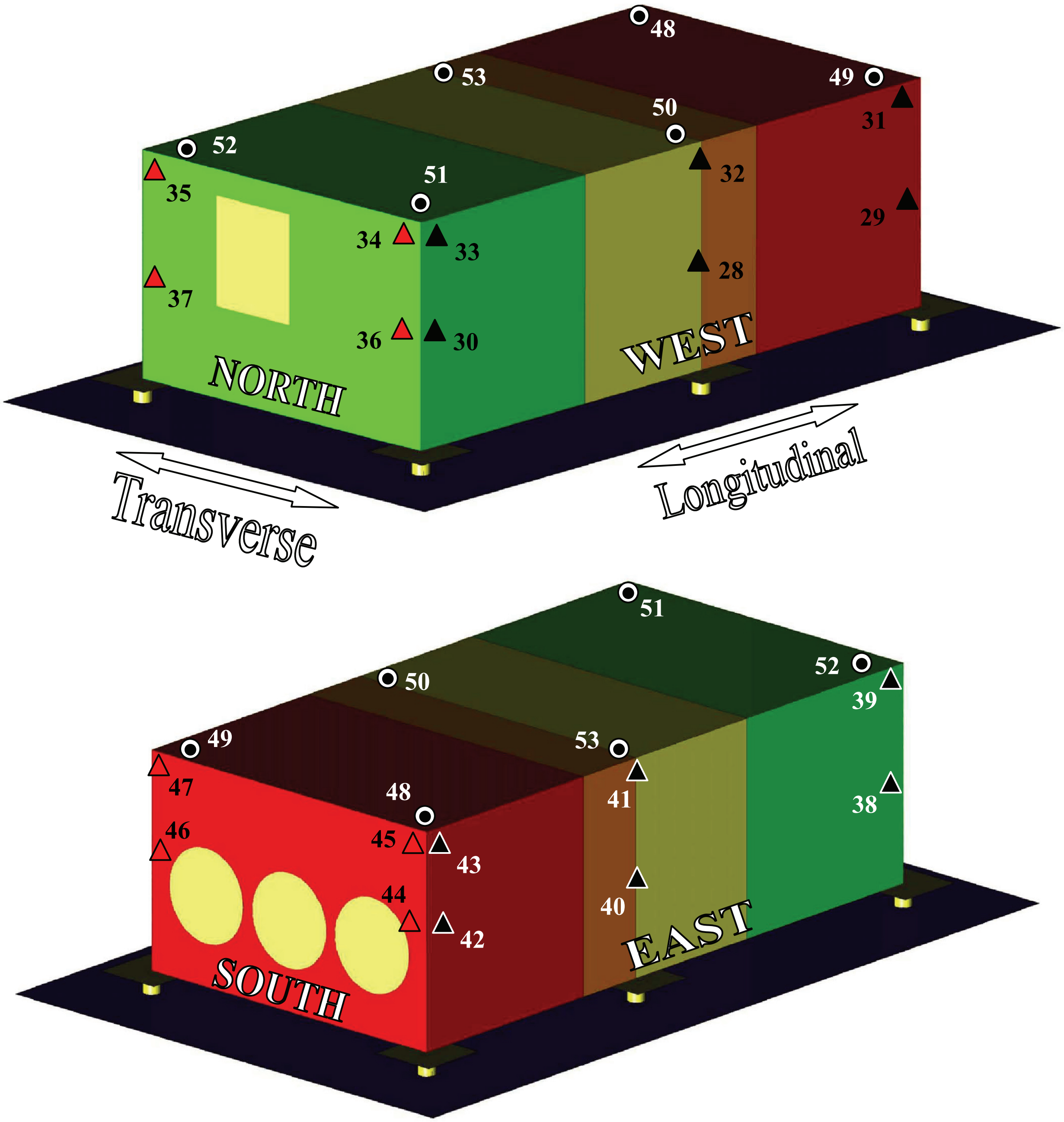

Figure 4-11 Arrangement of Accelerometers on Test Specimen Housing, Channels #28 to #53, Phase II: Rigidly Mounted Test Specimen

Table 4-6 Instrumentation List, Load Cells, Phase II: Rigidly Mounted Test Specimen

Channel #	Qty.	Type	Symbol	Direction	Location
54	1	Load Cell	☆	Transverse Shear	South East Corner (Load Cell No.1)
55	1	Load Cell		Longitudinal Shear	
56	1	Load Cell		Normal Force	
57	1	Load Cell		Moment around Transverse Axis	
58	1	Load Cell		Moment around Longitudinal Axis	
59	1	Load Cell	☆	Transverse Shear	South West Corner (Load Cell No.2)
60	1	Load Cell		Longitudinal Shear	
61	1	Load Cell		Normal Force	
62	1	Load Cell		Moment around Transverse Axis	
63	1	Load Cell		Moment around Longitudinal Axis	
64	1	Load Cell	☆	Transverse Shear	Mid West Support (Load Cell No.3)
65	1	Load Cell		Longitudinal Shear	
66	1	Load Cell		Normal Force	
67	1	Load Cell		Moment around Transverse Axis	
68	1	Load Cell		Moment around Longitudinal Axis	
69	1	Load Cell	☆	Transverse Shear	North West Corner (Load Cell No.4)
70	1	Load Cell		Longitudinal Shear	
71	1	Load Cell		Normal Force	
72	1	Load Cell		Moment around Transverse Axis	
73	1	Load Cell		Moment around Longitudinal Axis	
74	1	Load Cell	☆	Transverse Shear	North East Corner (Load Cell No.5)
75	1	Load Cell		Longitudinal Shear	
76	1	Load Cell		Normal Force	
77	1	Load Cell		Moment around Transverse Axis	
78	1	Load Cell		Moment around Longitudinal Axis	
79	1	Load Cell	☆	Transverse Shear	Mid East Support (Load Cell No.6)
80	1	Load Cell		Longitudinal Shear	
81	1	Load Cell		Normal Force	
82	1	Load Cell		Moment around Transverse Axis	
83	1	Load Cell		Moment around Longitudinal Axis	

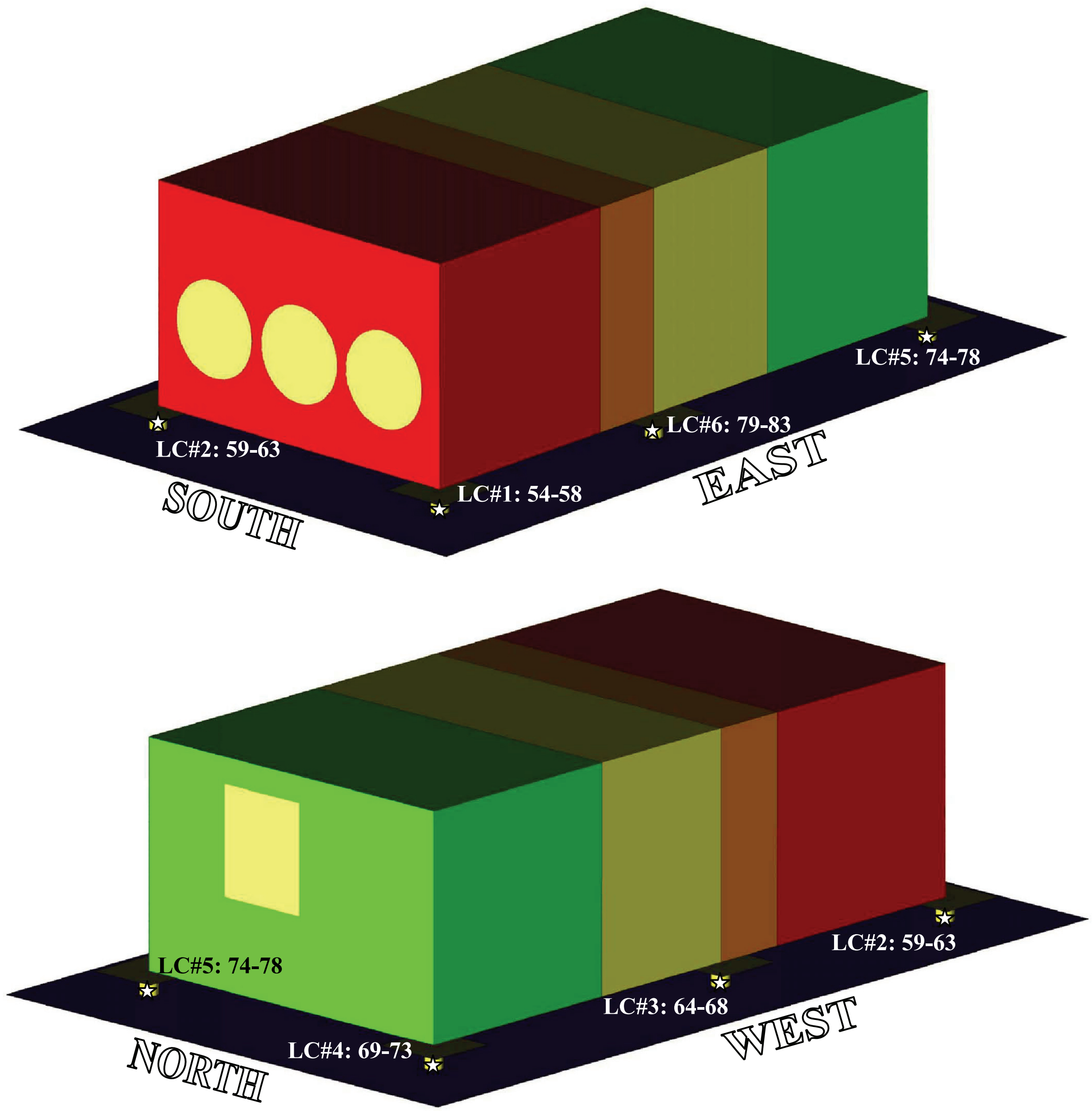

Figure 4-12 Arrangement of Six Load Cells under Test Specimen, Channels #54 to #83, Phase II: Rigidly Mounted Test Specimen

Table 4-7 Instrumentation List, Coordinate Measurement Machine LEDs and Displacement Transducers, Rigidly Mounted Test Specimen, Phase II: Rigidly Mounted Test Specimen

Channel #	Qty.	Type	Symbol	Direction	Location
84-85	2	Displacement Transducer		Diagonal	AHU Top Surface
86-87	2	Displacement Transducer		Diagonal	AHU West Face
88-89	2	Displacement Transducer		Diagonal	AHU North Face
90-91	2	Displacement Transducer		Diagonal	AHU East Face
92-100	9	KRYPTON LED		Triaxial	AHU South Face
101-102	2	KRYPTON LED		Triaxial	Top of Load Cell No.1
103-104	2	KRYPTON LED		Triaxial	Top of Load Cell No.2
105	1	KRYPTON LED		Triaxial	Table Extension South Edge

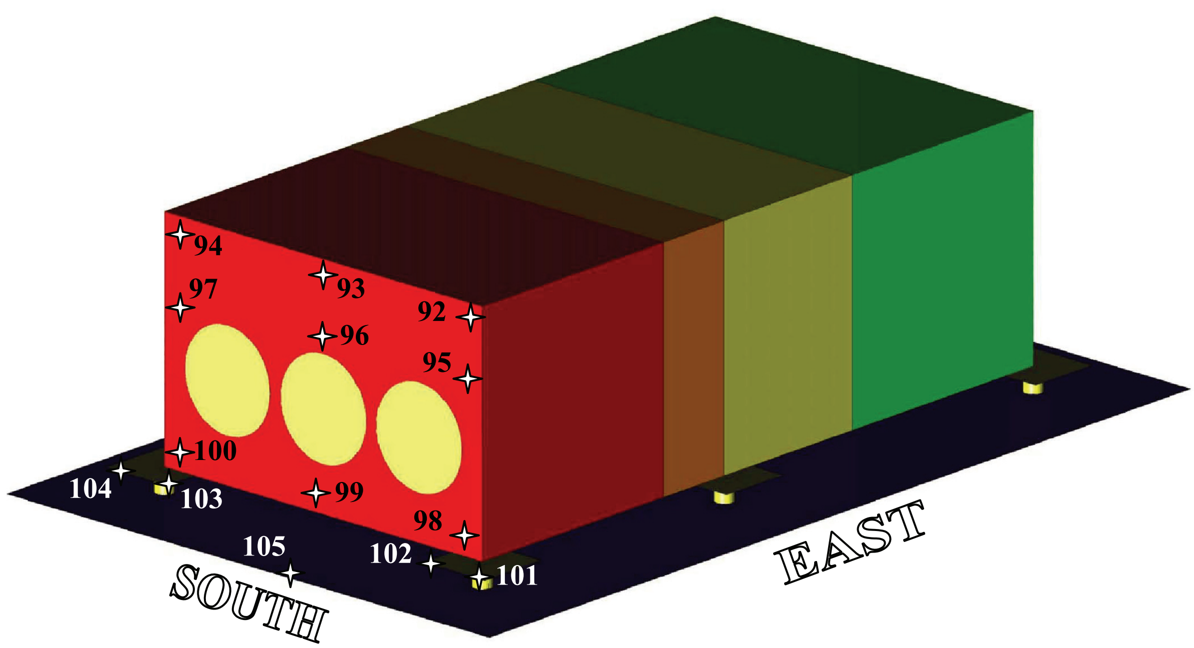

Figure 4-13 Arrangement of KRYPTON LEDs on Test Specimen Housing, on Top Level of Load Cells, and on Earthquake Simulator Extension, Channels #92 to #105, Phase II: Rigidly Mounted Test Specimen

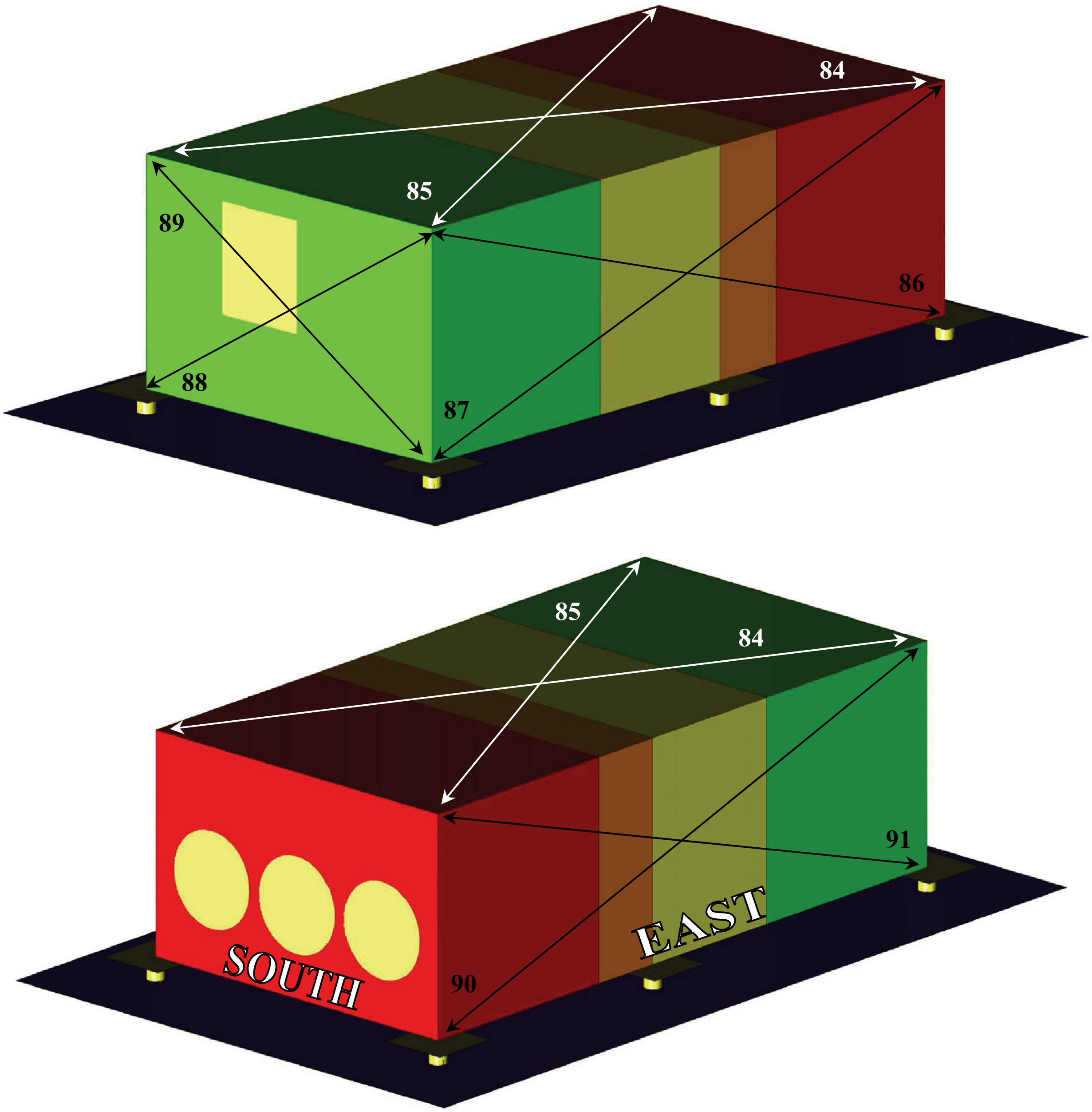

Figure 4-14 Arrangement of Displacement Transducers on Test Specimen Housing, Channels #84 to #91, Phase II: Rigidly Mounted Test Specimen

SECTION 5

EARTHQUAKE SIMULATOR TESTS

The experimental study presented in this report included two phases of earthquake simulator testing. In Phase I, the test specimen was mounted on six of the I/R systems. The test plan of Phase I included triaxial seismic tests with different input motion amplitudes, and incorporated different configuration properties of the restraint components of the I/R systems. Pulse tests were also conducted for the system identification of the test specimen supported by the isolation components of the I/R systems.

In Phase II of the experiments, the test specimen was rigidly mounted on the earthquake simulator. The test plan of Phase II included unidirectional white noise tests and triaxial seismic tests with different amplitudes. The following sections describe the input motion used for the three types of earthquake simulator tests, the test plan, and test setup procedure.

5.1 Earthquake Simulator Input Motions

5.1.1 Seismic Tests

A set of triaxial input motion was generated for the seismic tests to match the Required Response Spectrum (RRS) of the AC156 testing protocol (ICC-ES, 2004). The generated input motion was intended to represent the roof motion of a building structure located on a site class D in an area of high seismicity. Figure 5-1 shows the parametric 5%-damped horizontal and vertical RRS specified by the AC156 testing protocol.

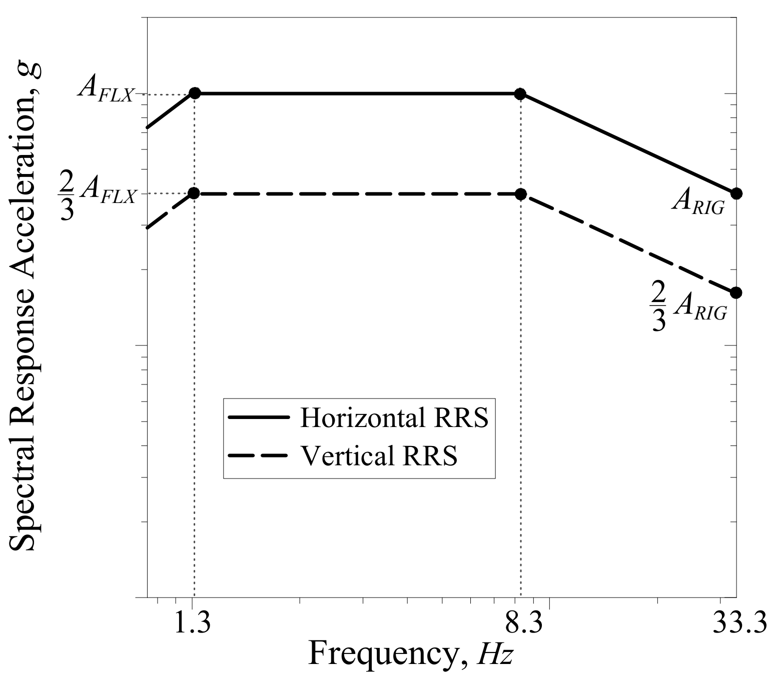

Figure 5-1 AC156 5%-Damped Horizontal and Vertical Required Response Spectra (RRS)

For all frequencies, the amplitude of the vertical RRS is two third of the amplitude of the horizontal RSS. According to the AC156 testing protocol, the horizontal spectral acceleration for a piece of flexible equipment (A_{FLX}) and for a piece of rigid equipment (A_{RIG}) are calculated as:

$$A_{FLX} = S_{DS}\left(1+2\frac{z}{h}\right) \le 1.6S_{DS} \tag{5-1}$$

$$A_{RIG} = 0.4S_{DS}\left(1+2\frac{z}{h}\right) \tag{5-2}$$

where:

z = height of the level in the structure where the equipment is located with respect to base
h = average roof height of the structure with respect to base
S_{DS} = design 5%-damped spectral response acceleration at short period

The height ratio $\frac{z}{h}$ is equal to one for the roof level of building structures. S_{DS} was selected as 1.0 g for a site class D in an area of high seismicity (ICC, 2003). Hence, A_{FLX} and A_{RIG} were calculated as 1.6 g and 1.2 g, respectively. The triaxial acceleration histories generated to match the corresponding RRS are shown in Figure 5-2. The peak input acceleration of the generated input motion in the transverse, longitudinal, and vertical direction were 0.80 *g*, 0.79 *g*, and 0.53 *g*, respectively. The transverse and longitudinal component of the input motion was associated with the short and long direction of the test specimen, respectively. The Required Response Spectra (RRS) and the Test Response Spectra (TRS) for a full-scale test are compared in Figure 5-3. The TRS envelopes the RRS over almost the entire 1.3 to 33 *Hz* frequency range.

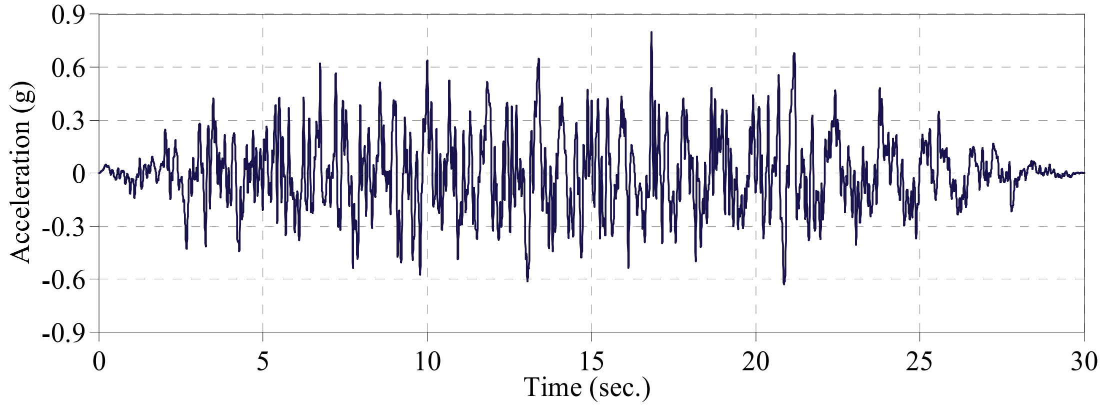

(a) Transverse Direction

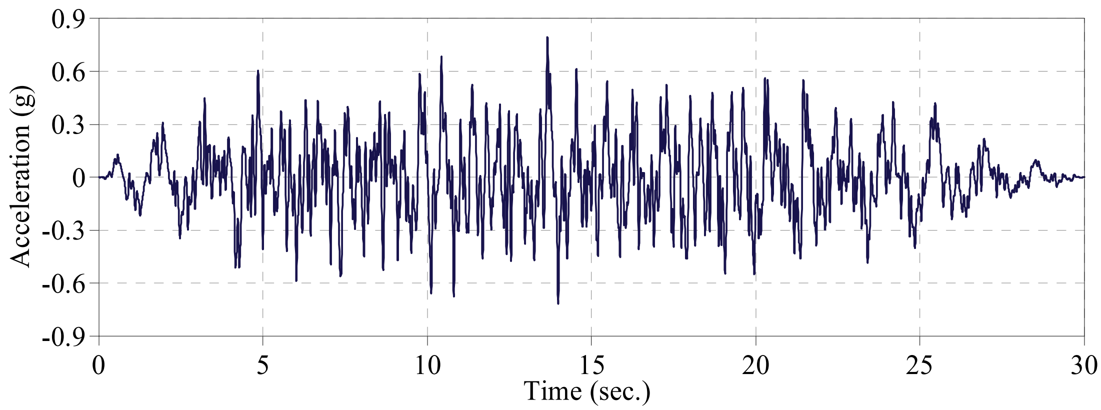

(b) Longitudinal Direction

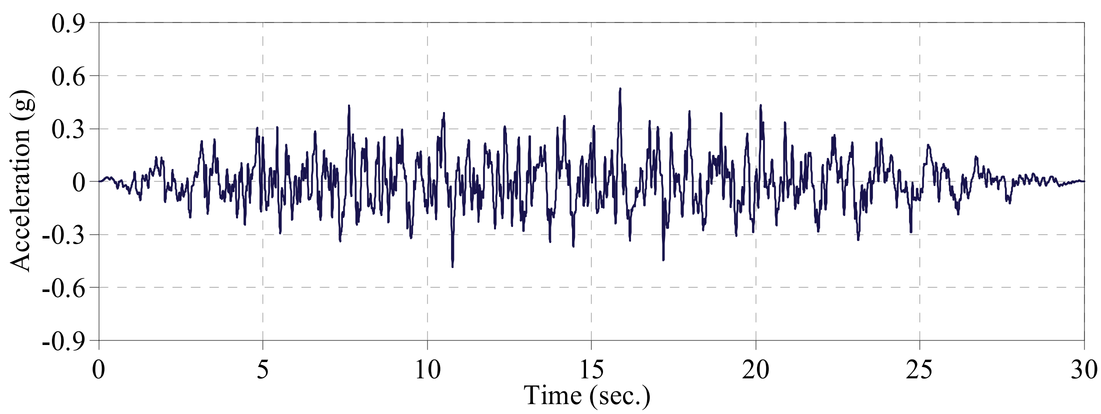

(c) Vertical Direction

Figure 5-2 Acceleration Histories of Triaxial Input Motion Generated to Match AC156 RRS, Roof Level of a Building Located on a Site Class D in an Area of High Seismicity

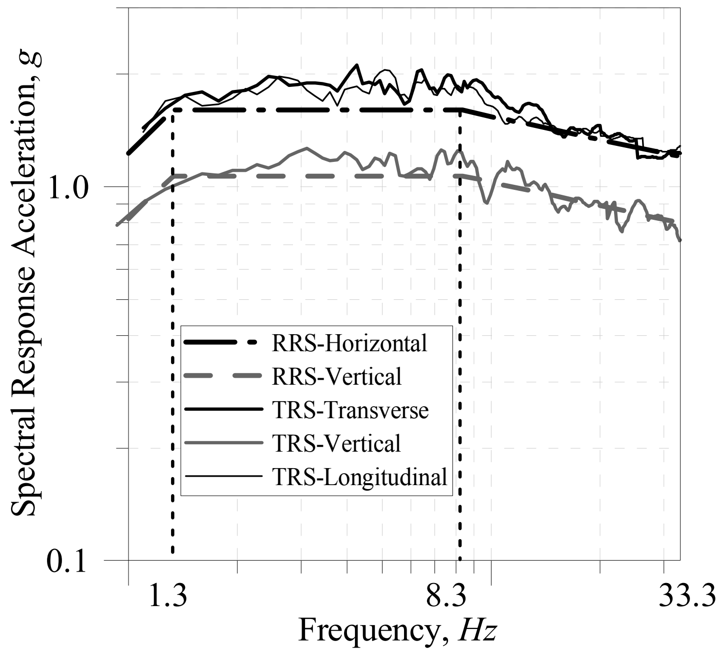

Figure 5-3 Comparison of RRS and TRS for a Full-Scale Triaxial Seismic Test

5.1.2 Pulse-Type System-Identification Tests

In Phase I of the experiments, pulse-type system-identification tests were conducted before and after each seismic test to establish and monitor changes to the natural frequencies and mode shapes of the test specimen supported by the isolation components of the I/R systems.

The input motion of the pulse tests consisted of three full-cycle sinusoidal pulses occurring in the transverse, longitudinal, and vertical direction, respectively, with a ten-second interval between each pulse. Each of the three pulses had a period of 0.1 second and an amplitude of 0.05 g. The amplitude of the pulses was calibrated to insure that the restraint components of the I/R systems would not be engaged. Equation 5-3 presents the desired input acceleration of the pulse tests. Figure 5-4 shows the portion of the acceleration history in each of the three orthogonal directions, which includes the pulse.

$$a=\begin{cases}(0.05\,sin(20\pi t))g\ ; & t_s\leq t\leq t_s+0.1\\ 0\ ; & t\leq t_s\ or\ t\geq t_s+0.1\end{cases} \tag{5-3}$$

where:

a = input (desired) acceleration
g = acceleration due to gravity
t_s = 5 sec. for the transverse direction, 15 sec. for the longitudinal direction, and 25 sec. for the vertical direction

The ten-second interval between the pulses was introduced to allow the test specimen to return to an at-rest condition (no vibration) before the application of each pulse. From the response to the pulse in each direction, natural frequencies and mode shapes of the isolated test specimen were established based on the procedure described in Section 6.1.2.

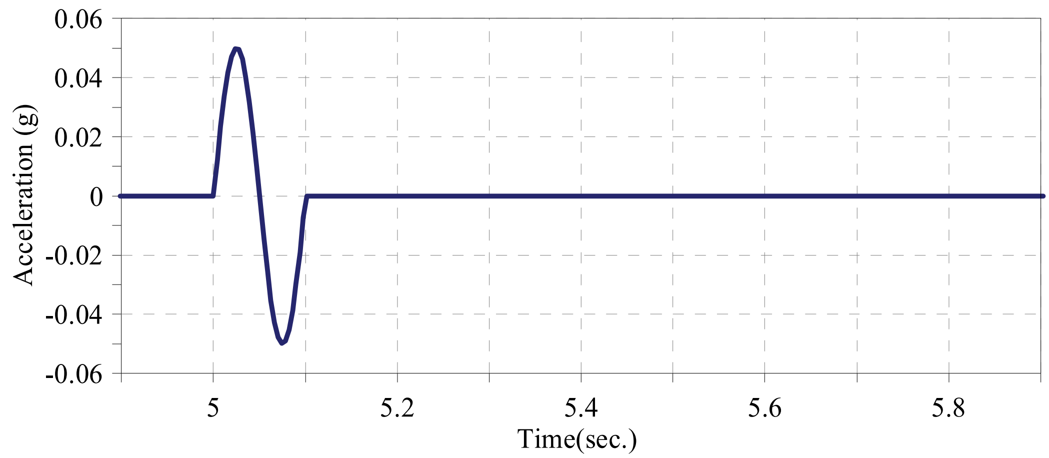

(a) Transverse Direction

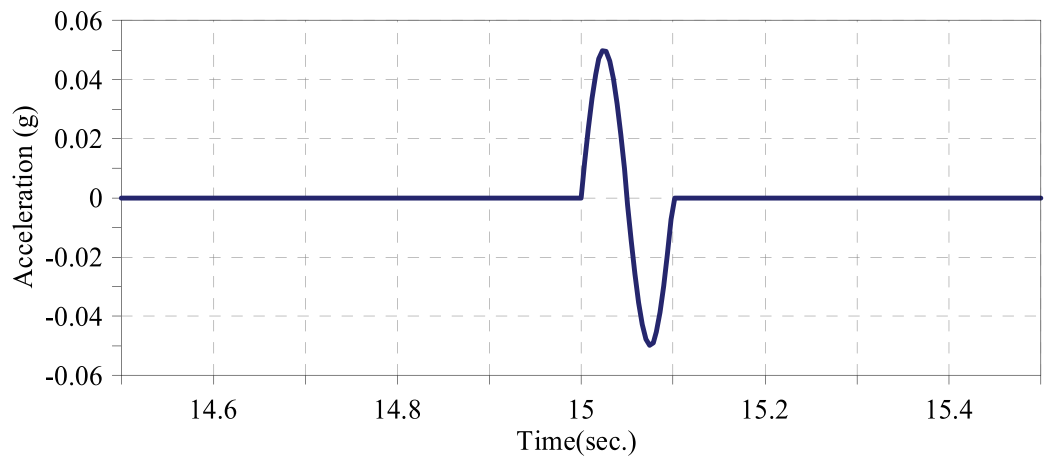

(b) Longitudinal Direction

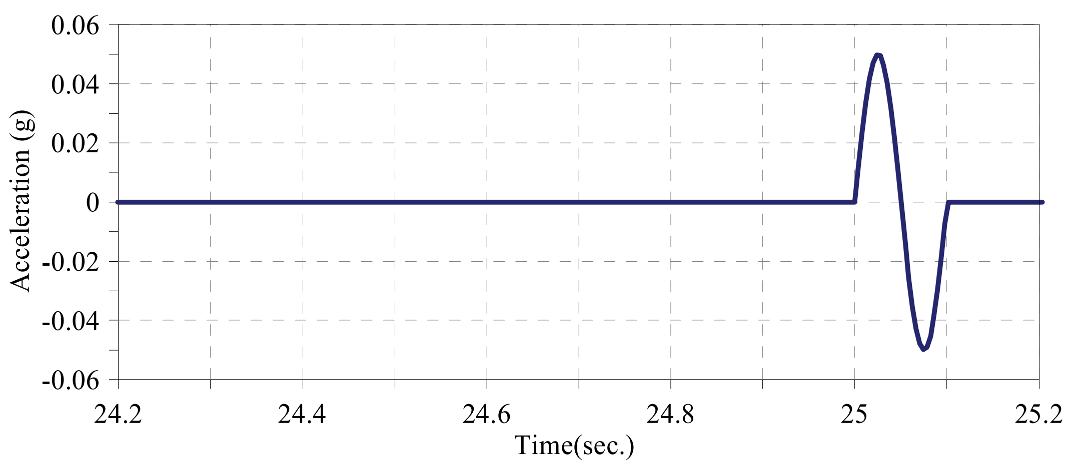

(b) Vertical Direction

Figure 5-4 Triaxial Input Acceleration for Pulse-Type System-Identification Tests

5.1.3 White Noise System-Identification Tests

Unidirectional white noise tests were conducted at the beginning and conclusion of Phase II to establish and monitor changes to dynamic properties of the rigidly mounted test specimen. The input motion of the unidirectional white noise tests was a three-minute-long, acceleration-controlled, broadband excitation extended from 0.25 to 40 *Hz*. The root mean square and peak acceleration of the input motion were 0.05 *g* and 0.20 *g*, respectively. The acceleration history of the white noise test input is shown in Figure 5-5.

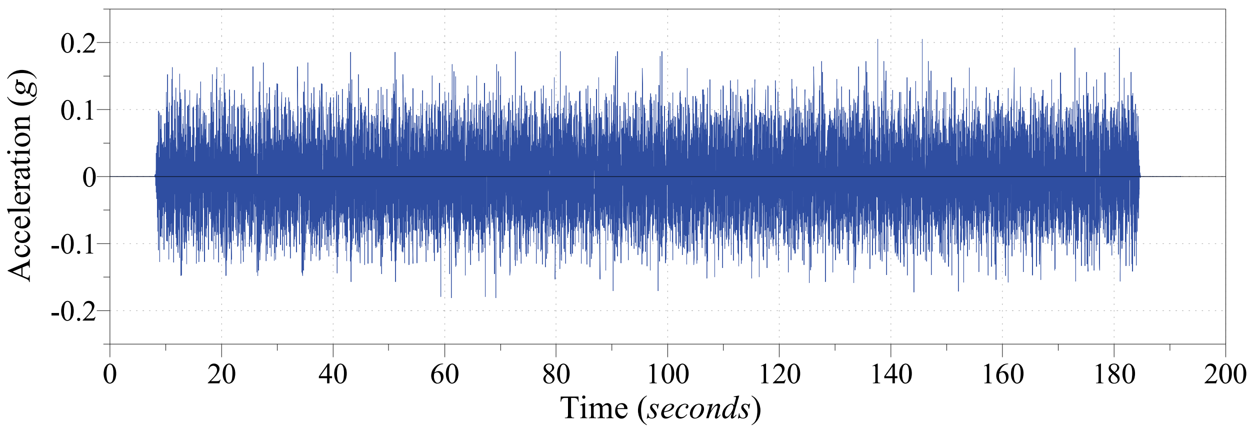

Figure 5-5 Input Acceleration History for Unidirectional White Noise Tests

5.2 Test Plan

The test plan was elaborated by the authors in collaboration with the members of the ASHRAE Technical Committee 2.7. As shown in Table 5-1, Phase I of the experiments included 11 test series. Each test series was defined by 5 configuration properties of the restraint components of the I/R systems. The test specimen mounted on the I/R systems with specified configuration properties was subjected to the triaxial input motions scaled to different amplitudes during each test series. Each seismic test of Phase I of the experiments was preceded and followed by a pulse-type system-identification test (for brevity the system-identification tests are not included in Table 5-1). Therefore, throughout the 11 test series of Phase I of the experiments, a total of 47 system-identification tests and 46 seismic tests were conducted.

Test Series 11 was conducted after the rubber tubes and washers of all the I/R systems were removed. The full-scale test of Test Series 7 was repeated after the vibration isolators supporting the motor and fan inside the fan module were activated. In addition, the full-scale test of Test Series 6 was repeated after retrofitting the connections between the base rail and modules. More details about retrofitting the test specimen housing during Test Series 6 are described in Section 6.2.2.

Phase II of the experiments, with the test specimen rigidly mounted on the earthquake simulator, started with three unidirectional white noise tests in the transverse, longitudinal, and vertical direction, respectively. The white noise tests were followed by five seismic tests with the input motion amplitude increasing from 10% to 100% of the AC156 qualification level (see Section 5.1.1). At the end of the seismic tests, the three unidirectional white noise tests were conducted once again in the same order. Then, the vibration isolators supporting the fan and motor inside the fan module of the test specimen were activated, and the experiments were concluded by conducting a pulse test and a full-scale triaxial seismic test. The sequence of the tests in Phase II of the experiments is listed in Table 5-2.

Table 5-1[*] Test Plan, Phase I: Isolated Test Specimen

Test #	Test Name	Gap, *mm (in.)*	Horizontal Snubber: Rubber Tube Thickness, *mm (in.)*	Horizontal Snubber: Rubber Tube Hardness, *Duro.*	Vertical Snubber: Rubber Washer Thickness, *mm (in.)*	Vertical Snubber: Rubber Washer Hardness, *Duro.*	Input Motion Amplitude *(%)*
1	TS1-S1	6 (0.25)	19 (0.75)	40	19 (0.75)	40	10
2	TS1-S2						25
3	TS1-S3						50
4	TS1-S4						100
5	TS2-S1	6 (0.25)	19 (0.75)	60	19 (0.75)	60	10
6	TS2-S2						25
7	TS2-S3						50
8	TS2-S4						100
9	TS3-S1	6 (0.25)	13 (0.5)	40	13 (0.5)	40	10
10	TS3-S2						25
11	TS3-S3						50
12	TS3-S4						75
13	TS3-S5						100
14	TS4-S1	6 (0.25)	13 (0.5)	60	13 (0.5)	60	10
15	TS4-S2						25
16	TS4-S3						50
17	TS4-S4						100
18	TS5-S1	13 (0.5)	6 (0.25)	40	6 (0.25)	40	10
19	TS5-S2						25
20	TS5-S3						50
21	TS5-S4						100
22	TS6-S1	13 (0.5)	6 (0.25)	60	6 (0.25)	60	10
23	TS6-S2						25
24	TS6-S3						50
25	TS6-S4						100
26	TS6-S5						100

Table 5-1 (cont'd) Test Plan, Phase I: Isolated Test Specimen

Test #	Test Name	Gap, *mm (in.)*	Horizontal Snubber: Rubber Tube		Vertical Snubber: Rubber Washer		Input Motion Amplitude *(%)*
			Thickness, *mm (in.)*	Hardness, *Duro.*	Thickness, *mm (in.)*	Hardness, *Duro.*	
27	TS7-S1	6 (0.25)	6 (0.25)	40	6 (0.25)	40	10
28	TS7-S2						25
29	TS7-S3						50
30	TS7-S4						100
31	TS7-S5						100
32	TS8-S1	6 (0.25)	6 (0.25)	60	6 (0.25)	60	10
33	TS8-S2						25
34	TS8-S3						50
35	TS8-S4						100
36	TS9-S1	6 (0.25)	3 (0.125)	40	6 (0.25)	40	10
37	TS9-S2						25
38	TS9-S3						50
39	TS9-S4						100
40	TS10-S1	6 (0.25)	3 (0.125)	60	6 (0.25)	60	10
41	TS10-S2						25
42	TS10-S3						50
43	TS10-S4						100
44	TS11-S1	10 (0.375)	—	—	—	—	10
45	TS11-S2						25
46	TS11-S3						50

*- The horizontal and vertical snubber gap sizes were nominally equal (the third column of the table)
- The test specimen housing was damaged during TS6-S4
- TS6-S5 was conducted after the test specimen housing was retrofitted by additional connection plates (see Section 6.2.2)
- TS7-S5 was conducted after the internal isolation system inside the fan module was activated
- The three seismic tests of Test Series TS11 were conducted after rubber snubbers were removed from the restraint components of the I/R systems

Table 5-2[*] Test Plan, Phase II: Rigidly Mounted Test Specimen

Test #	Test Name	Input Motion		
		Type	Direction	Amplitude (%)
1	TS12-w1x	White Noise	Transverse	100
2	TS12-w1y	White Noise	Longitudinal	100
3	TS12-w1z	White Noise	Vertical	100
4	TS12-S1	Seismic	Triaxial	10
5	TS12-S2	Seismic	Triaxial	25
6	TS12-S3	Seismic	Triaxial	50
7	TS12-S4	Seismic	Triaxial	75
8	TS12-S5	Seismic	Triaxial	100
9	TS12-w2x	White Noise	Transverse	100
10	TS12-w2y	White Noise	Longitudinal	100
11	TS12-w2z	White Noise	Vertical	100
12	TS12-P1	Pulse	Triaxial	100
13	TS12-S6	Seismic	Triaxial	100

*- TS12-S6 was conducted after the internal isolation system inside the fan module was activated

5.3 Test Setup

The test setup for Phase I of the experiments was initiated by bolting the interface steel plates to the earthquake simulator extension. Then, the load cells were bolted to the steel plates. Figure 5-6 shows the six load cells bolted to the interface plates. The I/R systems were assembled and bolted to the load cells such that the orientation of the isolation component of the I/R systems be parallel to the transverse direction of the test specimen. Finally, the test specimen was mounted on top of the I/R systems, and at each support location the top plate of the isolation and restraint component of the I/R system and the base plate of the test specimen were all tied together by four bolts. After mounting the test specimen on the I/R systems, the leveling bolts of the isolation component and the two nuts on the rods of the restraint component were adjusted to provide the required vertical gaps in the restraint component according to the test plan. Figure 5-7 shows the test specimen at the end of the test setup mounted on the I/R systems.

For Phase II of the experiments, the I/R systems were unbolted and removed. Then, at each support location the test specimen base plate was directly bolted to the load cell. Figure 5-8 shows the test specimen at the end of the test setup for the Phase II of the experiments.

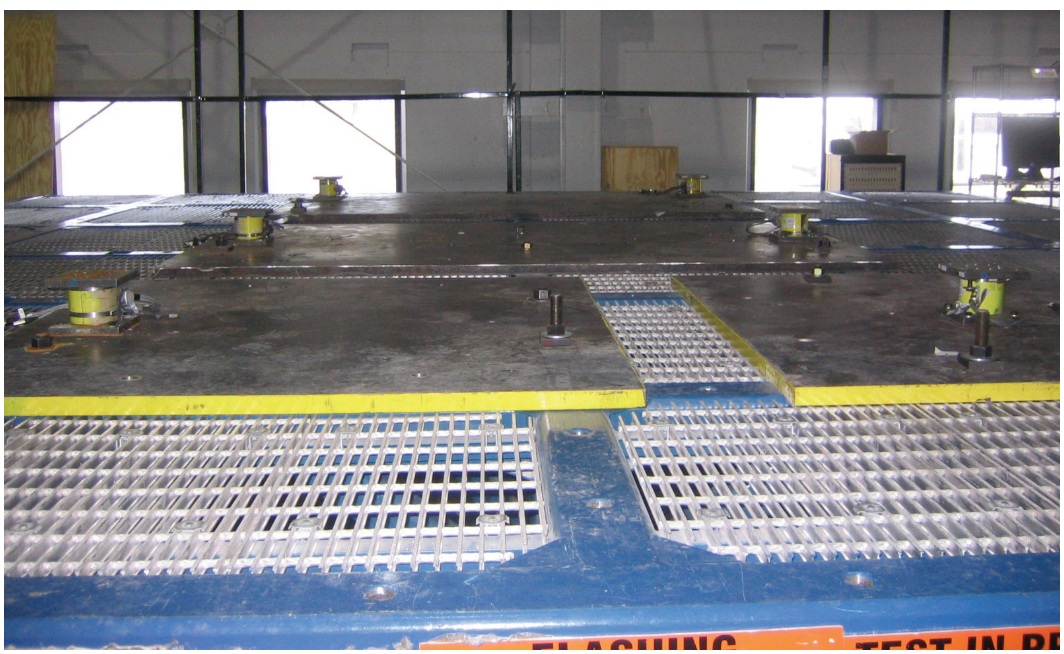

Figure 5-6 Six Load Cells Bolted to Interface Plates

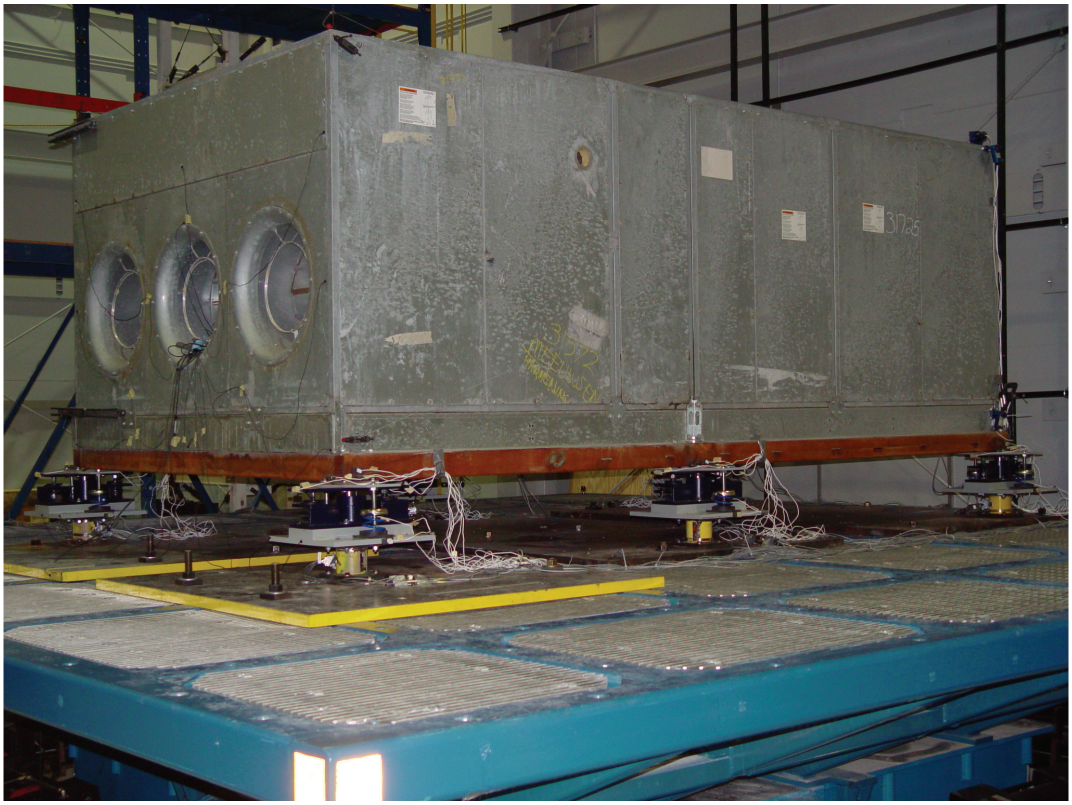

Figure 5-7 Test Setup, Phase I: Test Specimen Mounted on Six I/R Systems

Figure 5-8 Test Setup, Phase II: Rigidly Mounted Test Specimen

SECTION 6

TEST RESULTS

The dynamic characteristics of the rigidly mounted and isolated test specimen obtained from the system-identification tests results, the modal equivalent viscous damping ratios of the isolated test specimen obtained form the seismic tests results, and selected response envelopes during the seismic tests are presented in this section.

6.1 System-Identification Tests Results

6.1.1 Dynamic Characteristics of Rigidly Mounted Test Specimen

The acceleration responses measured during the white noise tests were analyzed to establish the natural frequencies and mode shapes of the first three modes of the rigidly mounted test specimen. The amplitude transfer-function between the input motion and the acceleration response has local peaks at the natural frequencies of the system (Wheeler and Ganji, 2004). The amplitude transfer-function was established between the input acceleration and acceleration responses at several points on the test specimen. Each amplitude transfer-function had several local peaks. The first three global natural frequencies of the rigidly mounted test specimen were detected among the common local peaks of the amplitude transfer-functions as 9.6, 17.9, and 27 *Hz*.

The phase and amplitude transfer functions between the acceleration response at several locations at the top level of the side faces and on the perimeter of the top face of the test specimen were used to establish the normalized mode shapes of the first three modes of vibration of the test specimen. The results showed that the vertical motion of the test specimen in the first three modes was negligible. Therefore, as listed in Table 6-1, the normalized mode shapes of the first three modes of the test specimen were defined by the values of the rotation around the vertical axis and the translation along the transverse and longitudinal axis at the center of the top face of the test specimen. The coordinate system used to calculate the values listed in Table 6-1 is the coordinate system previously shown in Figure 2-6.

Table 6.1 Normalized Modal Displacements and Rotation at Center of Top Face, Rigidly Mounted Test Specimen

Mode No.	x, *m*	y, *m*	θ_z , *rad*
1st Mode (9.6 *Hz*)	0.012	1.000	-0.043
2nd Mode (17.9 *Hz*)	1.000	-0.161	-0.038
3rd Mode (27.0 *Hz*)	-0.191	0.572	1.000

The results show that the first two mode shapes are attributed to almost pure translation in the transverse and longitudinal direction, respectively, and the third mode is a combination of the horizontal translation and rotation around the vertical axis. The mode shapes of the first three modes of vibration of the rigidly mounted test specimen are schematically shown in Figure 6-1.

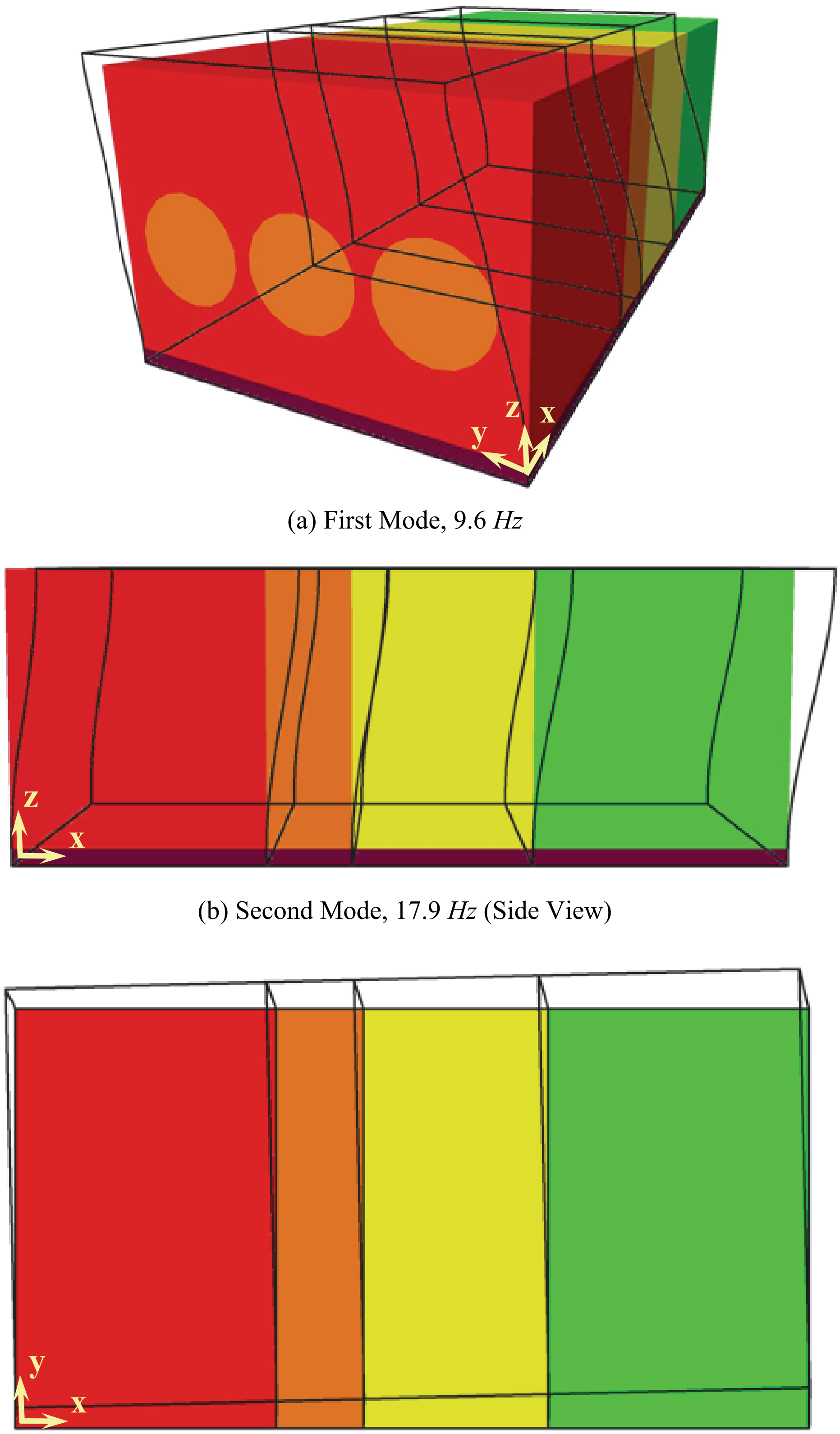

(a) First Mode, 9.6 *Hz*

(b) Second Mode, 17.9 *Hz* (Side View)

(c) Third Mode, 27 *Hz* (Top View)

Figure 6-1 Schematic Representation of Normalized Mode Shapes of Rigidly Mounted Test Specimen

6.1.2 Dynamic Characteristics of Isolated Test Specimen

The acceleration responses measured during the free vibrations between the three pulses during the pulse tests were used to establish the natural frequencies of the isolated tests specimen. The frequency content of the acceleration responses showed that the isolated test specimen responded to each pulse like a rigid body with six distinct natural frequencies. Table 6-2 lists the natural frequencies and periods of the six modes of vibrations of the isolated test specimen.

Table 6-2 Natural Frequencies / Periods of Isolated Test Specimen

Mode No.	**1**	**2**	**3**	**4**	**5**	**6**
Frequency, *Hz*	1.23	1.55	2.06	2.38	2.80	3.60
Period, *seconds*	0.81	0.65	0.49	0.42	0.36	0.28

To establish the normalized mode shapes, one of the measured acceleration responses was selected as the reference. Then, the amplitude and phase transfer-functions between the acceleration response at several other points and the reference acceleration response were established. At the frequency of the target mode, multiplying the amplitude transfer-function by the cosine of the phase-transfer function (+1 or -1) of each point yielded the normalized modal translation of that point. With the modal translations of several points on the test specimen and assuming that the mode shapes are associated with rigid body motion, the geometry-based kinematics equations were used to calculate the displacement and rotation at the center of mass of the test specimen. The procedure for establishing the modal displacements and rotations at the center of mass from the normalized modal translations of other points of a rigid body is explained in details in Fathali and Filiatrault (2007).

The values established as modal displacement and rotations at the center of mass of test specimen were normalized so that the largest displacement at the center of mass has value of +1 *m*. The procedure for establishing the mode shapes was repeated with the results of all of the pulse tests conducted throughout the test series TS5, TS6, and TS11. These three test series were selected to establish the mode shape because the gap size of the restraint components in these test series was larger than that in the other test series. The large gap size of the restraint components allowed the test specimen to respond to the pulses without engagement of the restraint components. The results obtained form different pulse tests of the three test series were coherent and, therefore, the mode shapes were calculated as an average of the results.

Table 6.3 lists the modal displacements and rotations at the center of mass of the isolated test specimen. The values in Table 6.3 are referred to the coordinate system previously defined in Figure 2.6. The results show that the first three mode shapes are mainly associated with pure translation along the transverse, longitudinal, and vertical direction, respectively. However, all of the first three modes of the isolated test specimen incorporated some rotational movements. The mode shapes of the fourth, fifth, and sixth mode of the isolated test specimen involved more rotations. The mode shapes of the six modes of the isolated test specimen show that the total response of the isolated test specimen always involves some rotational components.

As it was mentioned earlier, the seismic tests TS7-S5 and TS12-S6 were conducted after the vibration isolators supporting the fan and motor inside the fan module were activated. The triaxial acceleration responses on top of the motor during the pulse tests conducted before these two seismic tests were analyzed to establish the first three natural frequencies of the isolated motor and fan. The power spectrum of the triaxial acceleration responses identified the first three natural frequencies of the isolated motor and fan as 2.9 *Hz,* 3.0 *Hz,* and 3.8 *Hz.* The instrumentation attached to the motor was not sufficient to establish the mode shapes of the isolated fan and motor. However, the power spectra of the triaxial acceleration responses on top of the motor showed that the largest displacement of the first three mode shapes were in the transverse, vertical, and longitudinal direction, respectively. The two coil springs interfacing the fan encasing-frame and the test specimen housing (see Figure 2-4 (b)) increased the stiffness of the isolated fan and motor in the longitudinal direction.

Table 6-3 Measured Modal Displacements and Rotations at Center of Mass of Isolated Test Specimen

Modal Displacements at Center of Mass	**x**, ***m***	**y**, ***m***	**z**, ***m***
	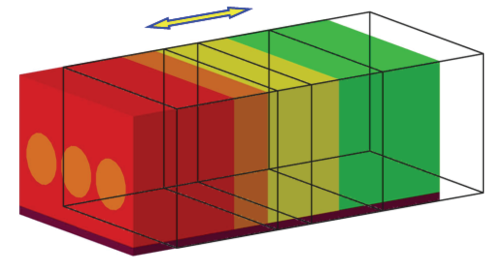	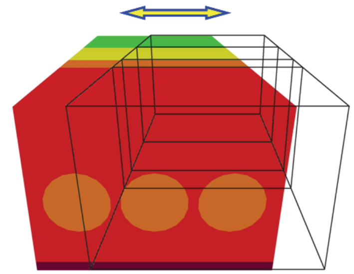	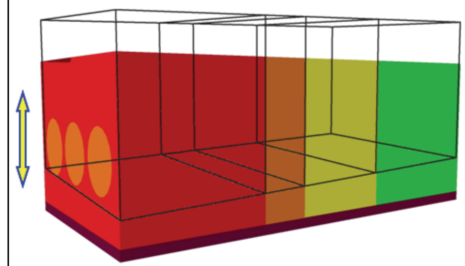
1st Mode (1.23 Hz)	-0.1590	1.0000	0.0539
2nd Mode (1.55 Hz)	1.0000	0.1461	0.1606
3rd Mode (2.06 Hz)	-0.0879	-0.1001	1.0000
4th Mode (2.38 Hz)	-0.4513	-0.5812	1.0000
5th Mode (2.80 Hz)	1.0000	-0.5236	0.0697
6th Mode (3.60 Hz)	1.0000	-0.0016	0.2923
Modal Rotations at Center of Mass	θ_x, ***rad***	θ_y, ***rad***	θ_z, ***rad***
	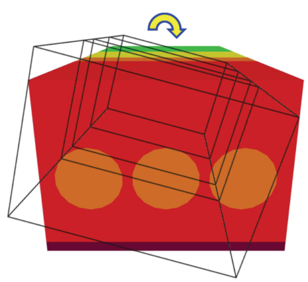	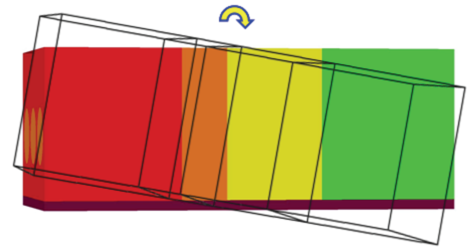	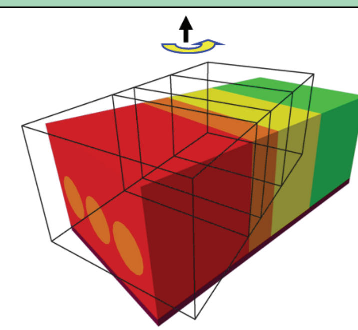
1st Mode (1.23 Hz)	-0.3673	-0.0621	-0.0454
2nd Mode (1.55 Hz)	0.0761	0.1664	-0.0310
3rd Mode (2.06 Hz)	-0.0265	0.0246	-0.2990
4th Mode (2.38 Hz)	-0.3323	0.4346	0.1271
5th Mode (2.80 Hz)	-2.6106	-2.4666	0.1728
6th Mode (3.60 Hz)	2.7924	-1.8718	-0.3989

6.2 Seismic Tests Results

6.2.1 Estimation of Modal Equivalent Viscous Damping Ratios for Isolated Test Specimen

The equivalent viscous damping ratio can be quantified by measuring the decrement of the peak response amplitudes. Double peak amplitudes are used to eliminate the effect of the potential offset of the response with respect to the time axis (Filiatrault, 2002). As annotated in Figure 6-2, the double amplitude response is defined as the difference between the maximum and minimum response within one response cycle. The equivalent viscous damping ratio for attributed to the decay of responses in any two consecutive cycles is calculated by Equation 6-1 (Fathali and Filiatrault, 2007):

$$\zeta_n = \frac{1}{2\pi} ln(\frac{R_i}{R_{i+1}}) \quad (6\text{-}1)$$

where,

ζ_n = equivalent viscous damping ratio of the n[th] mode
R_i and R_{i+1} = double response amplitude of two consecutive cycles

The equivalent viscous damping ratio calculated in equation 6-1 is attributed to R_a, the average amplitude of the two consecutive cycles, which is calculated by Equation 6-2:

$$R_a = \frac{(R_i + R_{i+1})}{4} \quad (6\text{-}2)$$

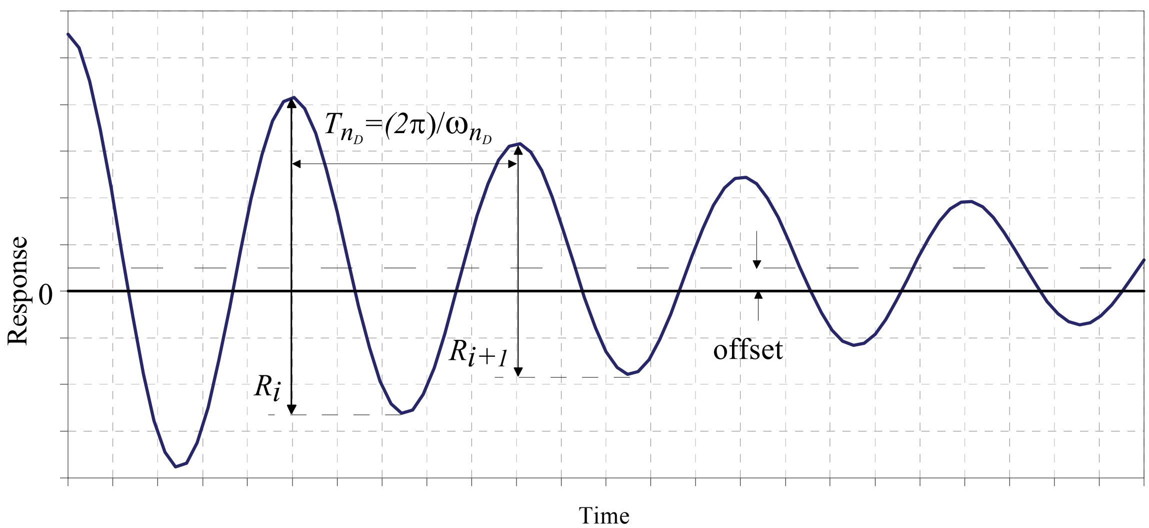

Figure 6-2 Decay of Response Attributed to Viscous Damping

Variation of the equivalent viscous damping ratio with the response amplitude should be established for a range of response amplitudes. The decay of acceleration and displacement responses of the isolated test specimen during the tale of the seismic tests were used to establish the equivalent viscous damping ratios for the first three modes of vibration of the isolated test specimen.

Before implementing Equation 6-1 on the decay of a measured response to calculate the damping ratio for a particular mode, the contribution of other modes to the response must be filtered out. For this purpose, band-pass filters were implemented. Three band-pass filters were selected such that each one includes only a very narrow frequency band centered on one of the first three modes. The decaying measured responses during the tale of seismic tests subjected to the three band pass filters provided several data sets for each of the first three modes to calculate the equivalent viscous damping ratios.

The results showed that the equivalent viscous damping ratios of the first two modes of vibration of the isolated test specimen were around 3% of the critical damping and the equivalent viscous damping ratio of the third mode was around 1% of the critical damping. It should be noted that the results were obtained for peak acceleration and displacement responses at the top level of the test specimen limited to 0.1 *g* and 15 *mm* (0.6 *in.*), respectively. The low damping property of the isolation components of the I/R systems proves why coil springs are successful vibration isolators.

6.2.2 Damage Observations during Seismic Tests

During the 11 tests series of Phase I of the experiments, the I/R systems sustained no damage. However, the test specimen housing was damaged after the full-scale (100%) test of Test Series 6. The base rail separated from the housing around the perimeter of the fan module. The separation of the base rail and the housing resulted in a slight separation of the fan and coil module. After observation of this damage, the joint between the test specimen and housing was strengthened by adding connection plates and the test with the full-scale input motion was repeated as TS6-S5. Figure 6-3 shows photographs of the damaged and retrofitted test specimen housing. During the repeated seismic test and the seismic tests conducted afterward, the test specimen did not sustain any damage. The responses of the test specimen during Seismic Test TS6-S4 and the repeated test (Seismic Test TS6-S5) are compared to each other in Section 7.4.

(a) Damaged Connection Plate between Base Rail and Test Specimen Housing

(b) Separation of Modules Resulting from Damage to Connection Plates between Base Rail and Test Specimen Housing

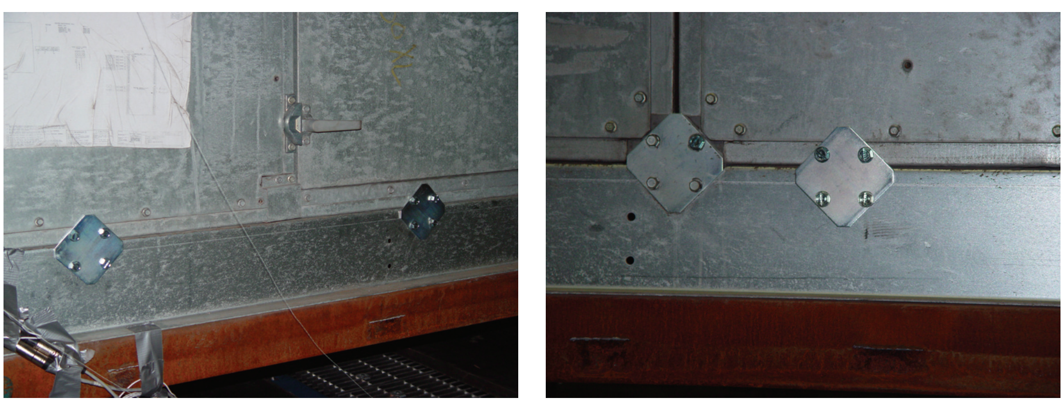

(c) Strengthening of Test Specimen Housing by Additional Connection Plates between Base Rail and Housing

Figure 6-3 Damaged and Retrofitted Test Specimen Housing after Seismic Test TS6-S4

6.2.3 Selected Response Envelopes during Seismic Tests

The peak triaxial acceleration responses at the top of the motor, the peak horizontal (transverse, and longitudinal) acceleration responses on the test specimen housing, the peak dynamic shear and normal forces induced into the I/R systems, and the peak relative displacement responses at three levels of the south face of the test specimen housing during the 46 seismic tests of Phase I of the experiments (with the isolated test specimen) are listed in Tables 6-4 through 6-8, respectively.

The peak triaxial acceleration responses at the top of the motor, the peak horizontal acceleration responses on the housing, and the peak dynamic shear and normal forces experienced at the support locations of the rigidly mounted test specimen during the six seismic tests of Phase II of the experiments are listed in Tables 6-9 through 6-12, respectively.

As mentioned earlier, the diagonal string displacement transducers were mainly used to measure the permanent deformation of the test specimen housing. Instead of the peak values, the difference between the initial and final values was the important quantity measured during each test. Furthermore, the peak values of the data recorded by the diagonal displacement transducers on the four faces of the test specimen throughout the tests were smaller than 5 *mm* (0.2 *in.*). These small values were in fact a combination of three effects: diagonal deformation of the test specimen housing, out-of-plane vibration of the transducer strings, and displacements of the magnets attaching the two ends of the transducer to the test specimen housing (which were not measured during the tests). Therefore, it was decided not to include the peak values recorded by the diagonal transducers in this section.

The response envelopes obtained during the 46 seismic test of Phase I and the six seismic test of Phase II of the experiments are analyzed and discussed in Section 7.

Table 6-4[*] Peak Acceleration Responses at Top of Motor near Center of Mass of Test Specimen during Seismic Tests, Phase I: Isolated Test Specimen

Test #	Test Name	Gap, *mm (in.)*	Horizontal Snubber: Rubber Tube		Vertical Snubber: Rubber Washer		Input Motion Amplitude (%)	Peak Acceleration Response, *g*		
			Thickness, *mm (in.)*	Hardness, *Duro.*	Thickness, *mm (in.)*	Hardness, *Duro.*		Transverse	Longitudinal	Vertical
1	TS1-S1	6 (0.25)	19 (0.75)	40	19 (0.75)	40	10	0.66	0.75	0.80
2	TS1-S2						25	1.30	1.57	1.30
3	TS1-S3						50	2.48	2.37	2.50
4	TS1-S4						100	3.21	4.20	2.82
5	TS2-S1	6 (0.25)	19 (0.75)	60	19 (0.75)	60	10	0.55	0.48	0.56
6	TS2-S2						25	1.05	0.99	1.51
7	TS2-S3						50	2.44	2.33	1.87
8	TS2-S4						100	3.24	3.65	2.69
9	TS3-S1	6 (0.25)	13 (0.5)	40	13 (0.5)	40	10	0.55	0.38	0.55
10	TS3-S2						25	1.04	1.07	1.15
11	TS3-S3						50	2.75	2.62	1.97
12	TS3-S4						75	2.76	3.65	2.10
13	TS3-S5						100	3.86	4.17	2.98
14	TS4-S1	6 (0.25)	13 (0.5)	60	13 (0.5)	60	10	0.49	0.46	0.42
15	TS4-S2						25	0.95	1.27	0.94
16	TS4-S3						50	1.78	2.84	1.54
17	TS4-S4						100	4.08	4.39	2.56

Table 6-4 (cont'd) Peak Acceleration Responses at Top of Motor near Center of Mass of Test Specimen during Seismic Tests, Phase I: Isolated Test Specimen

Test #	Test Name	Gap, *mm (in.)*	Horizontal Snubber: Rubber Tube		Vertical Snubber: Rubber Washer		Input Motion Amplitude (%)	Peak Acceleration Response, *g*		
			Thickness, *mm (in.)*	Hardness, *Duro.*	Thickness, *mm (in.)*	Hardness, *Duro.*		Transverse	Longitudinal	Vertical
18	TS5-S1	13 (0.5)	6 (0.25)	40	6 (0.25)	40	10	0.44	0.52	0.50
19	TS5-S2						25	1.07	1.14	0.93
20	TS5-S3						50	2.49	2.37	1.63
21	TS5-S4						100	3.89	3.83	2.23
22	TS6-S1	13 (0.5)	6 (0.25)	60	6 (0.25)	60	10	0.47	0.59	0.36
23	TS6-S2						25	0.96	1.18	0.87
24	TS6-S3						50	1.82	1.99	1.57
25	TS6-S4						100	5.19	4.83	3.07
26	TS6-S5						100	3.76	4.08	2.76
27	TS7-S1	6 (0.25)	6 (0.25)	40	6 (0.25)	40	10	0.69	0.79	0.49
28	TS7-S2						25	1.09	1.03	0.97
29	TS7-S3						50	1.84	2.63	1.54
30	TS7-S4						100	2.99	3.47	2.38
31	TS7-S5						100	6.02	5.60	3.83
32	TS8-S1	6 (0.25)	6 (0.25)	60	6 (0.25)	60	10	0.67	0.64	0.67
33	TS8-S2						25	1.68	1.43	0.89
34	TS8-S3						50	2.29	2.00	1.54
35	TS8-S4						100	3.12	2.89	2.25

Table 6-4 (cont'd) Peak Acceleration Responses at Top of Motor near Center of Mass of Test Specimen during Seismic Tests, Phase I: Isolated Test Specimen

Test #	Test Name	Gap, *mm (in.)*	Horizontal Snubber: Rubber Tube		Vertical Snubber: Rubber Washer		Input Motion Amplitude (%)	Peak Acceleration Response, *g*		
			Thickness, *mm (in.)*	Hardness, *Duro.*	Thickness, *mm (in.)*	Hardness, *Duro.*		Transverse	Longitudinal	Vertical
36	TS9-S1	6 (0.25)	3 (0.125)	40	6 (0.25)	40	10	0.55	0.67	0.49
37	TS9-S2						25	1.22	1.22	1.14
38	TS9-S3						50	1.41	2.05	1.45
39	TS9-S4						100	2.87	3.19	2.59
40	TS10-S1	6 (0.25)	3 (0.125)	60	6 (0.25)	60	10	0.36	0.62	0.40
41	TS10-S2						25	0.90	1.07	0.82
42	TS10-S3						50	1.83	1.53	1.47
43	TS10-S4						100	3.49	3.72	2.48
44	TS11-S1	10 (0.375)	—	—	—	—	10	0.74	0.86	0.65
45	TS11-S2						25	1.27	1.04	0.97
46	TS11-S3						50	1.77	2.56	1.86

*- The horizontal and vertical snubber gap sizes were nominally equal (the third column of the table)
- The test specimen housing was damaged during TS6-S4
- TS6-S5 was conducted after the test specimen housing was retrofitted by additional connection plates (see Section 6.2.2)
- TS7-S5 was conducted after the internal isolation system inside the fan module was activated
- The three seismic tests of Test Series TS11 were conducted after rubber snubbers were removed from the restraint components of the I/R systems

Table 6-5[*] Peak Horizontal Acceleration Responses of Test Specimen Housing during Seismic Tests, Phase I: Isolated Test Specimen

Test #	Test Name	Peak Transverse Acceleration, *g*		Peak Longitudinal Acceleration, *g*	
		Intermediate Level	Top Level	Intermediate Level	Top Level
1	TS1-S1	0.73	0.74	0.42	0.49
2	TS1-S2	1.07	1.21	0.76	0.86
3	TS1-S3	1.74	2.34	1.68	1.42
4	TS1-S4	3.58	4.23	2.94	2.56
5	TS2-S1	0.50	0.48	0.31	0.36
6	TS2-S2	1.07	1.28	0.63	0.63
7	TS2-S3	1.48	1.84	1.47	1.15
8	TS2-S4	3.50	4.03	2.65	2.69
9	TS3-S1	0.56	0.68	0.41	0.34
10	TS3-S2	1.46	1.58	0.66	0.79
11	TS3-S3	1.85	1.94	1.84	1.29
12	TS3-S4	3.12	3.68	2.67	1.84
13	TS3-S5	3.70	4.15	3.34	2.69
14	TS4-S1	0.47	0.57	0.30	0.42
15	TS4-S2	1.11	1.29	0.70	0.68
16	TS4-S3	1.79	2.37	1.68	1.32
17	TS4-S4	3.93	4.34	3.42	2.25
18	TS5-S1	0.67	0.70	0.39	0.48
19	TS5-S2	1.65	1.56	1.03	1.00
20	TS5-S3	2.93	4.27	1.65	1.61
21	TS5-S4	4.62	5.77	3.91	2.99
22	TS6-S1	1.01	1.06	0.40	0.58
23	TS6-S2	1.30	1.60	1.12	1.37
24	TS6-S3	2.57	3.58	1.76	1.94
25	TS6-S4	4.75	6.20	3.40	3.46
26	TS6-S5	4.35	4.45	2.67	3.30

Table 6-5 (cont'd) Peak Horizontal Acceleration Responses of Test Specimen Housing during Seismic Tests, Phase I: Isolated Test Specimen

Test #	Test Name	Peak Transverse Acceleration, *g*		Peak Longitudinal Acceleration, *g*	
		Intermediate Level	Top Level	Intermediate Level	Top Level
27	TS7-S1	0.94	0.94	0.47	0.45
28	TS7-S2	1.63	1.69	0.71	0.80
29	TS7-S3	2.15	2.17	1.41	1.77
30	TS7-S4	3.08	4.28	2.46	2.62
31	TS7-S5	3.24	4.05	2.33	2.41
32	TS8-S1	0.73	0.70	0.51	0.41
33	TS8-S2	1.48	1.74	0.80	0.78
34	TS8-S3	1.89	2.42	1.33	1.30
35	TS8-S4	2.97	4.03	2.52	2.75
36	TS9-S1	0.60	0.63	0.40	0.44
37	TS9-S2	1.28	1.41	0.81	0.86
38	TS9-S3	1.70	1.92	1.19	1.66
39	TS9-S4	2.67	3.22	2.23	2.97
40	TS10-S1	0.62	0.74	0.41	0.33
41	TS10-S2	1.26	1.44	0.95	0.94
42	TS10-S3	1.39	2.02	1.48	1.46
43	TS10-S4	2.81	3.63	2.76	2.59
44	TS11-S1	1.04	1.25	0.65	0.51
45	TS11-S2	1.42	1.77	0.81	1.00
46	TS11-S3	2.34	2.87	1.97	1.83

*- See footnotes of Table 6-4

Table 6-6[*] Peak Dynamic Shear Forces Induced into I/R Systems during Seismic Tests, *kN*, Phase I: Isolated Test Specimen

Test #	Test Name	I/R System #1		I/R System #2		I/R System #3		I/R System #4		I/R System #5		I/R System #6	
		Trans.	Long.	Trans.	Long.	Trans.	Long.	Trans.	Long.	Trans.	Long.	Trans.	Long.
1	TS1-S1	2.02	1.19	2.38	1.48	1.16	1.59	2.07	1.97	1.30	6.02	1.87	2.01
2	TS1-S2	2.41	2.69	2.98	2.61	2.17	2.78	3.17	2.97	2.24	8.41	3.30	3.25
3	TS1-S3	3.37	3.94	4.32	3.74	2.82	3.96	5.15	4.00	4.37	13.35	3.96	5.47
4	TS1-S4	4.81	4.92	5.73	5.46	5.06	9.26	9.34	7.10	9.22	22.48	7.01	5.84
5	TS2-S1	0.97	0.98	2.18	1.48	0.44	1.75	0.94	1.03	1.52	5.76	1.23	0.68
6	TS2-S2	2.76	2.33	3.22	2.23	1.17	2.55	2.84	1.81	2.54	7.72	2.22	1.92
7	TS2-S3	3.59	3.55	4.25	3.16	1.94	4.91	3.83	3.43	3.88	9.70	3.25	3.70
8	TS2-S4	5.63	5.42	6.62	5.39	4.90	8.08	10.30	6.22	7.42	18.23	5.79	5.36
9	TS3-S1	0.92	0.70	1.56	1.11	1.28	4.07	1.16	1.49	2.07	6.79	0.98	0.77
10	TS3-S2	1.86	1.92	3.30	2.60	2.41	5.18	3.20	2.20	2.81	12.25	2.03	1.64
11	TS3-S3	3.52	3.98	5.95	3.87	3.00	8.92	4.99	4.94	3.83	13.40	3.34	4.16
12	TS3-S4	4.24	4.64	6.57	4.98	3.64	9.85	10.30	4.88	5.72	16.21	4.39	4.68
13	TS3-S5	5.93	6.13	7.45	6.03	5.40	11.49	10.52	6.60	7.49	22.50	5.62	6.72
14	TS4-S1	1.61	1.07	2.41	1.68	0.57	1.81	1.95	1.81	1.83	5.57	0.55	0.76
15	TS4-S2	3.12	2.40	3.46	2.31	2.25	4.16	1.95	2.98	2.75	8.88	1.89	2.25
16	TS4-S3	3.74	3.69	4.40	4.00	2.94	5.88	5.22	3.52	4.44	14.11	3.20	3.90
17	TS4-S4	5.89	5.46	6.37	5.46	5.45	12.11	11.66	5.90	8.56	22.59	5.35	5.86

Table 6-6 (cont'd) Peak Dynamic Shear Forces Induced into I/R Systems during Seismic Tests, *kN*, Phase I: Isolated Test Specimen

Test #	Test Name	I/R System #1		I/R System #2		I/R System #3		I/R System #4		I/R System #5		I/R System #6	
		Trans.	Long.	Trans.	Long.	Trans.	Long.	Trans.	Long.	Trans.	Long.	Trans.	Long.
18	TS5-S1	1.89	1.51	2.73	2.78	0.46	1.07	1.68	1.60	1.30	6.54	0.74	0.46
19	TS5-S2	3.79	2.90	3.87	5.03	1.50	5.93	3.65	3.32	2.32	16.54	2.27	1.54
20	TS5-S3	4.78	4.14	6.18	4.68	3.06	6.64	5.62	4.59	4.39	15.35	3.08	3.56
21	TS5-S4	6.48	7.86	7.62	7.30	6.50	12.79	16.22	9.30	9.90	26.13	6.79	9.74
22	TS6-S1	1.24	0.88	2.74	1.81	0.81	1.30	1.61	1.87	0.75	4.31	1.79	0.53
23	TS6-S2	2.93	3.48	3.47	2.77	1.80	5.59	2.85	3.80	2.29	16.90	2.07	1.87
24	TS6-S3	4.46	4.09	6.63	4.98	2.80	7.11	7.13	4.54	4.74	14.39	4.15	4.66
25	TS6-S4	7.87	7.54	8.30	6.92	6.38	13.03	16.18	9.91	10.89	27.70	5.36	10.85
26	TS6-S5	6.61	9.24	10.37	8.87	7.61	13.89	16.27	11.95	10.21	25.29	6.19	10.05
27	TS7-S1	1.45	0.99	3.50	2.24	0.92	3.98	2.02	1.47	1.55	7.24	0.74	0.67
28	TS7-S2	3.31	2.34	4.12	2.95	1.53	7.70	4.88	2.81	2.24	11.50	2.77	2.93
29	TS7-S3	4.26	7.34	4.48	5.96	2.59	11.30	4.96	5.78	3.04	14.22	2.60	6.13
30	TS7-S4	6.41	7.39	7.76	10.05	4.07	13.12	9.56	8.47	6.36	25.21	5.27	7.42
31	TS7-S5	4.80	6.70	9.94	8.76	3.89	15.89	11.30	8.25	6.94	25.33	5.74	7.37
32	TS8-S1	1.67	0.78	3.04	2.07	0.84	0.70	2.31	3.08	1.70	10.53	0.72	0.57
33	TS8-S2	3.43	2.40	3.50	2.75	1.30	4.92	4.65	4.48	2.80	14.24	2.40	1.73
34	TS8-S3	4.42	5.26	5.80	6.30	2.83	9.49	5.58	6.74	3.75	21.85	3.20	5.02
35	TS8-S4	6.81	8.60	7.04	8.24	3.88	12.27	12.68	11.86	8.73	24.83	4.52	6.71

Table 6-6 (cont'd) Peak Dynamic Shear Forces Induced into I/R Systems during Seismic Tests, *kN*, Phase I: Isolated Test Specimen

Test #	Test Name	I/R System #1		I/R System #2		I/R System #3		I/R System #4		I/R System #5		I/R System #6	
		Trans.	Long.	Trans.	Long.	Trans.	Long.	Trans.	Long.	Trans.	Long.	Trans.	Long.
36	TS9-S1	2.05	1.39	3.13	2.41	0.56	1.29	1.87	1.62	1.33	6.27	1.33	2.04
37	TS9-S2	2.74	4.28	2.96	3.49	1.02	2.19	2.88	3.79	1.70	9.97	2.35	3.81
38	TS9-S3	3.77	5.66	5.56	4.35	2.78	9.40	4.07	4.55	3.53	21.76	2.69	6.02
39	TS9-S4	7.61	7.47	10.15	8.46	4.46	12.28	8.67	8.45	5.44	23.14	4.43	8.25
40	TS10-S1	1.75	1.65	2.78	2.81	0.57	2.03	1.33	1.51	1.25	10.00	1.34	0.99
41	TS10-S2	2.37	2.71	3.18	4.81	0.80	4.25	3.26	2.59	2.42	12.81	2.45	2.25
42	TS10-S3	3.58	4.41	5.83	6.26	2.25	4.94	5.06	4.28	2.93	16.39	3.00	3.48
43	TS10-S4	5.78	6.35	8.03	11.39	5.03	15.26	8.01	9.49	7.43	28.65	4.56	6.39
44	TS11-S1	2.82	1.79	3.01	2.95	0.56	0.81	3.50	1.78	1.78	15.08	1.28	0.54
45	TS11-S2	3.48	3.28	4.37	4.45	1.46	5.52	4.77	3.27	3.05	16.94	3.03	3.12
46	TS11-S3	4.70	6.06	8.23	6.40	2.54	10.76	6.57	7.36	4.49	24.26	3.76	5.24

*- Trans.: Transverse (Dynamic Shear Force)
- Long.: Longitudinal (Dynamic Shear Force)
- See footnotes of Table 6-4

Table 6-7* Peak Dynamic Normal Forces Induced into I/R Systems during Seismic Tests, *kN*, Phase I: Isolated Test Specimen

Test #	Test Name	I/R System #1		I/R System #2		I/R System #3		I/R System #4		I/R System #5		I/R System #6	
		Tens.	Comp.	Tens.	Comp.	Tens.	Comp.	Tens.	Comp.	Tens.	Comp.	Tens.	Comp.
1	TS1-S1	2.81	1.48	2.20	1.65	0.66	1.80	2.85	2.59	4.84	8.41	1.82	2.53
2	TS1-S2	5.39	3.81	4.35	3.34	3.17	3.03	6.17	3.71	14.32	11.97	2.18	3.78
3	TS1-S3	6.63	5.20	6.23	5.04	6.20	5.58	11.27	4.45	16.86	16.86	3.25	6.53
4	TS1-S4	10.25	9.25	12.05	7.15	9.89	7.85	14.76	6.17	20.99	19.68	4.18	6.27
5	TS2-S1	2.62	1.67	1.42	1.19	1.70	1.04	2.37	2.89	7.70	7.42	1.69	2.13
6	TS2-S2	3.53	3.58	3.57	2.84	3.17	2.08	4.71	3.24	12.68	9.16	2.09	2.98
7	TS2-S3	5.63	6.10	5.08	4.58	6.01	4.92	9.11	5.31	19.39	17.52	2.98	3.78
8	TS2-S4	9.82	9.82	10.58	8.43	8.33	7.99	12.87	7.21	23.95	20.10	4.98	4.80
9	TS3-S1	2.29	1.91	1.79	1.01	0.99	1.70	2.07	1.64	5.02	9.49	1.38	1.47
10	TS3-S2	3.34	2.48	3.80	3.39	2.41	3.12	4.32	3.89	9.30	10.85	1.82	1.69
11	TS3-S3	6.15	5.05	6.09	5.04	5.68	3.97	8.46	5.09	13.52	16.48	2.09	2.76
12	TS3-S4	7.39	7.06	7.47	6.92	6.01	5.58	12.91	5.87	22.21	18.27	2.80	4.40
13	TS3-S5	10.92	9.20	11.04	8.57	9.22	7.33	15.07	6.78	21.65	20.90	3.47	4.13
14	TS4-S1	2.77	1.19	1.47	2.75	0.62	0.85	1.73	1.77	4.88	8.08	1.02	1.33
15	TS4-S2	4.34	2.57	3.57	4.08	2.37	2.55	3.54	3.80	8.92	12.02	1.16	2.36
16	TS4-S3	5.24	5.53	5.45	5.18	5.06	3.64	8.50	5.05	16.86	19.11	2.62	3.91
17	TS4-S4	11.11	8.58	9.53	8.84	9.32	8.04	14.46	6.82	25.03	25.36	5.02	5.65

Table 6-7 (cont'd) Peak Dynamic Normal Forces Induced into I/R Systems during Seismic Tests, *kN*, Phase I: Isolated Test Specimen

Test #	Test Name	I/R System #1		I/R System #2		I/R System #3		I/R System #4		I/R System #5		I/R System #6	
		Tens.	Comp.	Tens.	Comp.	Tens.	Comp.	Tens.	Comp.	Tens.	Comp.	Tens.	Comp.
18	TS5-S1	2.57	0.91	2.89	1.42	1.14	0.99	2.85	1.29	5.78	11.60	1.42	1.56
19	TS5-S2	8.01	2.48	7.33	3.12	1.61	1.47	4.62	3.93	10.28	19.49	2.53	3.25
20	TS5-S3	9.11	4.82	11.09	5.04	6.24	4.68	7.38	5.27	20.33	17.05	3.25	4.27
21	TS5-S4	15.02	11.54	22.81	9.48	16.23	9.18	16.84	7.04	28.18	32.82	9.20	12.09
22	TS6-S1	2.19	1.67	1.65	1.56	0.90	1.09	1.99	1.68	3.76	12.21	2.09	3.87
23	TS6-S2	9.54	2.67	5.91	3.30	1.51	1.56	4.83	3.89	15.87	20.05	4.80	4.09
24	TS6-S3	8.58	5.77	8.29	4.90	3.97	4.49	11.48	5.53	18.55	16.39	4.00	3.38
25	TS6-S4	14.02	11.06	14.25	9.57	14.00	9.46	14.63	7.12	28.13	36.39	10.49	8.22
26	TS6-S5	14.35	10.01	14.34	8.89	9.98	11.59	15.54	11.09	32.31	33.58	8.80	5.60
27	TS7-S1	3.58	1.53	1.51	1.97	0.76	0.95	2.20	2.33	6.72	10.80	0.93	1.16
28	TS7-S2	3.81	2.72	4.63	3.39	2.93	3.08	6.39	4.01	12.02	13.34	1.38	2.49
29	TS7-S3	6.34	4.62	6.51	6.41	4.68	5.11	8.81	5.91	20.00	20.19	2.13	2.85
30	TS7-S4	11.35	6.44	10.22	13.01	11.31	8.52	13.69	10.06	26.30	32.26	2.71	4.93
31	TS7-S5	11.40	6.91	11.50	10.35	7.38	7.95	13.38	8.72	26.44	25.26	2.67	4.36
32	TS8-S1	3.58	2.05	2.02	2.25	0.76	1.70	2.37	2.68	6.72	12.54	1.07	2.31
33	TS8-S2	4.58	2.86	4.72	3.16	2.55	2.70	6.17	4.10	12.21	12.91	1.24	3.11
34	TS8-S3	5.77	5.29	6.78	5.68	4.54	5.72	8.33	6.22	15.03	20.33	2.76	2.67
35	TS8-S4	10.25	6.68	11.09	10.77	8.51	9.18	11.44	9.32	23.81	23.43	4.18	4.89

Table 6-7 (cont'd) Peak Dynamic Normal Forces Induced into I/R Systems during Seismic Tests, *kN*, Phase I: Isolated Test Specimen

Test #	Test Name	I/R System #1		I/R System #2		I/R System #3		I/R System #4		I/R System #5		I/R System #6	
		Tens.	Comp.	Tens.	Comp.	Tens.	Comp.	Tens.	Comp.	Tens.	Comp.	Tens.	Comp.
36	TS9-S1	1.19	2.05	2.15	1.28	0.80	1.14	2.07	2.37	5.07	13.57	1.02	2.62
37	TS9-S2	3.86	3.48	4.63	3.76	2.55	2.41	5.14	3.54	8.12	13.95	1.60	2.09
38	TS9-S3	5.39	4.39	7.38	6.18	3.83	5.44	7.47	5.35	13.52	14.32	2.00	3.11
39	TS9-S4	8.44	9.11	8.02	12.55	8.56	8.75	12.13	9.97	22.92	14.56	3.87	5.33
40	TS10-S1	2.43	1.81	2.24	1.56	0.52	0.85	1.68	1.42	4.46	7.23	1.07	1.60
41	TS10-S2	4.62	3.10	3.76	4.31	2.55	2.51	4.27	2.85	8.36	9.63	1.56	2.71
42	TS10-S3	5.72	4.20	7.05	5.59	4.78	5.82	7.04	5.66	11.51	10.42	2.62	2.45
43	TS10-S4	10.20	8.34	8.29	12.05	7.05	10.17	13.99	9.28	17.28	21.79	4.31	5.65
44	TS11-S1	5.05	0.67	2.70	2.02	0.71	2.60	2.20	3.28	7.84	12.63	1.33	3.82
45	TS11-S2	6.06	2.72	5.13	3.71	2.70	4.02	5.27	4.01	16.29	12.26	2.18	4.53
46	TS11-S3	9.92	3.72	6.69	5.73	5.58	6.72	7.51	7.21	21.55	23.15	3.87	6.85

*- Tens.: Tension
- Comp.: Compression
- See footnotes of Table 6-4

Table 6-8[*] Peak Relative Displacement Responses at South Face of Test Specimen during Seismic Tests, *mm*, Phase I: Isolated Test Specimen

Test #	Test Name	Bottom Level			Intermediate Level			Top Level		
		Trans.	Long.	Vertical	Trans.	Long.	Vertical	Trans.	Long.	Vertical
1	TS1-S1	17.4	15.6	10.1	16.2	14.8	10.0	12.3	12.4	9.9
2	TS1-S2	25.1	17.8	13.1	22.6	17.4	13.3	13.6	13.2	12.6
3	TS1-S3	28.9	22.9	14.8	26.2	23.2	15.6	15.6	15.1	15.1
4	TS1-S4	63.8	105.3	25.0	32.5	26.0	18.4	19.3	127.1	17.0
5	TS2-S1	15.0	15.1	9.0	13.9	13.9	8.7	9.5	12.6	8.8
6	TS2-S2	21.5	16.4	10.7	19.3	15.2	11.1	12.1	13.2	11.0
7	TS2-S3	24.5	22.3	12.8	21.8	22.2	13.4	13.1	14.9	13.3
8	TS2-S4	60.5	94.6	22.4	29.2	26.0	16.6	17.1	16.8	15.6
9	TS3-S1	16.1	11.1	9.9	15.0	11.3	10.3	10.8	11.1	9.7
10	TS3-S2	22.9	16.1	11.5	20.7	15.8	11.5	12.9	14.7	11.4
11	TS3-S3	28.9	20.7	13.3	25.9	20.6	13.8	15.0	16.2	13.4
12	TS3-S4	30.3	33.7	15.1	26.9	24.5	15.7	15.5	16.3	15.0
13	TS3-S5	58.2	103.8	23.4	32.4	25.3	18.9	19.0	16.5	16.3
14	TS4-S1	15.6	12.1	8.8	14.5	11.2	8.7	10.6	10.8	8.6
15	TS4-S2	21.9	14.9	10.3	19.7	13.8	10.2	12.3	12.8	9.9
16	TS4-S3	24.4	19.0	11.6	21.8	18.2	12.0	12.5	13.8	11.1
17	TS4-S4	56.8	104.9	21.7	28.9	26.3	16.3	16.9	16.1	13.0

Table 6-8 (cont'd) Peak Relative Displacement Responses at South Face of Test Specimen during Seismic Tests, *mm*, Phase I: Isolated Test Specimen

Test #	Test Name	Bottom Level			Intermediate Level			Top Level		
		Trans.	Long.	Vertical	Trans.	Long.	Vertical	Trans.	Long.	Vertical
18	TS5-S1	23.5	18.2	13.7	22.1	17.5	13.8	17.0	16.2	13.7
19	TS5-S2	29.0	22.8	16.5	26.6	22.0	17.0	20.2	20.2	15.9
20	TS5-S3	39.9	28.9	19.9	36.2	27.6	20.5	22.8	21.9	18.2
21	TS5-S4	61.0	110.8	24.5	40.8	39.0	24.8	23.8	24.8	21.5
22	TS6-S1	23.7	19.7	14.2	22.2	18.4	13.8	17.3	17.2	13.9
23	TS6-S2	27.7	22.7	14.7	25.4	22.0	14.8	18.3	19.2	14.6
24	TS6-S3	35.6	27.6	16.7	31.8	26.7	16.8	20.2	21.7	16.4
25	TS6-S4	51.3	104.0	24.9	37.1	39.4	20.9	21.3	24.3	19.7
26	TS6-S5	54.4	108.5	31.1	37.0	36.3	23.7	23.4	26.6	18.8
27	TS7-S1	16.9	10.3	8.6	15.5	9.7	8.4	10.5	9.4	8.4
28	TS7-S2	21.9	14.3	10.0	19.6	14.1	10.7	11.3	11.8	9.5
29	TS7-S3	23.9	19.3	13.5	21.1	19.0	12.6	11.5	13.6	11.4
30	TS7-S4	51.3	92.6	20.6	26.4	23.8	15.9	14.1	15.2	13.4
31	TS7-S5	56.5	99.9	28.2	26.8	22.4	16.7	14.3	15.5	12.5
32	TS8-S1	14.1	10.0	8.4	12.9	9.2	8.1	8.6	9.4	7.9
33	TS8-S2	20.6	14.4	9.3	18.5	13.6	9.2	10.7	12.7	8.7
34	TS8-S3	23.7	17.9	14.0	21.0	18.8	11.2	12.0	13.7	9.5
35	TS8-S4	49.7	70.5	28.0	25.4	25.5	13.5	14.2	16.2	11.6

Table 6-8 (cont'd) Peak Relative Displacement Responses at South Face of Test Specimen during Seismic Tests, *mm*, Phase I: Isolated Test Specimen

Test #	Test Name	Bottom Level			Intermediate Level			Top Level		
		Trans.	Long.	Vertical	Trans.	Long.	Vertical	Trans.	Long.	Vertical
36	TS9-S1	12.2	7.8	8.7	11.2	7.3	8.6	6.8	6.9	8.5
37	TS9-S2	16.2	11.1	10.7	14.1	11.2	11.9	7.3	8.2	10.6
38	TS9-S3	18.0	13.4	12.8	16.1	13.1	13.1	8.2	9.5	11.8
39	TS9-S4	57.2	85.2	19.3	25.0	18.1	17.5	11.9	10.0	15.3
40	TS10-S1	10.8	7.4	9.3	9.7	6.7	9.1	5.5	5.9	9.1
41	TS10-S2	16.2	10.0	10.0	14.3	10.0	10.3	5.9	7.0	9.6
42	TS10-S3	18.2	12.8	14.1	15.8	13.4	11.8	7.3	8.5	10.3
43	TS10-S4	54.4	69.7	23.0	23.1	18.3	17.0	11.2	12.9	13.1
44	TS11-S1	17.3	10.6	7.9	15.8	10.0	8.1	10.0	9.5	7.3
45	TS11-S2	21.3	15.7	8.6	19.0	15.0	9.1	11.1	12.9	8.3
46	TS11-S3	24.7	19.3	13.5	22.2	19.5	10.2	13.1	14.1	8.9

*- Trans.: Transverse
- Long.: Longitudinal
- See footnotes of Table 6-4

Table 6-9[*] Peak Acceleration Responses at Top of Motor Close to Center of Mass of Test Specimen during Seismic Tests, Phase II: Rigidly Mounted Test Specimen

Test #	Test Name	Input Motion Amplitude (%)	Peak Acceleration Response, *g*		
			Transverse	Longitudinal	Vertical
1	TS12-S1	10	0.43	0.29	0.28
2	TS12-S2	25	0.85	0.49	0.63
3	TS12-S3	50	1.05	1.16	0.95
4	TS12-S4	75	1.52	1.98	1.23
5	TS12-S5	100	2.98	2.50	1.70
6	TS12-S6	100	3.34	3.75	2.44

*- TS12-S6 was conducted after the internal isolation system inside the fan module was activated

Table 6-10[*] Peak Horizontal Acceleration Responses of Test Specimen Housing during Seismic Tests, Phase II: Rigidly Mounted Test Specimen

Test #	Test Name	Peak Transverse Acceleration, *g*		Peak Longitudinal Acceleration, *g*	
		Intermediate Level	Top Level	Intermediate Level	Top Level
1	TS12-S1	0.14	0.14	0.13	0.17
2	TS12-S2	0.30	0.35	0.28	0.32
3	TS12-S3	0.58	0.69	0.53	0.56
4	TS12-S4	1.10	1.37	0.79	0.80
5	TS12-S5	1.83	2.52	1.18	1.24
6	TS12-S6	2.10	1.79	0.97	1.15

*- See footnote of Table 6-9

Table 6-11[*] Peak Dynamic Shear Forces Induced into I/R Systems during Seismic Tests, *kN*, Phase II: Rigidly Mounted Test Specimen

Test #	Test Name	Support #1		Support #2		Support #3		Support #4		Support #5		Support #6	
		Trans.	Long.	Trans.	Long.	Trans.	Long.	Trans.	Long.	Trans.	Long.	Trans.	Long.
1	TS12-S1	0.37	0.41	0.41	0.42	0.37	0.50	0.67	0.42	0.33	0.11	0.20	0.46
2	TS12-S2	0.90	0.90	0.85	1.01	1.02	1.40	1.20	1.06	0.58	0.45	0.49	1.10
3	TS12-S3	1.70	1.78	1.76	1.81	2.14	2.83	3.03	2.02	1.21	1.13	0.99	2.67
4	TS12-S4	2.92	2.50	2.64	2.92	3.16	3.90	6.88	2.88	1.93	2.98	1.57	4.62
5	TS12-S5	3.72	3.54	3.63	3.94	3.79	5.68	11.51	4.45	2.32	4.73	2.54	5.90
6	TS12-S6	3.12	3.22	3.39	3.56	3.41	5.57	12.58	4.49	2.81	4.97	2.41	5.25

*- Trans.: Transverse (Dynamic Shear Force), Long.: Longitudinal (Dynamic Shear Force)
- See footnote of Table 6-9

Table 6-12[*] Peak Dynamic Normal Forces Induced into I/R Systems during Seismic Tests, *kN*, Phase II: Rigidly Mounted Test Specimen

Test #	Test Name	Support #1		Support #2		Support #3		Support #4		Support #5		Support #6	
		Tens.	Comp.	Tens.	Comp.	Tens.	Comp.	Tens.	Comp.	Tens.	Comp.	Tens.	Comp.
1	TS12-S1	0.54	0.51	0.41	0.56	0.66	0.52	0.61	0.40	0.50	1.23	0.58	0.69
2	TS12-S2	0.80	0.75	1.00	0.64	1.31	1.19	1.06	1.31	1.75	1.81	1.26	1.30
3	TS12-S3	1.97	1.10	1.42	1.44	2.29	2.54	2.42	2.20	3.14	1.81	2.40	2.12
4	TS12-S4	3.02	2.39	2.42	2.48	3.55	3.55	4.35	4.22	7.33	12.09	2.98	2.52
5	TS12-S5	5.08	3.24	3.36	3.88	4.84	4.79	6.48	5.28	15.94	18.55	4.04	3.67
6	TS12-S6	3.85	2.86	2.59	3.03	3.98	[illegible].94	7.37	5.11	9.37	13.67	3.66	3.06

*- Tens.: Tension, Comp.: Compression
- See footnote of Table 6-9

SECTION 7

SEISMIC TEST RESULTS ANALYSES

The seismic test results, presented earlier in Section 6, are analyzed in this section. Effects of variation of the restraint component properties on the seismic performance of the I/R systems are investigated in this section. The seismic response and damaged assessment of both the isolated and rigidly mounted test specimen are presented. Finally, the comparison of seismic responses of the test specimen before and after activation of the internal isolation systems concludes this section. Throughout this section, whenever possible, seismic responses of the isolated and rigidly mounted test specimen during similar seismic tests are compared to each other.

7.1 Test Specimen Response

The peak acceleration responses near the center of mass, the peak acceleration responses on the housing, and the peak relative displacement responses on the south face of the test specimen during the seismic tests are presented and discussed in Sections 7.1.1 through 7.1.3, respectively.

7.1.1 Acceleration Response near Center of Mass of Test Specimen

One of the most important unknowns regarding the seismic protection of nonstructural components is the amplification of acceleration response. Depending on the nonstructural component characteristics and its support conditions, the acceleration response experienced by the nonstructural component can be much larger than the input acceleration. Flexibility of the nonstructural component and presence of flexible supports generally increase the amplification of acceleration response. The amplification of the acceleration response can be different for different locations on a nonstructural component. However, since the seismic requirements for nonstructural components in most of the code provisions and guidelines deal with an equivalent static force applied at the center of mass of the nonstructural component (Tauby et al., 1999), it is always essential to know the amplification of the acceleration response at (or near) the center of mass. The amplification of acceleration response at the center of mass is quantified by an Acceleration Amplification Factor (*AAF*), which is calculated as:

$$AAF = \frac{a_{max,CM}}{a_{max,Inp}} \tag{7-1}$$

where,

$a_{max,CM}$ = the peak acceleration response at the center of mass
$a_{max,Inp}$ = the corresponding peak input acceleration

The *AAF* can be calculated for the acceleration response in a given direction (such as the longitudinal, transverse, and vertical acceleration response) or for the resultant acceleration responses. It should be noted that the *AAF* can be calculated at any other point rather than the center of mass by using the peak acceleration response of that point in the numerator of Equation 7-1.

As it was mentioned in Section 4, the top of the motor inside the fan module was the closest location to the center of mass of the test specimen for which the triaxial acceleration responses were measured during the seismic tests. Therefore, the triaxial peak acceleration responses on top of the motor during the seismic tests were used as numerator of Equation 7-1 to calculate the *AAF* near the center of mass of the test specimen.

To calculate the horizontal and resultant *AAF* on the top of the motor, the horizontal and resultant acceleration response histories were required. The triaxial acceleration responses measured on the top of the motor can be used to calculate the horizontal and resultant acceleration response histories on the top of the motor as follows:

$$|a_H(t)| = \sqrt{a_T(t)^2 + a_L(t)^2} \tag{7-2}$$

$$|a_R(t)| = \sqrt{a_T(t)^2 + a_L(t)^2 + a_V(t)^2} \tag{7-3}$$

where,

$a_T(t)$ = the transverse acceleration response
$a_L(t)$ = the longitudinal acceleration response
$a_V(t)$ = the vertical acceleration response
$a_H(t)$ = the horizontal acceleration response
$a_R(t)$ = the resultant acceleration response

The variations of the transverse, longitudinal, horizontal, vertical, and resultant *AAF* on top of the motor with the corresponding peak input acceleration during the 46 seismic tests of Phase I and the six seismic tests of Phase II are presented in Figures 7-1(a) through 7-1(e), respectively. According to Equation 7-1, for any given seismic test, multiplying the peak input acceleration (the horizontal axis in Figure 7-1) by the *AAF* (the vertical axis in Figure 7-1) yields the peak acceleration response on top of the motor during that test.

The maximum *AAF*, minimum *AAF*, and maximum acceleration responses on top of the motor during the seismic tests of Phase I are listed in Tables 7-1 through 7-3, respectively. To find the extreme values presented in these tables, results of Test Series TS11 (the test series conducted without rubber snubbers), Seismic Tests TS6-S4 (the test during which the test specimen housing was damaged), and TS7-S5 (the test conducted after activation of the isolation systems inside the fan module) were not considered. The transverse, longitudinal, horizontal, vertical, and resultant *AAF* on the top of motor of the isolated test specimen varied in the range of 3.5 to 8.7, 3.6 to 9.9, 4.0 to 11.2, 4.2 to 15.1, and 4.5 to 13.8, respectively. The test results show that near the center of mass of the test specimen, the vertical *AAF* was remarkably larger than the horizontal *AAF*.

With the peak horizontal and vertical input acceleration limited to 0.81 *g* and 0.53 *g* in the seismic tests, the horizontal and vertical acceleration responses experienced near the center of mass of the isolated test specimen were as high as 4.71 *g* and 2.98 *g*, respectively. As listed in Table 7-1, even with the 10%-amplitude input motion, the resultant acceleration response on top of the motor exceeded 1.0 *g*.

The test results show that during the seismic tests, the *AAF* near the center of mass of the isolated test specimen varied with a change in the input motion amplitude or with a change in the restraint component properties. The sensitivity of the *AAF* near the center of mass of the isolated test specimen to the variation of the restraint component properties decreased with an increase of the input motion amplitude. In terms of reducing the acceleration responses near the center of mass of the test specimen, among different I/R systems tested throughout the 11 test series, the I/R systems with small gap size and thin rubber snubbers (Test Series TS7 through TS10) exhibited the best performance (lowest AAF values).

During most of the seismic tests of Phase I, when the input motion amplitude was high enough to engage the restraint components of the I/R systems, the *AAF* near the center of mass of the isolated test specimen decreased with an increase of the input motion amplitude. However, the peak acceleration responses near the center of mass of the isolated test specimen always increased with an increase of the input motion amplitude. During each test series of Phase I, the maximum acceleration responses near the center of mass of the isolated test specimen were always experienced in the test with the full-scale input motion.

During the six seismic tests of Phase II of the experiments, the transverse *AAF* on top of the motor of the rigidly mounted test specimen decreased with an increase of the input motion amplitude. The longitudinal and vertical *AAF* on top of the motor of the rigidly mounted test specimen, on the other hand, hardly varied with a change in the input motion amplitude. This trend is attributed to the fact that the test specimen is more flexible in the transverse direction than in the longitudinal and vertical direction, thereby exhibited displacement-dependent damping in the transverse direction.

The *AAF* near the center of mass of the test specimen obtained in the seismic tests of this series of experiments is considerably larger than the *AAF* at the center of mass of a heavy centrifugal chiller obtained in similar earthquake-simulator experiments previously conducted by Fathali and Filiatrault (2007). This is mainly attributed to the fact that the test specimen used in this study was more flexible and six times lighter that centrifugal chiller previously tested. Effect of the flexibility of the test specimen on the amplification of the acceleration response was clearly seen in the test results obtained in Phase II of the experiments. As it is seen in Figure 7-1, regardless of the input motion amplitude, the horizontal and vertical *AAF* on top of the motor of the rigidly mounted were always larger than 3.

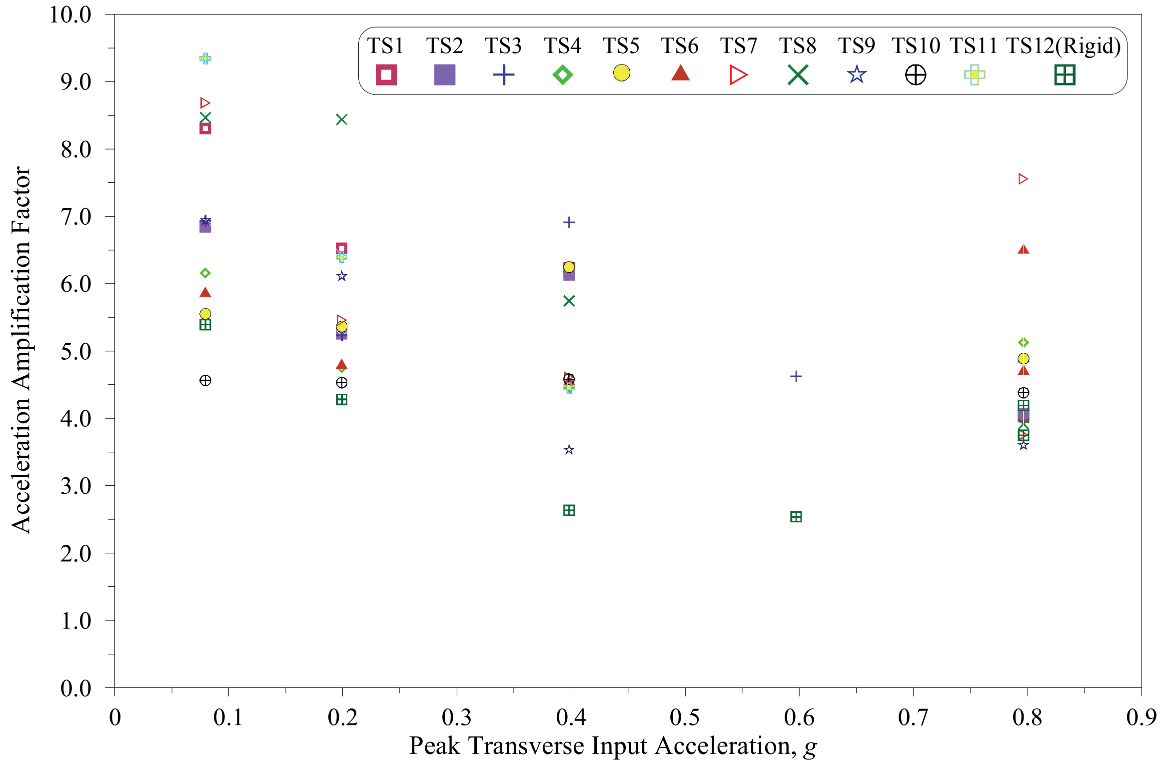

(a) Transverse *AAF* on Top of Motor Vs. Peak Transverse Input Acceleration

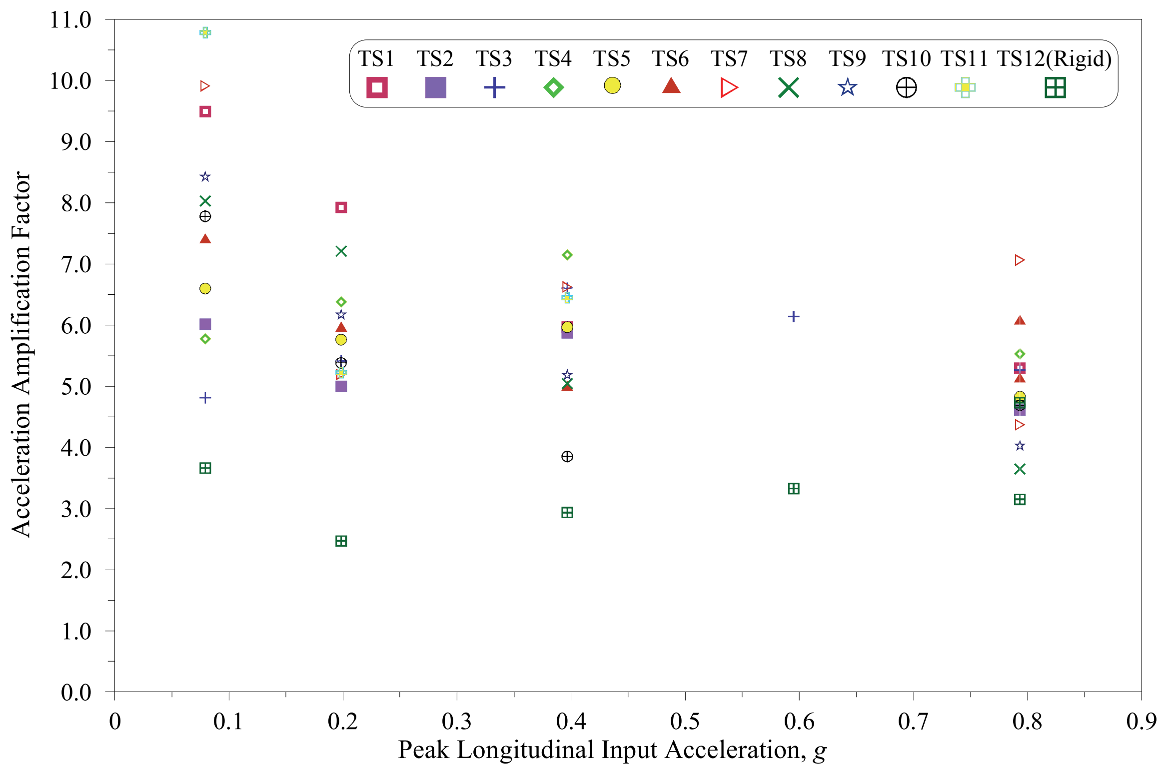

(b) Longitudinal *AAF* on Top of Motor Vs. Peak Longitudinal Input Acceleration

Figure 7-1 Variations of *AAF* near Center of Mass of Test Specimen (on Top of Motor) with Peak Input Acceleration

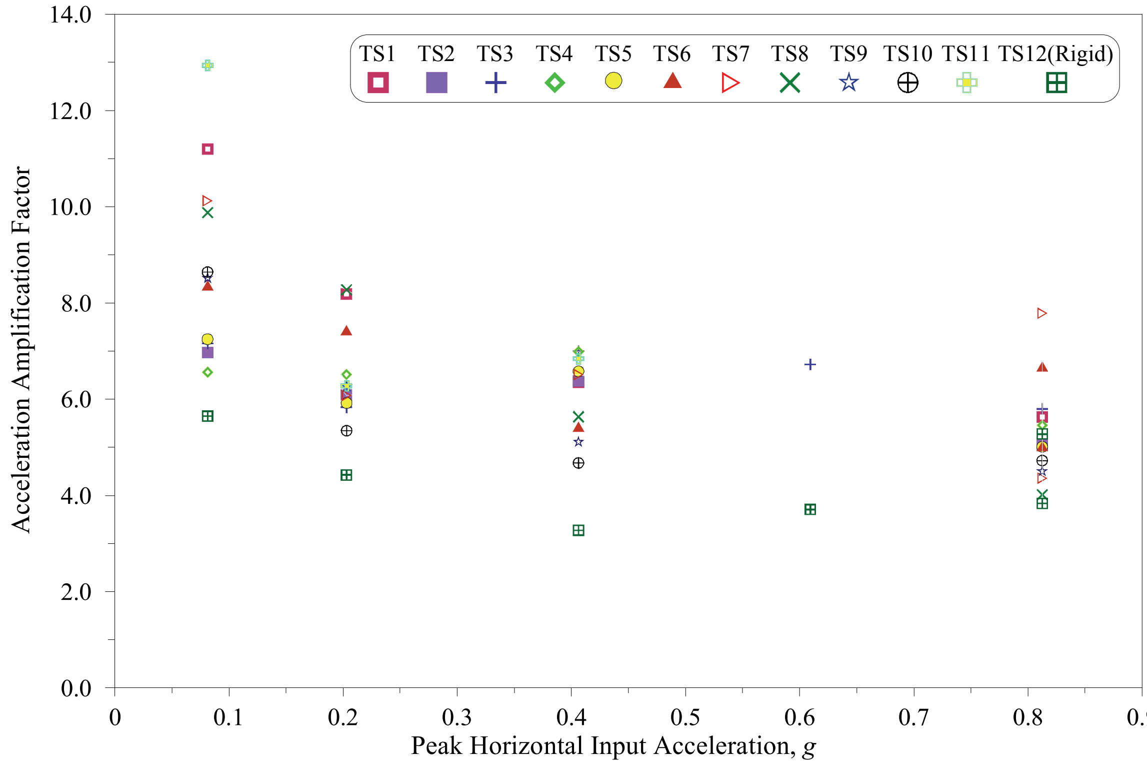

(c) Horizontal *AAF* on Top of Motor Vs. Peak Horizontal Input Acceleration

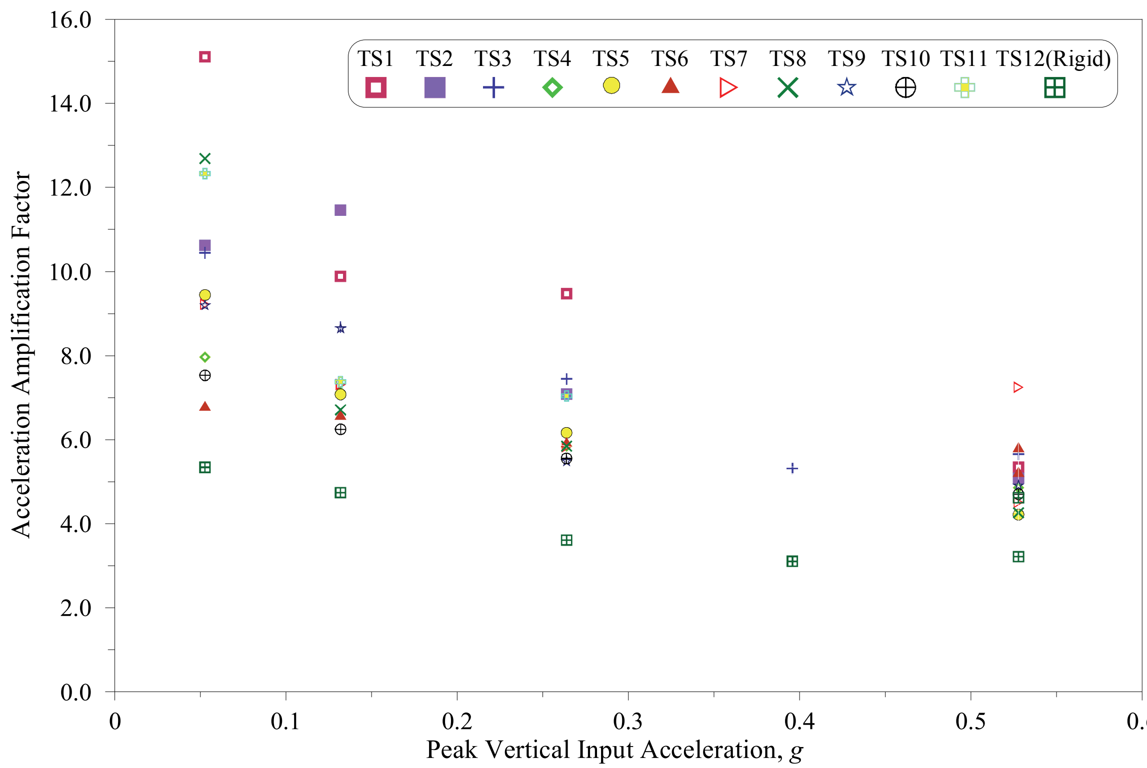

(d) Vertical *AAF* on Top of Motor Vs. Peak Vertical Input Acceleration

Figure 7-1 (cont'd) Variations of *AAF* near Center of Mass of Test Specimen (on Top of Motor) with Peak Input Acceleration

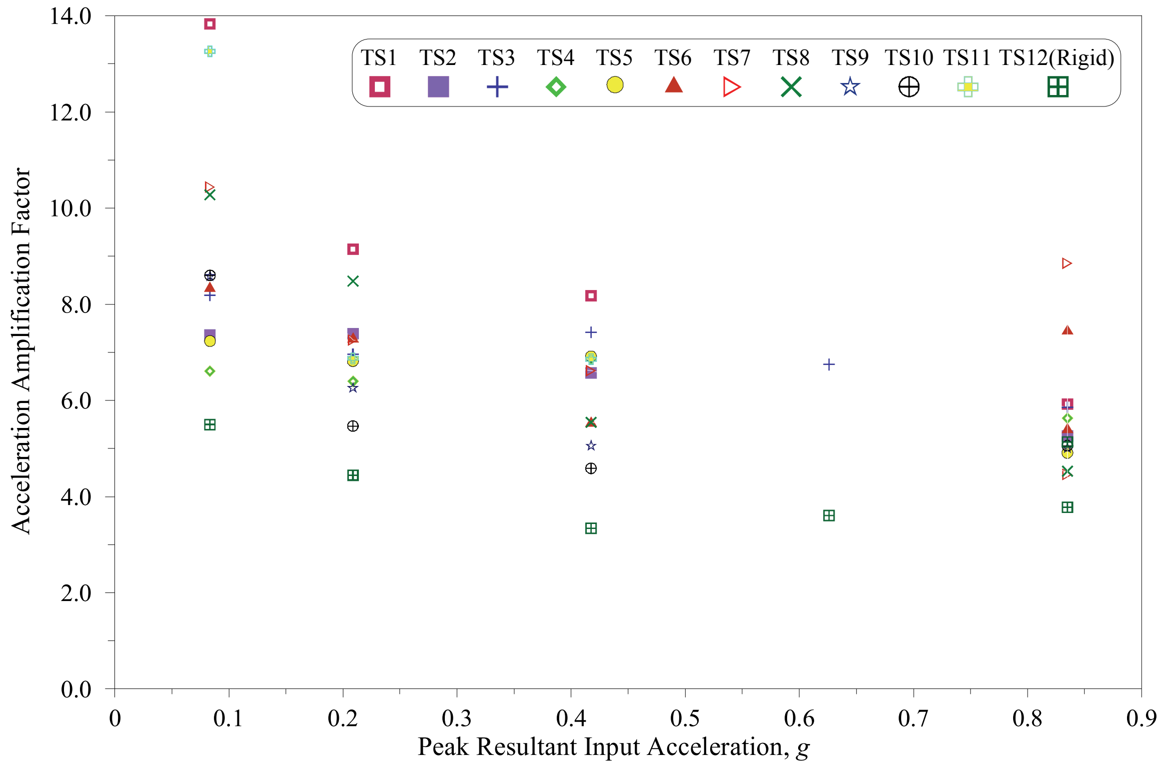

(e) Resultant *AAF* on Top of Motor Vs. Peak Resultant Input Acceleration

Figure 7-1 (cont'd) Variations of *AAF* near Center of Mass of Test Specimen (on Top of Motor) with Peak Input Acceleration

Table 7-1 Maximum *AAF* near Center of Mass of Test Specimen (on Top of Motor), Phase I: Test Series TS1 through TS10

Acceleration Component	Maximum *AAF*	Test Name	Input Motion		Peak Acceleration Response on Top of Motor, *g*
			Amplitude, %	Peak Acceleration, *g*	
Transverse	8.7	TS7-S1	10	0.08	0.69
Longitudinal	9.9	TS7-S1	10	0.08	0.79
Horizontal	11.2	TS1-S1	10	0.08	0.91
Vertical	15.1	TS1-S1	10	0.05	0.80
Resultant	13.8	TS1-S1	10	0.08	1.15

Table 7-2 Minimum *AAF* near Center of Mass of Test Specimen (on Top of Motor), Phase I: Test Series TS1 through TS10

Acceleration Component	Minimum *AAF*	Test Name	Input Motion		Peak Acceleration Response on Top of Motor, *g*
			Amplitude, %	Peak Acceleration, *g*	
Transverse	3.5	TS9-S3	50	0.40	1.41
Longitudinal	3.6	TS8-S4	100	0.79	2.89
Horizontal	4.0	TS8-S4	100	0.81	3.26
Vertical	4.2	TS5-S4	100	0.53	2.23
Resultant	4.5	TS7-S4	100	0.83	3.72

Table 7-3 Maximum Acceleration Responses near Center of Mass of Test Specimen (on Top of Motor), Phase I: Test Series TS1 through TS10

Acceleration Component	Maximum Acceleration Response on Top of Motor, *g*	Test Name	Input Motion		*AAF*
			Amplitude, %	Peak Acceleration, *g*	
Transverse	4.08	TS4-S4	100	0.80	5.1
Longitudinal	4.39	TS4-S4	100	0.79	5.5
Horizontal	4.71	TS3-S5	100	0.81	5.8
Vertical	2.98	TS3-S5	100	0.53	5.7
Resultant	4.94	TS1-S4	100	0.83	5.9

7.1.2 Acceleration Response on Test Specimen Housing

The transverse and longitudinal acceleration responses measured at several points on the intermediate and top level of the test specimen housing were used in Equation 7-1 to calculate the transverse and longitudinal *AAF* on the test specimen housing.

The variations of the transverse and longitudinal *AAF* on the intermediate and top level of the test specimen housing with the corresponding peak input acceleration during the 46 seismic tests of Phase I and the six seismic tests of Phase II of the experiments are presented in Figures 7-2 and 7-3, respectively.

The maximum *AAF*, minimum *AAF*, and maximum acceleration responses on the intermediate and top level of the test specimen housing during the seismic tests of Phase I are listed in Tables 7-4 through 7-6, respectively. To find the extreme values presented in these tables, results of Test Series TS11 (the test series conducted without rubber snubbers), Seismic Tests TS6-S4 (the test during which the test specimen housing was damaged), and TS7-S5 (the test conducted after activation of the isolation systems inside the fan module) were not considered. On the intermediate level of the housing of the isolated test specimen, the transverse and longitudinal *AAF* varied in the range of 3.4 to 12.7 and 2.8 to 6.5, respectively. On the top level of the housing of the isolated test specimen, the transverse and longitudinal *AAF* varied in the range of 4.0 to 13.4 and 2.8 to 7.3, respectively. The acceleration response and its variation range along the height of the housing of the isolated test specimen were larger in the transverse direction than in the longitudinal direction.

With the peak transverse and longitudinal input acceleration limited to 0.80 *g* and 0.79 *g* in the seismic tests, the transverse and longitudinal acceleration responses of the housing of the isolated test specimen exceeded 5.70 *g* and 3.90 *g*, respectively. As it is seen in Table 7-4, even with the 10%-amplitude input motion, the transverse acceleration response on the housing of the isolated test specimen exceeded 1.0 *g*.

The *AAF* on the housing of the isolated test specimen varied with a change in the input motion amplitude or with a change in the restraint component properties. However, the sensitivity of the acceleration response on the housing of the isolated test specimen to the changes in the restraint component properties decreased with an increase of the input motion amplitude. The housing of the test specimen mounted on the I/R systems with large gap size (Test Series TS5 and TS6) or without rubber snubbers (Test Series TS11) experienced the largest acceleration responses throughout the experiments.

During most of the seismic tests of Phase I, when the input motion amplitude was high enough to engage the restraint components of the I/R systems, the *AAF* on the test specimen housing decreased with an increase of the input motion amplitude. The peak acceleration responses on the test specimen housing, on the other hand, always increased with an increase of the input motion amplitude. The maximum acceleration responses on the housing of the isolated test specimen during each test series were always experienced in the test with the full-scale input motion.

As seen in Figure 7-2, during the six seismic tests of Phase II of the experiments, the transverse and longitudinal *AAF* on the housing of the rigidly mounted test specimen varied in the range of 1.5 to 3.2, and 1.2 to 2.1, respectively. The comparison of the *AAF* on the top of the motor and on top of the housing obtained during both phases of the experiments shows that the acceleration responses have been larger on the top level of the housing than on the top of the motor.

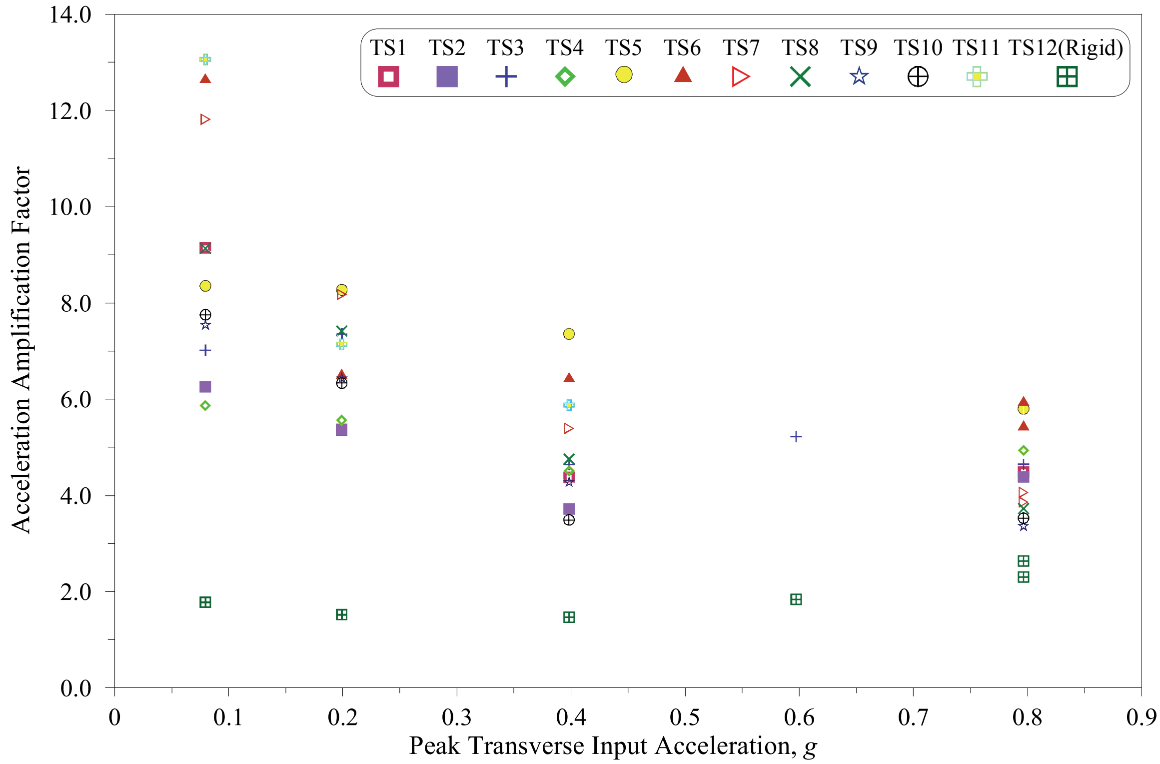

(a) Intermediate Level

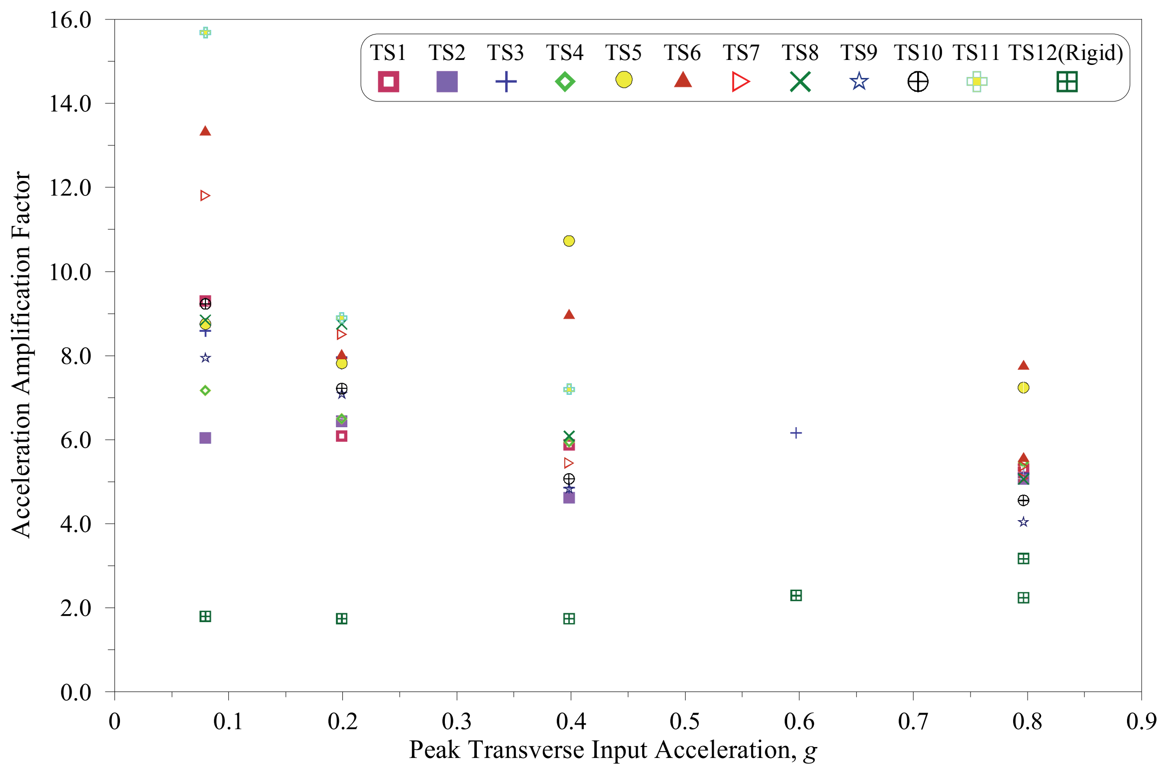

(b) Top Level

Figure 7-2 Variations of *AAF* on Test Specimen Housing with Peak Input Acceleration, Transverse Direction

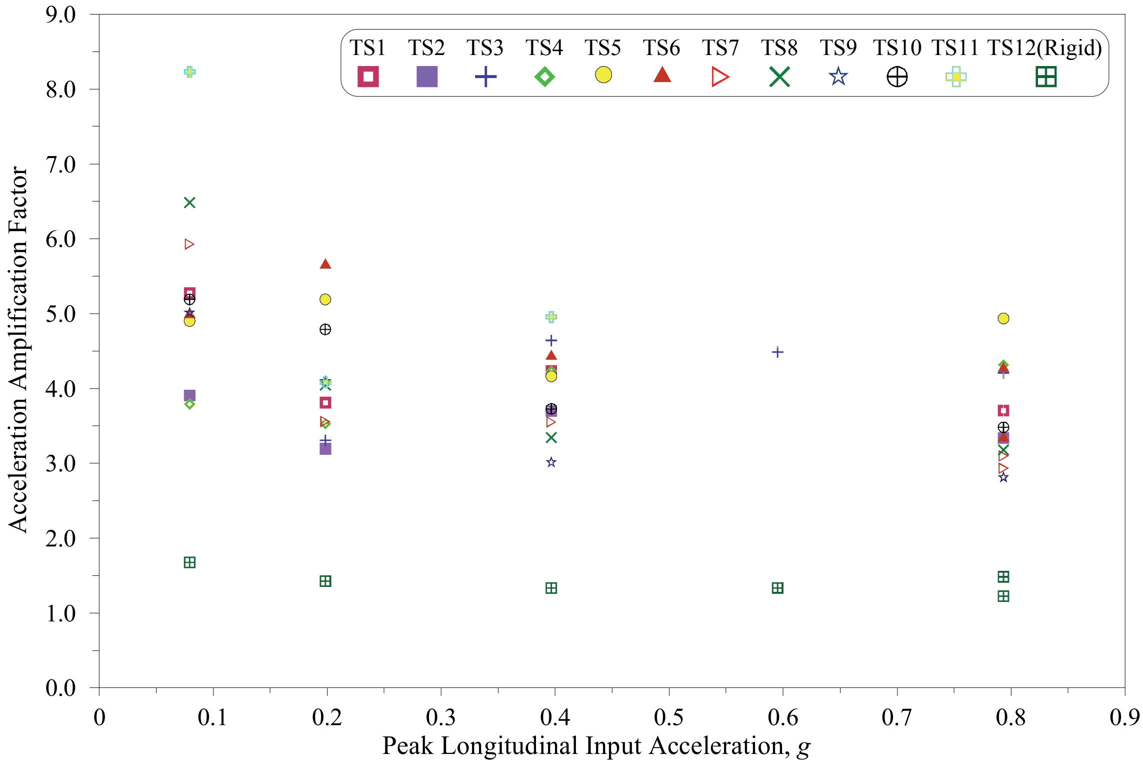

(a) Intermediate Level

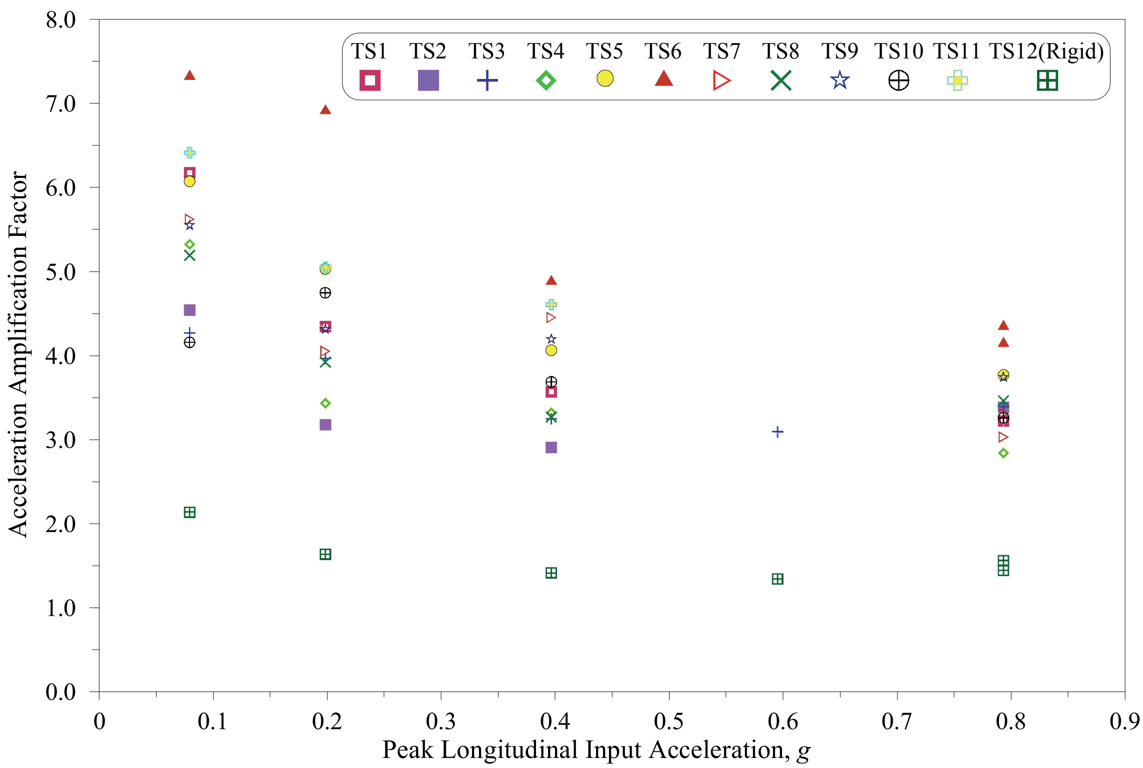

(b) Top Level

Figure 7-3 Variations of *AAF* on Test Specimen Housing with Peak Input Acceleration, Longitudinal Direction

Table 7-4 Maximum *AAF* on Test Specimen Housing, Phase I: Test Series TS1 through TS10

Direction	Level	Maximum *AAF*	Test Name	Input Motion		Peak Acceleration Response on Test Specimen Housing, *g*
				Amplitude, %	Peak Acceleration, *g*	
Transverse	Intermediate	12.7	TS6-S1	10	0.08	1.01
	Top	13.4	TS6-S1	10	0.08	1.06
Longitudinal	Intermediate	6.5	TS8-S1	10	0.08	0.51
	Top	7.3	TS6-S1	10	0.08	0.58

Table 7-5 Minimum *AAF* on Test Specimen Housing, Phase I: Test Series TS1 through TS10

Direction	Level	Minimum *AAF*	Test Name	Input Motion		Peak Acceleration Response on Test Specimen Housing, *g*
				Amplitude, %	Peak Acceleration, *g*	
Transverse	Intermediate	3.4	TS9-S4	100	0.80	2.67
	Top	4.0	TS9-S4	100	0.80	3.22
Longitudinal	Intermediate	2.8	TS9-S4	100	0.79	2.23
	Top	2.8	TS4-S4	100	0.79	2.25

Table 7-6 Maximum Horizontal Acceleration Responses on Test Specimen Housing, Phase I: Test Series TS1 through TS10

Direction	Level	Maximum Acceleration Response on Test Specimen Housing, *g*	Test Name	Input Motion		*AAF*
				Amplitude, %	Peak Acceleration, *g*	
Transverse	Intermediate	4.62	TS5-S4	100	0.80	5.8
	Top	5.77	TS5-S4	100	0.80	7.2
Longitudinal	Intermediate	3.91	TS5-S4	100	0.79	4.9
	Top	3.30	TS6-S5	100	0.79	4.2

7.1.3 Relative Displacement Response of Isolated Test Specimen

The absolute displacement responses of the nine instrumented locations on the south face of the test specimen and one instrumented location on the earthquake-simulator extension platform during the seismic tests were used to calculate the relative displacement response at three levels on the south face of the isolated test specimen. Figures 7-4 and 7-5 show the triaxial relative displacement response histories at the top-south-east corner of the isolated test specimen (channel #120, shown in Figure 4-10 and listed in Table 4-4) during Seismic Tests TS1-S4 and TS8-S1, respectively. These figures are useful to compare the displacement responses of the isolated test specimen during a test with the high amplitude input motion (TS1-S4) and during a test with the low amplitude input motion (TS8-S1).

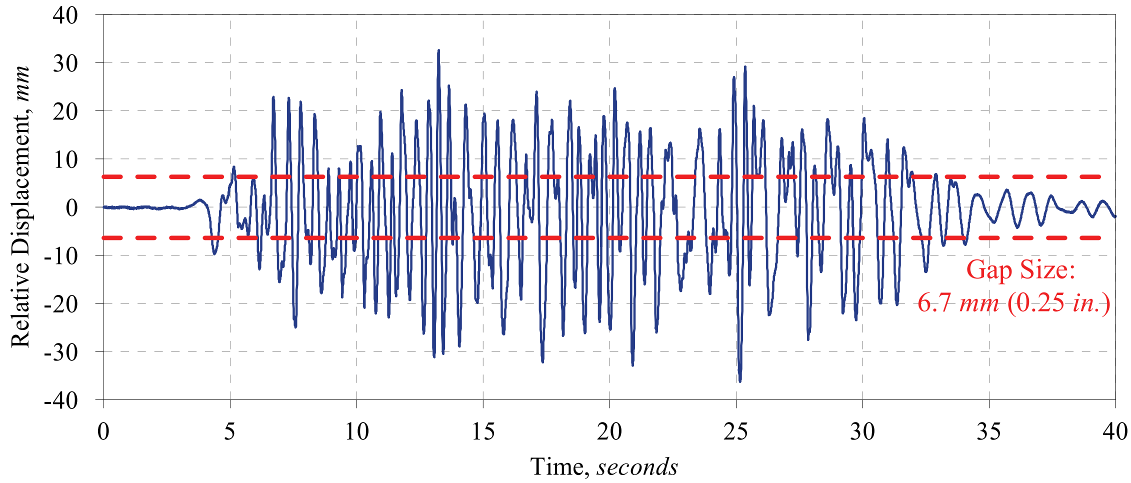

(a) Transverse Direction

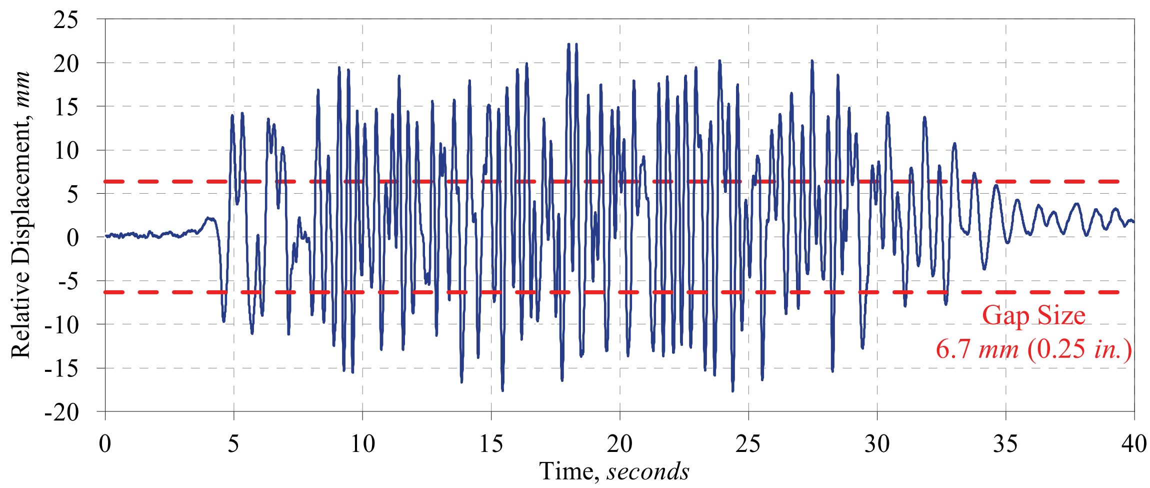

(b) Longitudinal Direction

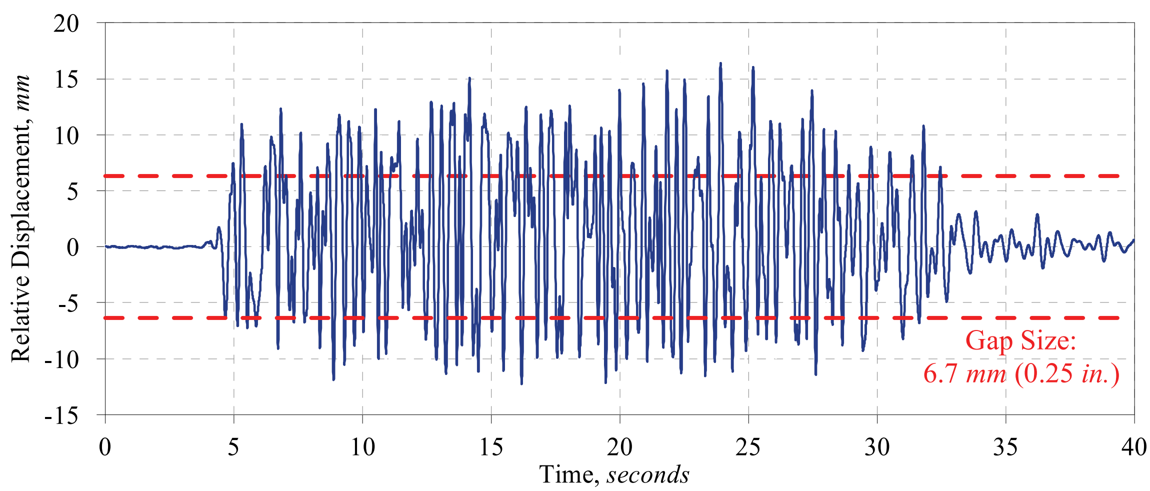

(c) Vertical Direction

Figure 7-4 Triaxial Relative Displacement Response Histories, Top-South-East Corner of Isolated Test Specimen, Seismic Test TS1-S4 (Full-Scale Input Motion)

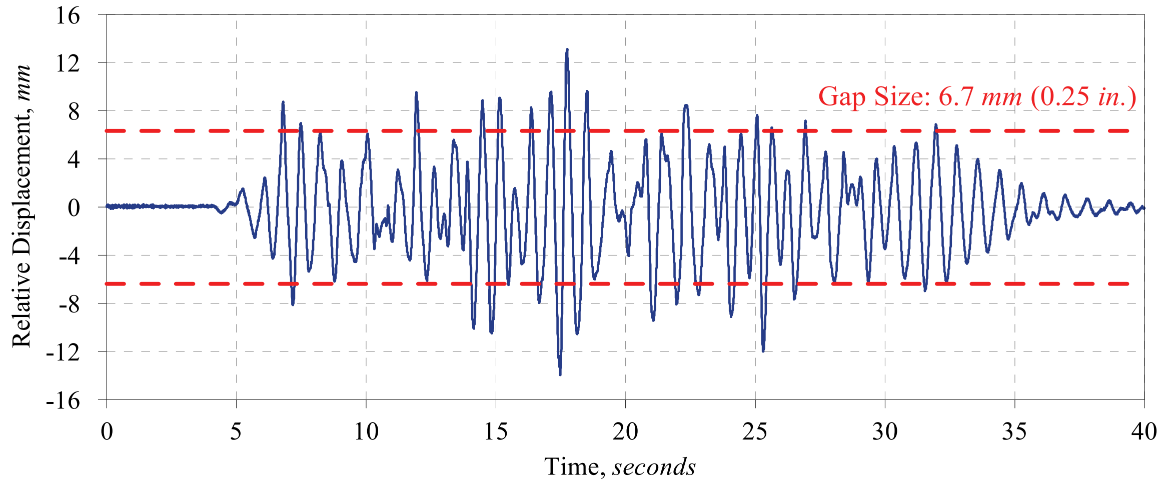

(a) Transverse Direction

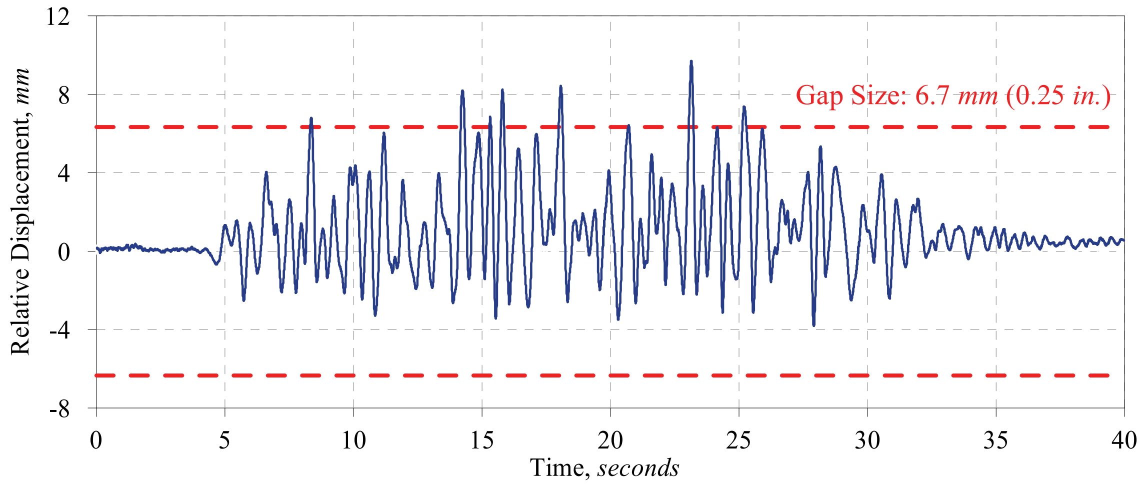

(b) Longitudinal Direction

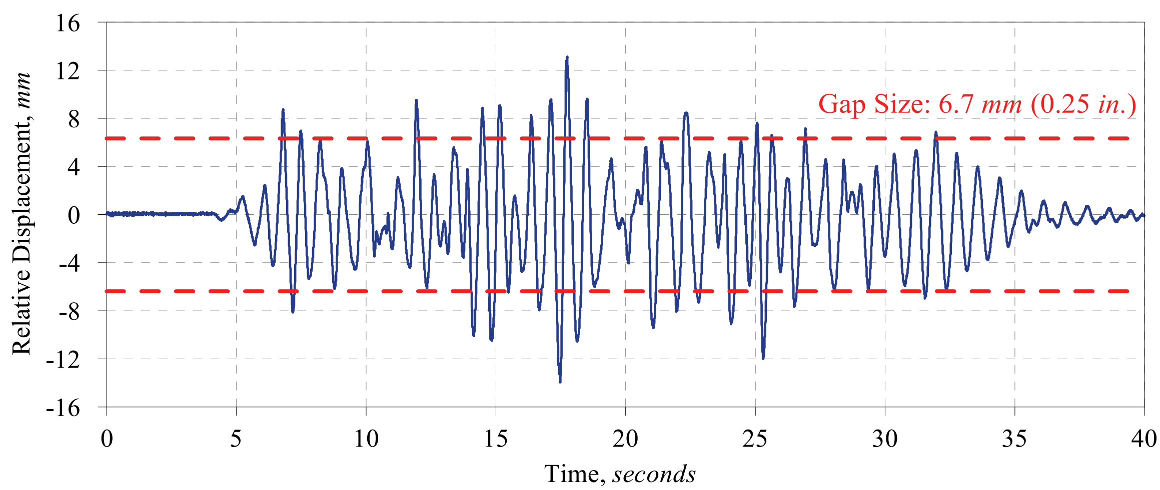

(c) Vertical Direction

Figure 7-5 Triaxial Relative Displacement Response Histories, Top-South-East Corner of Test Specimen, Seismic Test TS8-S1 (10%-Amplitude Input Motion)

If the isolated test specimen experienced only translation (no rotation) and the snubbers were incompressible, the relative displacement histories shown in Figures 7-4 and 7-5 would have been limited to the dashed lines representing the limits of the gap size. However, the seismic response of the isolated test specimen was always a combination of translation and rotation. Moreover, during the temporary engagement of the restraint components of the I/R systems, the rubber snubbers were compressed. Therefore, in most of the seismic tests, the relative displacement response measured on the south face of the isolated test specimen exceeded the gap size. In order to compare the peak relative displacement response of the isolated test specimen to the gap size of the restraint components, a dimensionless Relative Displacement Response Ratio (*RDRR*) can be defined as:

$$RDRR = \frac{\text{Peak Relative Displacement Response}}{\text{Gap Size}} \quad (7\text{-}4)$$

Figures 7-6 through 7-8 show the variations of the transverse, longitudinal, and vertical *RDRR* at the top and bottom of the southeast edge of the isolated test specimen with the corresponding peak input acceleration during the 46 seismic tests of Phase I of the experiments. The dashed lines in Figures 7-6 through 7-8, crossing the *RDRR* axis at value 1.0, corresponds to the peak relative displacement response equal to the gap size of the restraint component. As seen in these figures, the peak relative displacement response on the south face of the isolated test specimen during some of the seismic tests was six times larger than the gap size.

The comparison of the results for the *RDRR* in the three orthogonal directions shows that the displacement response of the isolated test specimen has been larger in the transverse direction than in the other two directions. Furthermore, the comparison of the *RDRR* on the top and bottom levels of the south face of the isolated test specimen shows that because of the rotational responses of the test specimen, the displacement response amplitude was proportionate to the elevation from the support locations.

The peak relative displacement response of the isolated test specimen was sensitive to a change of the input motion amplitude or to a change in the restraint component properties. The peak relative displacement responses of the isolated test specimen generally increased with an increase of any of the followings: the input motion amplitude, gap size, rubber snubber thickness, or softness.

The maximum and minimum relative displacement responses measured on the south face of the test specimen housing during the seismic tests of Phase I are listed in Tables 7-7 through 7-8, respectively. To find the extreme values presented in these tables, results of Test Series TS11 (the test series conducted without rubber snubbers), Seismic Tests TS6-S4 (the test during which the test specimen housing was damaged), and TS7-S5 (the test conducted after activation of the isolation systems inside the fan module) were not considered. During the seismic tests of Test Series TS6 and TS5 (gap size of the restraint component adjusted to 13 *mm* (0.5 *in.*)), the peak transverse, longitudinal, and vertical relative displacement response on the south face of the test specimen exceeded 45, 37, and 31 *mm* (1.8, 1.5, and 1.2 *in.*), respectively.

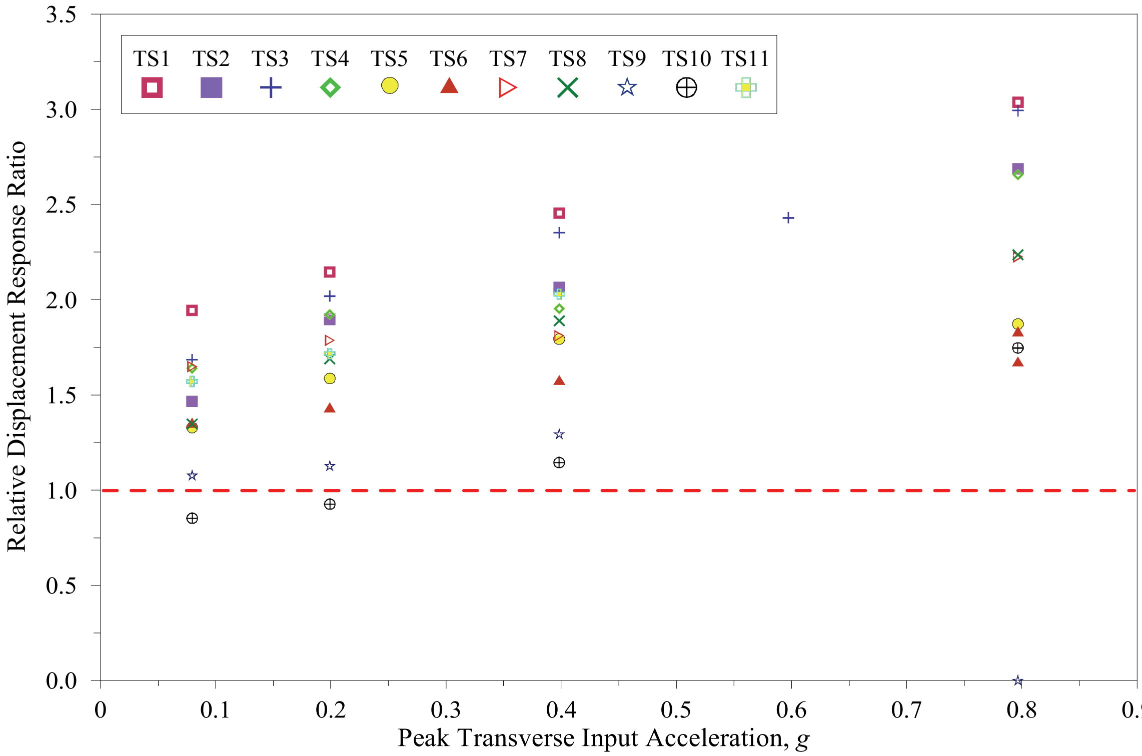

(a) Bottom Level

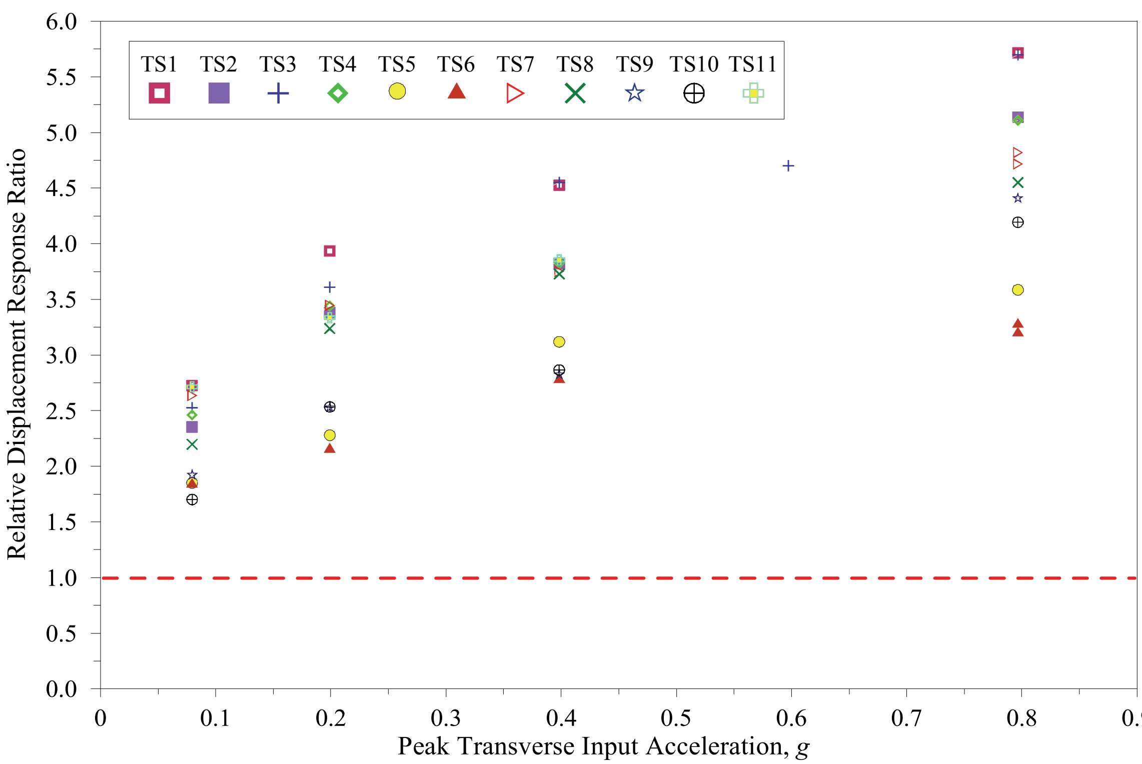

(b) Top Level

Figure 7-6 Variations of Transverse *RDRR* along South-East Edge of Test Specimen with Peak Transverse Input Acceleration

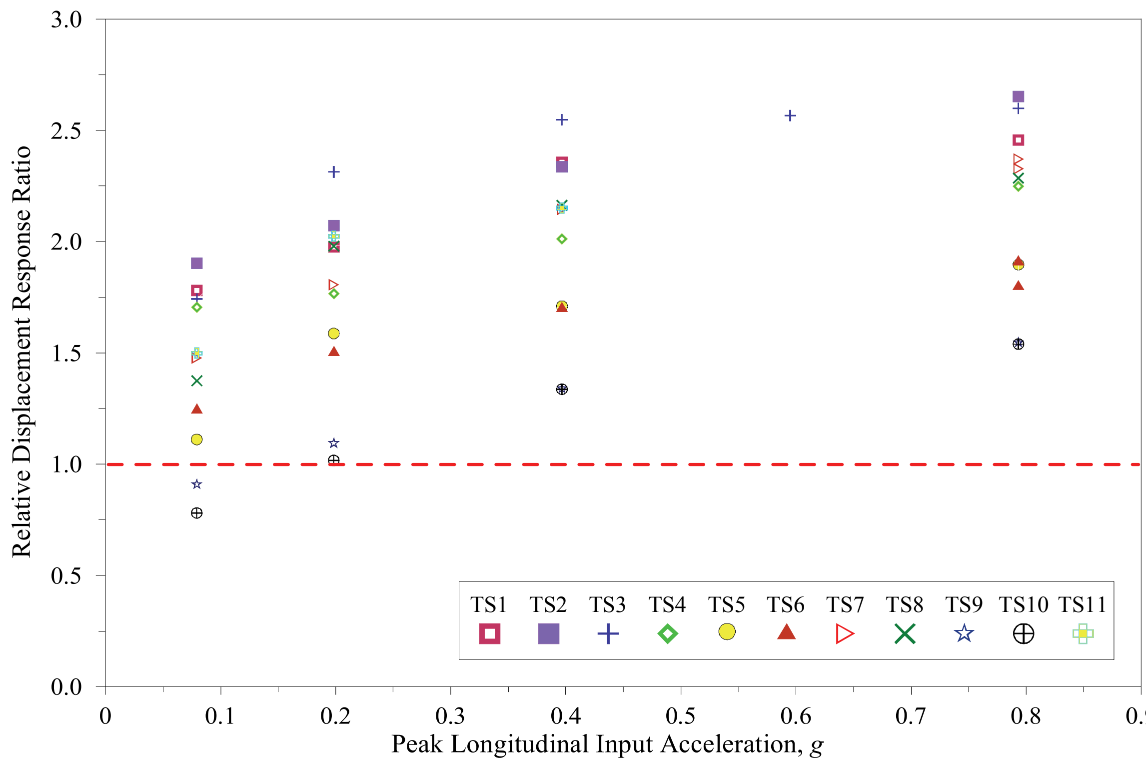

(a) Bottom Level

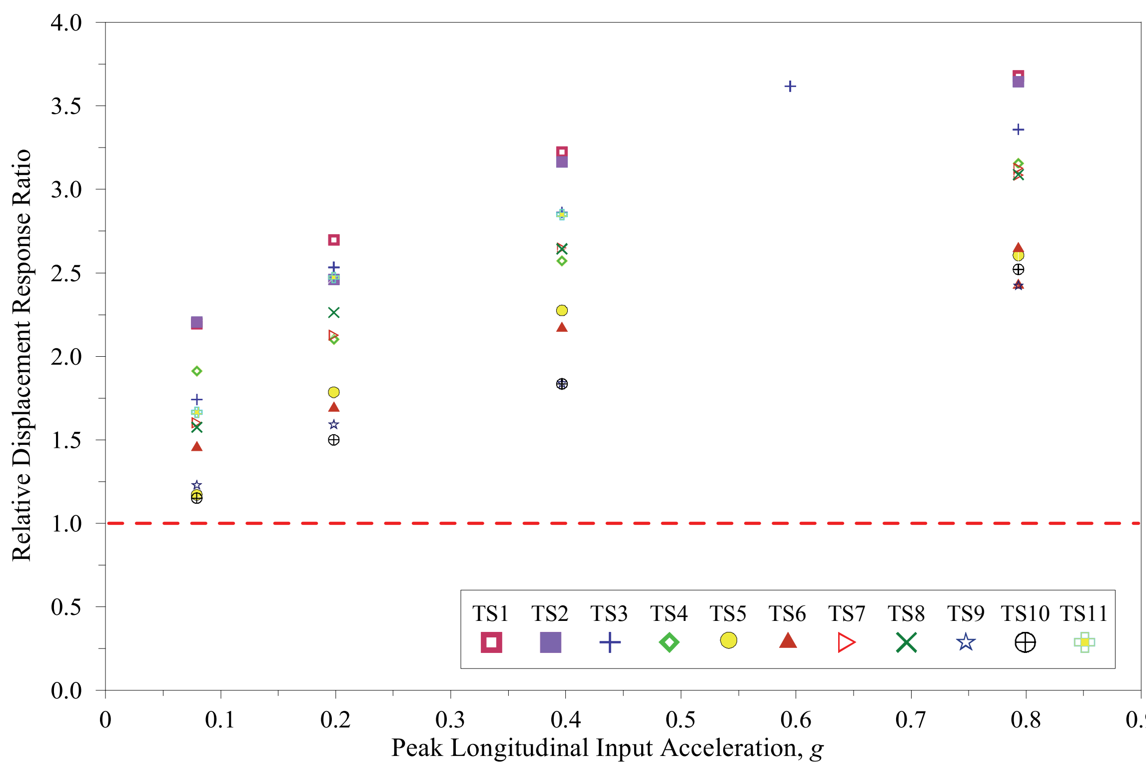

(b) Top Level

Figure 7-7 Variations of Longitudinal *RDRR* along South-East Edge of Test Specimen with Peak Longitudinal Input Acceleration

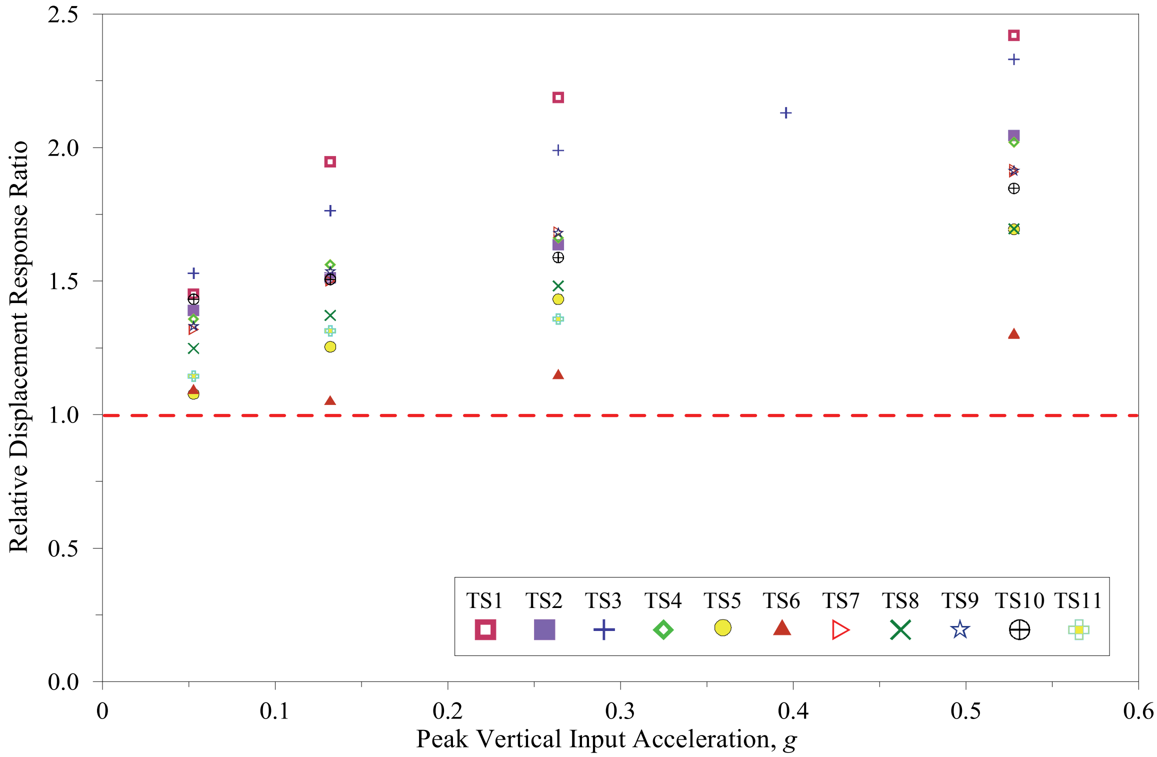

(a) Bottom Level

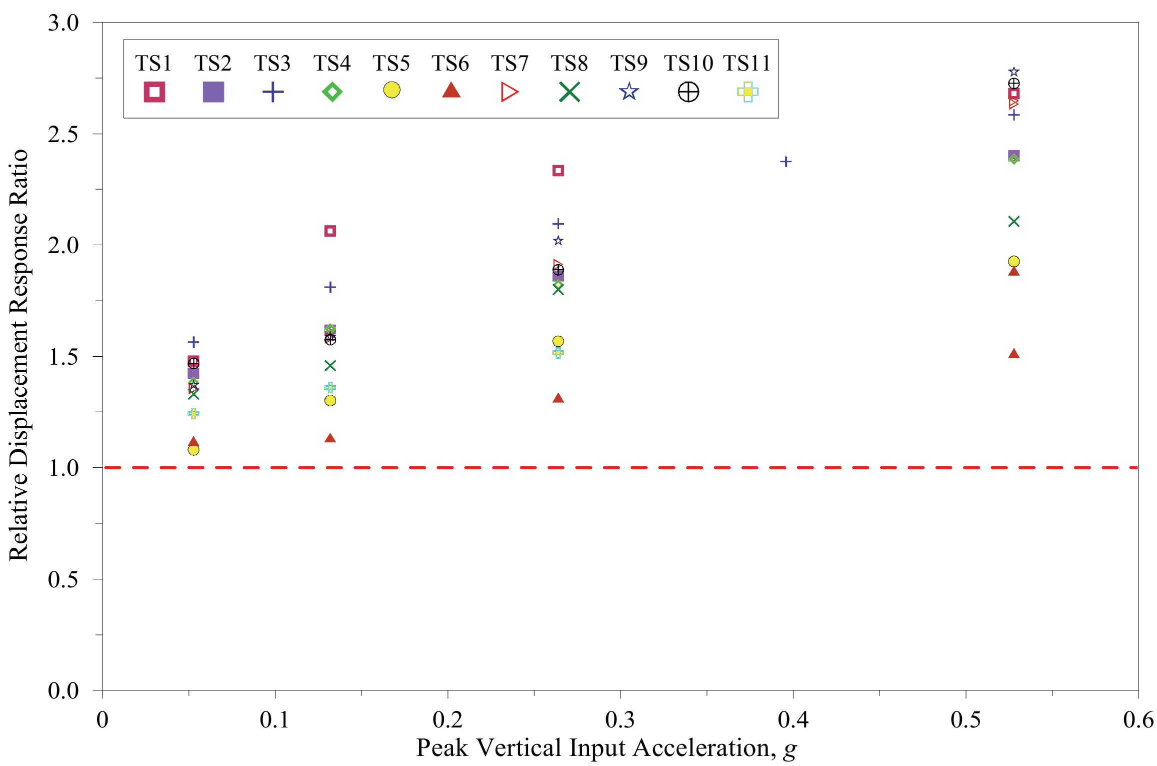

(b) Top Level

Figure 7-8 Variations of Vertical RDRR along South-East Edge of Test Specimen with Peak Vertical Input Acceleration

Table 7-7 Maximum Relative Displacement Response on Top Level of South Face of Test Specimen, Phase I: Test Series TS1 trough TS10

Direction	Maximum Relative Displacement Response, *mm*	Test Name	Input Motion	
			Amplitude, %	Peak Acceleration, *g*
Transverse	45.8	TS5-S4	100	0.80
Longitudinal	37.6	TS5-S4	100	0.79
Vertical	31.1	TS6-S5	100	0.53

Table 7-8 Minimum Relative Displacement Response on Top Level of South Face of Test Specimen, Phase I: Test Series TS1 trough TS10

Direction	Minimum Relative Displacement Response, *mm*	Test Name	Input Motion	
			Amplitude, %	Peak Acceleration, *g*
Transverse	10.4	TS10-S1	10	0.08
Longitudinal	7.0	TS9-S1	10	0.08
Vertical	6.9	TS9-S1	10	0.05

7.2 Isolation/Restraint Systems Response

The response quantities measured at the support locations during the seismic tests including the triaxial acceleration responses, and the dynamic forces are analyzed in this section.

7.2.1 Acceleration Response on Top Level of Isolation/Restraint Systems

The variations of the transverse, longitudinal, and vertical *AAF* on the top level of the six I/R systems during the 46 seismic tests of Phase I are presented in Figures 7-9 through 7-11, respectively. In these figures, the dashed lines crossing the *AAF* axis at value 1.0 correspond to the *AAF* at the support locations of the rigidly mounted test specimen.

The maximum *AAF*, minimum *AAF*, and maximum acceleration responses on the top level of the I/R systems during the seismic tests of Phase I are listed in Tables 7-9 through 7-11, respectively. To find the extreme values presented in these tables, results of Test Series TS11 (the test series conducted without rubber snubbers), Seismic Tests TS6-S4 (the test during which the test specimen housing was damaged), and TS7-S5 (the test conducted after activation of the isolation systems inside the fan module) were not considered. The transverse, longitudinal, and vertical *AAF* on the top level of the I/R systems varied in the range of 2.9 to 17.3, 2.7 to 9.5, and 4.2 to 27, respectively. With the peak transverse, longitudinal, and vertical input acceleration limited to 0.80 *g*, 0.79 *g*, and 0.53*g*, respectively, in the seismic tests, the transverse, longitudinal, and vertical acceleration responses on the top level of I/R systems exceeded 7.6 *g*, 6.7 *g*, and 6.3 *g*, respectively.

During some of the test series, even with the 25%-amplitude input motion, the peak acceleration responses experienced on the top level of the I/R systems exceeded their design peak acceleration (3.0 *g*). However, due the safety factors used in the design of the I/R systems, their actual capacity was larger than their nominal (static design) capacity, and they were not damaged during the experiments.

The *AAF* on the top level of the I/R systems varied with a change in the input motion amplitude or with a change in the restraint component properties. However, the sensitivity of the acceleration responses on top level of the I/R systems to changes in the restraint component properties decreased with an increase of the input motion amplitude. Among different I/R systems tested in 11 test series, the I/R systems with the large gap size (Test Series TS5 and TS6) or without rubber snubbers (Test Series TS11) experienced the highest acceleration responses on their top level.

The *AAF* was larger on the top level of the I/R systems than on top of the motor near the center of mass of the test specimen. This was mainly attributed to the rotational responses of the test specimen. The dynamic forces induced into the restraint components created translational acceleration responses at the support locations, but they created translational and rotational acceleration responses at the center of mass or other points of the test specimen. Therefore, the highest translational acceleration responses were always experienced at the support location where the peak dynamic forces where applied to the test specimen. Moreover, from an energy point of view, the energy of the impacts created in the restraint component at the support location was always partially absorbed by the test specimen housing and other components. Therefore, the energy induced on the top of the motor was always a fraction of the energy imparted at the support locations.

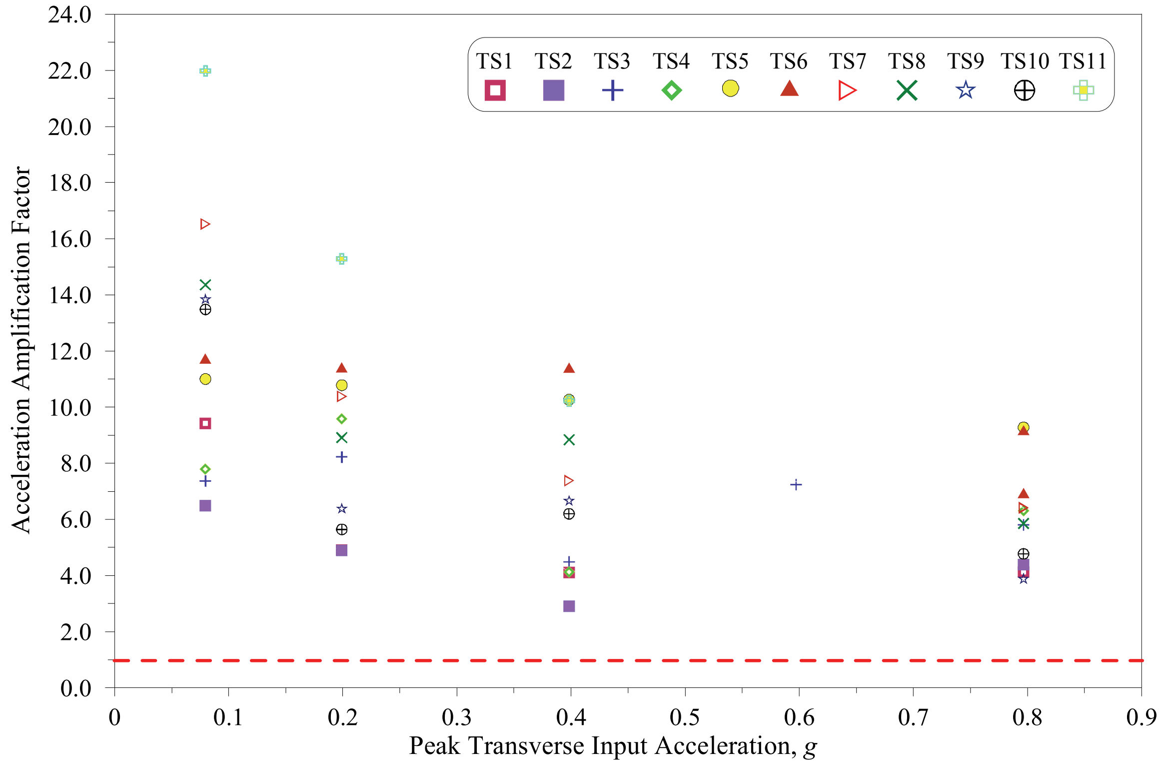

(a) I/R System #1

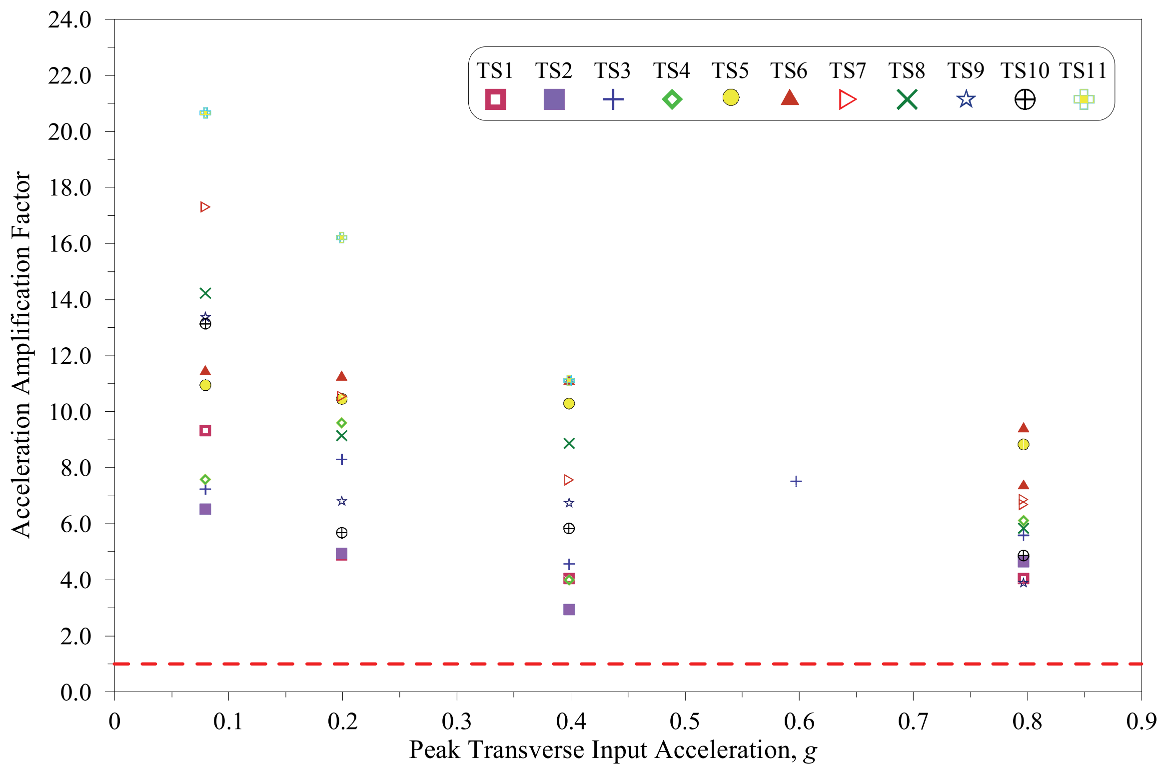

(b) I/R System #2

Figure 7-9 Variations of Transverse *AAF* on Top Level of I/R Systems with Peak Transverse Input Acceleration

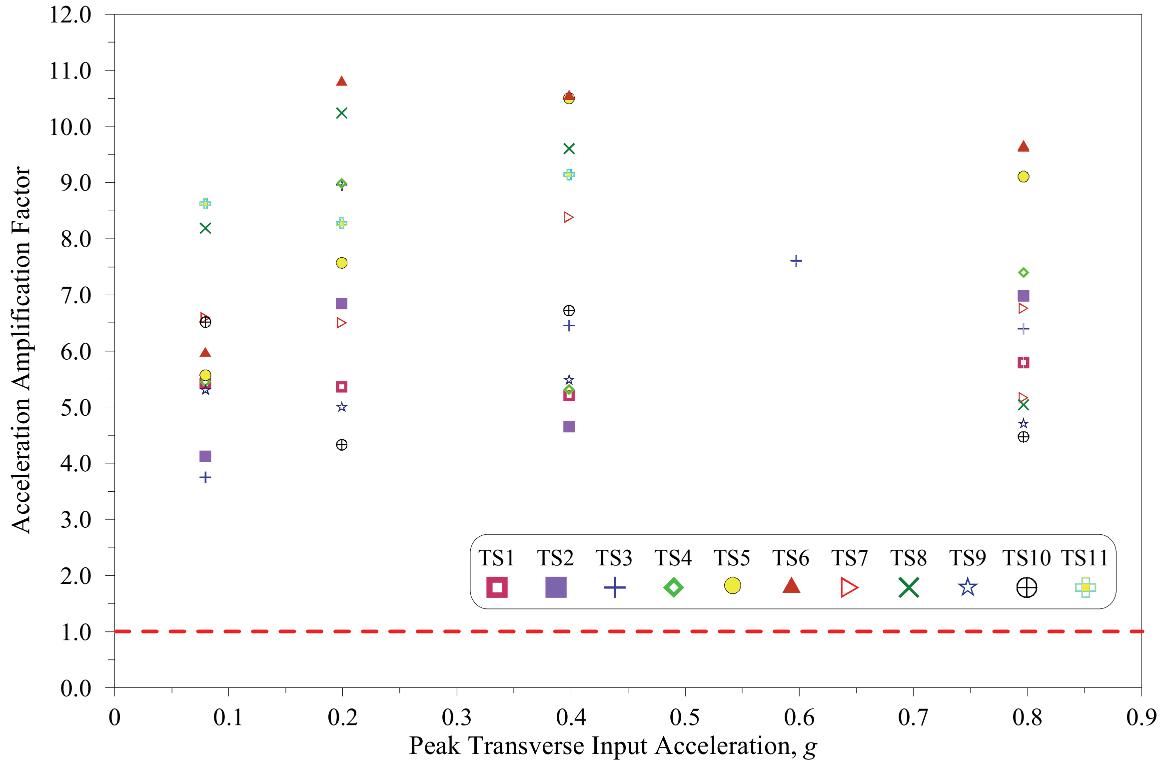

(c) I/R System #3

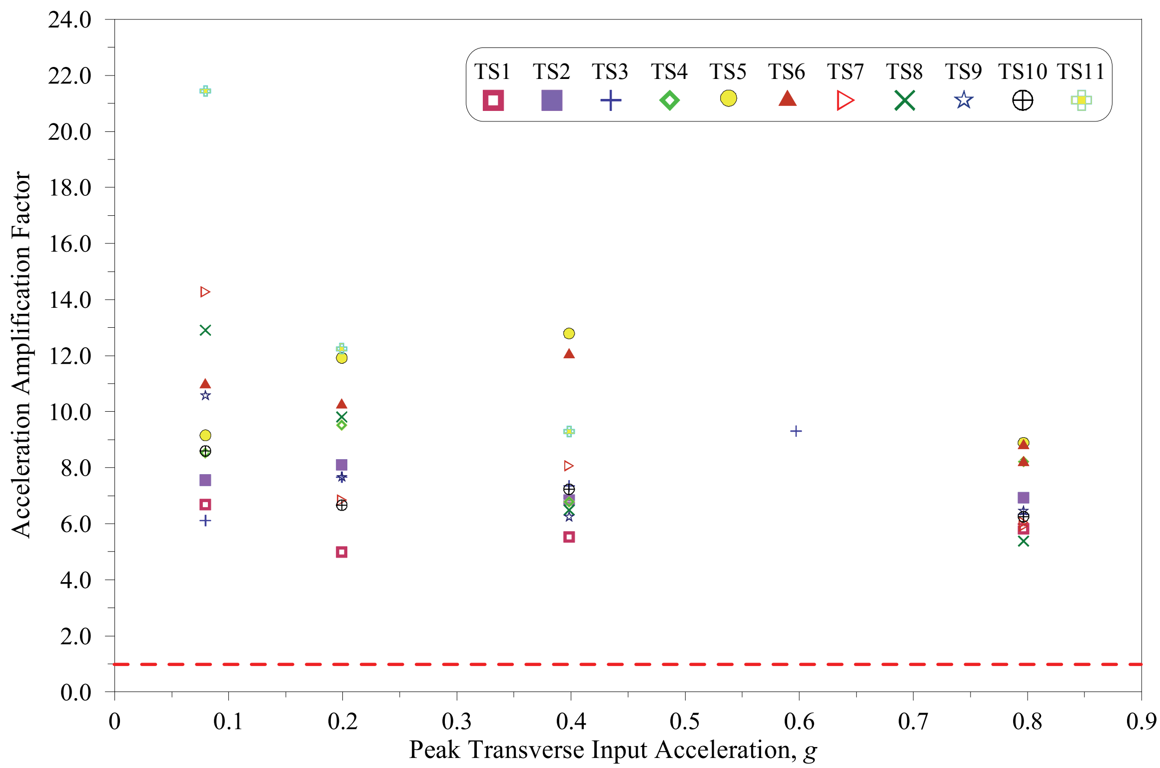

(d) I/R System #4

Figure 7-9 (cont'd) Variations of Transverse *AAF* on Top Level of I/R Systems with Peak Transverse Input Acceleration

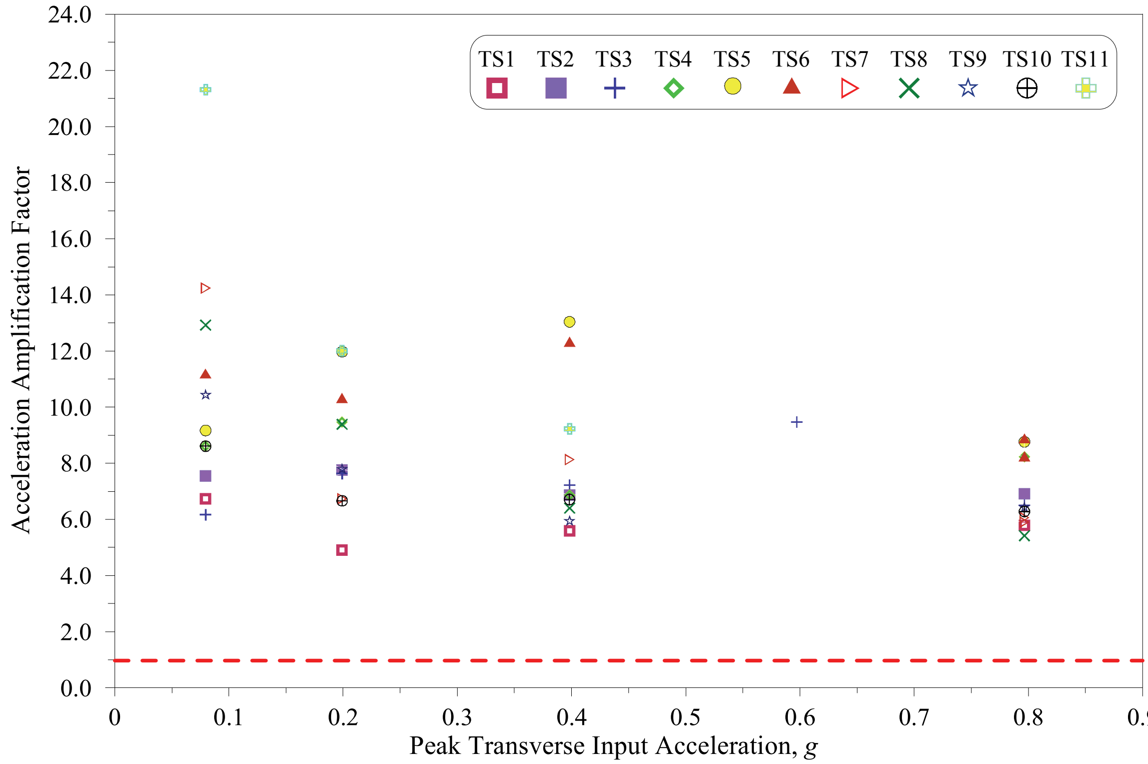

(e) I/R System #5

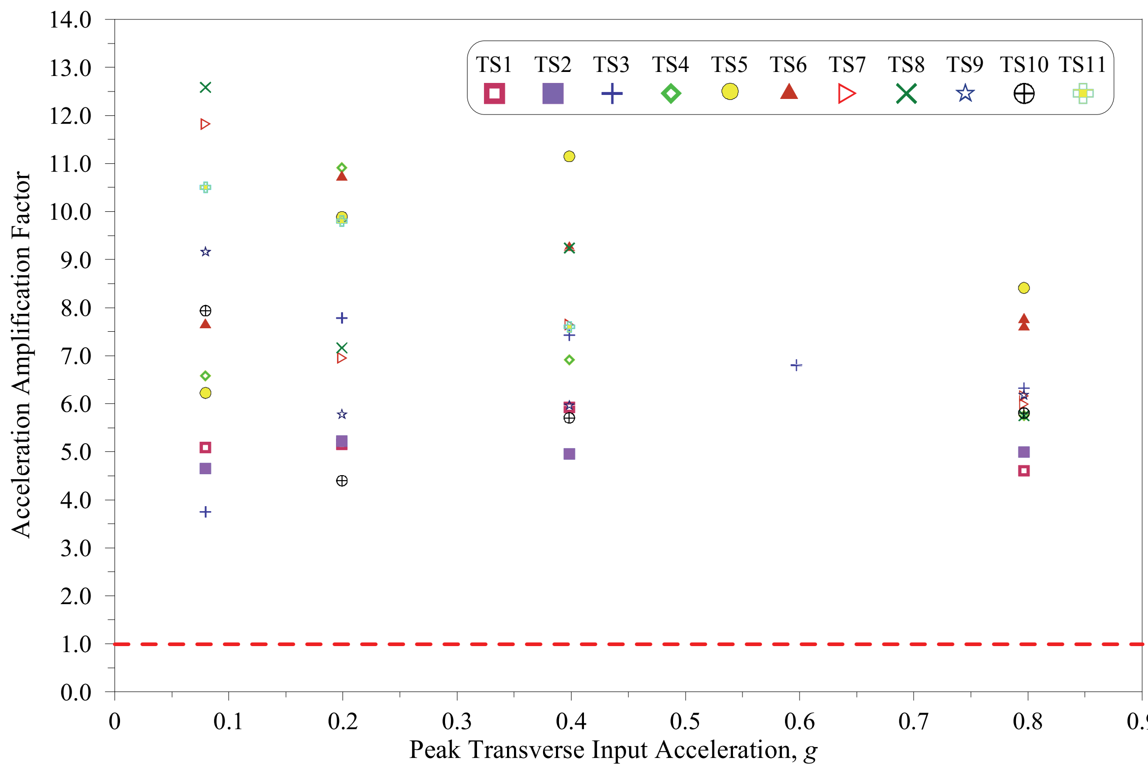

(f) I/R System #6

Figure 7-9 (cont'd) Variations of Transverse *AAF* on Top Level of I/R Systems with Peak Transverse Input Acceleration

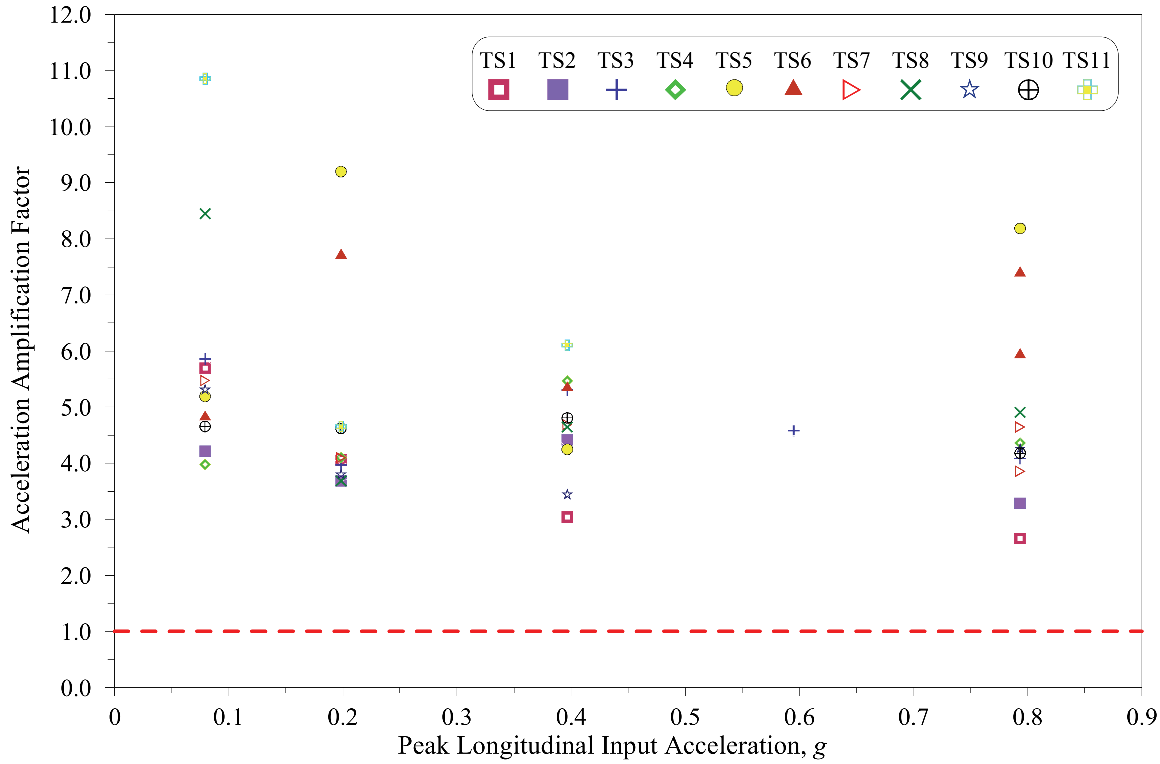

(a) I/R System #1

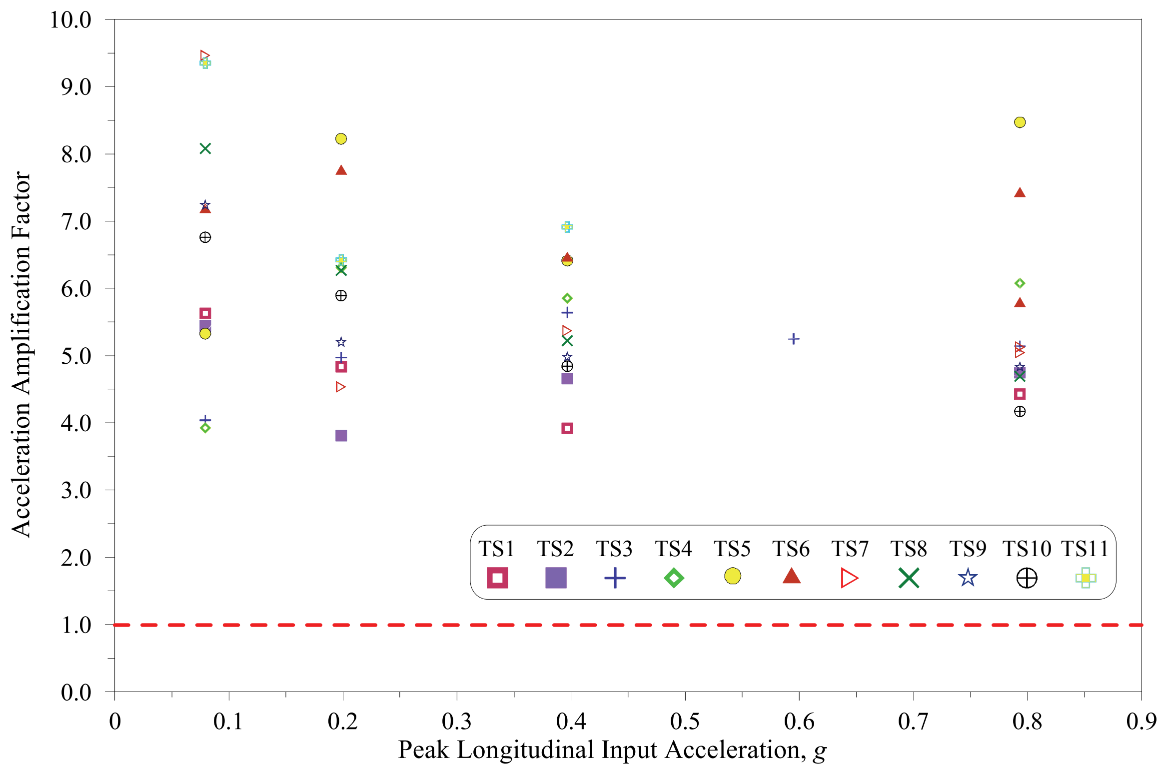

(b) I/R System #2

Figure 7-10 Variations of Longitudinal *AAF* on Top Level of I/R Systems with Peak Longitudinal Input Acceleration

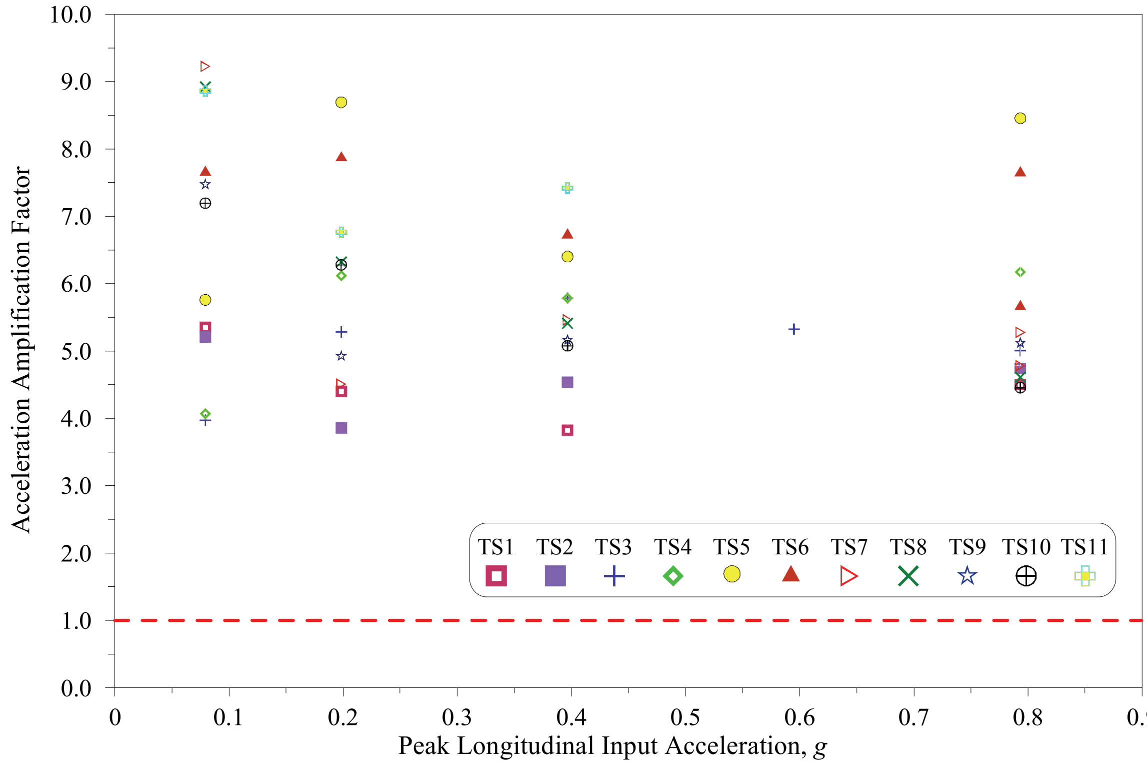

(c) I/R System #3

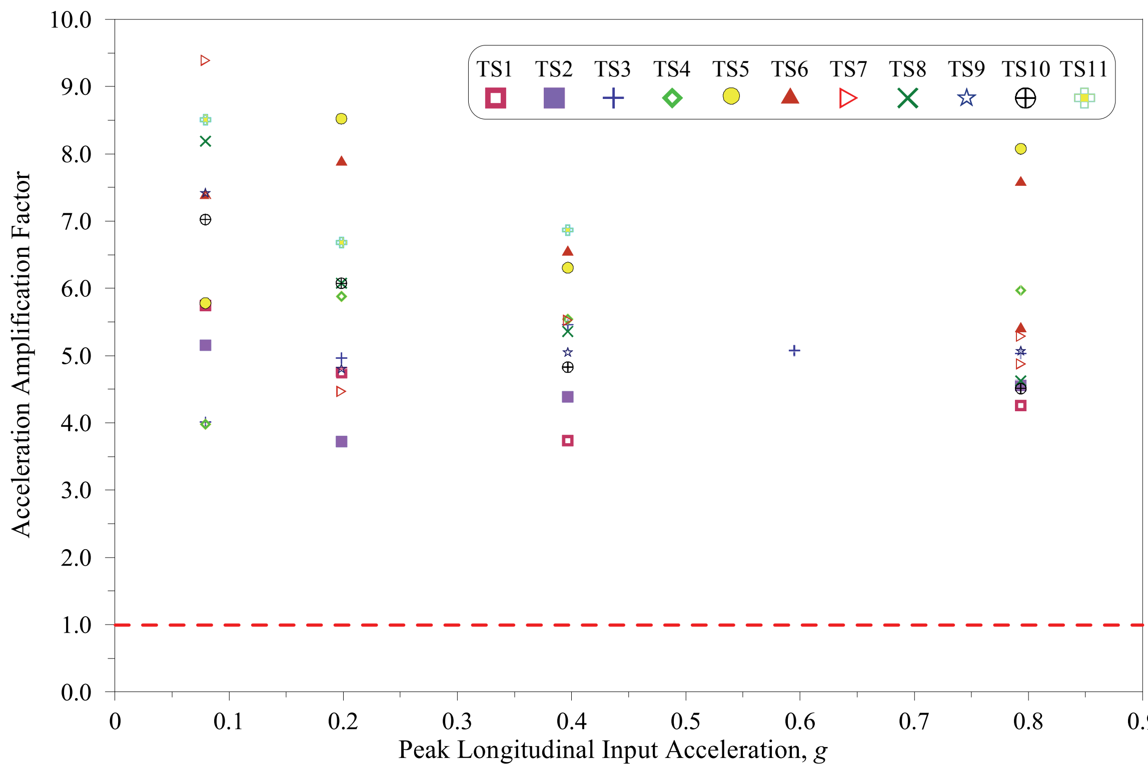

(d) I/R System #4

Figure 7-10 (cont'd) Variations of Longitudinal *AAF* on Top Level of I/R Systems with Peak Longitudinal Input Acceleration

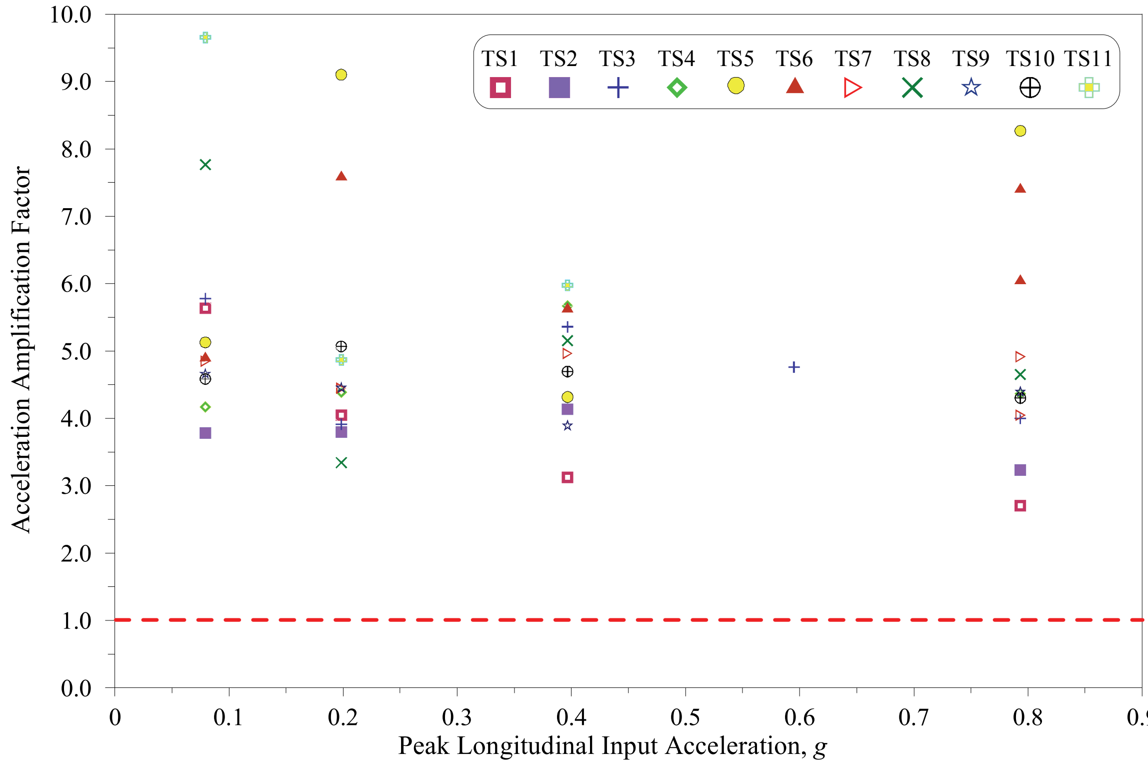

(e) I/R System #5

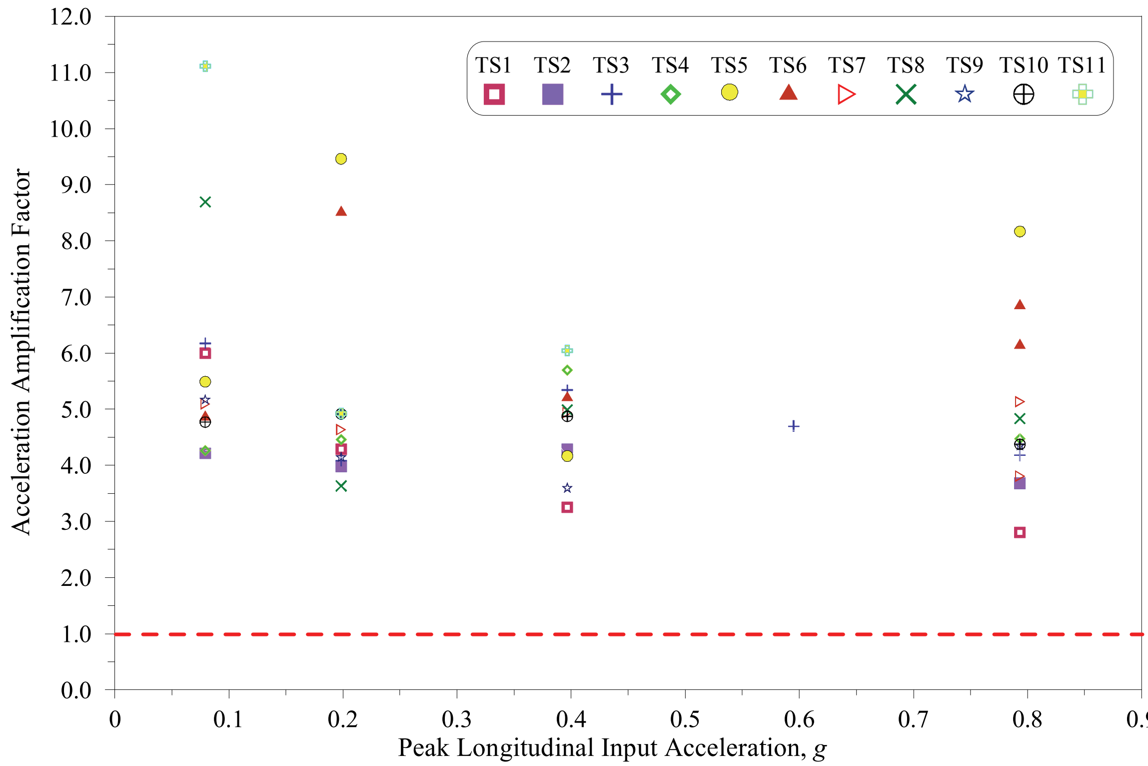

(f) I/R System #6

Figure 7-10 (cont'd) Variations of Longitudinal *AAF* on Top Level of I/R Systems with Peak Longitudinal Input Acceleration

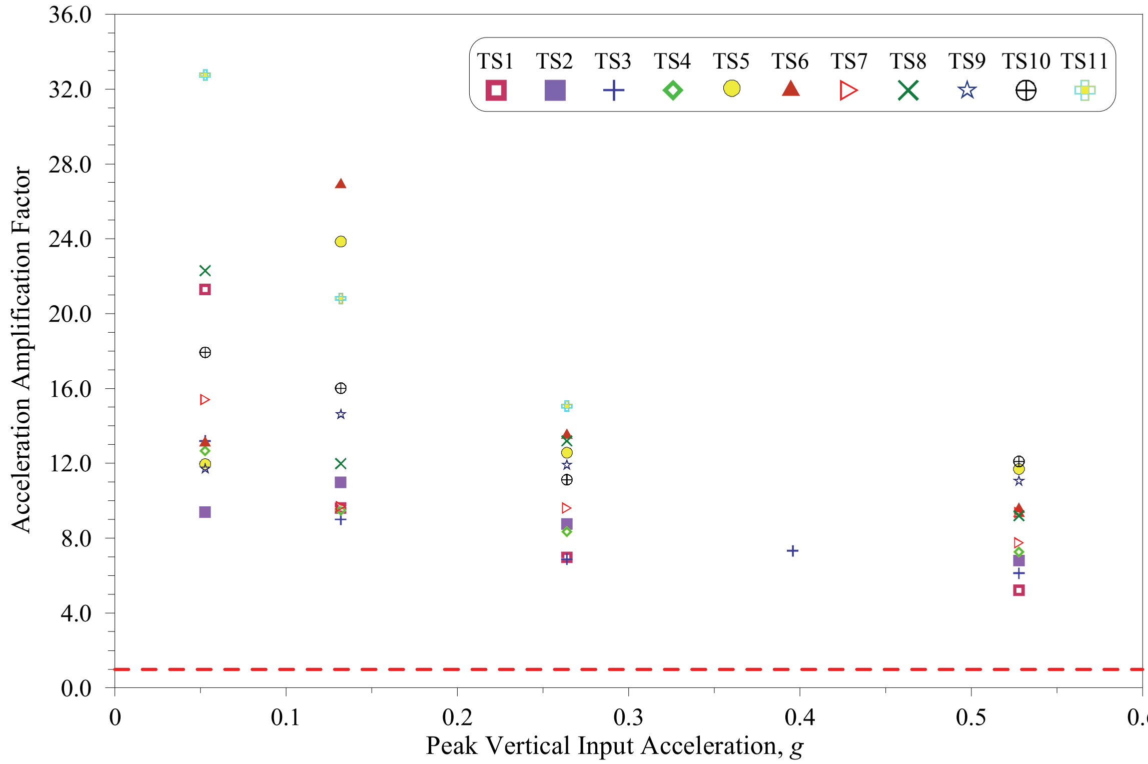

(a) I/R System #1

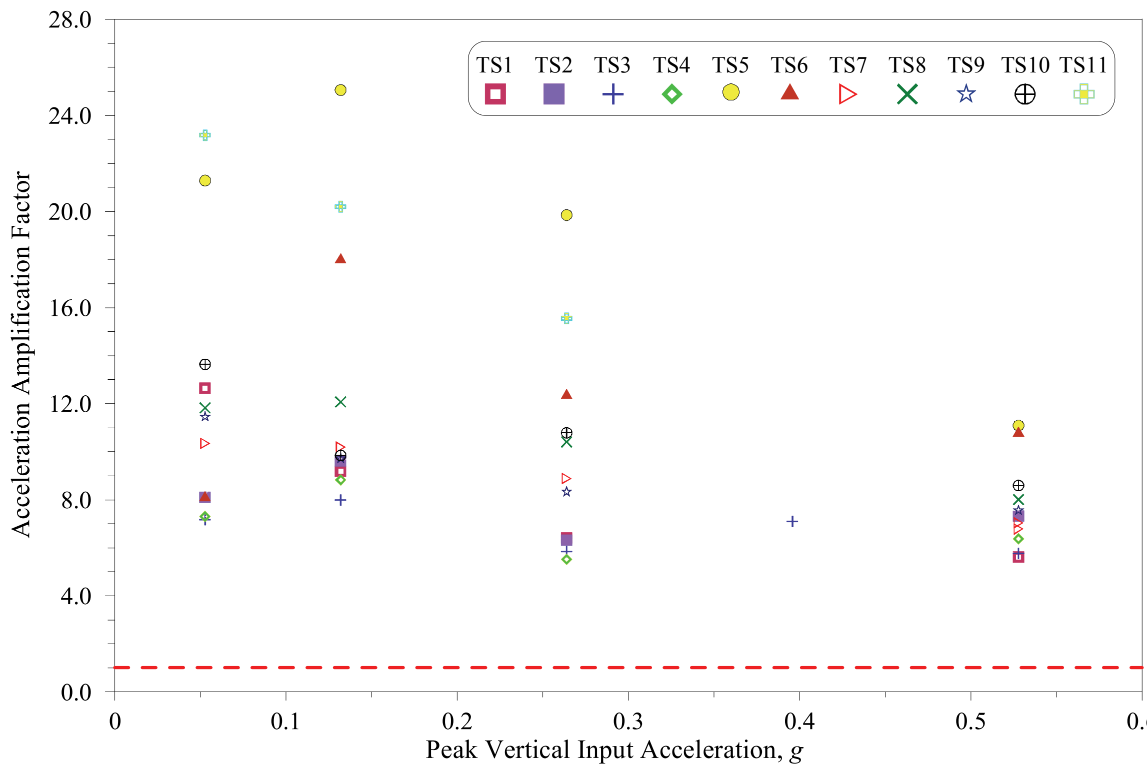

(b) I/R System #2

Figure 7-11 Variations of Vertical *AAF* on Top Level of I/R Systems with Peak Vertical Input Acceleration

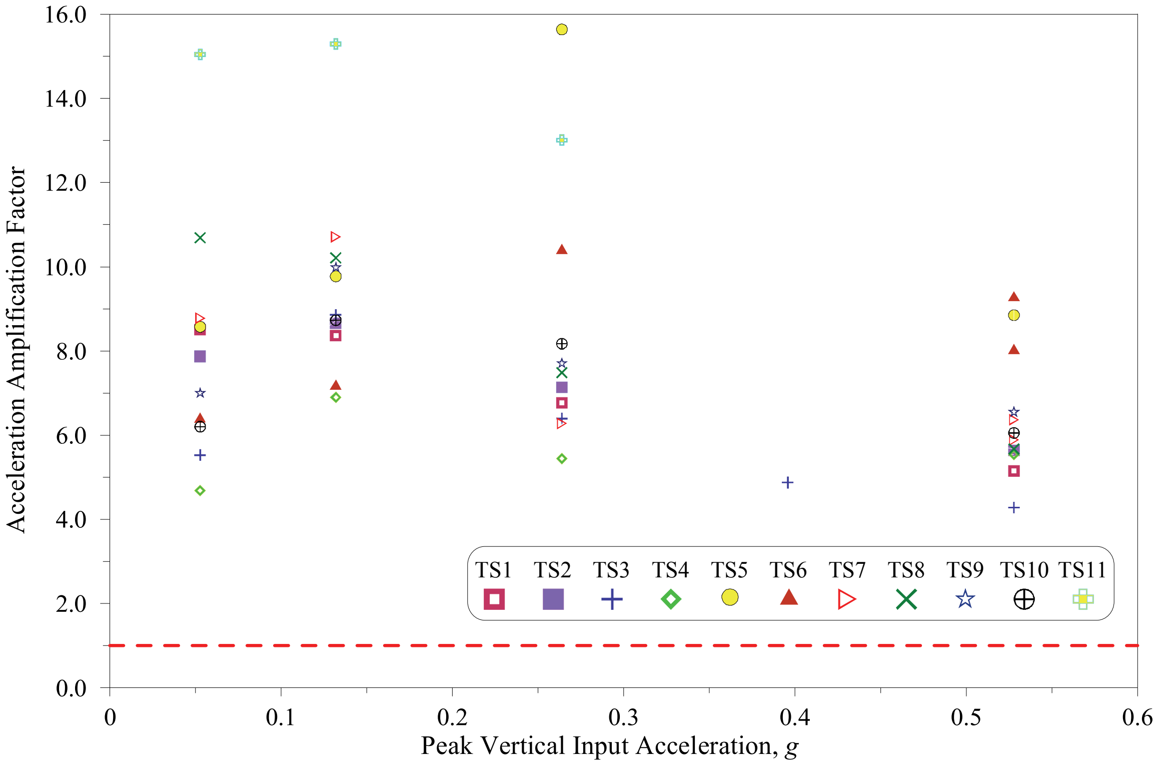

(c) I/R System #3

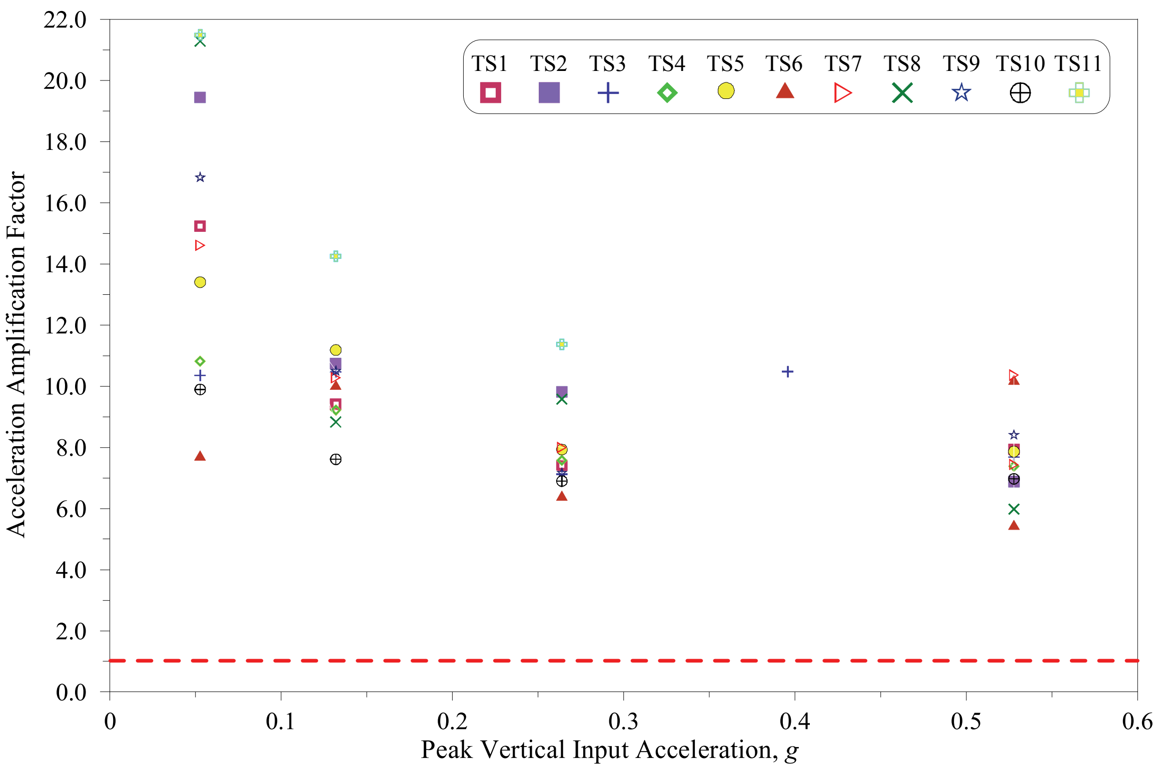

(d) I/R System #4

Figure 7-11 (cont'd) Variations of Vertical *AAF* on Top Level of I/R Systems with Peak Vertical Input Acceleration

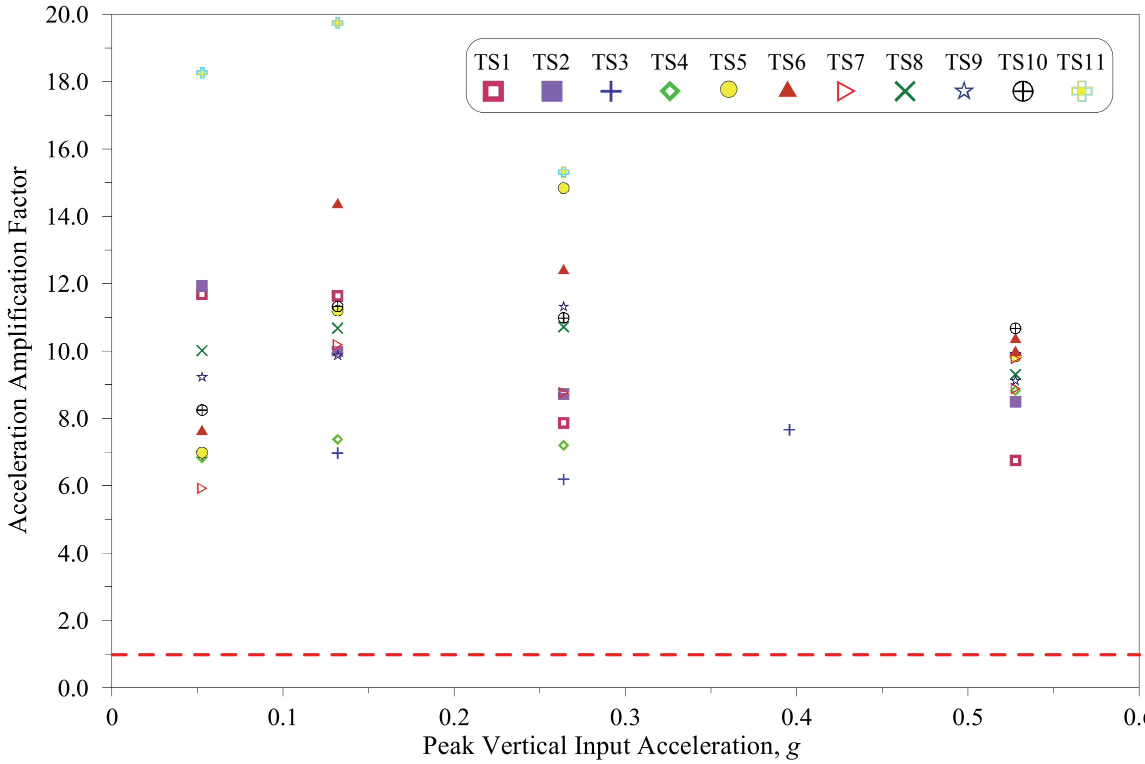

(e) I/R System #5

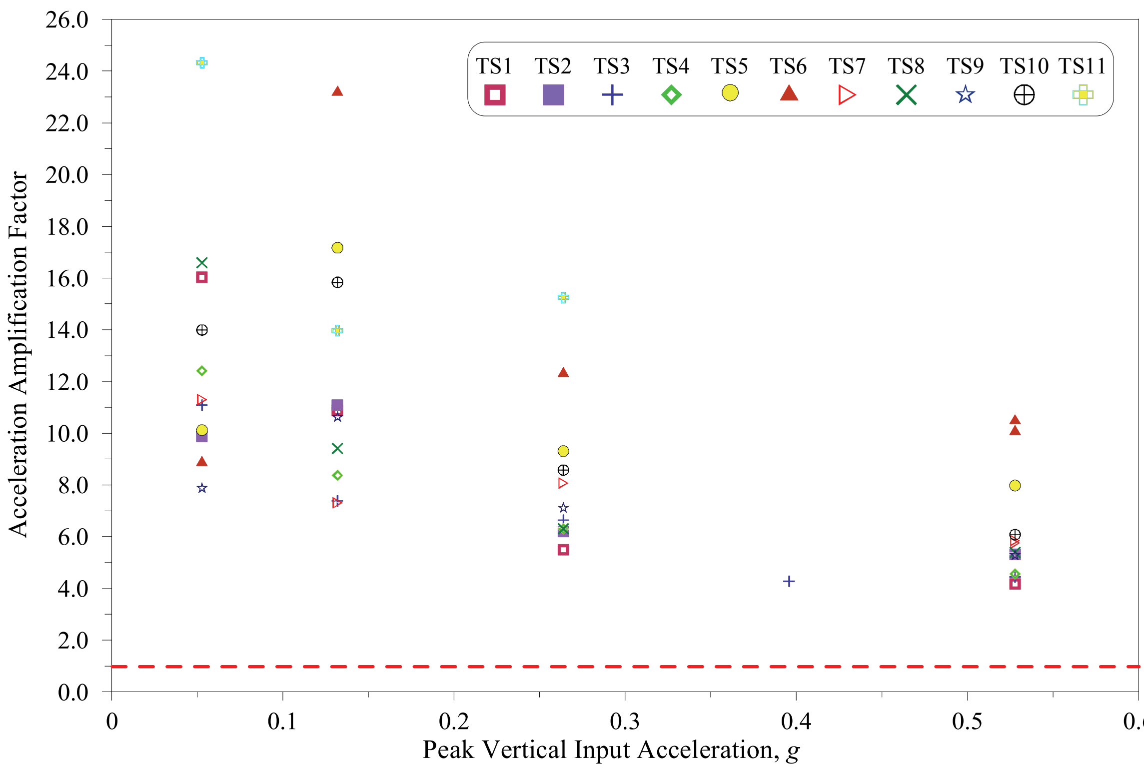

(f) I/R System #6

Figure 7-11 (cont'd) Variations of Vertical *AAF* on Top Level of I/R Systems with Peak Vertical Input Acceleration

Table 7-9 Maximum *AAF* on Top Level of I/R Systems, Phase I: Test Series TS1 through TS10

Direction	Maximum *AAF*	I/R System #	Test Name	Input Motion		Peak Acceleration Response on Top Level of I/R System, *g*
				Amplitude, %	Peak Acceleration, *g*	
Transverse	17.3	2	TS7-S1	10	0.08	1.38
Longitudinal	9.5	2	TS7-S1	10	0.08	0.75
Vertical	27.0	1	TS6-S2	25	0.13	3.56

Table 7-10 Minimum *AAF* on Top Level of I/R Systems, Phase I: Test Series TS1 through TS10

Direction	Minimum *AAF*	I/R System #	Test Name	Input Motion		Peak Acceleration Response on Top Level of I/R System, *g*
				Amplitude, %	Peak Acceleration, *g*	
Transverse	2.9	1	TS2-S3	50	0.40	1.16
Longitudinal	2.7	1	TS1-S4	100	0.79	2.11
Vertical	4.2	6	TS1-S4	100	0.53	2.20

Table 7-11 Maximum Triaxial Acceleration Responses on Top Level of I/R systems, Phase I: Test Series TS1 through TS10

Direction	Maximum Acceleration Response on Top Level of I/R System, *g*	I/R System #	Test Name	Input Motion		*AAF*
				Amplitude, %	Peak Acceleration, *g*	
Transverse	7.68	3	TS6-S5	100	0.80	9.6
Longitudinal	6.72	2	TS5-S4	100	0.79	8.5
Vertical	6.39	1	TS5-S4	100	0.53	11.7

7.2.2 Dynamic Forces Induced into I/R Systems

Variations of the peak dynamic transverse shear, longitudinal shear, resultant shear, and normal forces induced into the I/R systems with the corresponding peak input acceleration during the 46 seismic tests of Phase I of the experiments are presented in Figures 7-12 through 7-15, respectively. In order to compare the dynamic forces induced into the I/R systems to the dynamic forces experienced at the support locations of the rigidly mounted test specimen, variations of the peak dynamic forces measured at the support locations of the rigidly mounted test specimen during the six seismic tests of Phase II of the experiments were added to Figures 7-12 through 7-15.

The dynamic forces induced into the I/R systems varied with a change of the input motion amplitude or with a change in the restraint component properties. The peak dynamic forces induced into the I/R systems increased with an increase of the input motion amplitude. Among the I/R systems used in the 11 test series, those with thick rubber snubbers experienced the lowest dynamic forces. Removing the rubber snubbers of the restraint components during the seismic tests of Test Series 11 resulted in very large dynamic forces induced into the I/R systems. In fact, conducting a seismic test with the full-scale input motion during Test Series TS11 would have damaged the load cells.

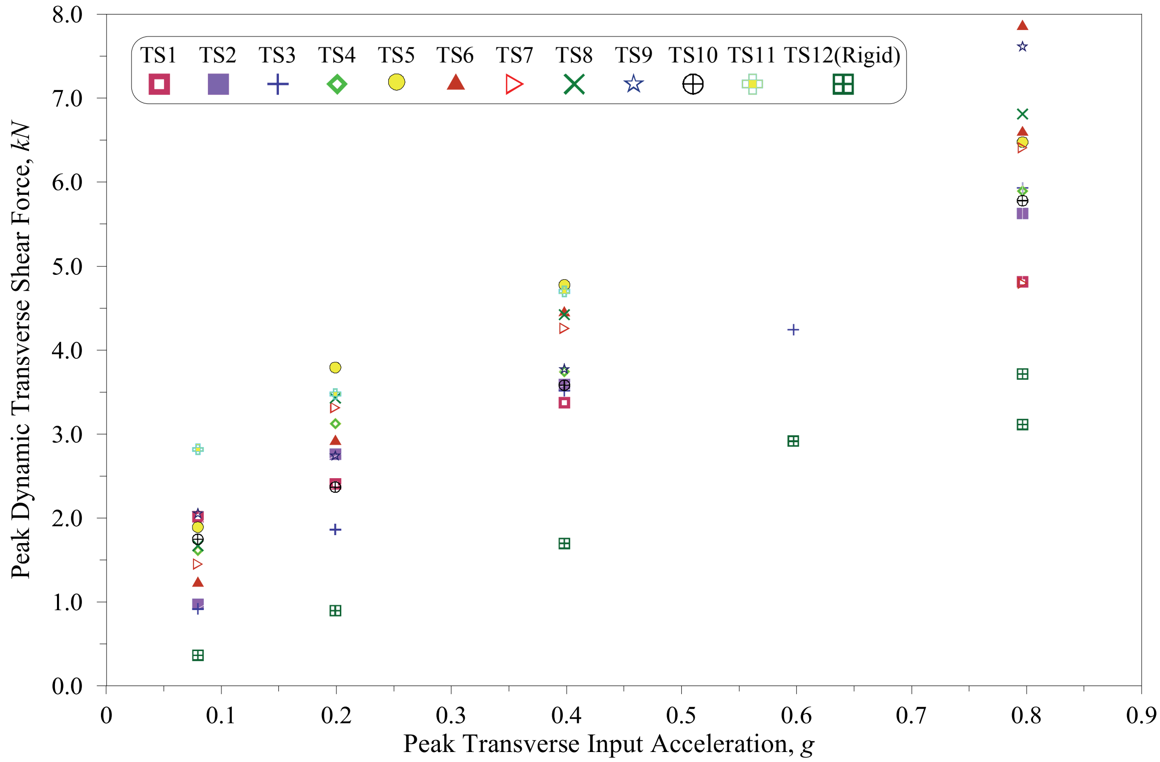

(a) I/R System #1

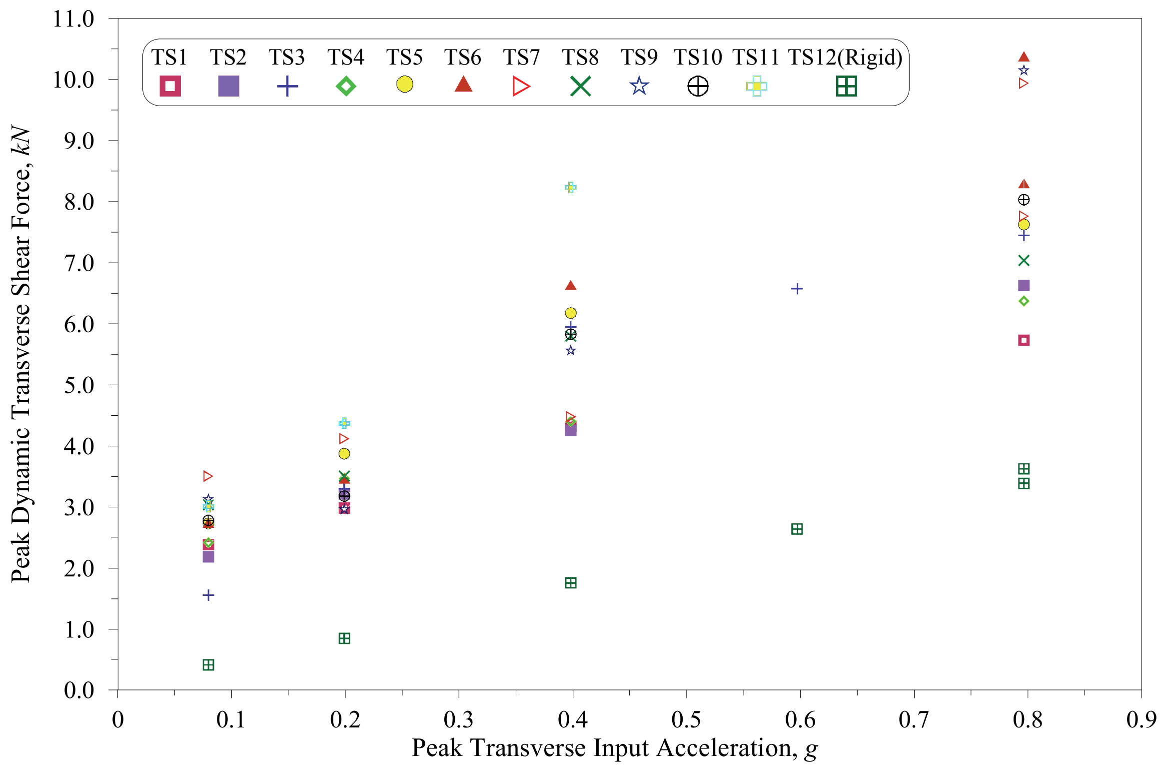

(b) I/R System #2

Figure 7-12 Variations of Peak Dynamic Shear Forces Induced into I/R Systems with Peak Input Acceleration, Transverse Direction

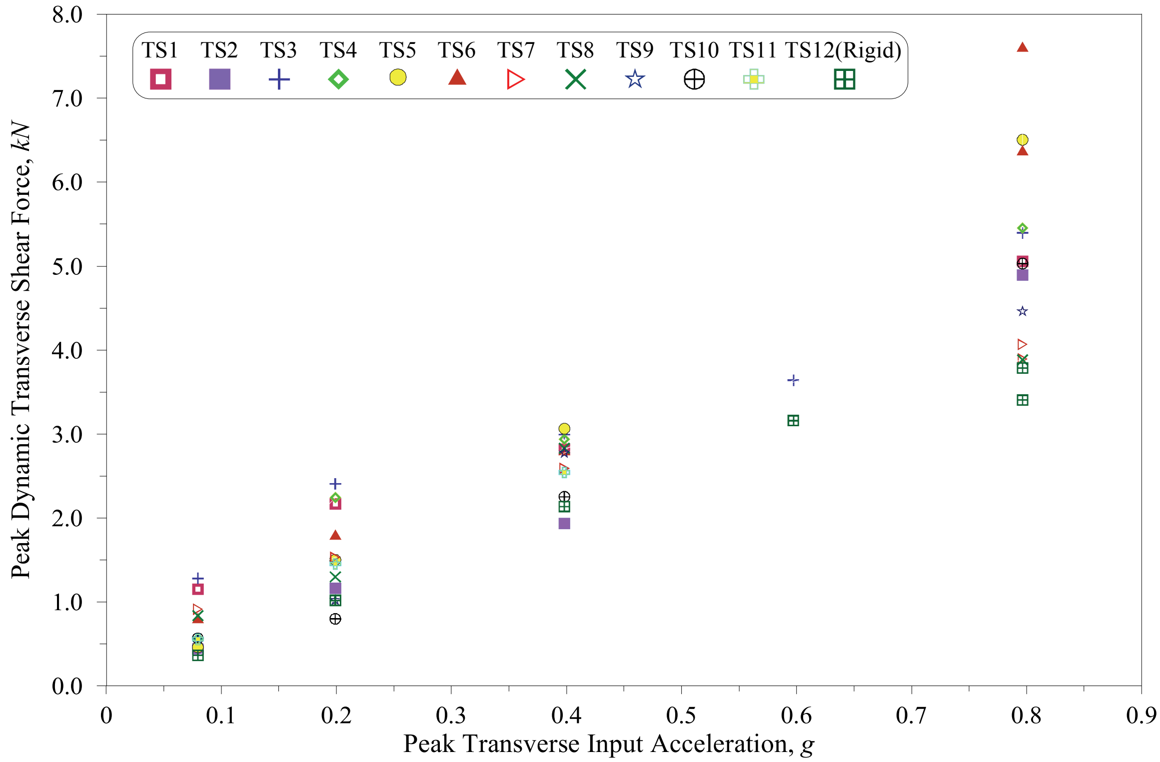

(c) I/R System #3

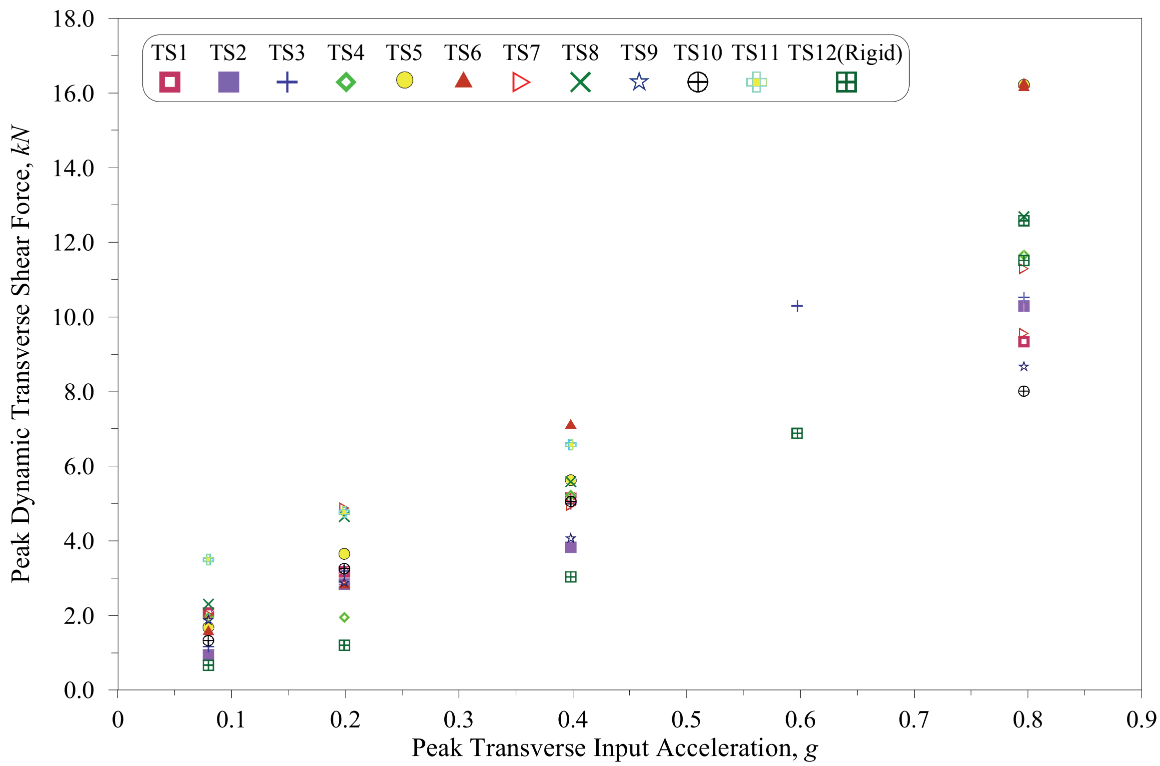

(d) I/R System #4

Figure 7-12 (cont'd) Variations of Peak Dynamic Shear Forces Induced into I/R Systems with Peak Input Acceleration, Transverse Direction

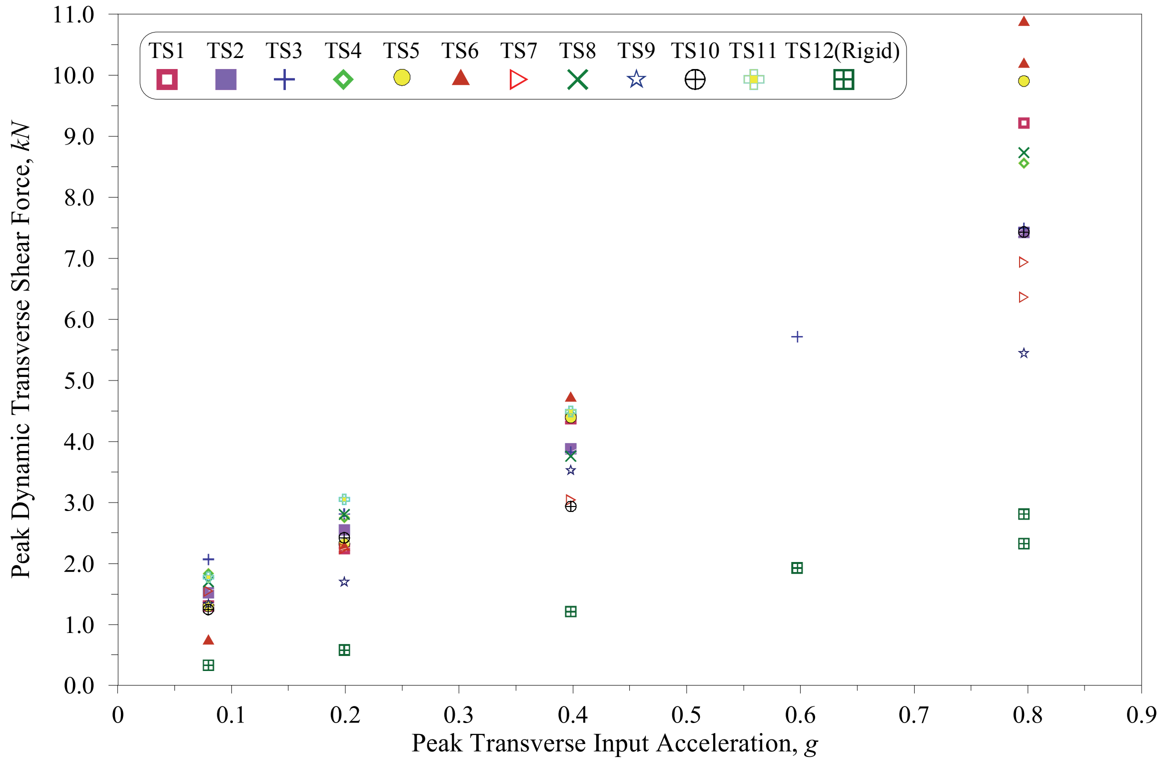

(e) I/R System #5

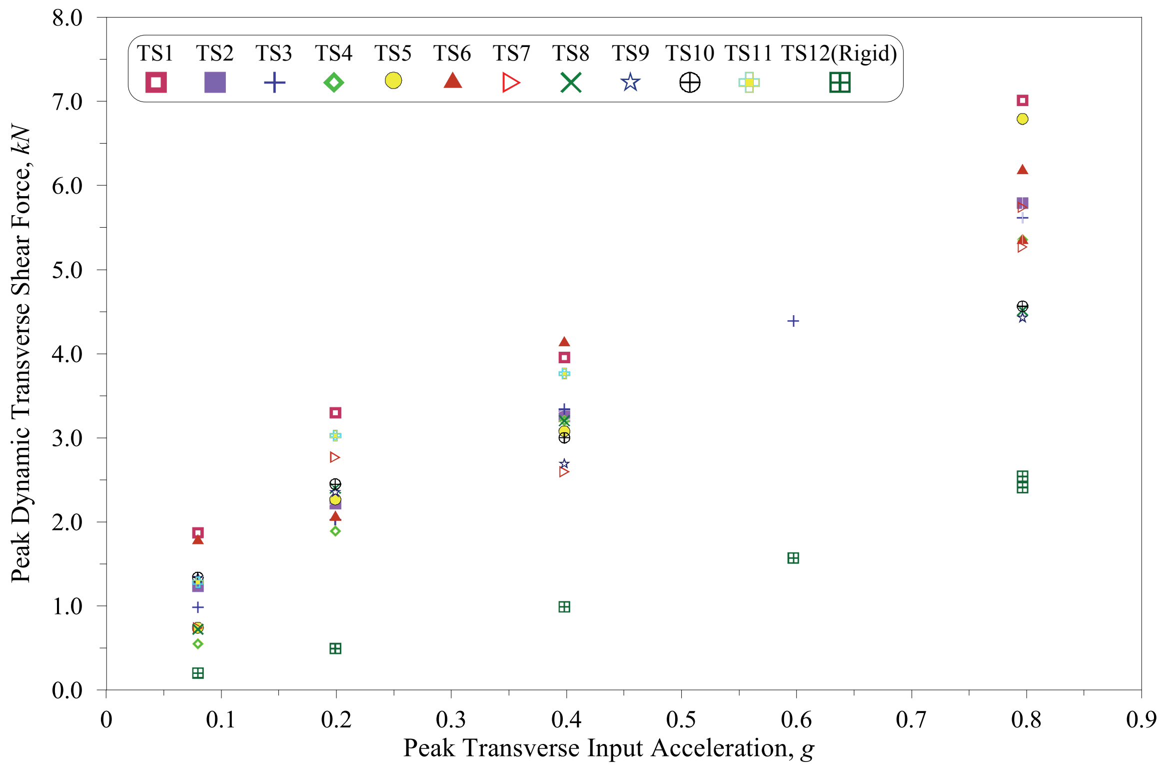

(f) I/R System #6

Figure 7-12 (cont'd) Variations of Peak Dynamic Shear Forces Induced into I/R Systems with Peak Input Acceleration, Transverse Direction

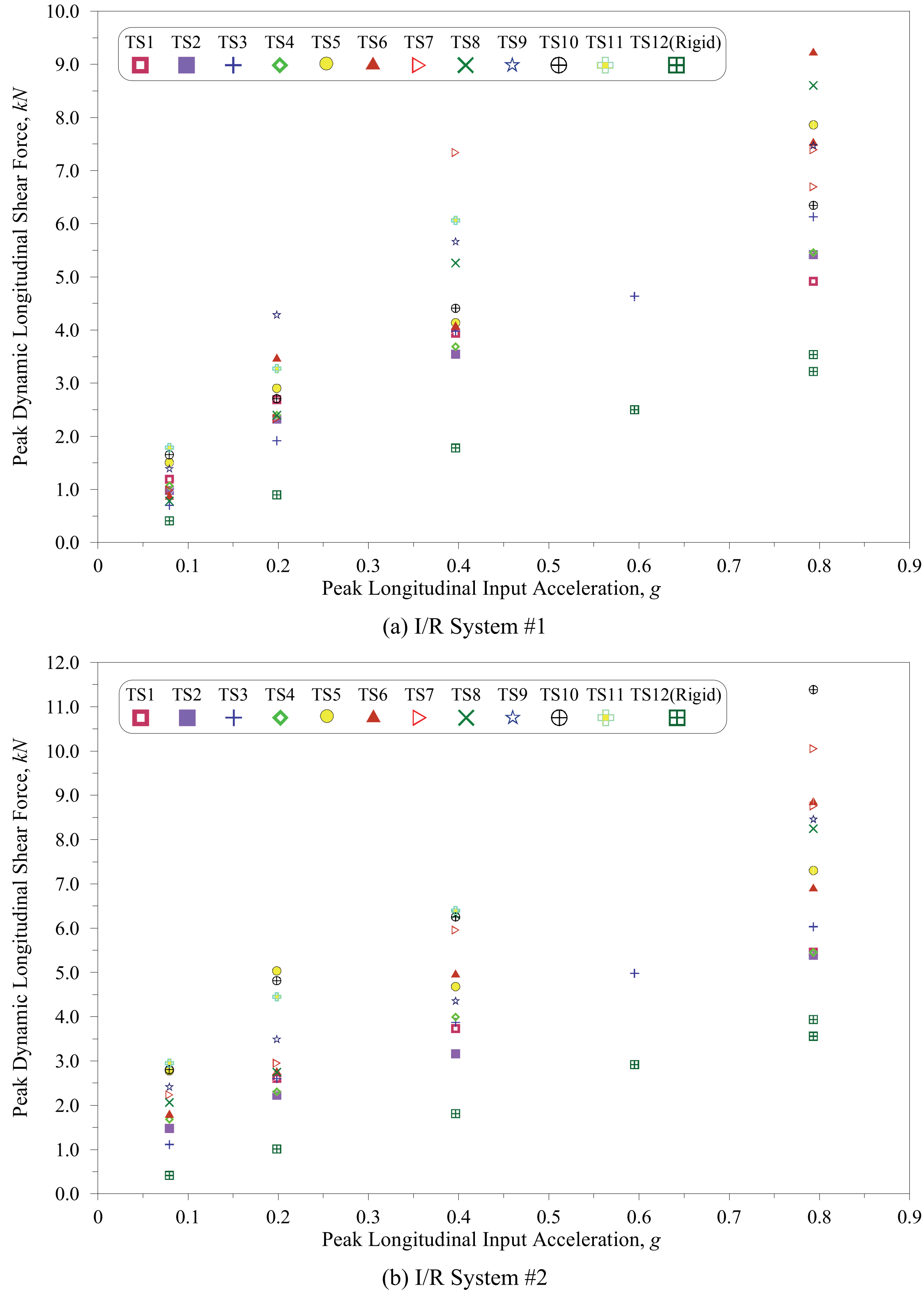

Figure 7-13 Variations of Peak Dynamic Shear Forces Induced into I/R Systems with Peak Input Acceleration, Longitudinal Direction

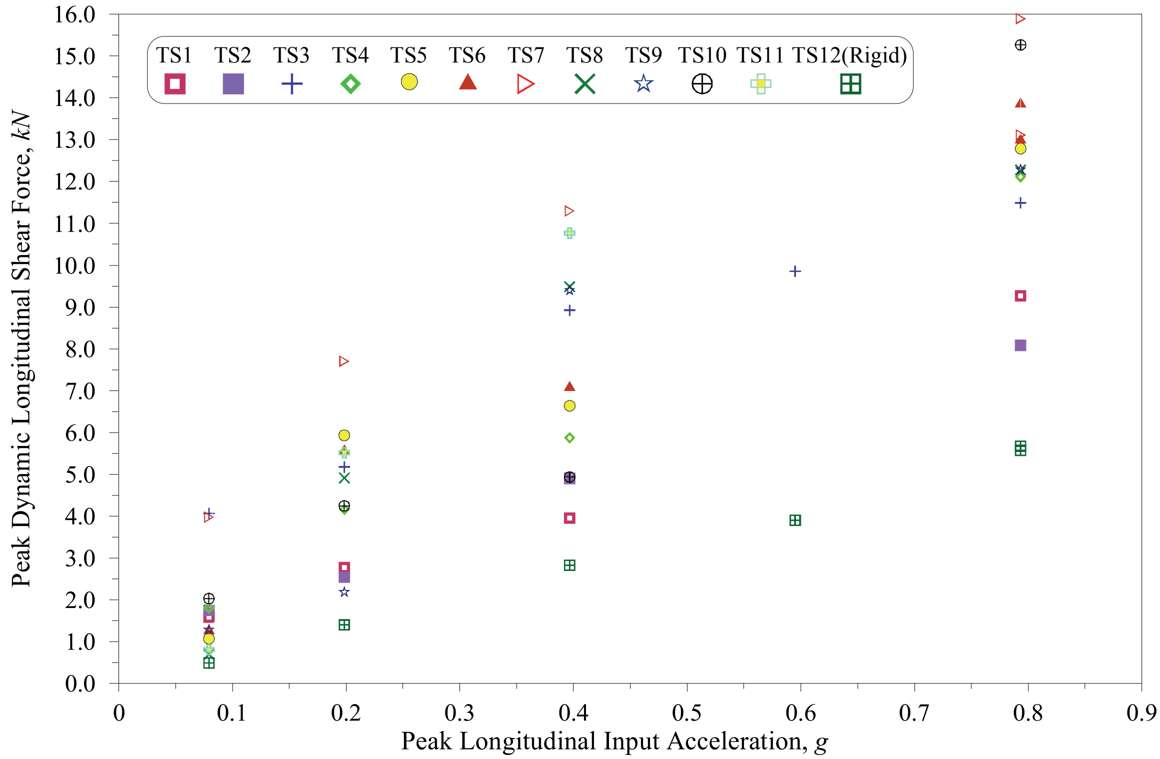

(c) I/R System #3

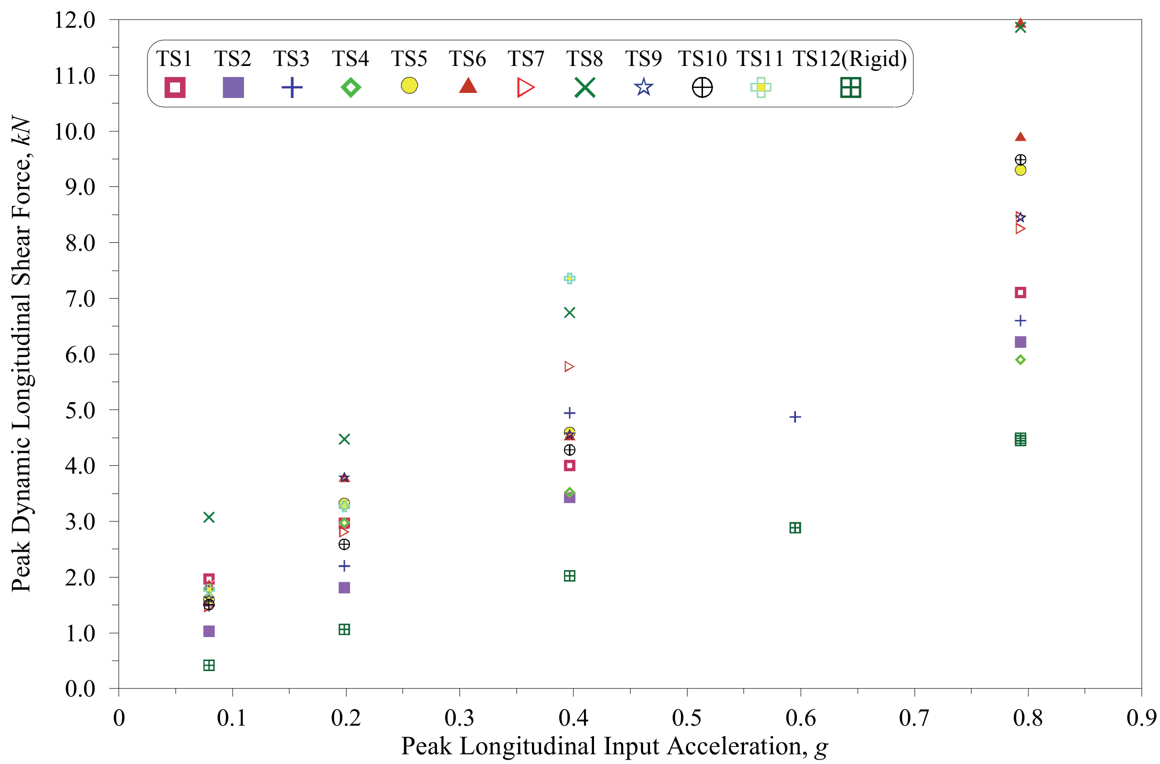

(d) I/R System #4

Figure 7-13 (cont'd) Variations of Peak Dynamic Shear Forces Induced into I/R Systems with Peak Input Acceleration, Longitudinal Direction

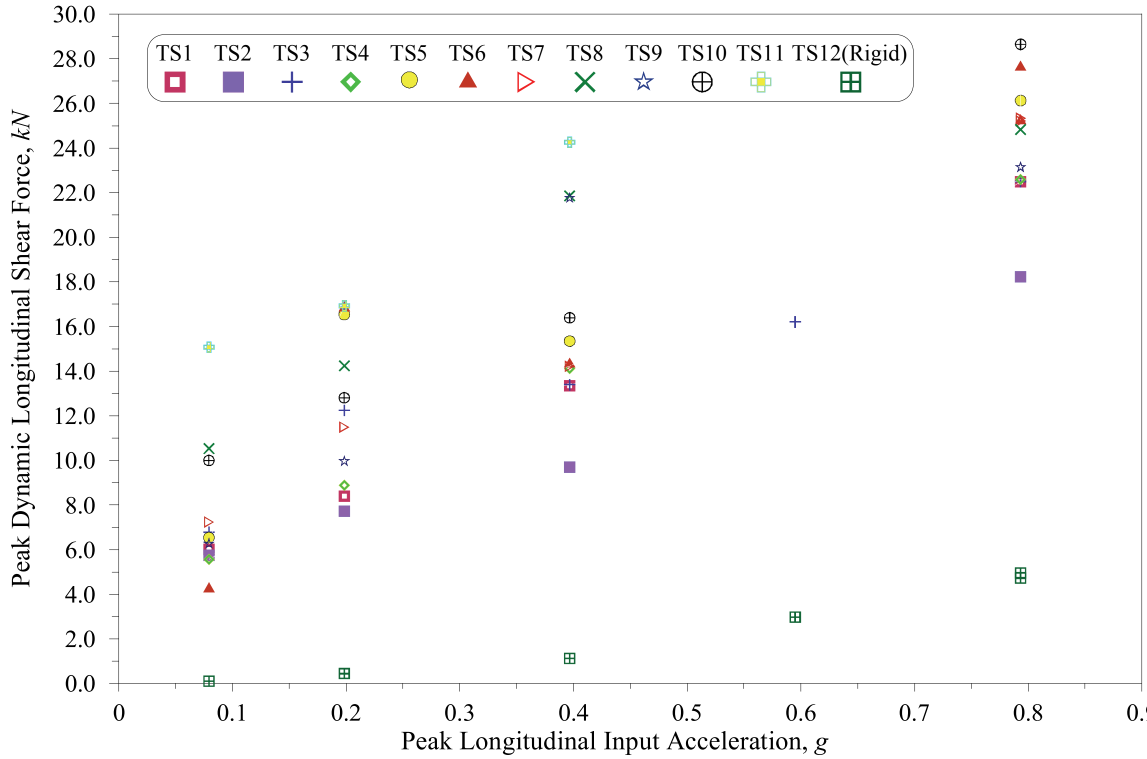

(e) I/R System #5

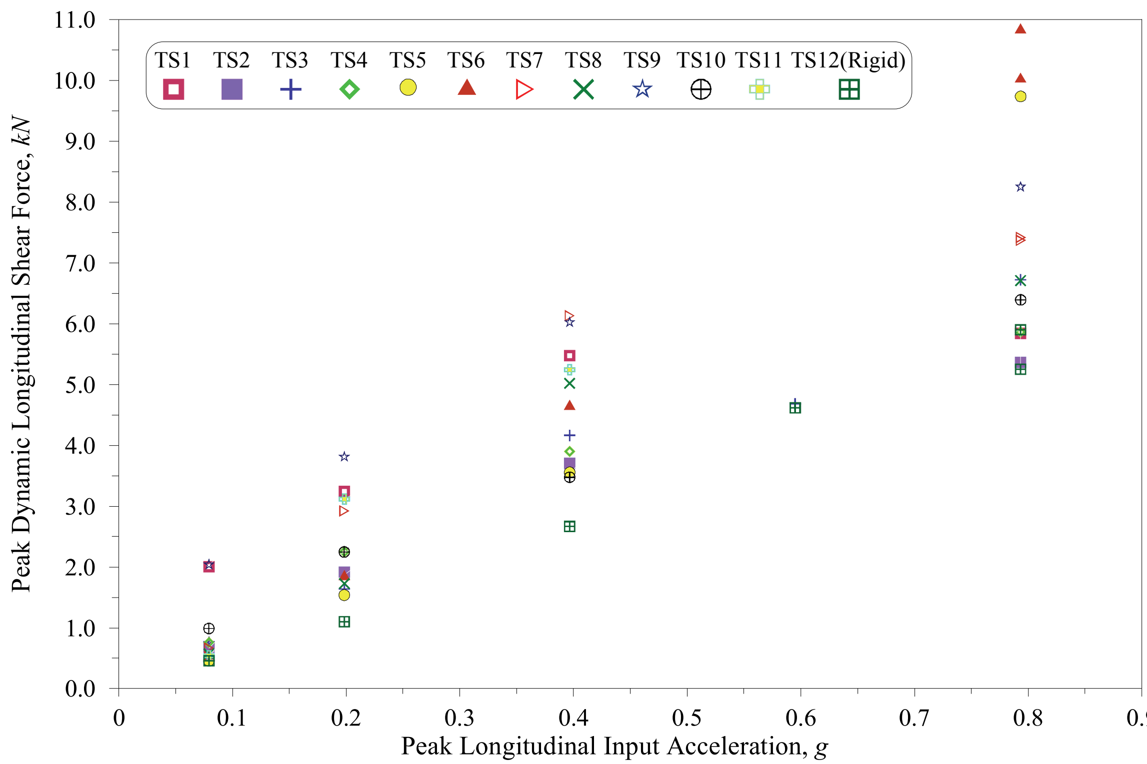

(f) I/R System #6

Figure 7-13 (cont'd) Variations of Peak Dynamic Shear Forces Induced into I/R Systems with Peak Input Acceleration, Longitudinal Direction

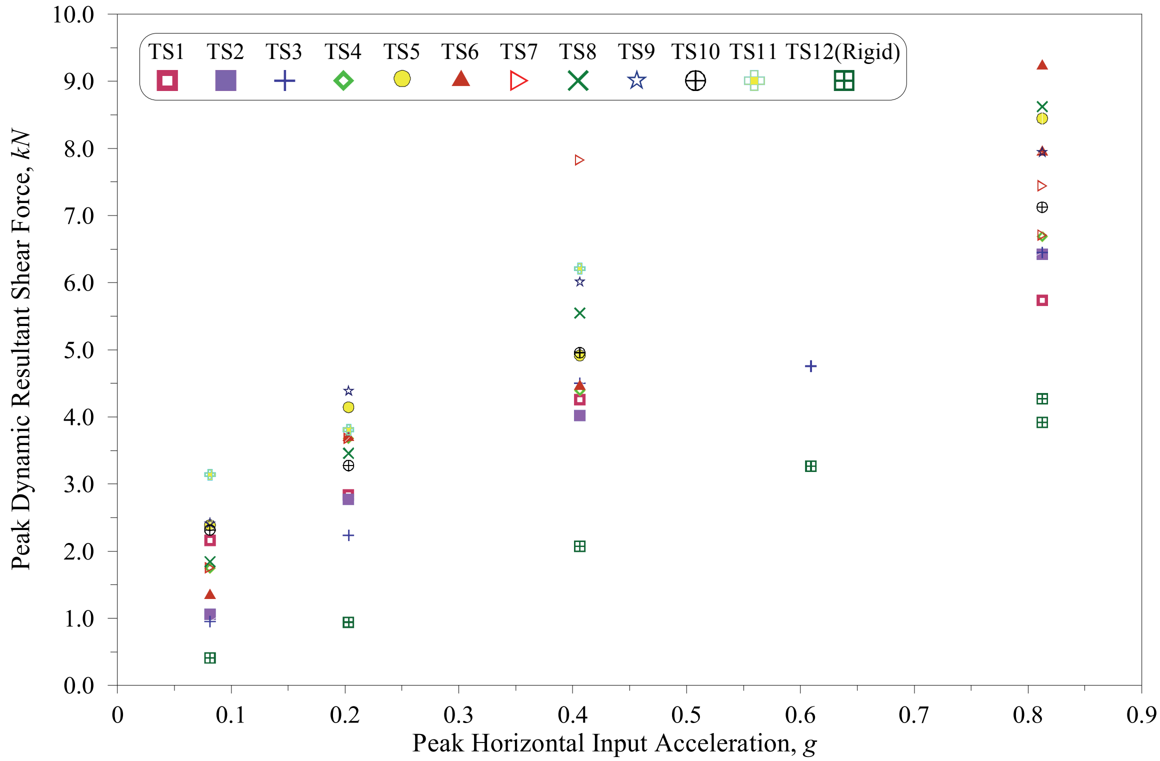

(a) I/R System #1

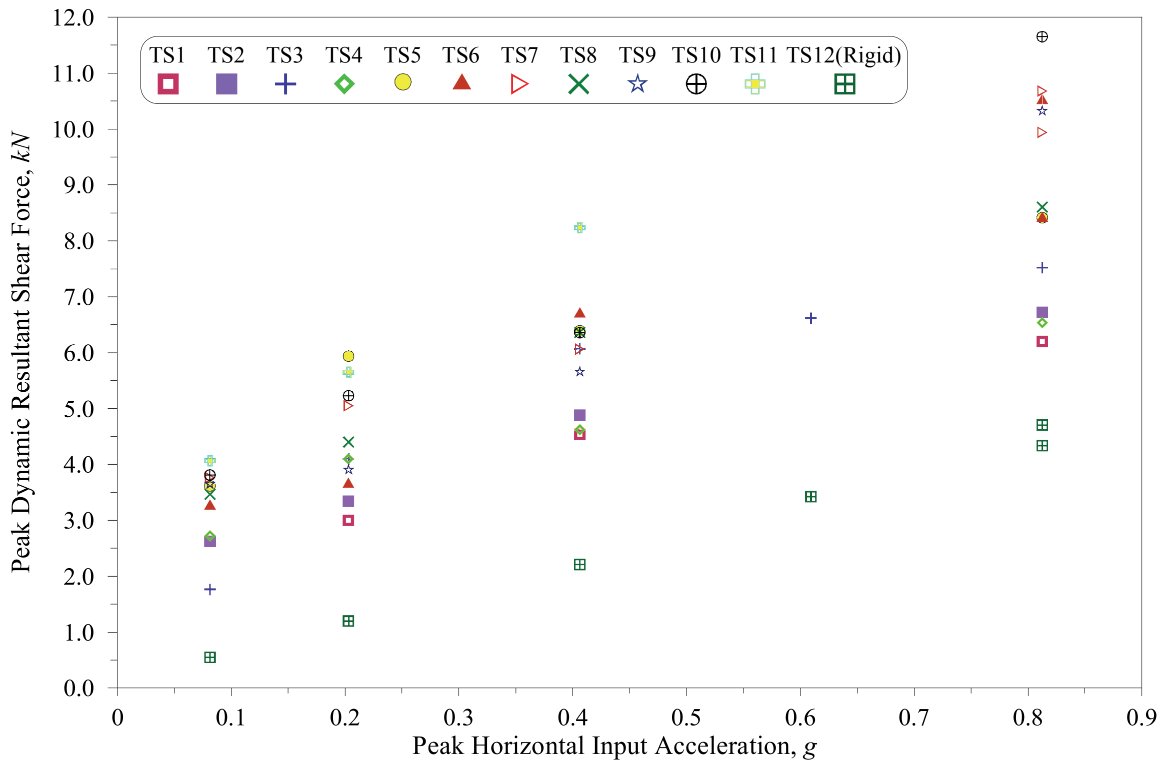

(b) I/R System #2

Figure 7-14 Variations of Peak Dynamic Resultant Shear Forces Induced into I/R Systems with Peak Horizontal Input Acceleration

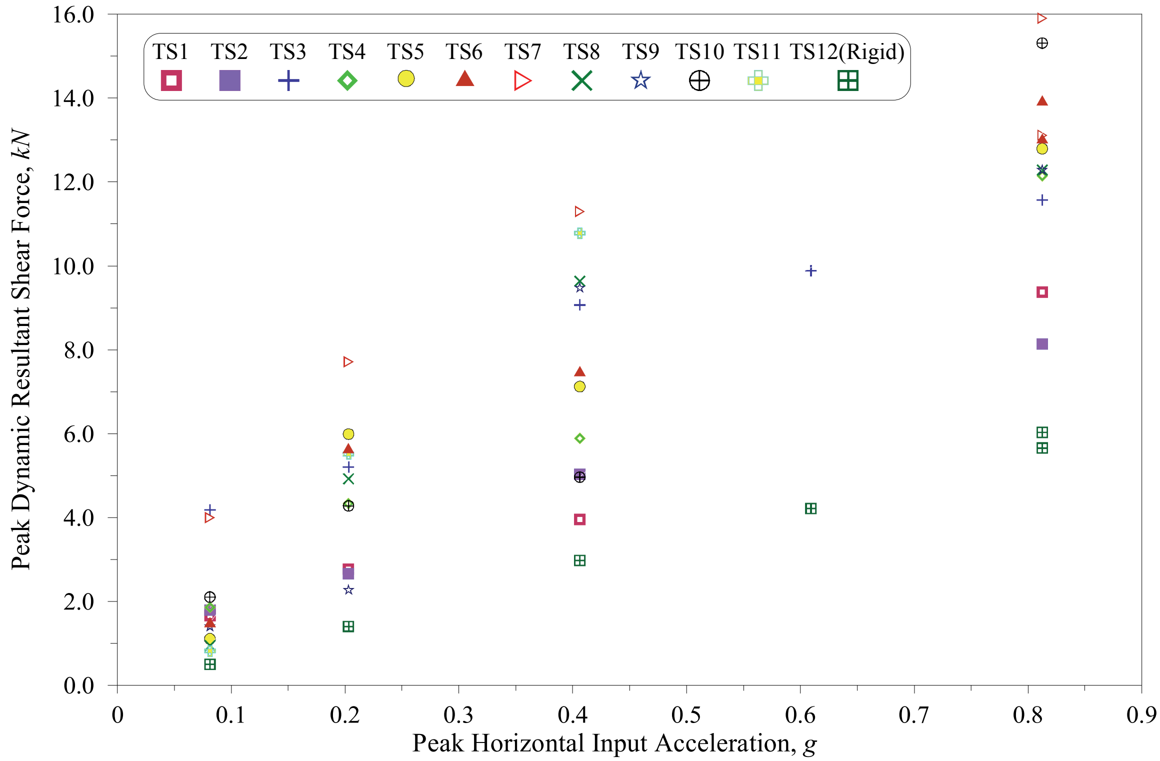

(c) I/R System #3

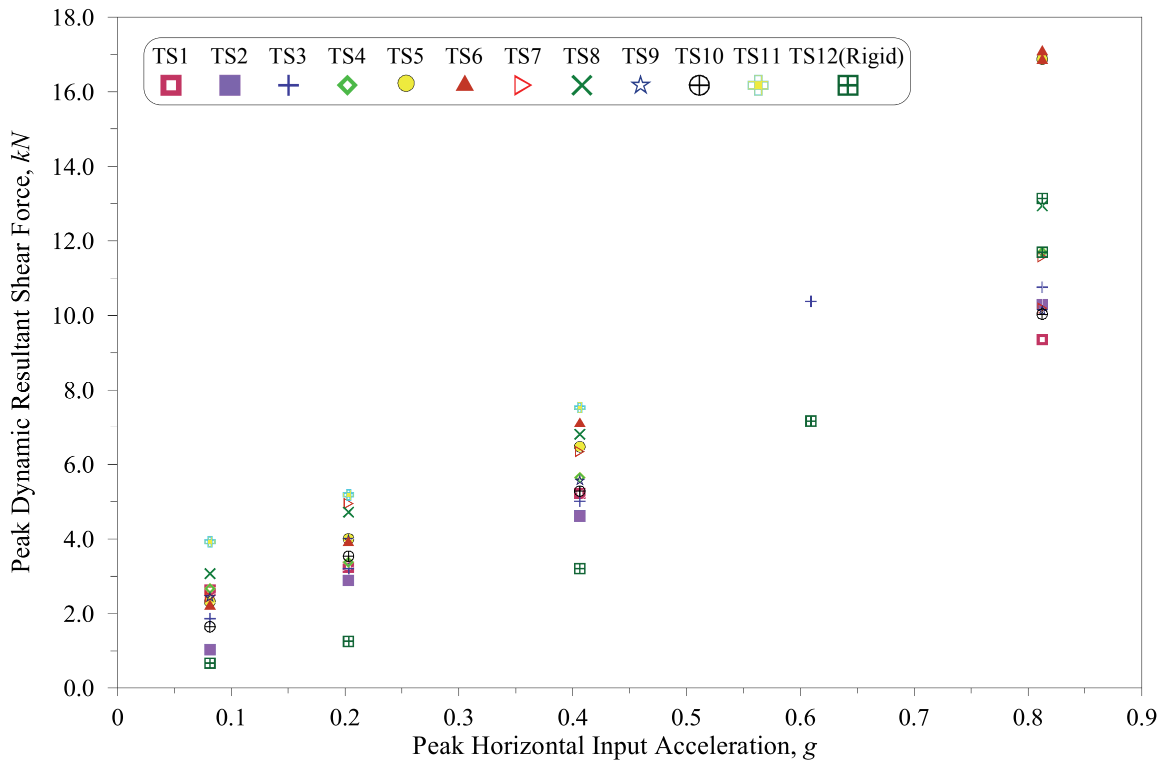

(d) I/R System #4

Figure 7-14 (cont'd) Variations of Peak Dynamic Resultant Shear Forces Induced into I/R Systems with Peak Horizontal Input Acceleration

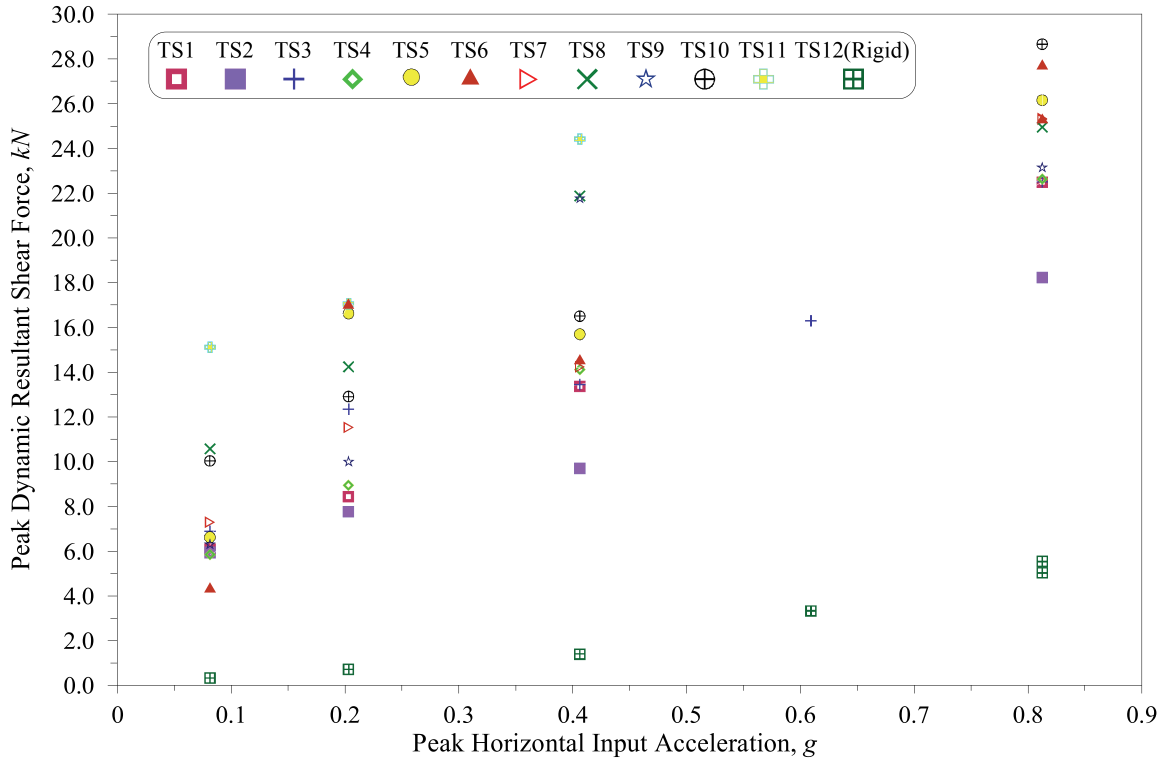

(e) I/R System #5

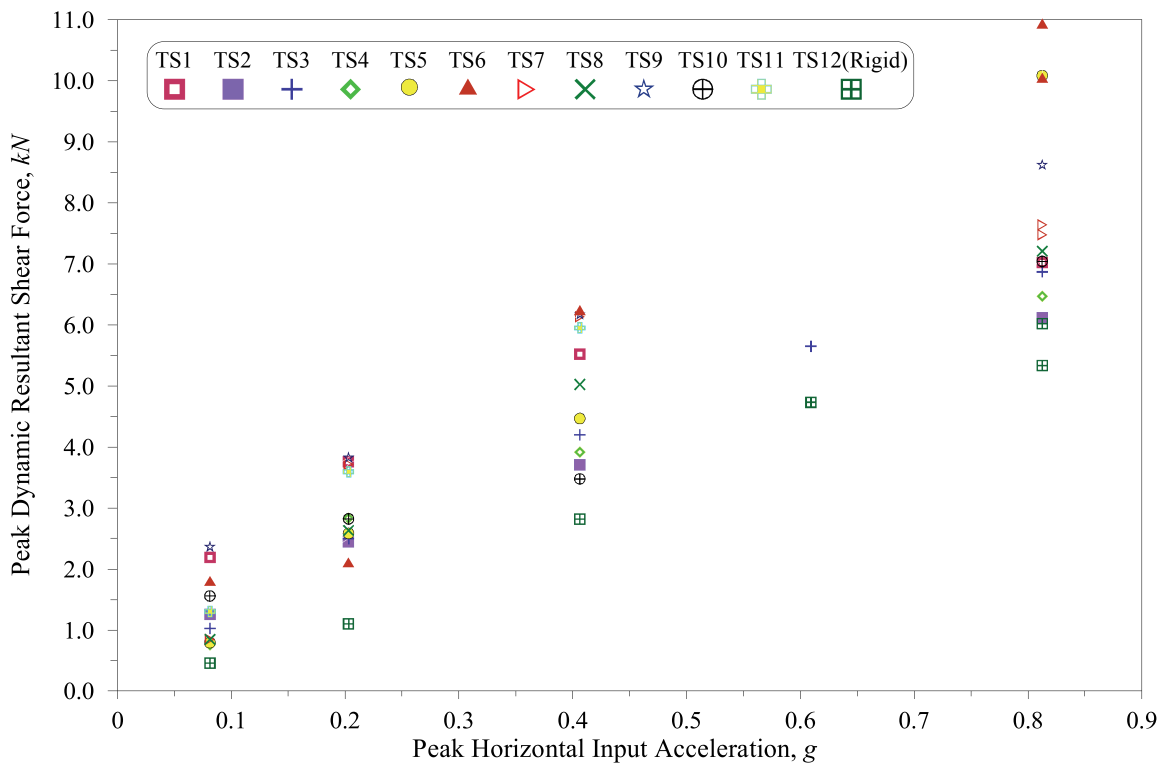

(f) I/R System #6

Figure 7-14 (cont'd) Variations of Peak Dynamic Resultant Shear Forces Induced into I/R Systems with Peak Horizontal Input Acceleration

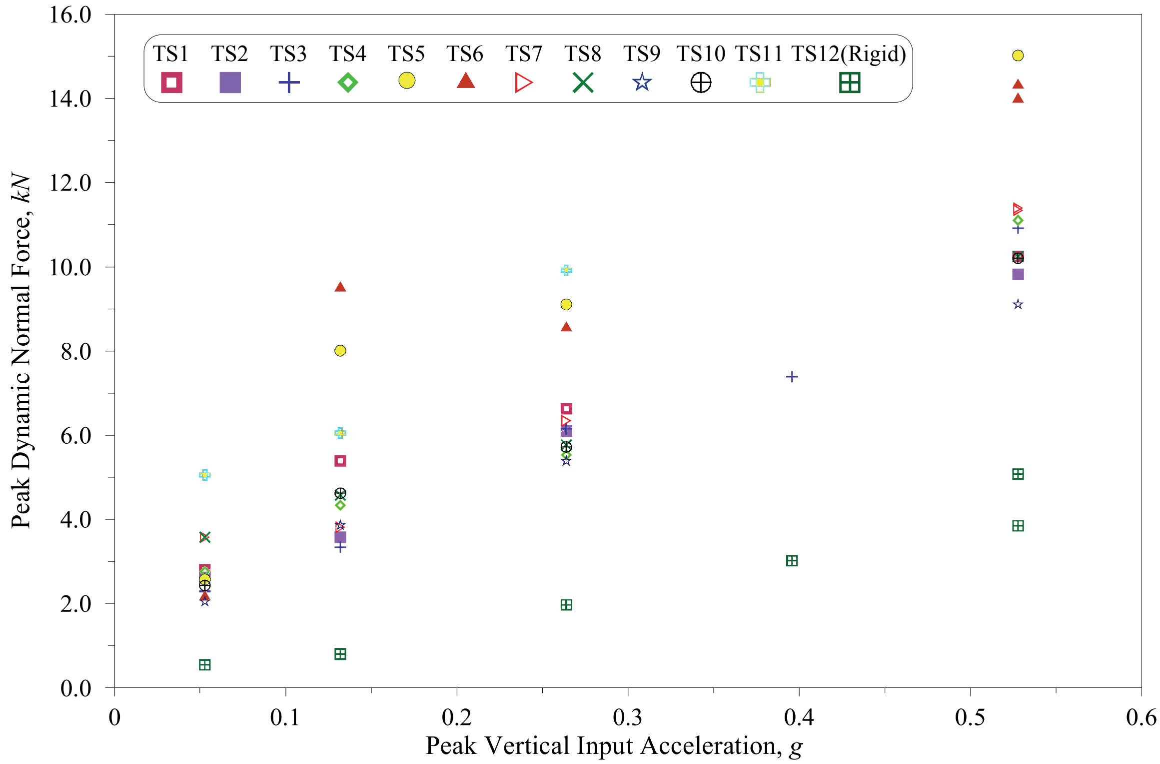

(a) I/R System #1

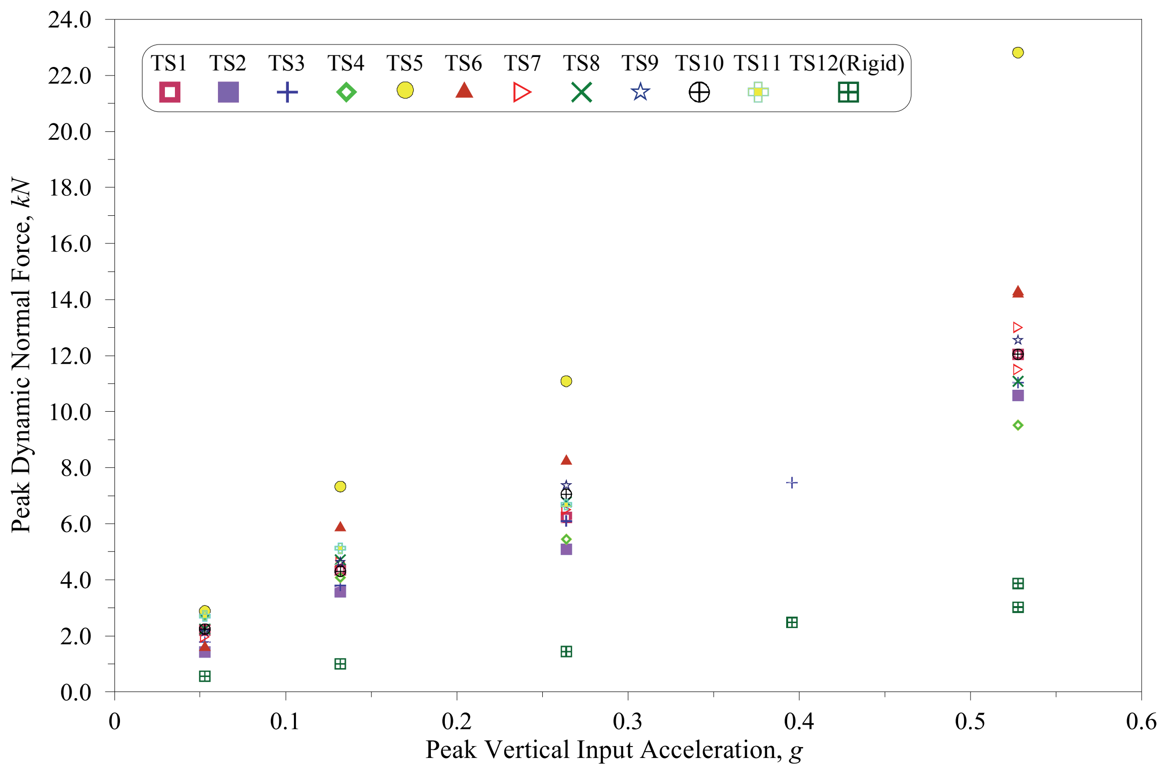

(b) I/R System #2

Figure 7-15 Variations of Peak Dynamic Normal Forces Induced into I/R Systems with Peak Vertical Input Acceleration

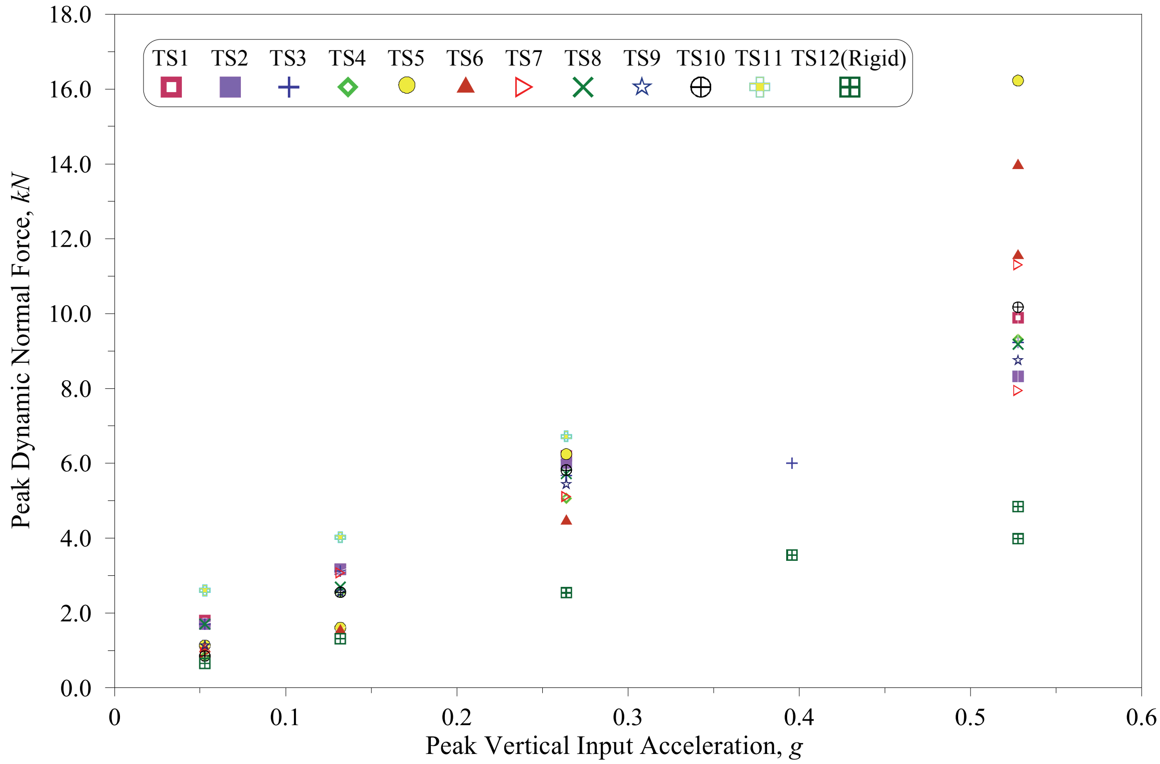

(c) I/R System #3

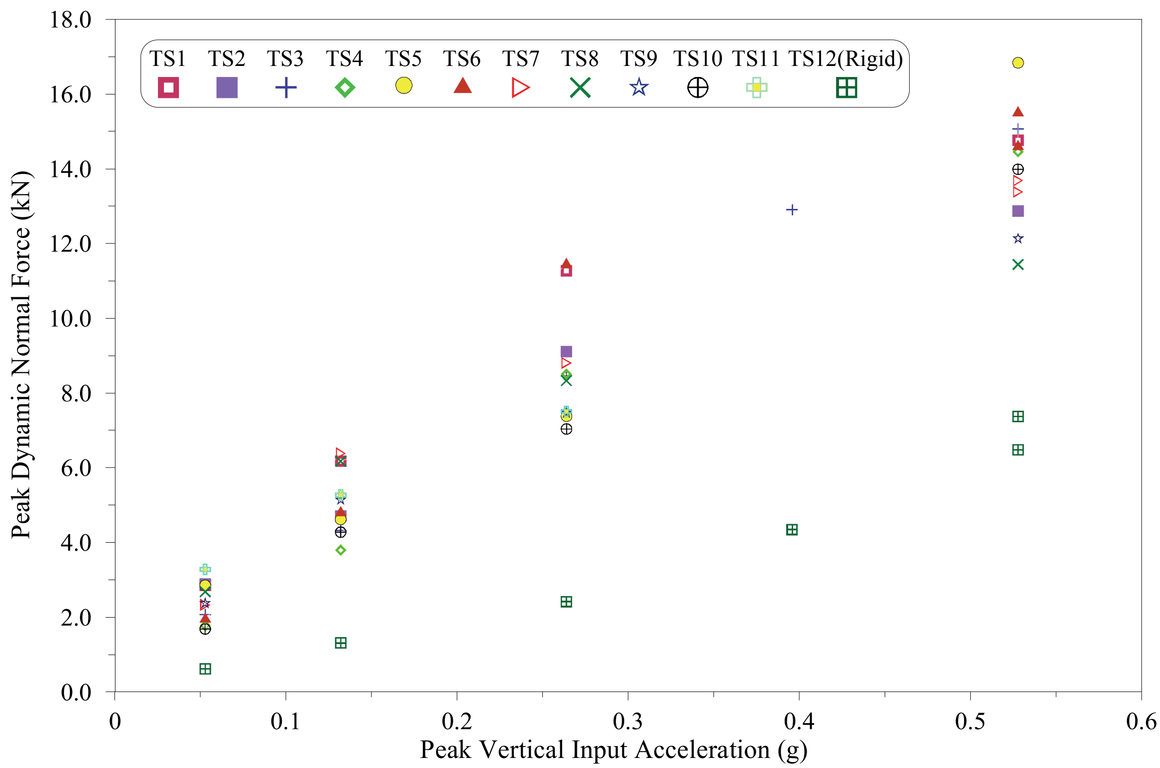

(d) I/R System #4

Figure 7-15 (cont'd) Variations of Peak Dynamic Normal Forces Induced into I/R Systems with Peak Vertical Input Acceleration

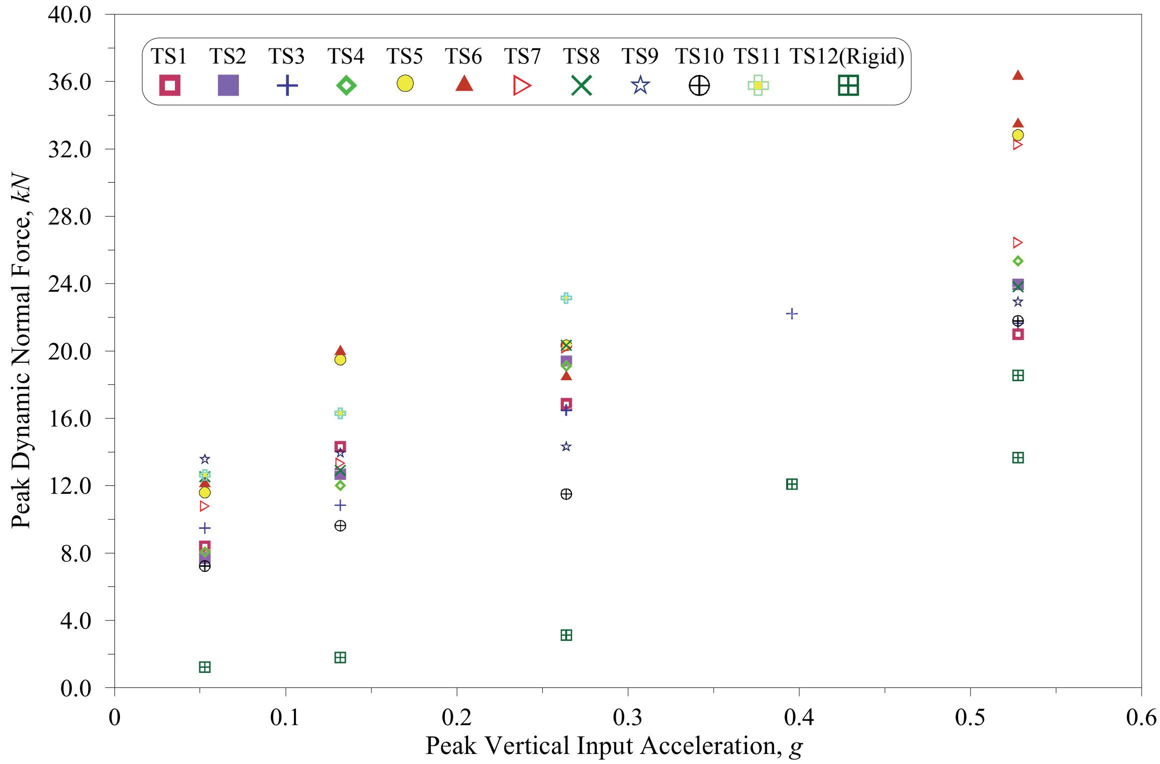

(e) I/R System #5

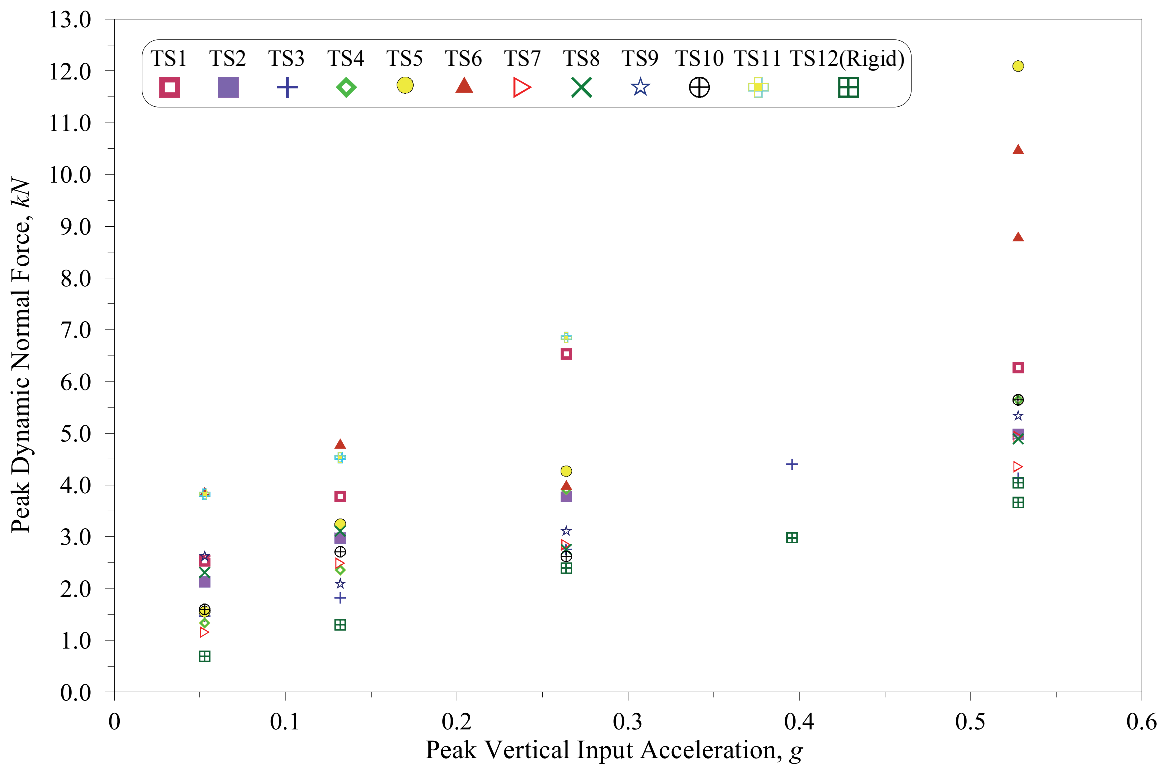

(f) I/R System #6

Figure 7-15 (cont'd) Variations of Peak Dynamic Normal Forces Induced into I/R Systems with Peak Vertical Input Acceleration

The maximum dynamic shear and normal forces experienced by the I/R systems are listed in Table 7-12. To find the extreme values presented in these tables, results of Test Series TS11 (the test series conducted without rubber snubbers), Test TS6-S4 (the test during which the test specimen housing was damaged), and Test TS7-S5 (the test conducted after activation of the isolation systems inside the fan module) were not considered. The I/R systems designed for a static load of 15 *kN* (3.4 *kips*) withstood dynamic shear and normal forces as strong as 29 *kN* (6.6 *kips*) and 34 *kN* (7.7 *kips*), respectively, without sustaining any damage.

Table 7-12 Maximum Dynamic Forces Induced into I/R Systems, Phase I: Test Series TS1 through TS10

Dynamic Force	Direction	Peak Response, *kN*	I/R System #	Test Name	Input Motion	
					Amplitude, %	Peak Acceleration, *g*
Shear	Transverse	16	4	TS6-S5	100	0.80
	Longitudinal	29	5	TS10-S4	100	0.79
	Resultant	29	5	TS10-S4	100	0.81
Normal	Vertical	34	5	TS6-S5	100	0.53

The test results show that the maximum dynamic forces were not necessarily induced into the I/R system supporting the largest tributary mass. Furthermore, despite the fact that the acceleration response (near the center of mass) of the test specimen was usually larger in the transverse direction than in the longitudinal direction, the maximum shear force was experienced in the longitudinal direction. These two important observations regarding the dynamic forces induced into the I/R systems are attributed to the rotational responses of the test specimen. The engagements of the restraint components were not only because of the translational movement but also because of the rotational movement of the test specimen. The relationship between the rotational responses of the test specimen on the dynamic forces induced into the I/R systems are explained more in Section 7.3.2.

For each of the input motion amplitudes, the maximum dynamic forces induced into the support locations of the isolated and rigidly mounted test specimen can be compared to each other by a dimensionless Force Amplification Factor (*FAF*) defined in Equation 7-5:

$$FAF = \frac{F_{max,isol}}{F_{max,rigid}} \tag{7-5}$$

where,

FAF = the Force Amplification Factor
$F_{max,isol}$ = the maximum dynamic resultant shear or normal force induced into the I/R systems
$F_{max,rigid}$ = the maximum dynamic resultant shear or normal force at the support locations of the rigidly mounted test specimen

The variations of the resultant shear and normal *FAF* with the corresponding peak input acceleration throughout the 46 seismic tests of Phase I of the experiments are shown in Figures 7-16 and 7-17, respectively. Throughout the seismic tests of Test Series TS1 through TS10, the resultant shear and normal *FAF* varied in the range of 1.5 to 15.8 and 1.1 to 11.1, respectively. Both resultant shear and normal *FAF* decreased with an increase of the input motion amplitude. During the tests with the full-scale input motion, the variation ranges of the resultant shear and normal *FAF* were limited to 1.5 to 2.5 and 1.0 to 2.0, respectively.

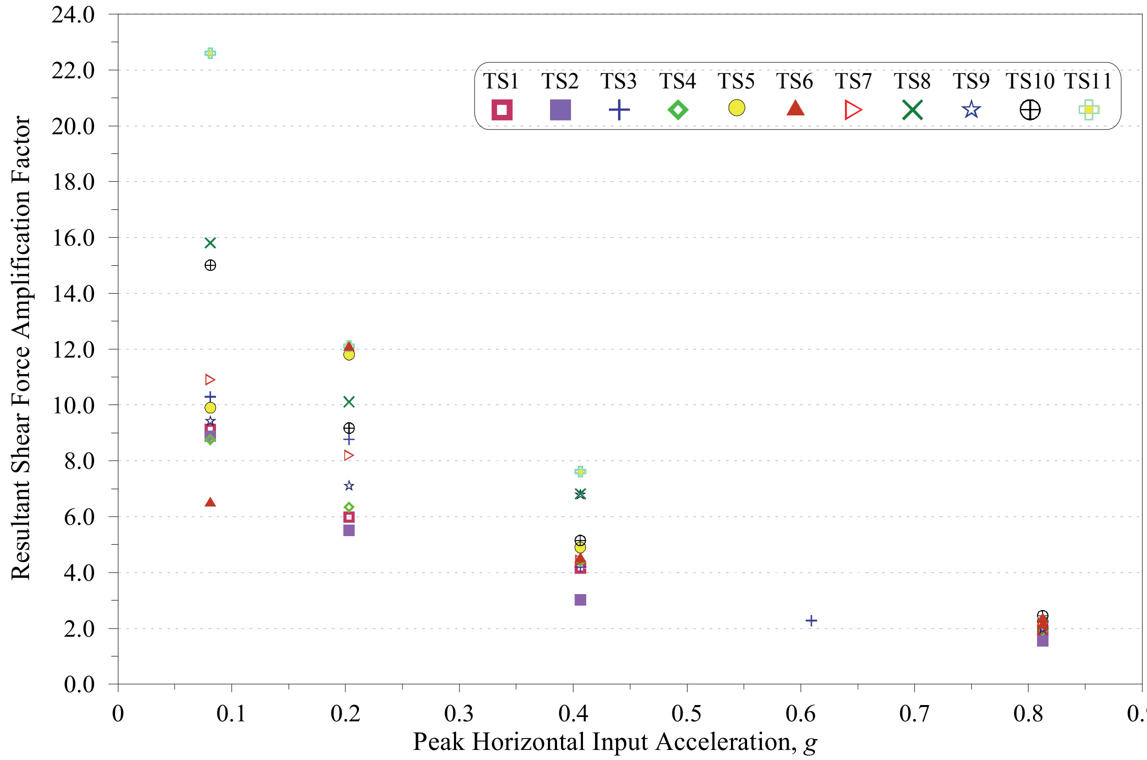

Figure 7-16 Variations of Resultant Shear *FAF* with Peak Horizontal Input Acceleration

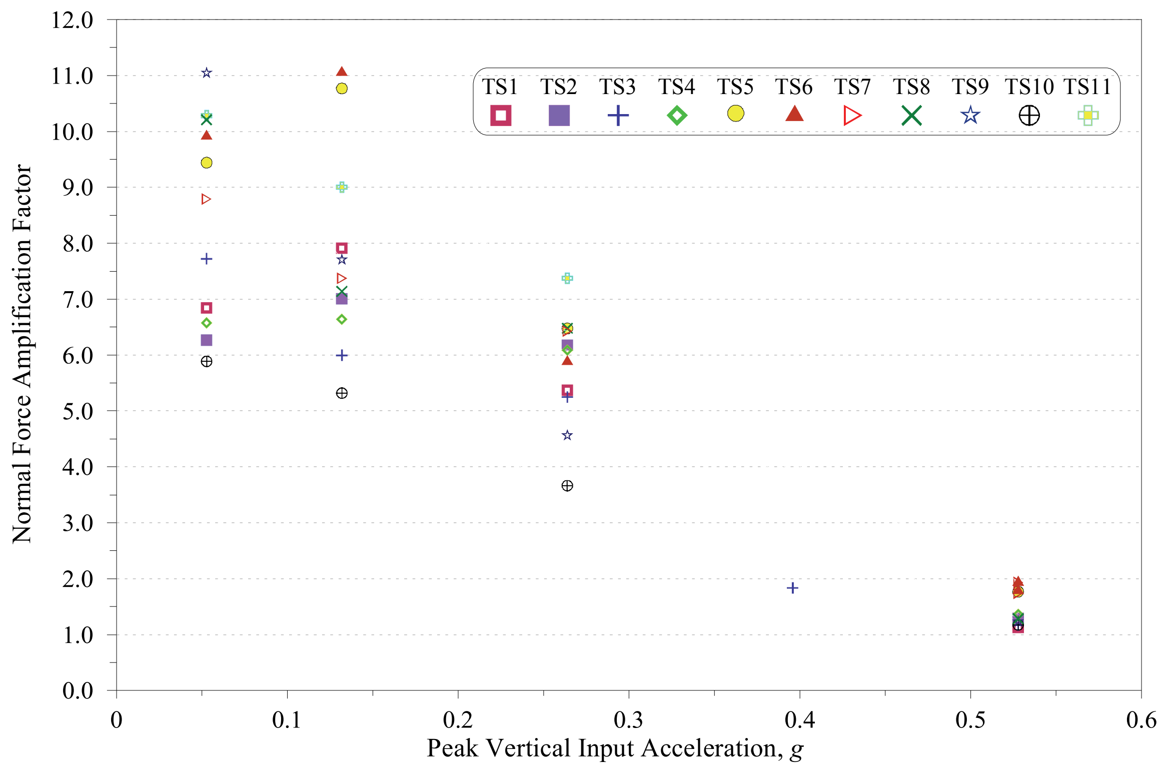

Figure 7-17 Variations of Normal *FAF* with Peak Vertical Input Acceleration

7.3 Effect of Restraint Component Properties on Seismic Performance of I/R Systems

The sensitivity of the seismic performance of the I/R systems to the variations of the restraint component properties are investigated in this section. Among several response quantities measured on the test specimen during the seismic tests, the horizontal, vertical, and resultant *AAF* near the center of mass, the peak relative displacement responses on top of the south face of the test specimen, and the maximum dynamic shear and normal forces induced into the I/R systems were selected as the main indicators of the seismic performance of the I/R system. Effects of variation of the gap size, rubber snubber thickness, and rubber snubber hardness on the seismic responses of the test specimen and on the dynamic forces induced into the I/R systems are described in Sections 7.3.1 through 7.3.3, respectively.

7.3.1 Effect of Gap Size

The test plan included two groups of test series that incorporated I/R systems with identical rubber snubber thickness and hardness, but different gap sizes. The first group of test series included TS5 and TS7, and the second group included TS6 and TS8. Table 7-13, lists the identical and variable properties of the restraint components of I/R systems incorporated in the test series of each group.

Table 7-13 Restraint Component Properties in Test Series Conducted to Study Effect of Gap Size on Seismic Performance of I/R System

	Test Series	Identical Properties: Rubber Snubber Thickness, *mm* (*in.*)		Identical Properties: Rubber Snubber Hardness, *Duro.*		Variable Property: Gap Size, *mm* (*in.*)
		Horizontal Snubber	Vertical Snubber	Horizontal Snubber	Vertical Snubber	
Group I	TS5	6 (0.25)	6 (0.25)	40	40	13 (0.5)
	TS7	6 (0.25)	6 (0.25)	40	40	6 (0.25)
Group II	TS6	6 (0.25)	6 (0.25)	60	60	13 (0.5)
	TS8	6 (0.25)	6 (0.25)	60	60	6 (0.25)

The variations of the horizontal, vertical, and resultant *AAF* on top of the motor with the corresponding peak input acceleration during the seismic tests of Groups I and II are shown in Figures 7-18 and 7-19, respectively. The results of Test Series TS12 have been added to these figures to compare the amplification of the acceleration response of the isolated and rigidly mounted test specimen to each other.

The effect of doubling the gap size of the restraint components from 6 *mm* (0.25 *in.*) to 13 *mm* (0.5 *in.*) on the acceleration responses on top of the motor varied with the input motion amplitude. In the tests with the low-to-moderate amplitude input motions, increasing the gap size from 6 *mm* (0.25 *in.*) to 13 *mm* (0.5 *in.*) resulted in a decrease of the acceleration response on the top of the motor. However, in the tests with the high amplitude input motions, doubling the gap size from 6 *mm* (0.25 *in.*) to 13 *mm* (0.5 *in.*) increased the acceleration response on the top of the motor. The reason for this trend is that the responses of the test specimen to the low-to-moderate amplitude input motions were relatively small and the large air gap precluded the engagement of the restraint components with high frequency and intensity. However, for the high amplitude input motions, engagement of the restraint components with high intensity and frequency was inevitable and the large air gap allowed the test specimen to accelerate more and engage the restraint components with higher momentum.

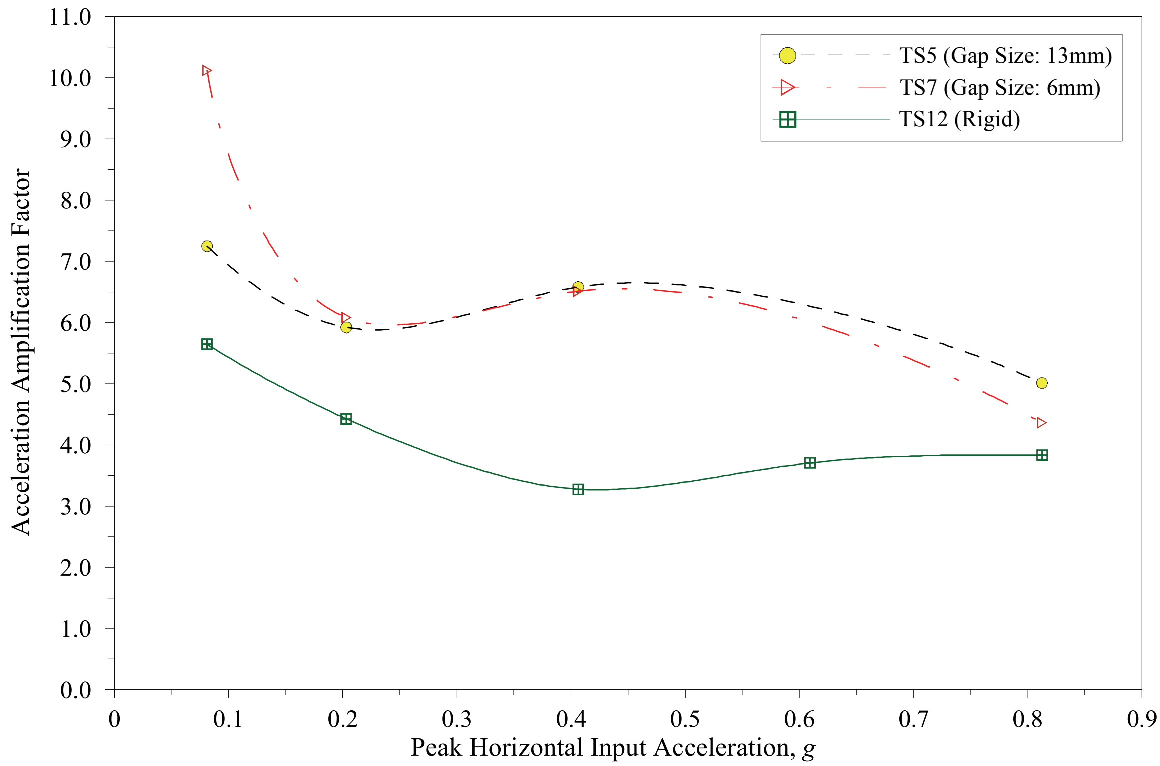

(a) Horizontal *AAF* on Top of Motor Vs. Peak Horizontal Input Acceleration

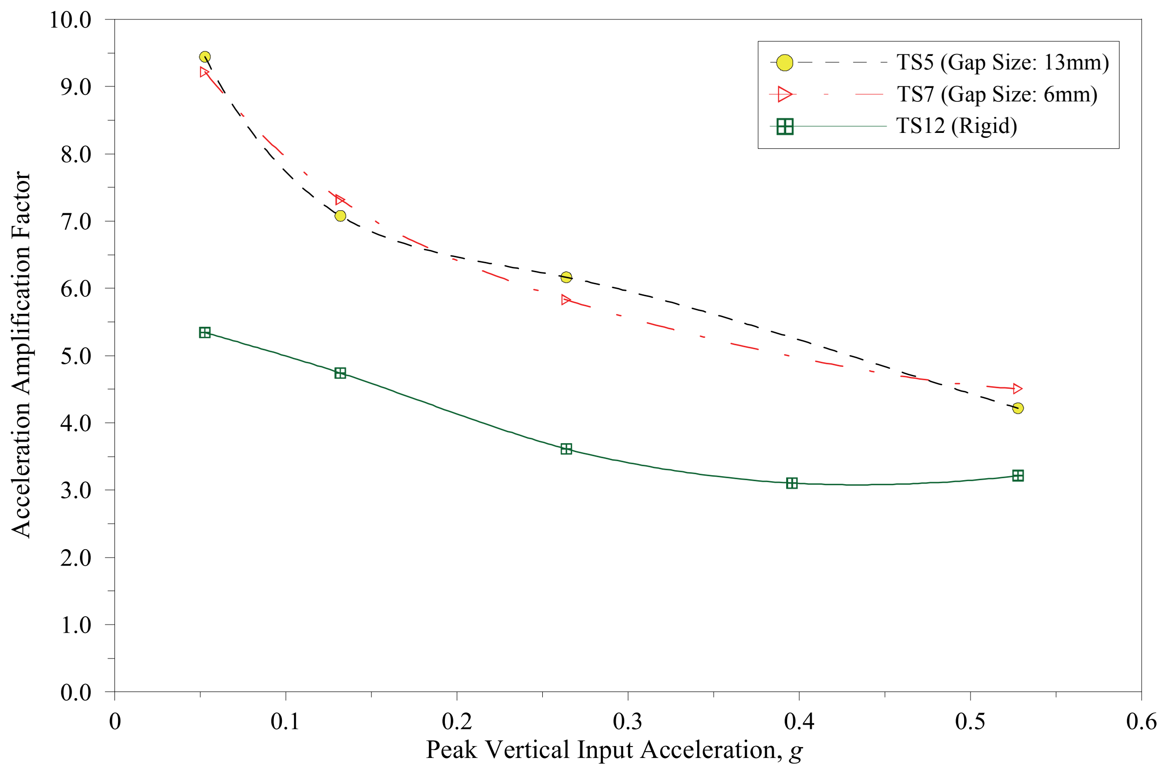

(b) Vertical *AAF* on Top of Motor Vs. Peak Vertical Input Acceleration

Figure 7-18 Effect of Variation of Restraint Component Gap Size on *AAF* near Center of Mass of Test Specimen (on Top of Motor), Comparison of Results of Test Series 5 and 7

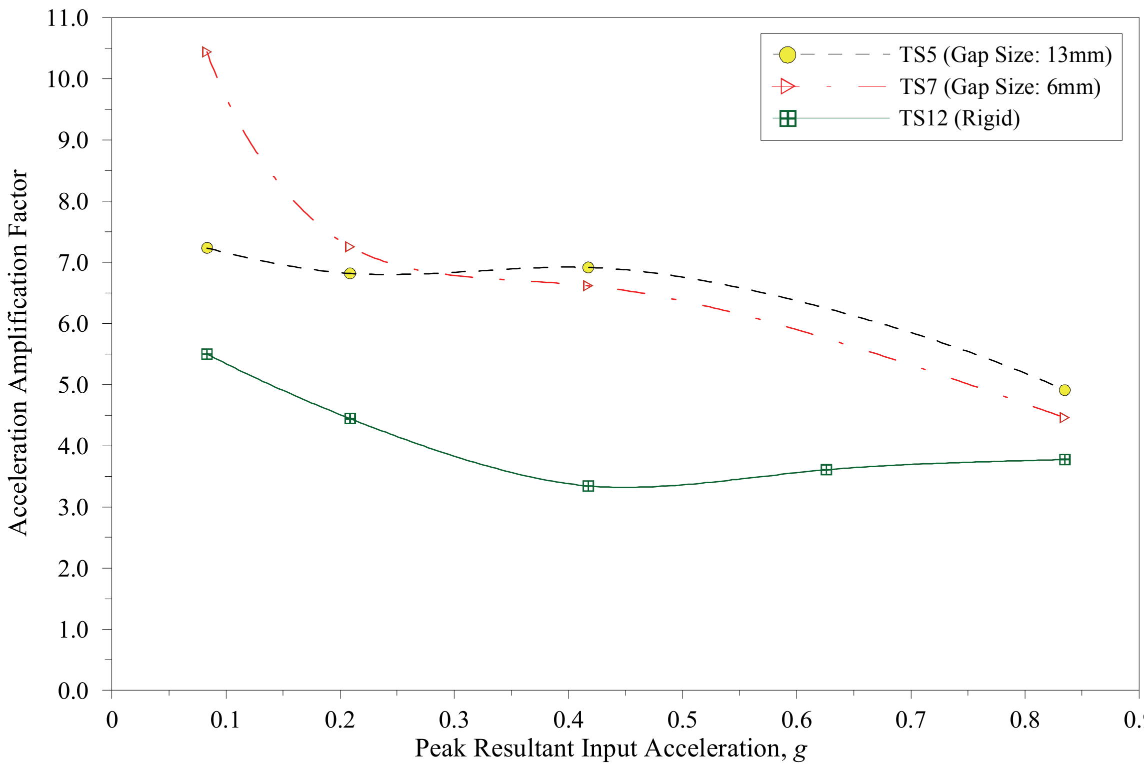

(c) Resultant *AAF* on Top of Motor Vs. Peak Resultant Input Acceleration

Figure 7-18 (cont'd) Effect of Variation of Restraint Component Gap Size on *AAF* near Center of Mass of Test Specimen (on Top of Motor), Comparison of Results of Test Series 5 and 7

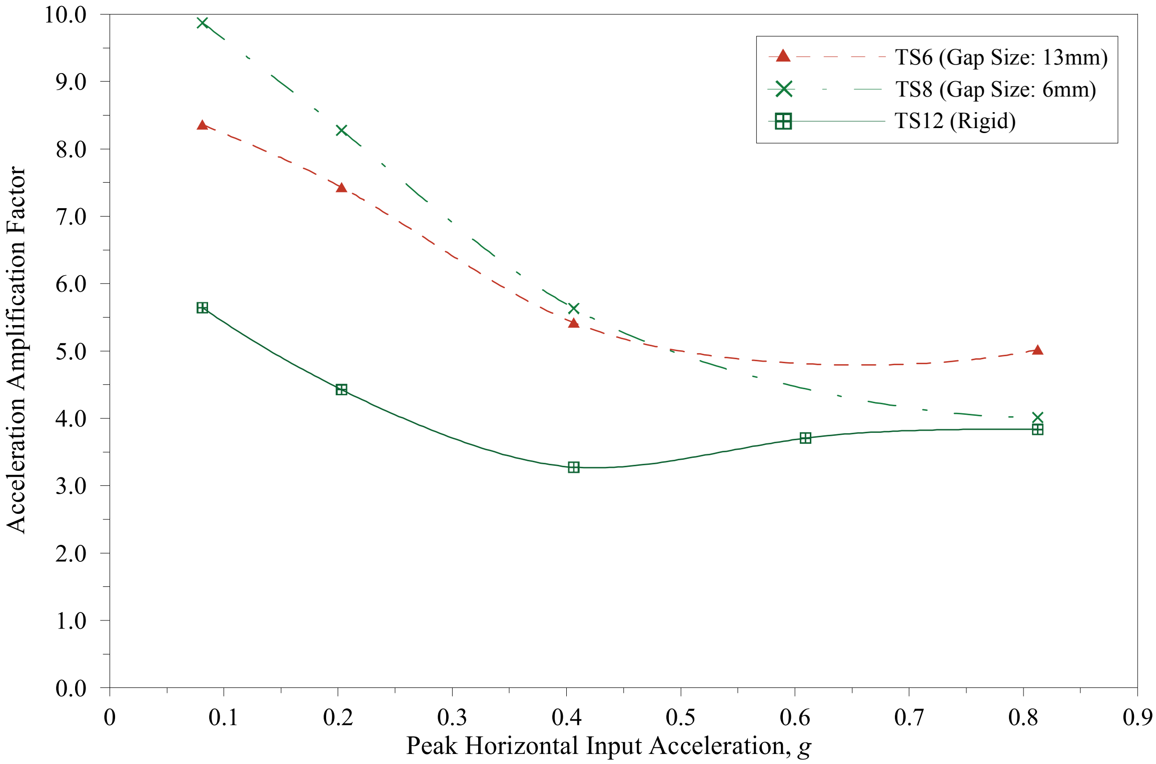

(a) Horizontal *AAF* on Top of Motor Vs. Peak Horizontal Input Acceleration

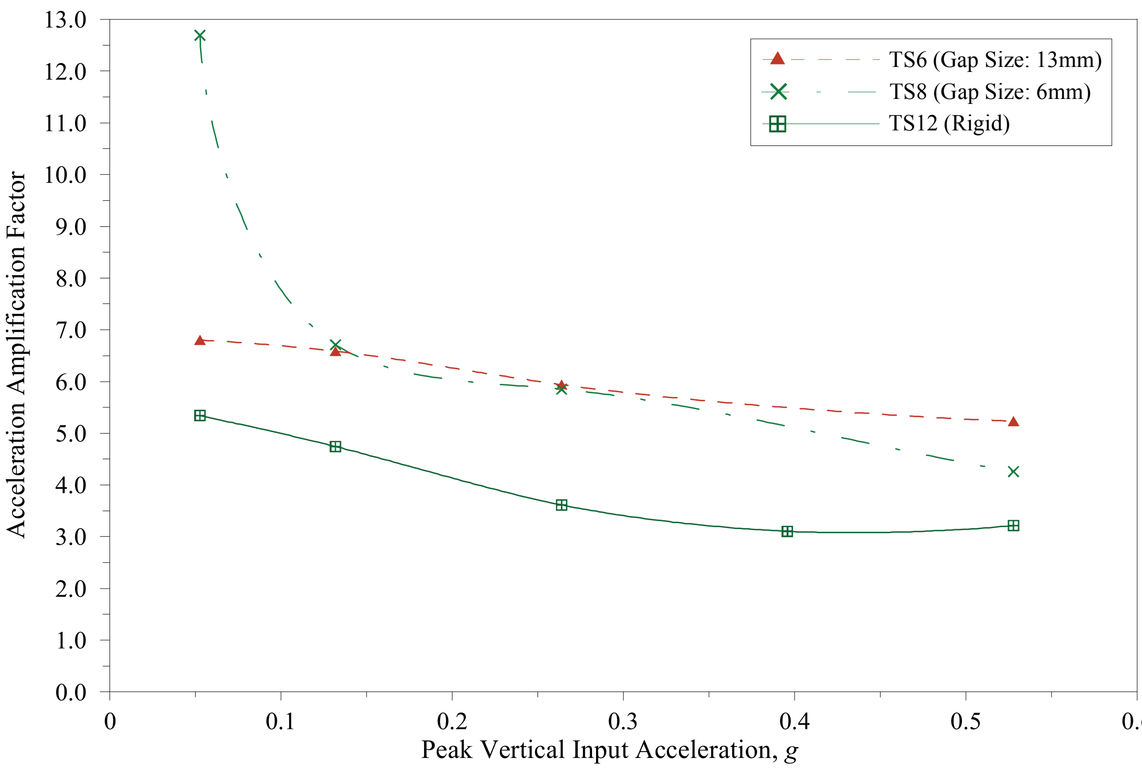

(b) Vertical *AAF* on Top of Motor Vs. Peak Vertical Input Acceleration

Figure 7-19 Effect of Variation of Restraint Component Gap Size on *AAF* near Center of Mass of Test Specimen (on Top of Motor), Comparison of Results of Test Series 6 and 8

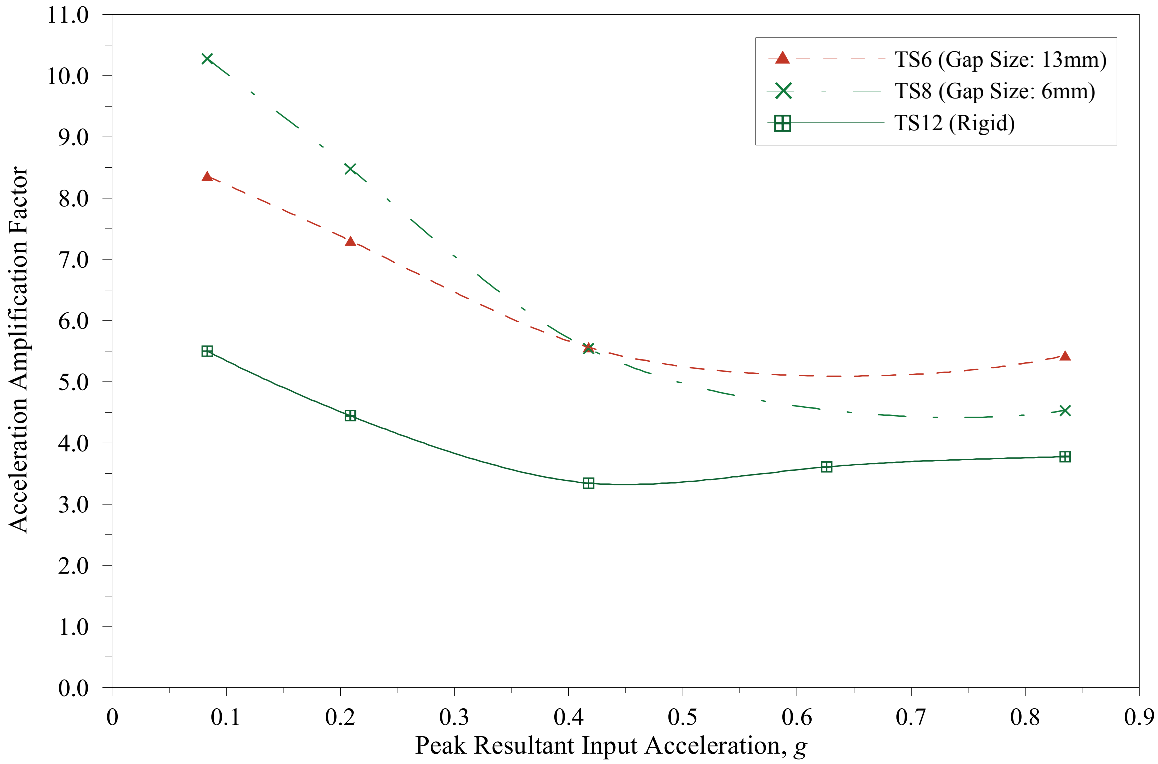

(c) Resultant *AAF* on Top of Motor Vs. Peak Resultant Input Acceleration

Figure 7-19 (cont'd) Effect of Variation of Restraint Component Gap Size on *AAF* near Center of Mass of Test Specimen (on Top of Motor), Comparison of Results of Test Series 6 and 8

The variations of the maximum horizontal and vertical relative displacement responses on the south face of the isolated test specimen with the corresponding peak input acceleration during the seismic tests of the test series of Group I and II are shown in Figures 7-20 and 7-21, respectively.

The test results show that regardless of the input motion amplitude, increasing the gap size from 6 *mm* (0.25 *in.*) to 13 *mm* (0.5 *in.*) resulted in a significant increase of the relative displacement responses of the test specimen. Due to the contributions of the rotational responses and deformation of the rubber snubbers to the displacement responses of the test specimen, the increase of the peak relative displacement response was usually larger than the 6 *mm* (0.25 *in.*) enlargement of the gap size. With an increase of the input motion amplitude, the rotational responses of the test specimen and intensity of the engagement of the rubber snubbers increased. Therefore, the effect of the large gap size on the amplification of the relative displacement responses of the test specimen increased with an increase of the input motion amplitude. For instance, with the full-scale input motion, doubling the gap size from 6 *mm* (0.25 *in.*) in Test Series TS7 to 13 *mm* (0.5 *in.*) in Test Series TS5 resulted in 19 *mm* (0.75 *in.*) increase of the horizontal relative displacement response on the south face of the test specimen.

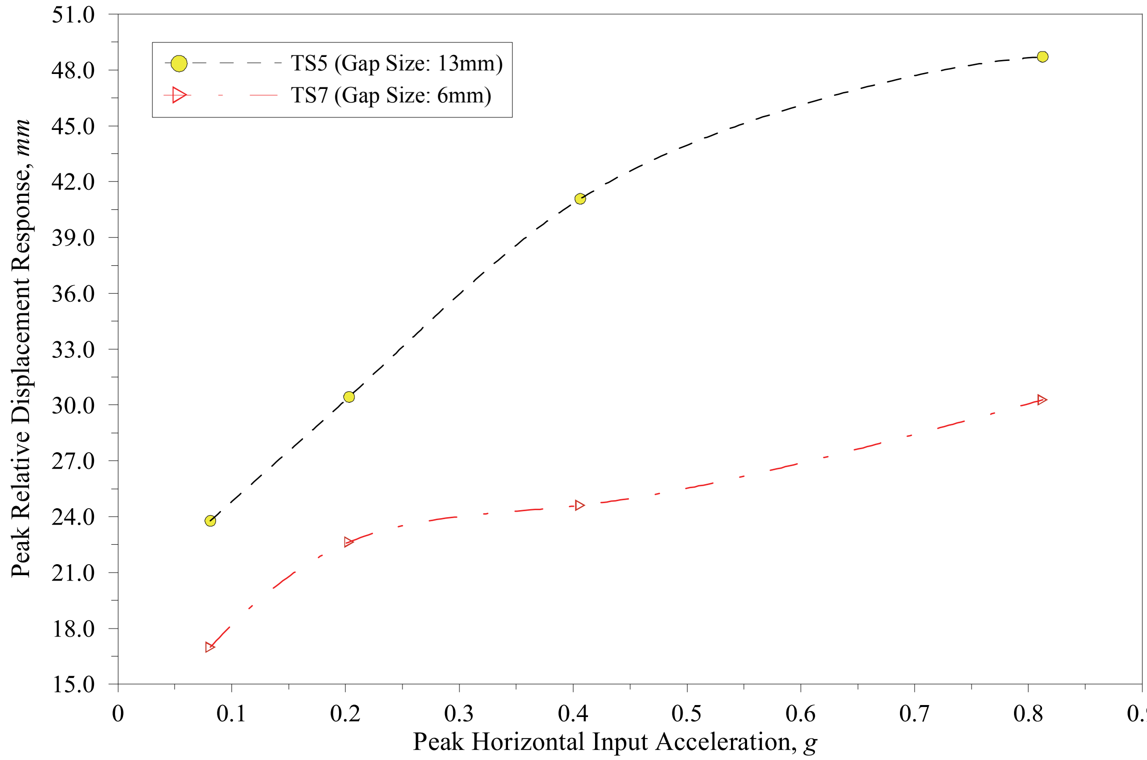

(a) Peak Horizontal Relative Displacement Response Vs. Peak Horizontal Input Acceleration

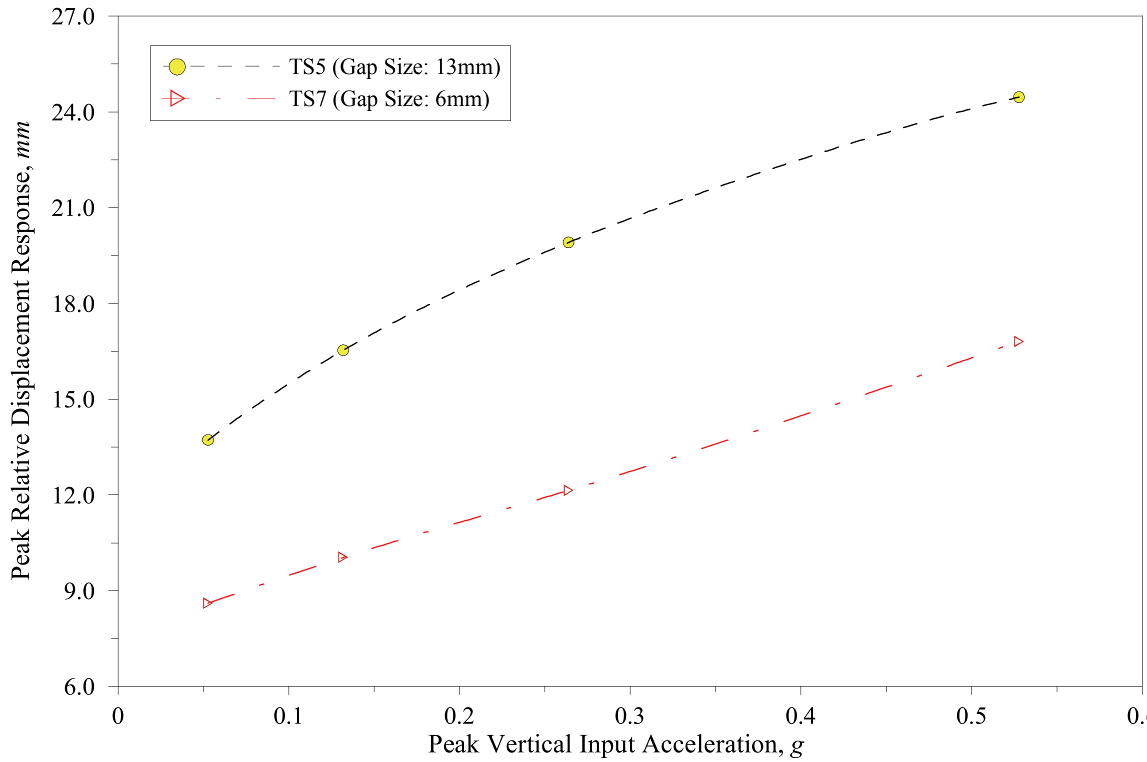

(b) Peak Vertical Relative Displacement Response Vs. Peak Vertical Input Acceleration

Figure 7-20 Effect of Variation of Restraint Component Gap Size on Peak Relative Displacement Responses at Top-South-East Corner of Test Specimen, Comparison of Results of Test Series 5 and 7

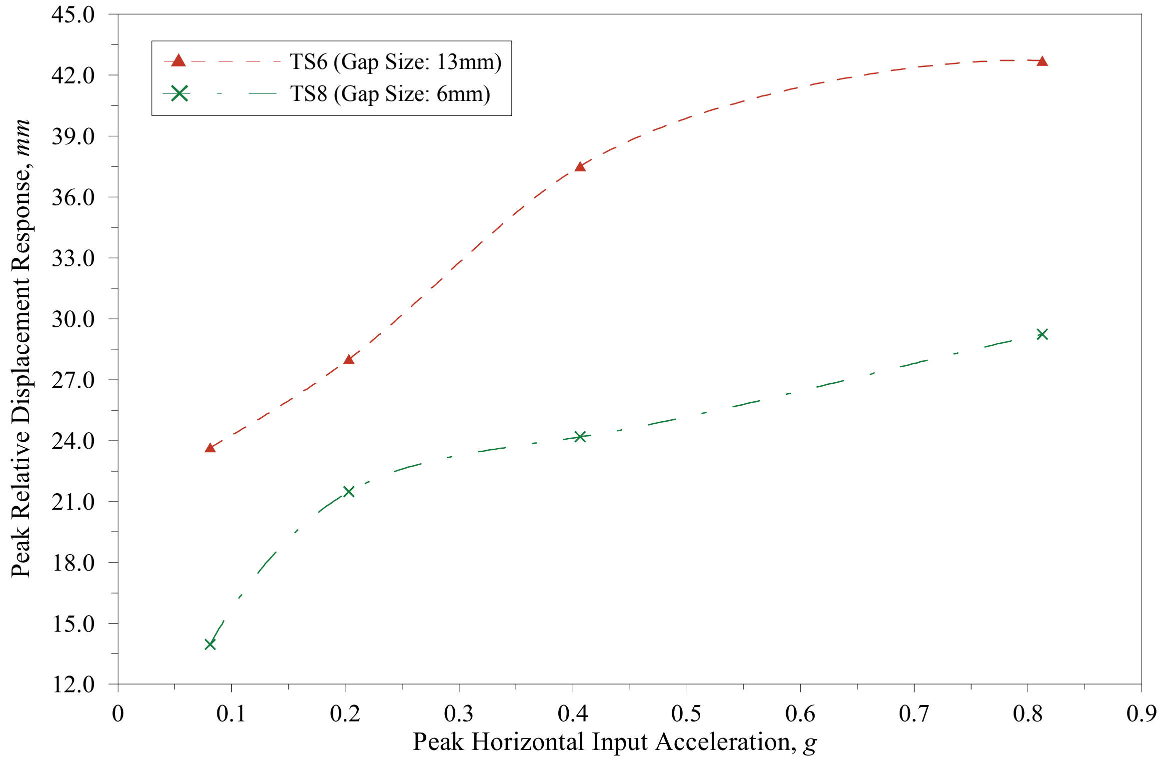

(a) Peak Horizontal Relative Displacement Response Vs. Peak Horizontal Input Acceleration

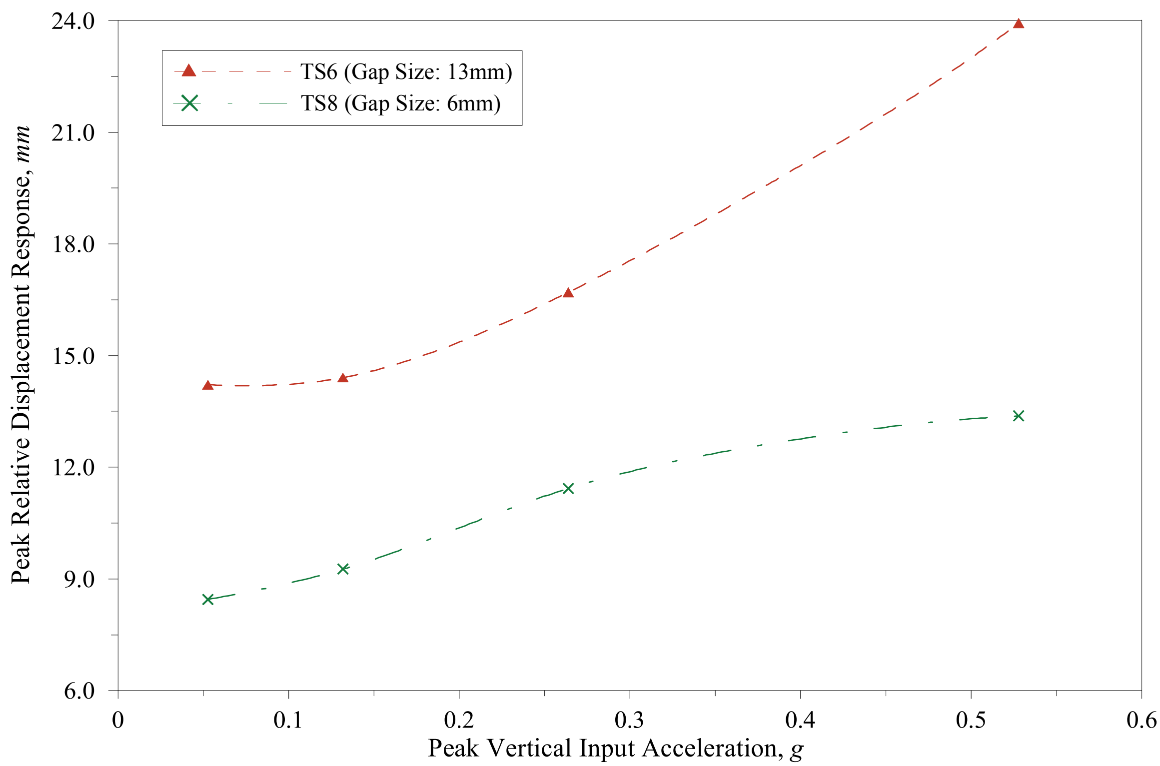

(b) Peak Vertical Relative Displacement Response Vs. Peak Vertical Input Acceleration

Figure 7-21 Effect of Variation of Restraint Component Gap Size on Peak Relative Displacement Responses at Top-South-East Corner of Test Specimen, Comparison of Results of Test Series 6 and 8

The variations of the maximum dynamic shear and normal forces induced into the I/R systems with the corresponding peak input acceleration during the seismic tests of the test series of Group I and II are shown in Figures 7-22 and 7-23, respectively. The results of Test Series TS12 have been added to these figures to compare the dynamic forces at the support locations of the isolated and rigidly mounted test specimen.

In the test series of Group I with the soft rubber snubber (Test Series TS5 and TS7), regardless of the input motion amplitude, increasing the gap size from 6 *mm* (0.25 *in.*) to 13 *mm* (0.5 *in.*) has resulted in an increase of the dynamic forces induced into the I/R systems. However, in the test series of Group II with the hard rubber snubber (Test Series TS6 and TS8), the effect of increasing the gap size on the dynamic forces induced into the I/R systems varied with the input motion amplitude. During these two test series, the detrimental effect of the enlargement of the gap size in increasing the dynamic forces (particularly the normal forces) induced into the I/R systems was mainly seen in the tests with full-scale input motion.

The results obtained in this study and the results of the previous study on the seismic performance of the I/R systems (Fathali and Filiatrault, 2007) show that depending on the response amplitude, the large air gap can be relatively beneficial or seriously detrimental. The large air gap might be beneficial by allowing the equipment to respond to the input motion without intense engagement of the restraint components or might be seriously problematic by allowing the equipment to accelerate in a larger domain and engage the snubbers with higher velocity and momentum. With so many uncertainties about the input motion characteristics and given the fact that increasing the gap size always results in a considerable increase of the displacement response of the equipment, it can be concluded that increasing the gap size degrades the overall seismic performance of the I/R system and should be avoided.

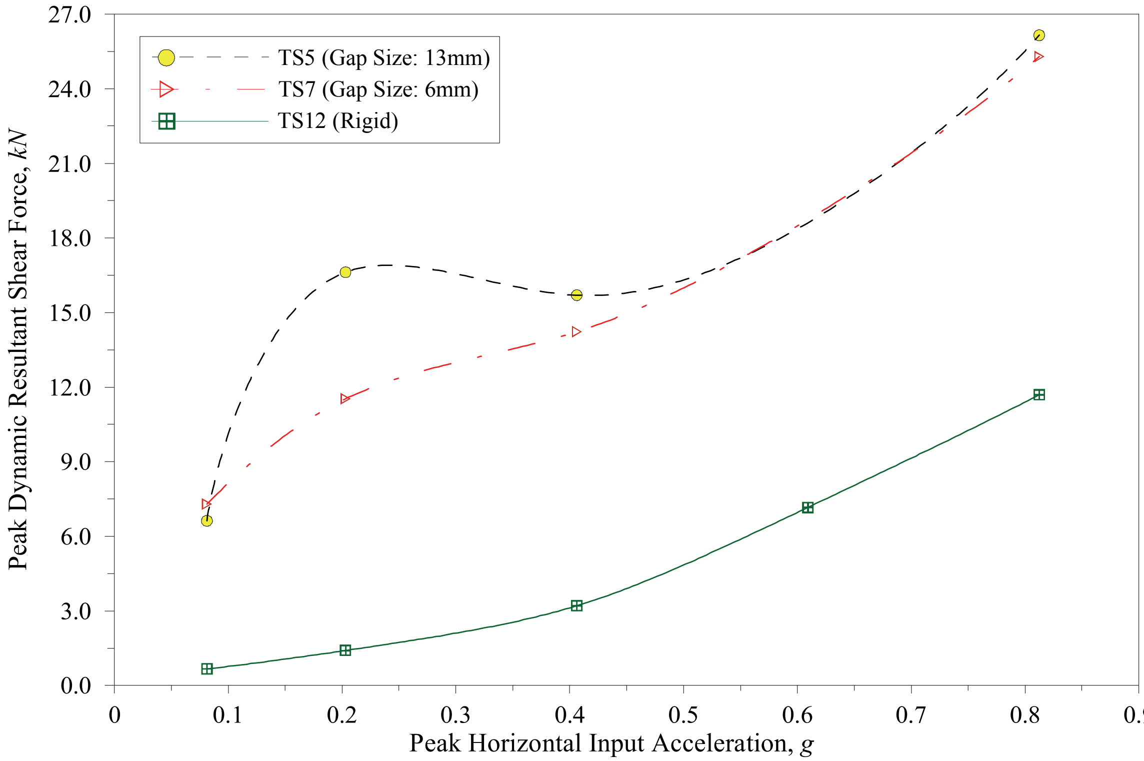

(a) Maximum Shear Force Induced into I/R Systems Vs. Peak Horizontal Input Acceleration

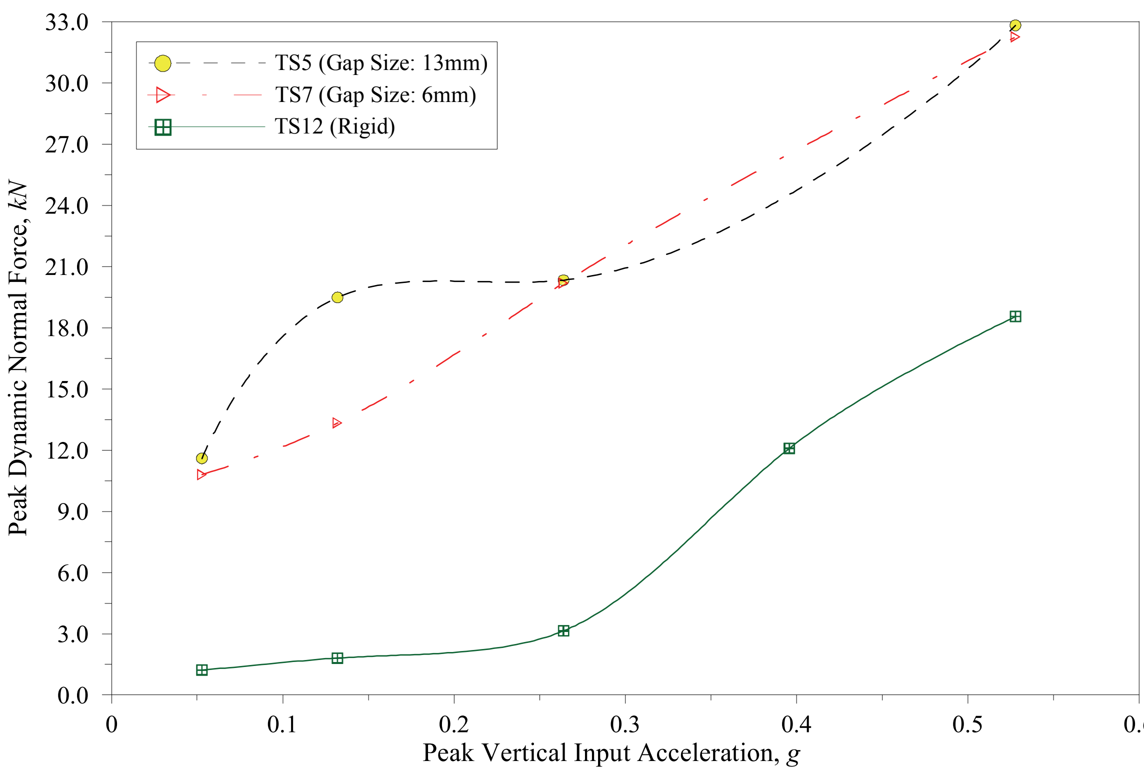

(b) Maximum Normal Force Induced into I/R Systems Vs. Peak Vertical Input Acceleration

Figure 7-22 Effect of Variation of Restraint Component Gap Size on Peak Dynamic Forces Induced into I/R Systems, Comparison of Results of Test Series 5 and 7

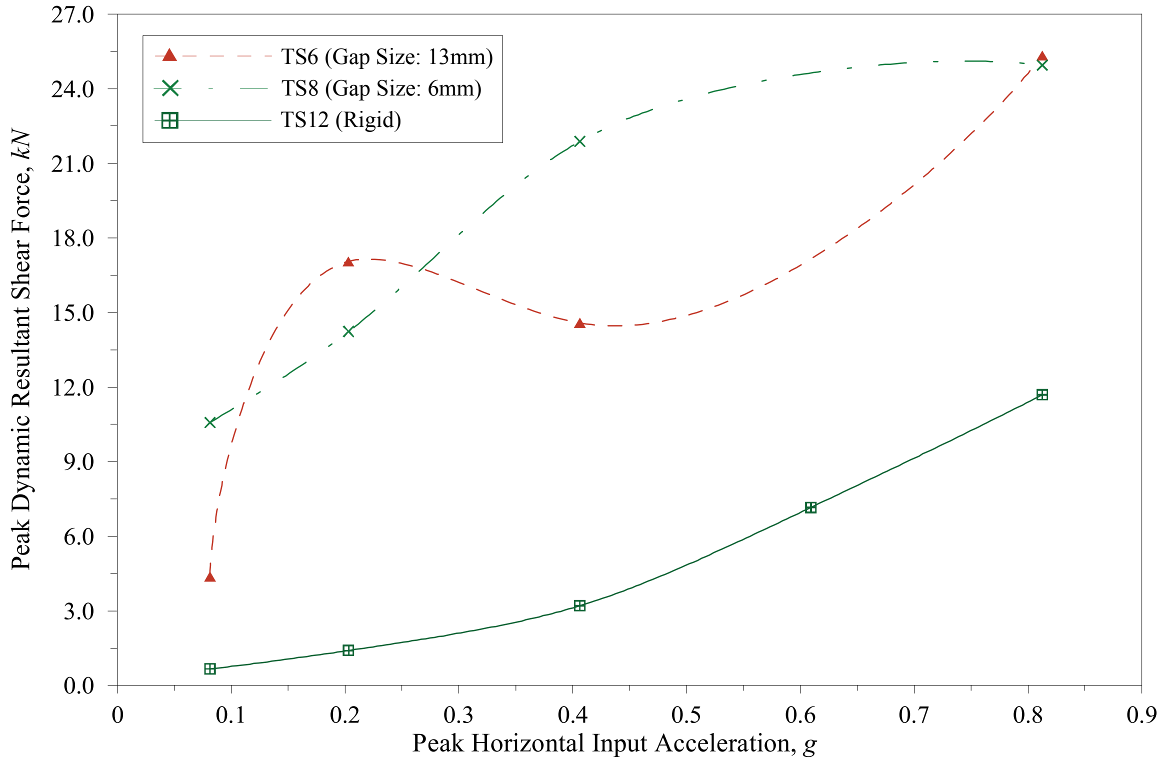

(a) Maximum Shear Force Induced into I/R Systems Vs. Peak Horizontal Input Acceleration

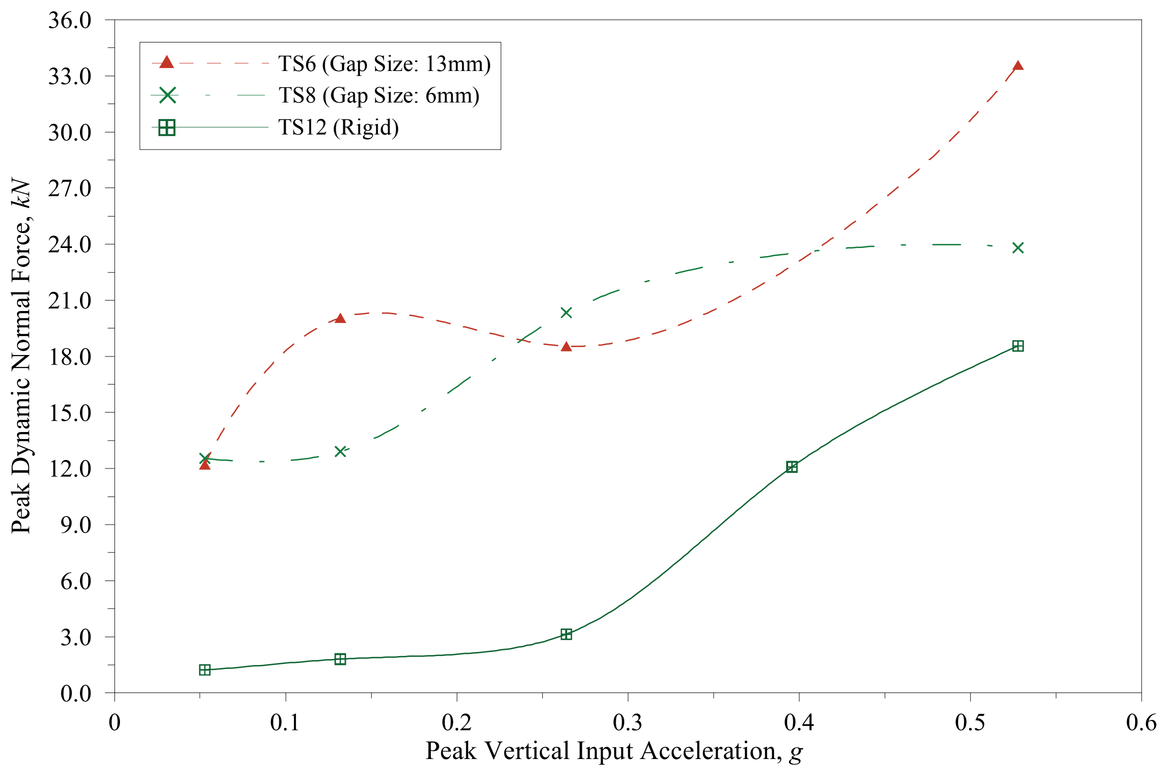

(b) Maximum Normal Force Induced into I/R Systems Vs. Peak Vertical Input Acceleration

Figure 7-23 Effect of Variation of Restraint Component Gap Size on Peak Dynamic Forces Induced into I/R Systems, Comparison of Results of Test Series 6 and 8

7.3.2 Effect of Rubber Snubber Thickness

The test plan included two groups of test series that incorporated I/R systems with identical rubber snubber hardness and equal gap size, but different rubber snubber thicknesses. The first group of test series included TS1, TS3, and TS7, and the second group included TS2, TS4, and TS8. Table 7-14, lists the identical and variable properties of the restraint components of I/R systems incorporated in the test series of each group.

Table 7-14 Restraint Component Properties in Test Series Conducted to Study Effect of Rubber Snubber Thickness on Seismic Performance of I/R System

	Test Series	Identical Properties:			Variable Property:	
		Gap Size, *mm* (*in.*)	Rubber Snubber Hardness, *Duro.*		Rubber Snubber Thickness, *mm* (*in.*)	
			Horizontal Snubber	Vertical Snubber	Horizontal Snubber	Vertical Snubber
Group I	TS1	6 (0.25)	40	40	19 (0.75)	19 (0.75)
	TS3				13 (0.5)	13 (0.5)
	TS7				6 (0.25)	6 (0.25)
Group II	TS2	6 (0.25)	60	60	19 (0.75)	19 (0.75)
	TS4				13 (0.5)	13 (0.5)
	TS8				6 (0.25)	6 (0.25)

The variations of the horizontal, vertical, and resultant *AAF* on the top of the motor with the corresponding peak input acceleration during the seismic tests of Groups I and II are shown in Figures 7-24 and 7-25, respectively. The results of Test Series TS12 have been added to these figures to compare the amplification of the acceleration response of the isolated and rigidly mounted test specimen. In addition, the results of Test Series TS11 have been included in these figures to investigate the effect of removing the rubber snubbers on the acceleration responses of the isolated test specimen. However, it should be considered that the gap size of the I/R systems in Test Series TS11 was 3 *mm* (0.125 *in.*) smaller than the gap size of the I/R systems in the other test series.

The test results show that in the tests with the low-to-moderate amplitude input motions, increasing the rubber snubber thickness resulted in a reduction of the acceleration response on top of the motor. However, the opposite trend took place during the tests with high amplitude input motions. Moreover, the test results show that the combination of reduced rubber hardness and increased rubber thickness resulted in very large acceleration responses on the top of the motor. As shown in Figure 7-24, regardless of the input motion amplitude, the resultant acceleration response on the top of the motor was always larger during Test Series TS1 (thickest and softer snubber) than during the other two test series of Group I (Test Series TS7 and TS3).

The variations of the peak relative displacement responses on the south face of the test specimen during the seismic tests of Groups I and II are shown in Figures 7-26 and 7-27, respectively. The results of Test Series TS11 have been included in these figures to investigate the effect of removing the rubber snubbers on the displacement responses of the isolated test specimen. The results show that, in most cases, increasing the rubber thickness resulted in an increase of the displacement response of the test specimen.

Given the fact that the gap size of the I/R systems in Test Series TS11 (I/R systems without rubber snubber) was 3 *mm* (0.125 *in.*) larger than the gap size of the I/R systems during the other test series, the reduction of the peak relative displacement responses of the test specimen during Test Series TS11 highlights the significant contribution of the rubber snubbers in increasing the displacement response of the test specimen.

The variations of the maximum dynamic shear and normal forces induced into the I/R systems with the corresponding peak input acceleration during the seismic tests of Groups I and II are shown in Figures 7-28 and 7-29, respectively. The results of Test Series TS12 have been added to these figures to compare the dynamic forces at the support locations of the isolated and rigidly mounted test specimen. In addition, the results of Test Series TS11 have been included in these figures to investigate the effect of removing the rubber snubbers on the dynamic forces induced into the I/R systems.

The test results show that despite the increased acceleration and displacement response of the test specimen, in most of the tests increasing the rubber snubber thickness resulted in a reduction of the peak dynamic forces induced into the I/R systems. Decreases in the translational acceleration responses of all points of the test specimen would certainly result in reductions of the dynamic forces induced into the I/R systems. Conversely however, as the tests results showed, reduction of the dynamic forces induced into the I/R systems does not mean that all the points of the test specimen experienced lower translational acceleration responses. In fact, increases of the translational acceleration responses near the center of mass of the test specimen and reductions of the dynamic forces induced into the I/R systems occurred often during the same seismic test. In order to understand these apparently contradictory observations, the following characteristics of the seismic response of the test specimen should be considered:

1) A large portion of the dynamic forces induced into the I/R systems was attributed to the rotational responses of the test specimen. In other words, the dynamic force applied to the test specimen at the support locations created both translational and rotational acceleration responses. Therefore, in the presence of rotational acceleration responses in the equilibrium equation, a reduction of the dynamic force could occur at the same time as an in increase of the translational acceleration response.

2) Due to the rotational and vertical responses of the test specimen, the dynamic mass supported by each I/R system was not constant. Therefore, any change in the peak dynamic forces could be attributed to a change in any of the two variables of the equilibrium equation at the support location, namely the supported dynamic mass and the translational acceleration response. In other words, with the variable dynamic mass supported by each I/R system a reduction in the induced dynamic force could occur at the same time as an increase in the translational response.

3) The translational acceleration responses at different points of a rigid body, which is experiencing a combination of translational and rotational displacement, are not necessarily equal. Therefore, even if the reduction in dynamic forces induced into the I/R systems was as a result of a reduction in the translational acceleration responses at the support locations, this could still coincide with an increase of the translational acceleration responses at other locations of the test specimen, such as the center of mass.

The results obtained during Test Series TS11 show that the retraining mechanism without the rubber snubbers, which involves impacts between steel surfaces, resulted in excessive dynamic forces induced into the I/R systems. In fact, the dynamic forces induced into the I/R systems were so high that performing a seismic test with the full-scale input motion would have damaged the load cells installed under the I/R systems.

Based on the test results obtained, it can be concluded that increasing the thickness of the rubber snubbers is a successful modification in the restraint component properties to reduce the dynamic forces induces into the I/R systems. However, it might result in an increase of the acceleration responses of the test specimen and it certainly results in an increase of the displacement responses of the test specimen.

With the large air gap, large acceleration and displacement response are already expected and increasing the thickness of the rubber snubbers will hardly worsen the seismic performance of the I/R systems from those points of view. However, thick rubber snubbers are capable of reducing the potential strong dynamic forces induced into the I/R systems. In other words, in presence of large air gaps, increasing the rubber snubber thickness is a reasonable solution, because the unwanted consequences of the solution are negligible compared to its required benefits.

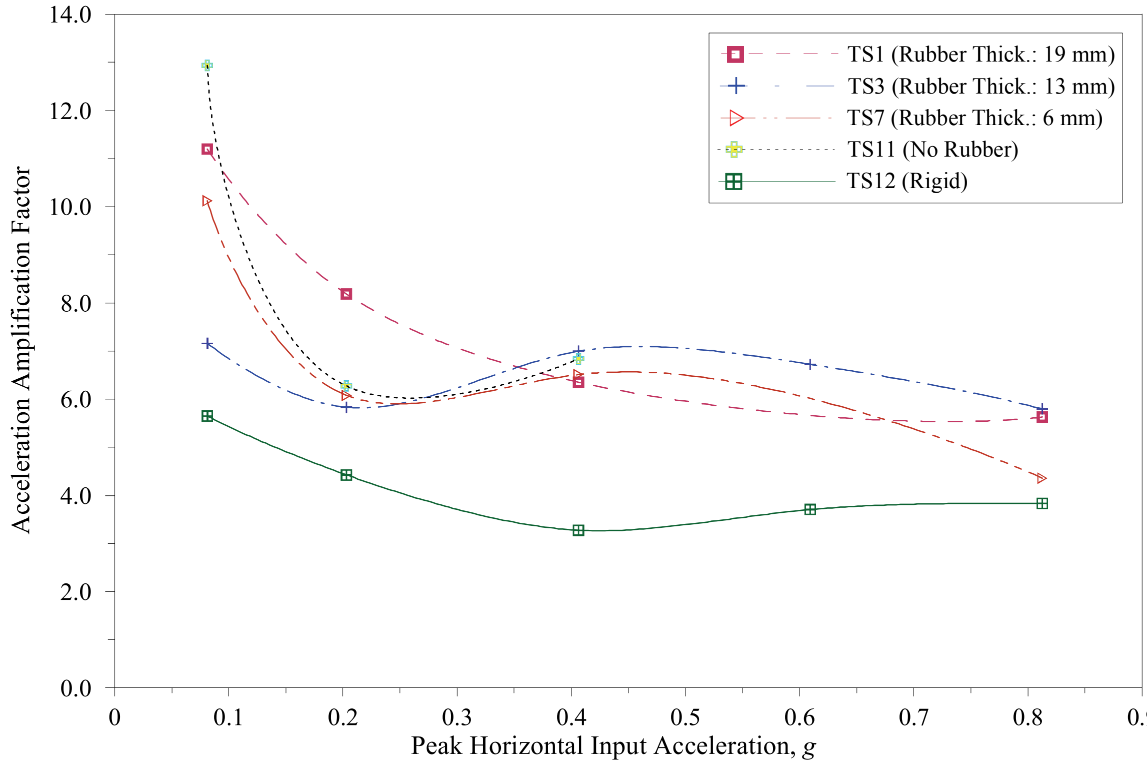

(a) Horizontal *AAF* on Top of Motor Vs. Peak Horizontal Input Acceleration

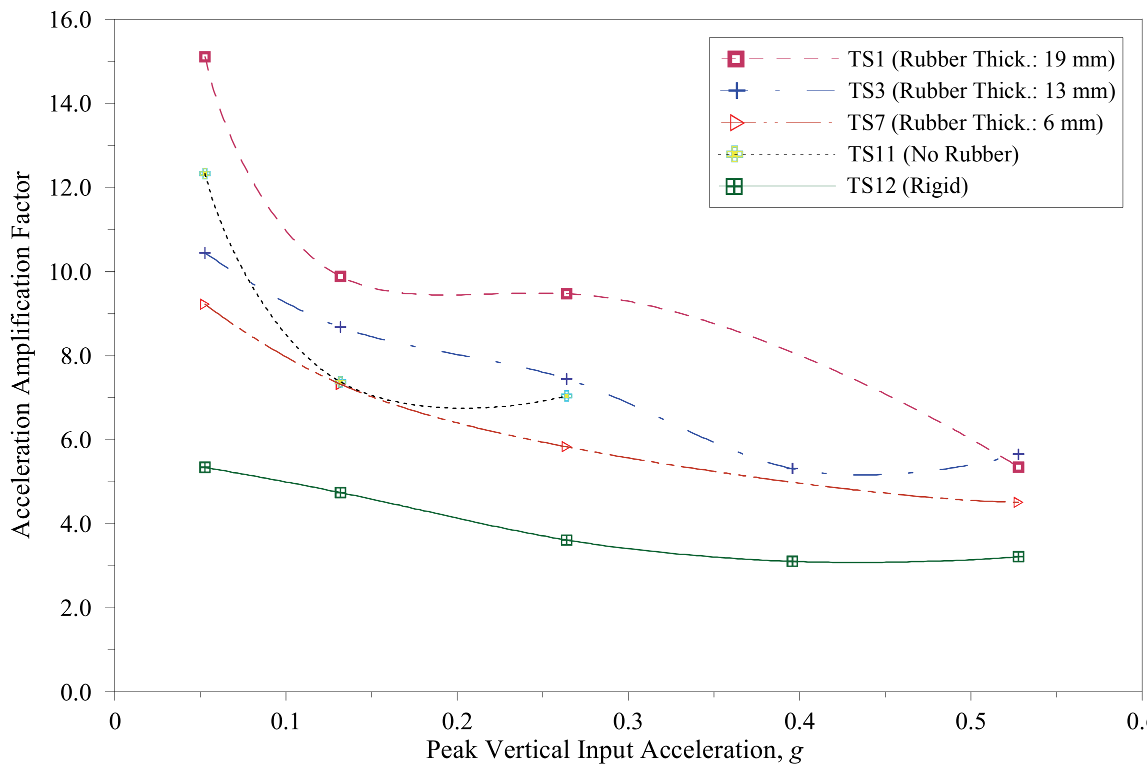

(b) Vertical *AAF* on Top of Motor Vs. Peak Vertical Input Acceleration

Figure 7-24 Effect of Variation of Rubber Snubber Thickness on *AAF* near Center of Mass of Test Specimen (on Top of Motor), Comparison of Results of Test Series 1, 3, 7, and 11

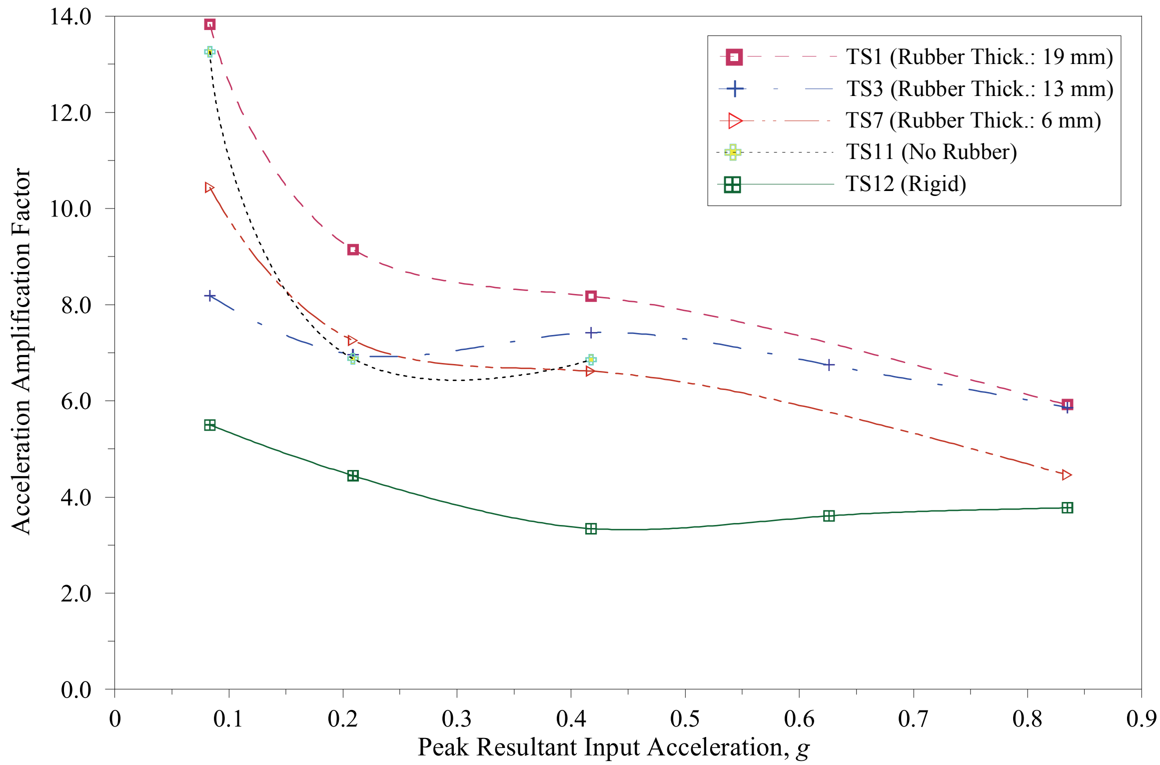

(c) Resultant *AAF* on Top of Motor Vs. Peak Resultant Input Acceleration

Figure 7-24 (cont'd) Effect of Variation of Rubber Snubber Thickness on *AAF* near Center of Mass of Test Specimen (on Top of Motor), Comparison of Results of Test Series 1, 3, 7, and 11

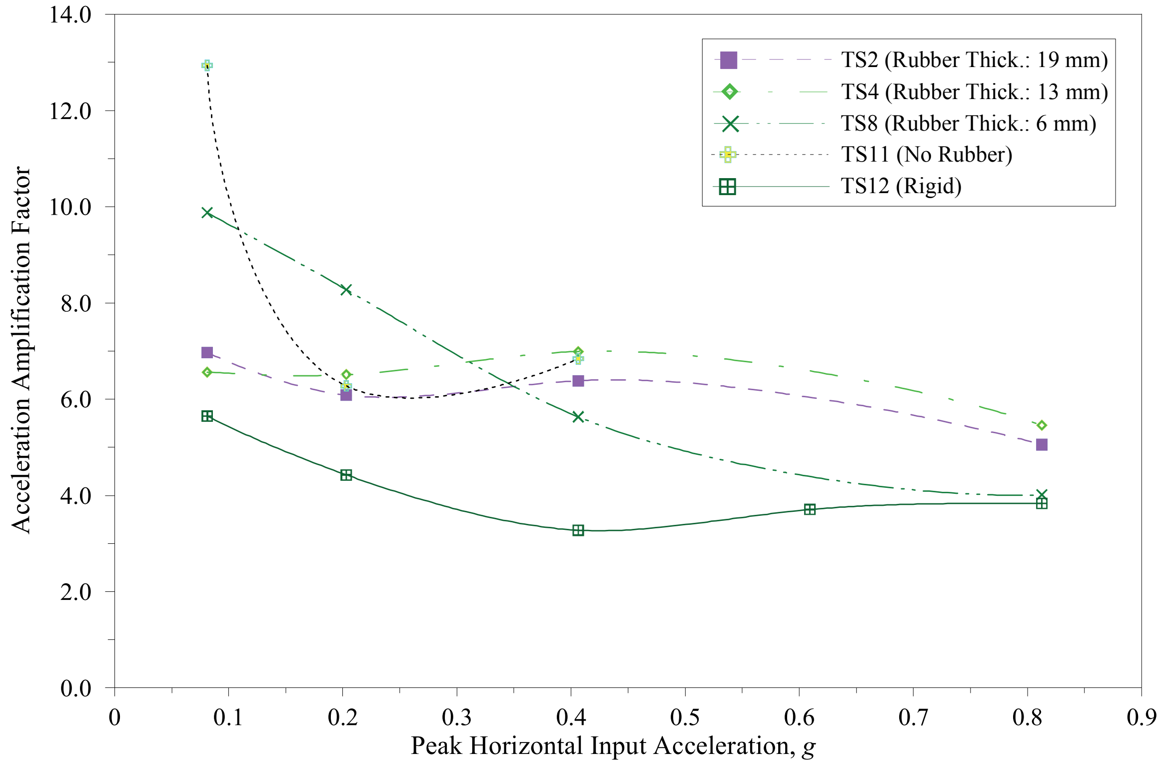

(a) Horizontal *AAF* on Top of Motor Vs. Peak Horizontal Input Acceleration

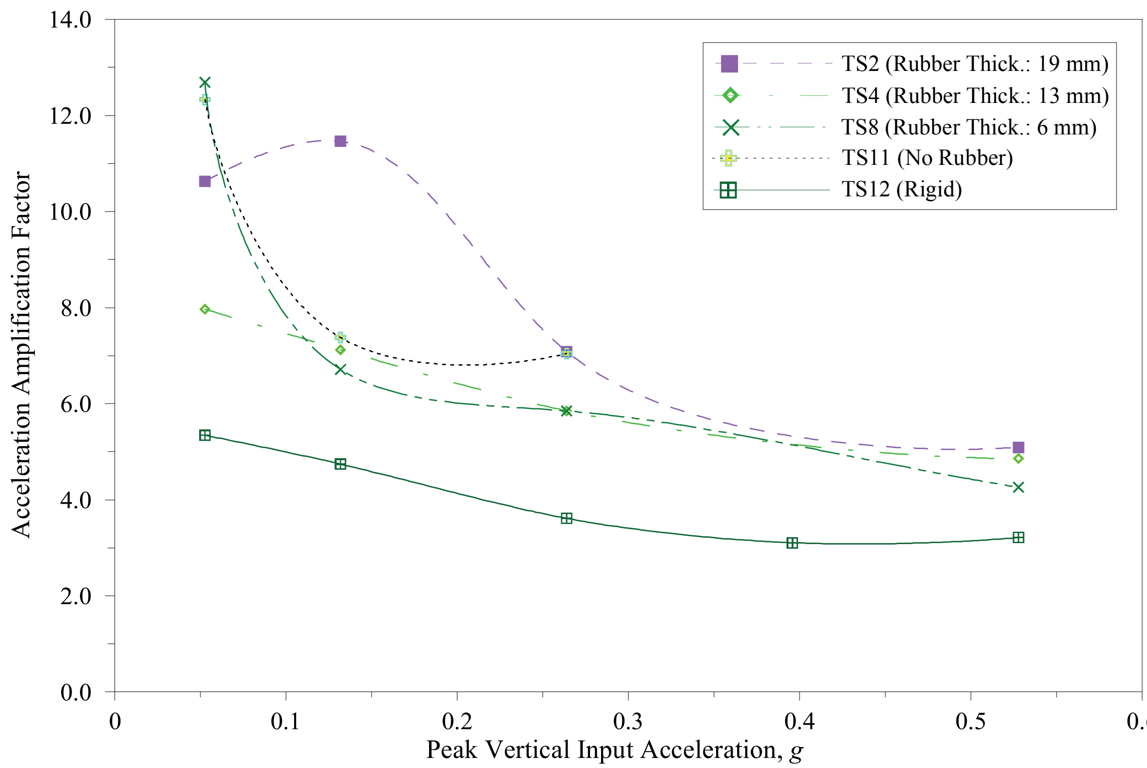

(b) Vertical *AAF* on Top of Motor Vs. Peak Vertical Input Acceleration

Figure 7-25 Effect of Variation of Rubber Snubber Thickness on *AAF* near Center of Mass of Test Specimen (on Top of Motor), Comparison of Results of Test Series 2, 4, 8, and 11

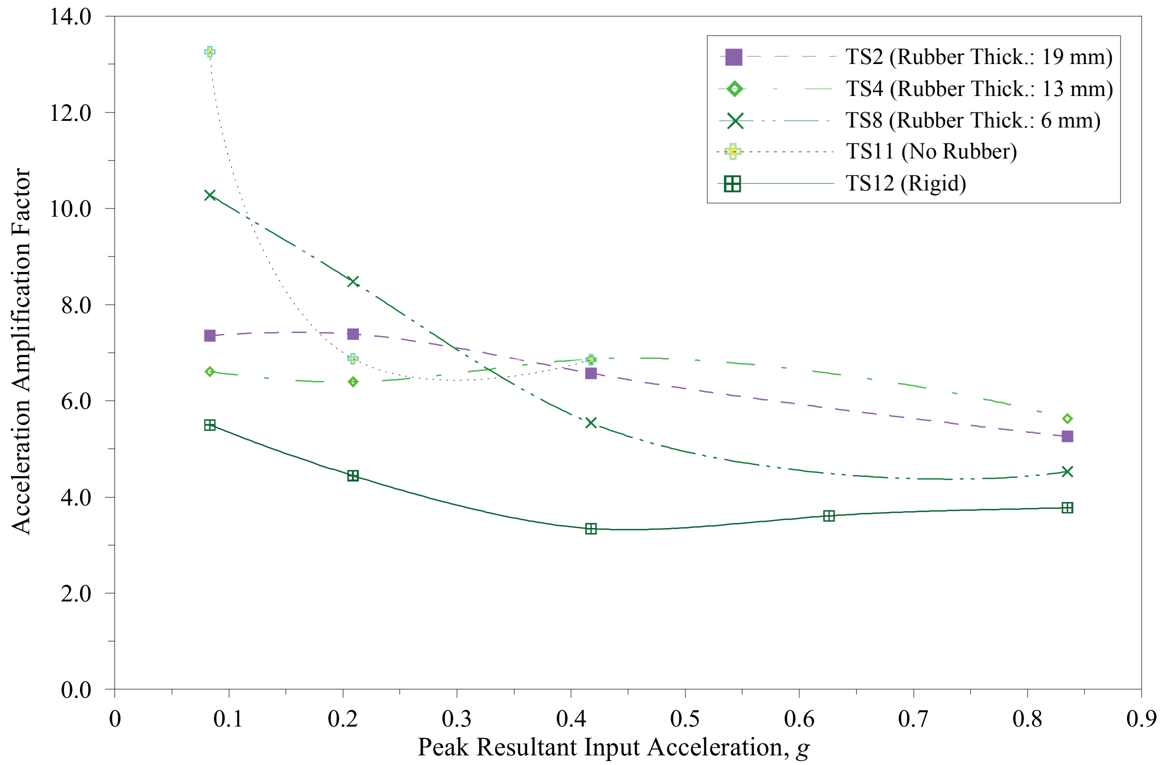

(c) Resultant *AAF* on Top of Motor Vs. Peak Resultant Input Acceleration

Figure 7-25 (cont'd) Effect of Variation of Rubber Snubber Thickness on *AAF* near Center of Mass of Test Specimen (on Top of Motor), Comparison of Results of Test Series 2, 4, 8, and 11

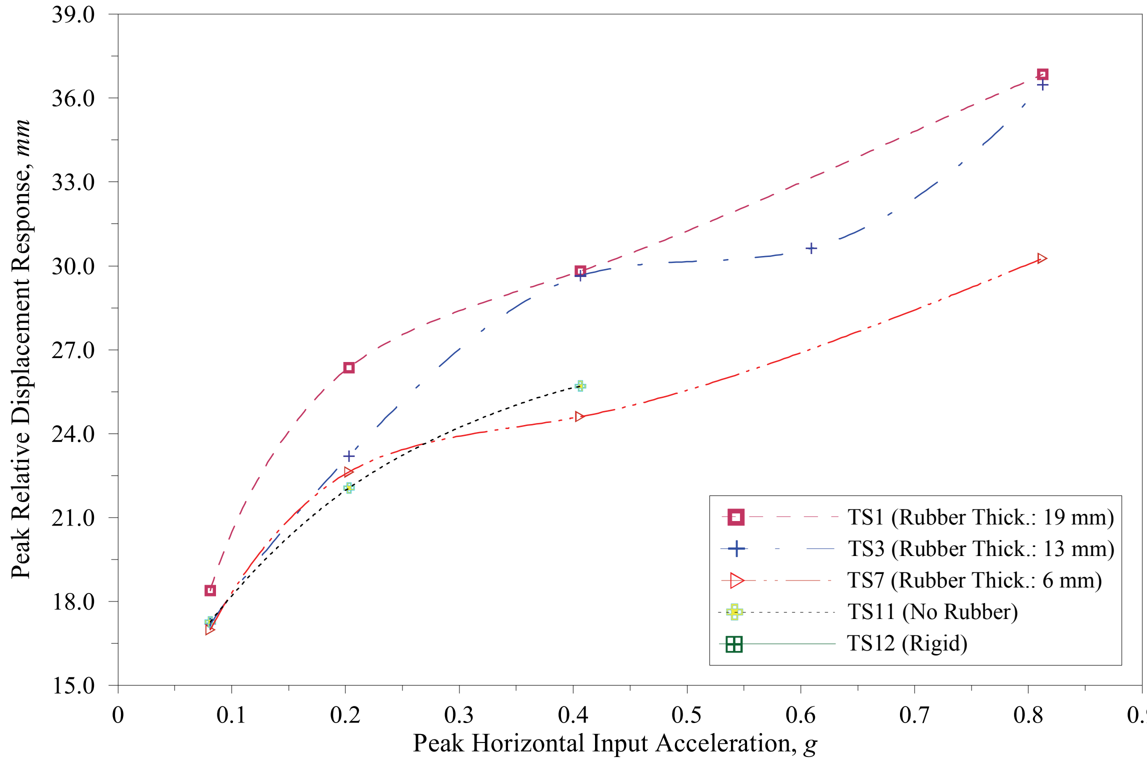

(a) Peak Horizontal Relative Displacement Response Vs. Peak Horizontal Input Acceleration

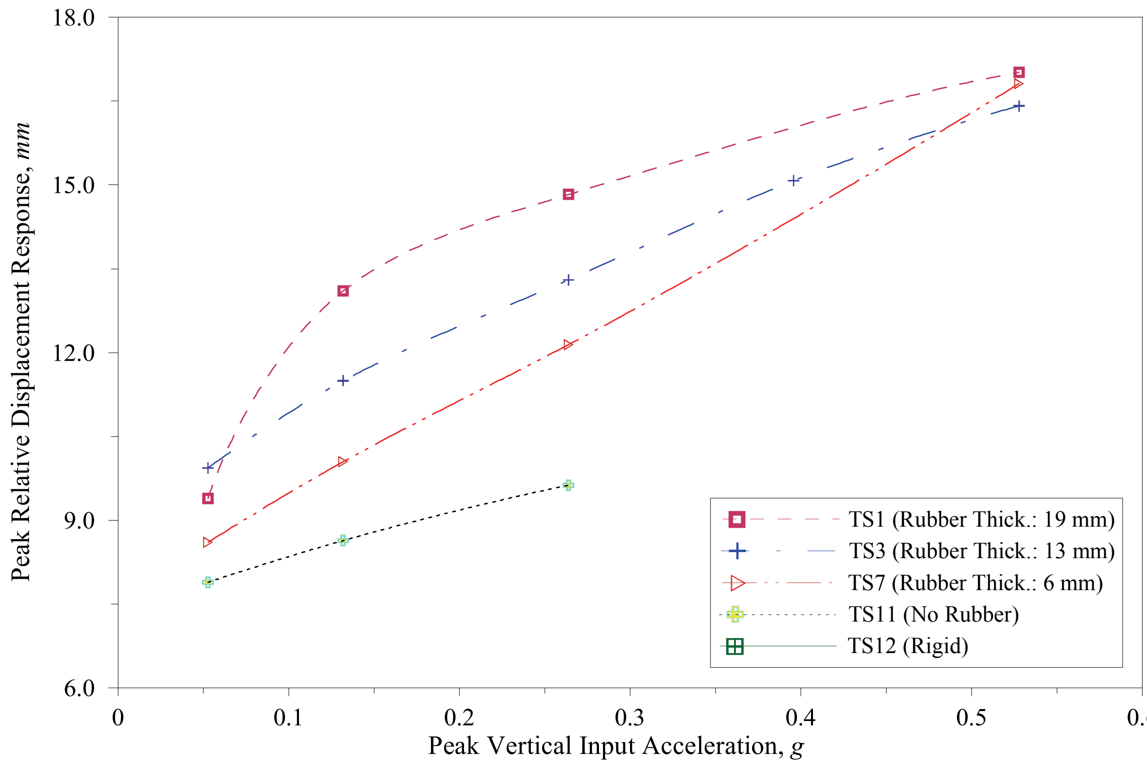

(b) Peak Vertical Relative Displacement Response Vs. Peak Vertical Input Acceleration

Figure 7-26 Effect of Variation of Rubber Snubber Thickness on Peak Relative Displacement Response at Top-South-East Corner of Test Specimen, Comparison of Results of Test Series 1, 3, 7, and 11

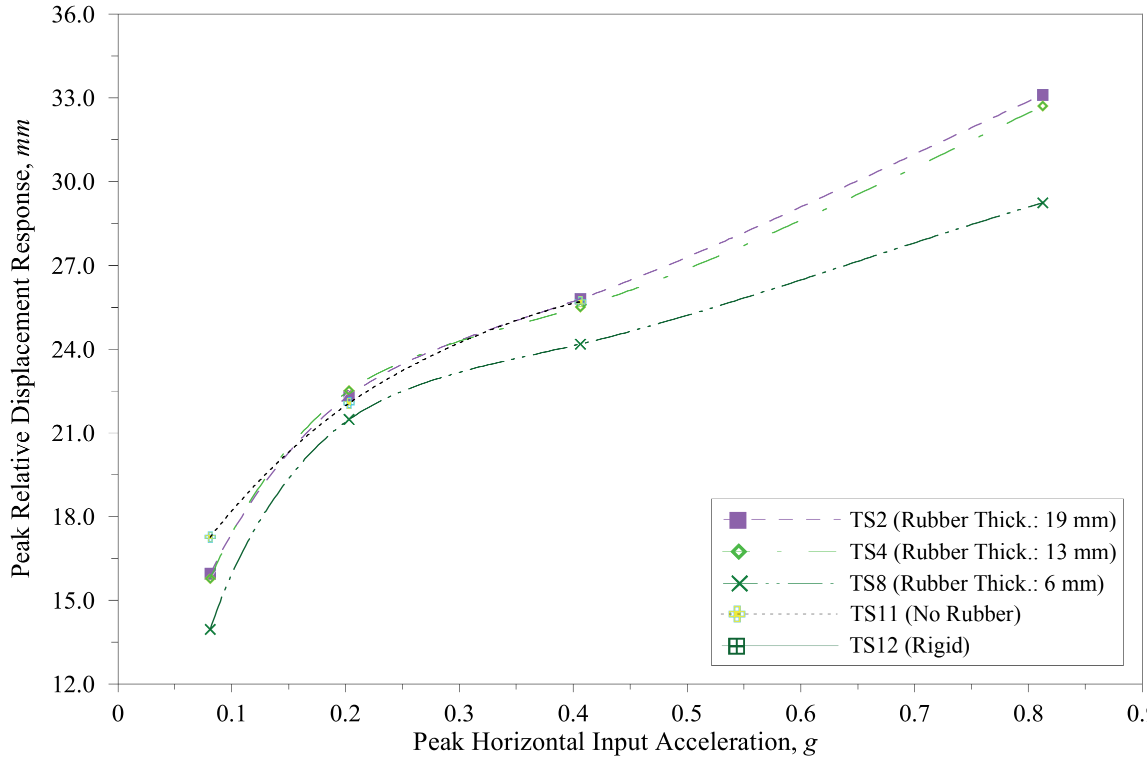

(a) Peak Horizontal Relative Displacement Response Vs. Peak Horizontal Input Acceleration

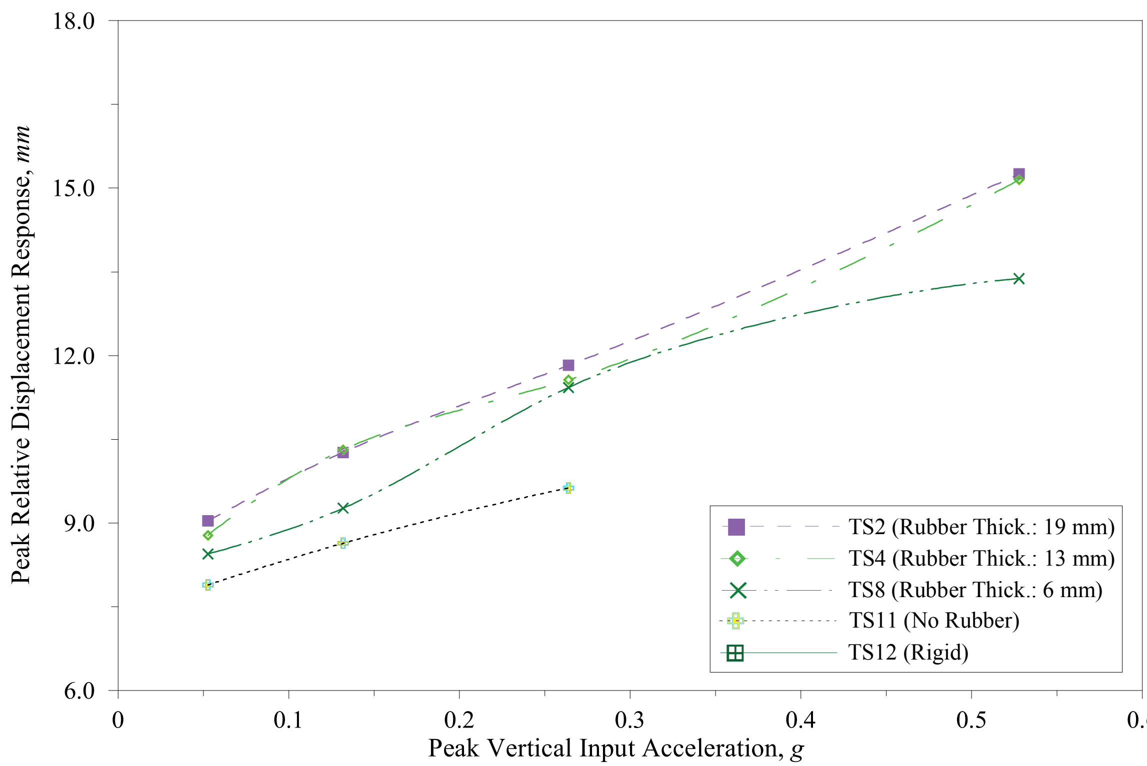

(b) Peak Vertical Relative Displacement Response Vs. Peak Vertical Input Acceleration

Figure 7-27 Effect of Variation of Rubber Snubber Thickness on Peak Relative Displacement Response at Top-South-East Corner of Test Specimen, Comparison of Results of Test Series 2, 4, 8, and 11

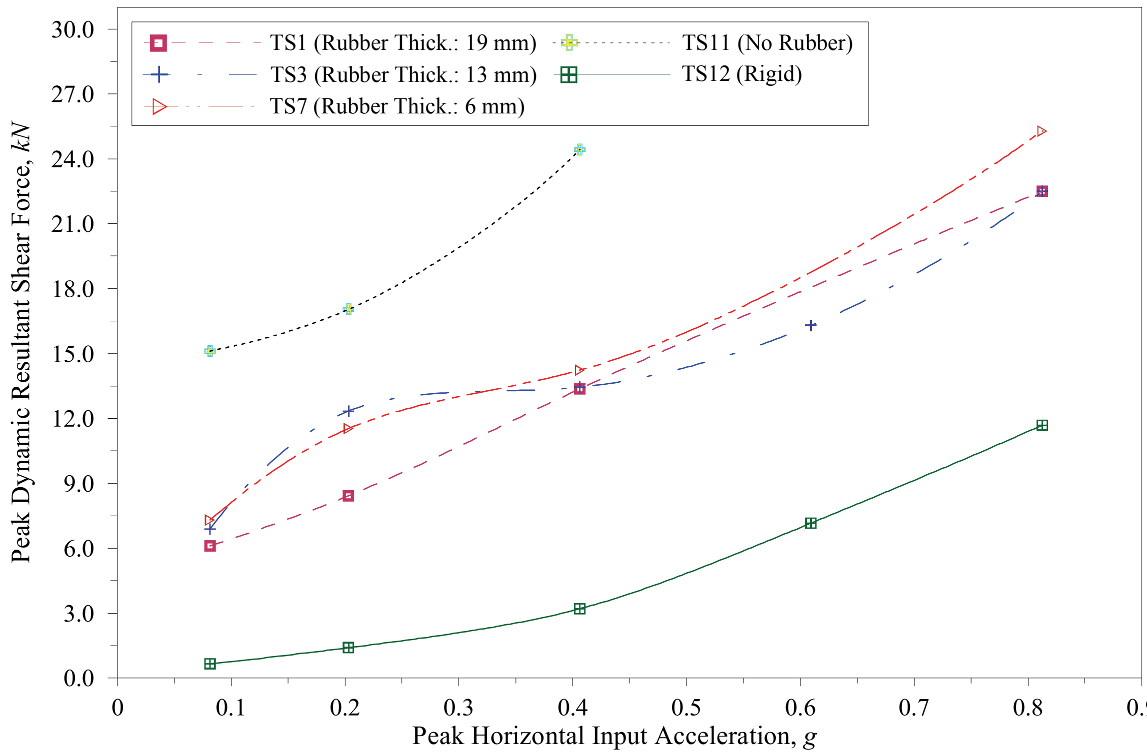

(a) Maximum Shear Force Induced into I/R Systems Vs. Peak Horizontal Input Acceleration

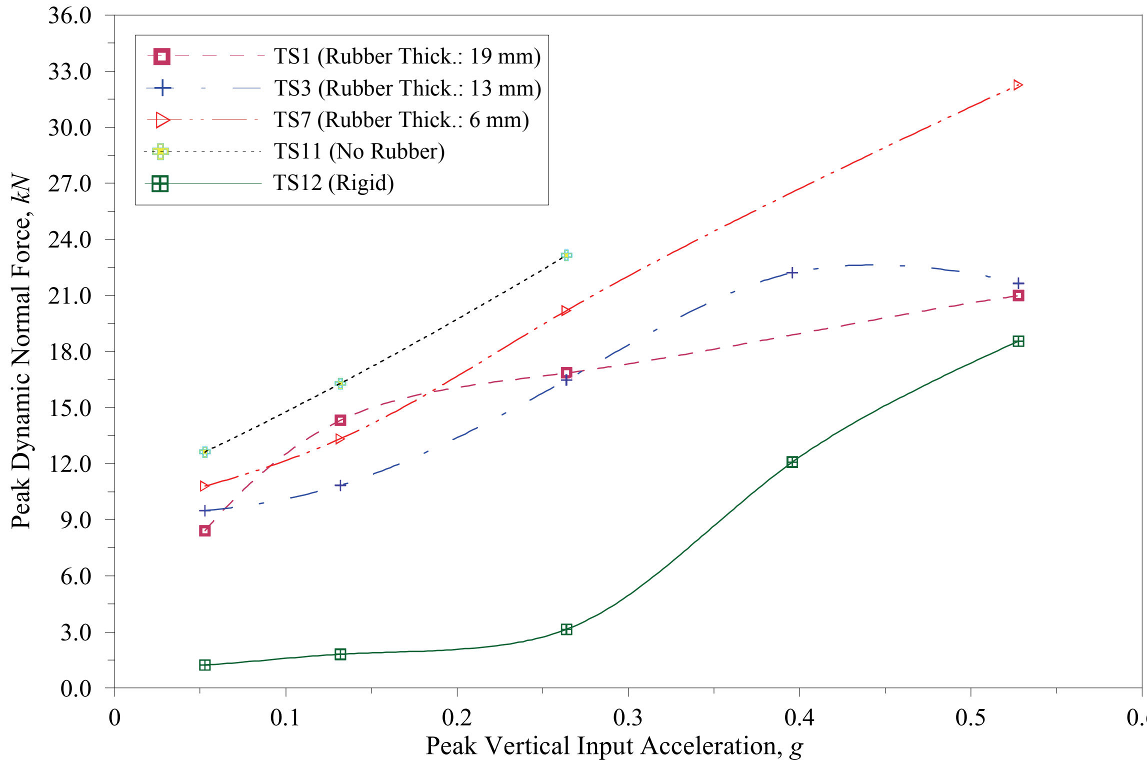

(b) Maximum Normal Force Induced into I/R Systems Vs. Peak Vertical Input Acceleration

Figure 7-28 Effect of Variation of Rubber Snubber Thickness on Peak Dynamic Forces Induced into I/R Systems, Comparison of Results of Test Series 1, 3, 7, and 11

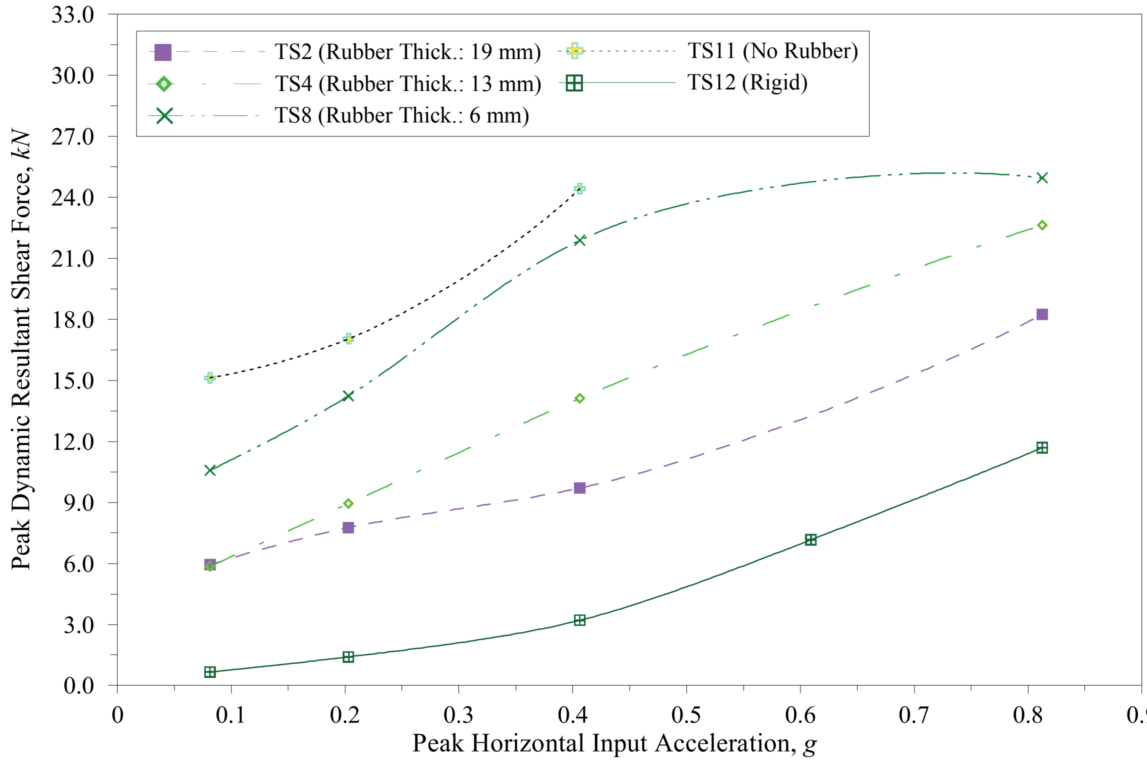

(a) Maximum Shear Force Induced into I/R Systems Vs. Peak Horizontal Input Acceleration

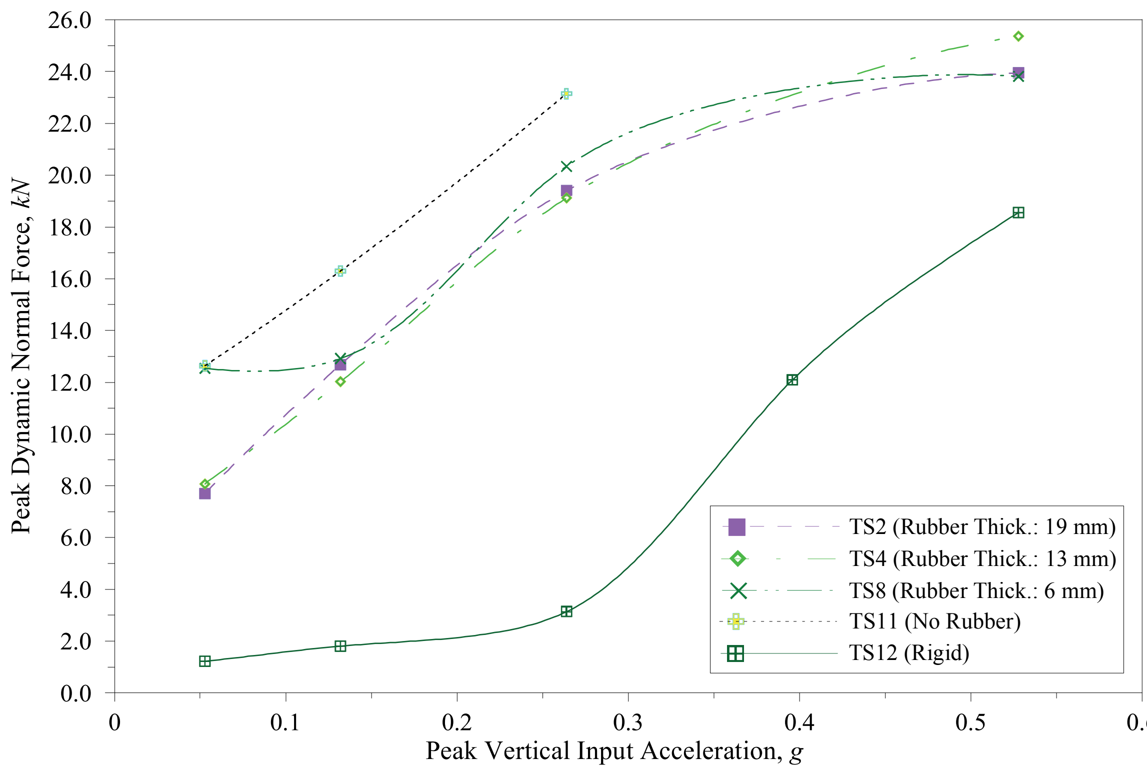

(b) Maximum Normal Force Induced into I/R Systems Vs. Peak Vertical Input Acceleration

Figure 7-29 Effect of Variation of Rubber Snubber Thickness on Peak Dynamic Forces Induced into I/R Systems, Comparison of Results of Test Series 2, 4, 8, and 11

7.3.3 Effect of Rubber Snubber Hardness

The test plan included five groups of test series that incorporated I/R systems with identical rubber thickness and equal gap size, but different rubber hardness. Each group consisted of a test series with 40 *Duro* rubber snubbers and a test series with 60 *Duro* rubber snubbers. Table 7-15, lists the identical and variable properties of the restraint components of I/R systems incorporated in the test series of each of the five groups.

Table 7-15 Restraint Component Properties in Test Series Conducted to Study Effect of Rubber Snubber Hardness on Seismic Performance of I/R System

	Test Series	Identical Properties:			Variable Property:	
		Gap Size, *mm* (*in.*)	Rubber Snubber Thickness, *mm* (*in.*)		Rubber Snubber Hardness, *Duro.*	
			Horizontal Snubber	Vertical Snubber	Horizontal Snubber	Vertical Snubber
Group I	TS1	6 (0.25)	19 (0.75)	19 (0.75)	40	40
	TS2				60	60
Group II	TS3	6 (0.25)	12 (0.5)	12 (0.5)	40	40
	TS4				60	60
Group III	TS5	13 (0.5)	6 (0.25)	6 (0.25)	40	40
	TS6				60	60
Group IV	TS7	6 (0.25)	6 (0.25)	6 (0.25)	40	40
	TS8				60	60
Group V	TS9	6 (0.25)	3 (0.125)	6 (0.25)	40	40
	TS10				60	60

The variations of the horizontal, vertical, and resultant *AAF* on top of the motor with the corresponding peak input acceleration during the seismic tests of Groups I through V are shown in Figures 7-30 through 7-34, respectively. The results of Test Series TS12 have been added to these figures to compare the amplification of the acceleration response of the isolated and rigidly mounted test specimen. The test results show that in most of the tests, reducing the rubber snubber hardness resulted in an increase of the acceleration response on the top of the motor.

The variations of the maximum horizontal and vertical relative displacement responses on the south face of the isolated test specimen with the corresponding peak input acceleration during the test series of Group I through V are shown in Figures 7-35 through 7-39, respectively. The results show that regardless of the input motion amplitude, reducing the rubber snubber hardness from 60 to 40 *Duro* resulted in an increase of the peak relative displacement responses of the test specimen.

The variations of the maximum dynamic shear and normal forces induced into the I/R systems with the corresponding peak input acceleration during the test series of Group I through V are shown in Figures 7-40 through 7-44, respectively. The results of Test Series TS12 have been added to these figures to compare the dynamic forces at the support locations of the isolated and rigidly mounted test specimen.

The test results show that despite the increased acceleration and displacement responses of the test specimen in most of the tests with the softer rubber snubber, still in some cases reducing the rubber snubber hardness resulted in a reduction of the dynamic forces induced into the I/R systems.

The immediate concern about the excessive displacement response of the equipment is the breakage of the connected pipes and wires. However, beyond this potential problem, the increased displacement of the equipment as a result of application of softer (or thicker) rubber snubbers can actually degrade the capability of the snubbers in reducing the dynamic forces induced into the I/R systems.

For a single impact between a punching mass and a rubber snubber, reducing the stiffness of the snubber by reducing its hardness (or increasing its thickness) will certainly result in a reduction of the dynamic force experienced by the object. The reduction of the snubber stiffness will also result in an increased compression of the rubber snubber during the impact. For a single impact, the increased compression of the rubber snubber will not be a concern. However, if the punching mass is moving within an air gap and there is a chance of a second impact in the opposite direction after rebounding, then the excessive compression of the rubber snubber during the first impact might be detrimental. The excessive compression of the rubber snubber in one direction can instantly enlarge the nominal gap size and allow the punching mass to accelerate and impact the snubber on the other side with a larger momentum. Analogously, in the seismic tests with the I/R systems, the capability of the soft (or thick) rubber snubbers could be degraded by their contribution in enlarging the nominal gap size and allowing the test specimen to move and accelerate within a larger domain.

As discussed previously, the increase of the snubber thickness in most of the cases was successful in reducing the dynamic forces induced into the I/R systems. However, the same level of success in reducing the dynamic forces was not repeated by reducing the rubber snubber hardness. In order to understand the reason behind this trend, the effect of rubber hardness and thickness on the snubber stiffness should be compared to each other. The stiffness of a rubber snubber can be estimated by (Kinetics Noise Control, 2004):

$$K = C_1 \frac{A_L}{t} (E_0 (1 + C_2 S^2)) \tag{7-6}$$

where,

K = snubber stiffness
A_L = loaded area
t = snubber thickness
E_0 = tangent modulus for a shape factor equal to zero
S = rubber snubber shape factor
C_1 and C_2 = constant coefficients that depend on the shape of the snubber (for instance, C_1 and C_2 for the rubber washer used as the snubbers in the vertical direction are equal to 1 and 2, respectively.)

As it is seen in Equation 7-6, the rubber hardness controls the snubber stiffness only through E_0. Increasing the rubber hardness from 40 to 60 *Duro* increases E_0 by a factor of about 2.2(Gent, 2001). Therefore, throughout the experiments, replacing the 40 *Duro*-rubber snubbers by the 60 *Duro*-rubber snubbers would amplify the stiffness of the restraint components by a factor of about 2.2.

The direct effect of the rubber thickness on the snubber stiffness is seen in the denominator of Equation 7-6. In addition, the rubber thickness variation affects the snubber stiffness indirectly through the shape factor in the numerator of Equation 7-6. The shape factor of a snubber is the ratio between the loaded area and the area free to bulge. With an increase of the thickness, the bulging area increases and therefore, the shape factor decreases. Therefore, in Equation 7-6, the rubber stiffness reduces nonlinearly with snubber thickness. For example, according to the manufacturer of the rubber snubbers, doubling and tripling the thickness of a 6 *mm* (0.25 *in.*)-thick rubber washer snubber would reduce the snubber stiffness by a factor of about 5 and 10, respectively.

Therefore, throughout the experiments, the stiffness of the rubber snubbers was reduced much more by increasing their thickness rather than by reducing their hardness. For instance, the 6 *mm* (0.25 *in.*)-thick washer snubber made from *40 Duro* was stiffer than a 19 *mm* (0.75 *in.*)-thick washer snubber made from 60 *Duro* rubber.

In general, the seismic performance of the I/R systems was more influenced by a change in the gap size or rubber thickness than by a change in the rubber snubber hardness. Moreover, the effect of the rubber snubber hardness on the seismic performance of the I/R systems could be overshadowed by the effects of the other two properties of the I/R systems. For instance, the results of Test Series TS5 and TS6 showed that in presence of the large gap size, variation of the rubber snubber hardness hardly affected the dynamic forces induced into the I/R systems.

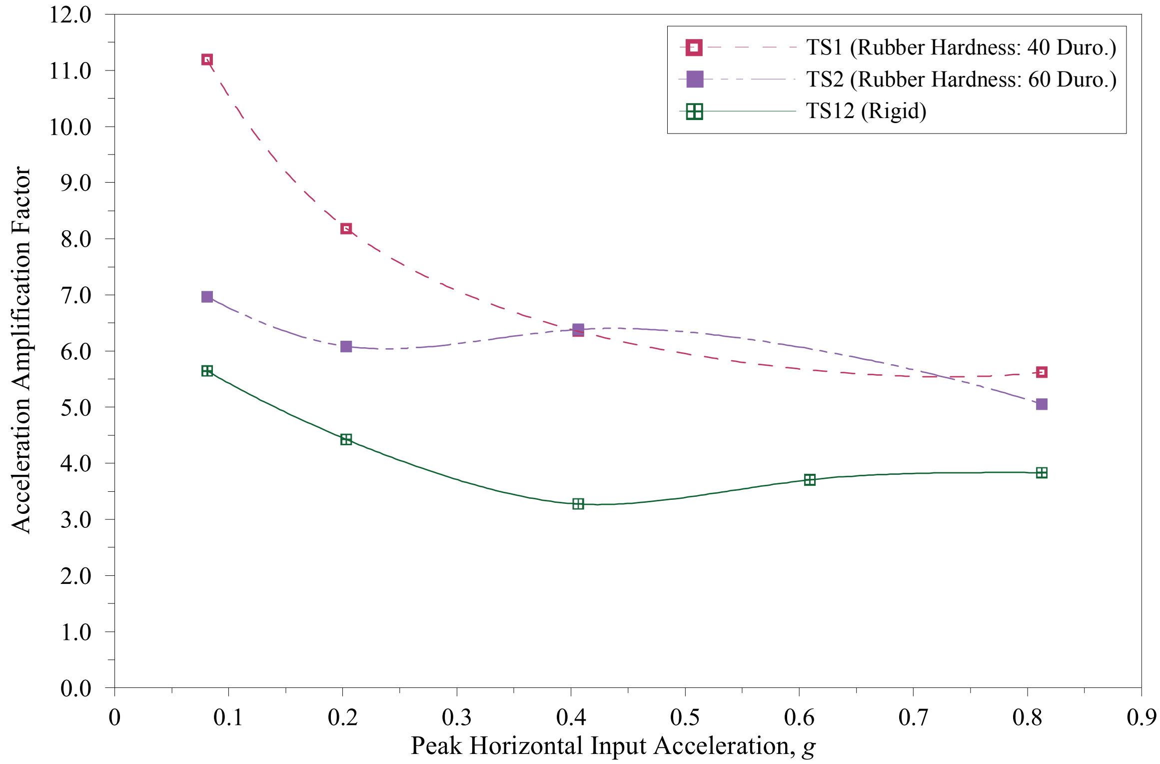

(a) Horizontal *AAF* on Top of Motor Vs. Peak Horizontal Input Acceleration

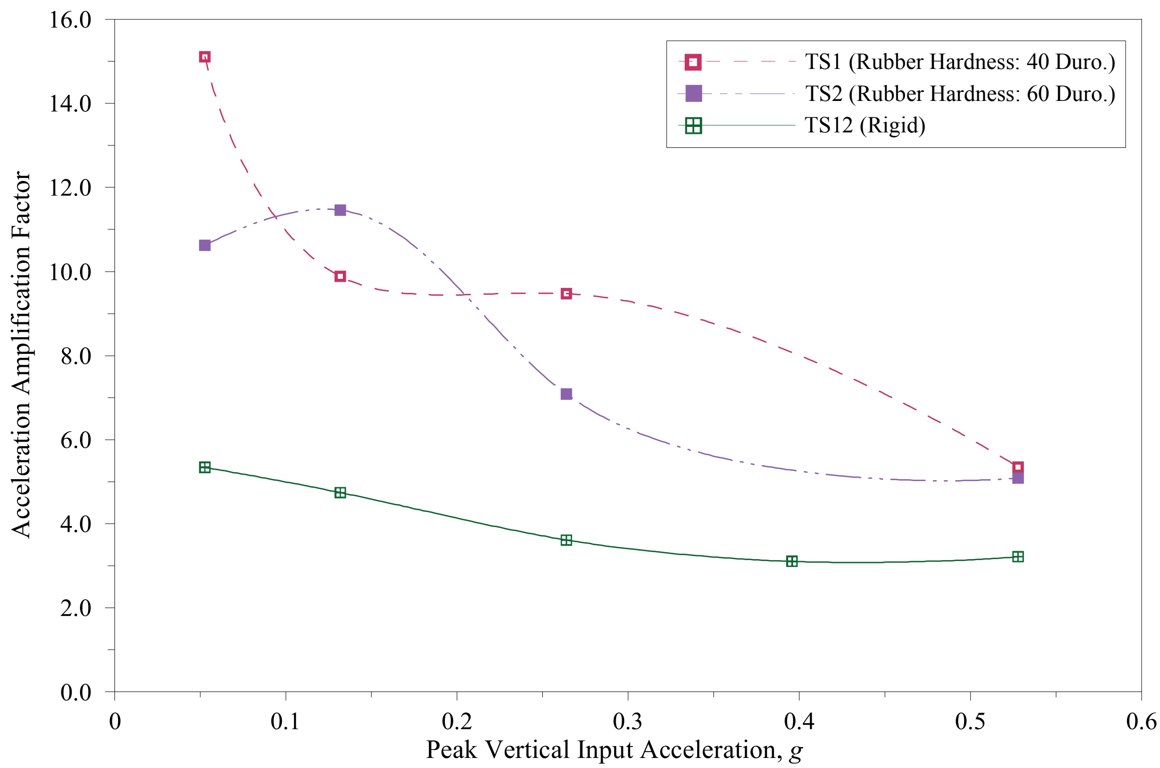

(b) Vertical AAF on Top of Motor Vs. Peak Vertical Input Acceleration

Figure 7-30 Effect of Variation of Rubber Snubber Hardness on *AAF* near Center of Mass of Test Specimen (on Top of Motor), Comparison of Results of Test Series 1 and 2

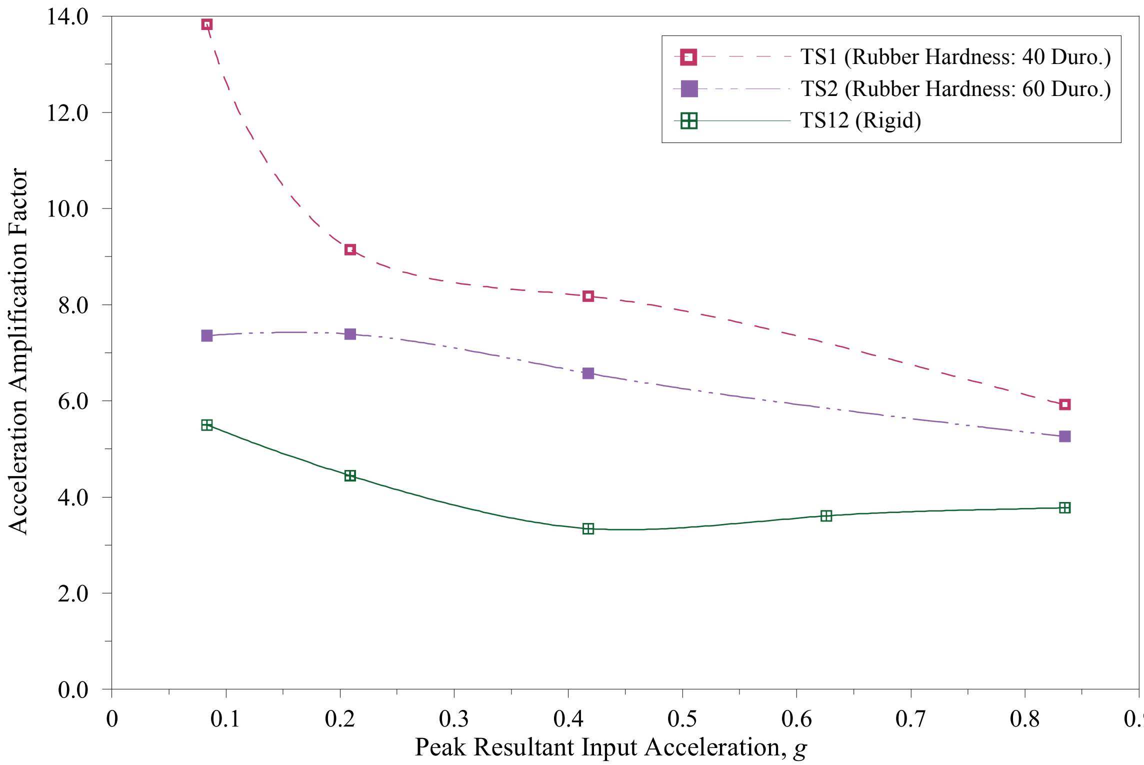

(c) Resultant *AAF* on Top of Motor Vs. Peak Resultant Input Acceleration

Figure 7-30 (cont'd) Effect of Variation of Rubber Snubber Hardness on *AAF* near Center of Mass of Test Specimen (on Top of Motor), Comparison of Results of Test Series 1 and 2

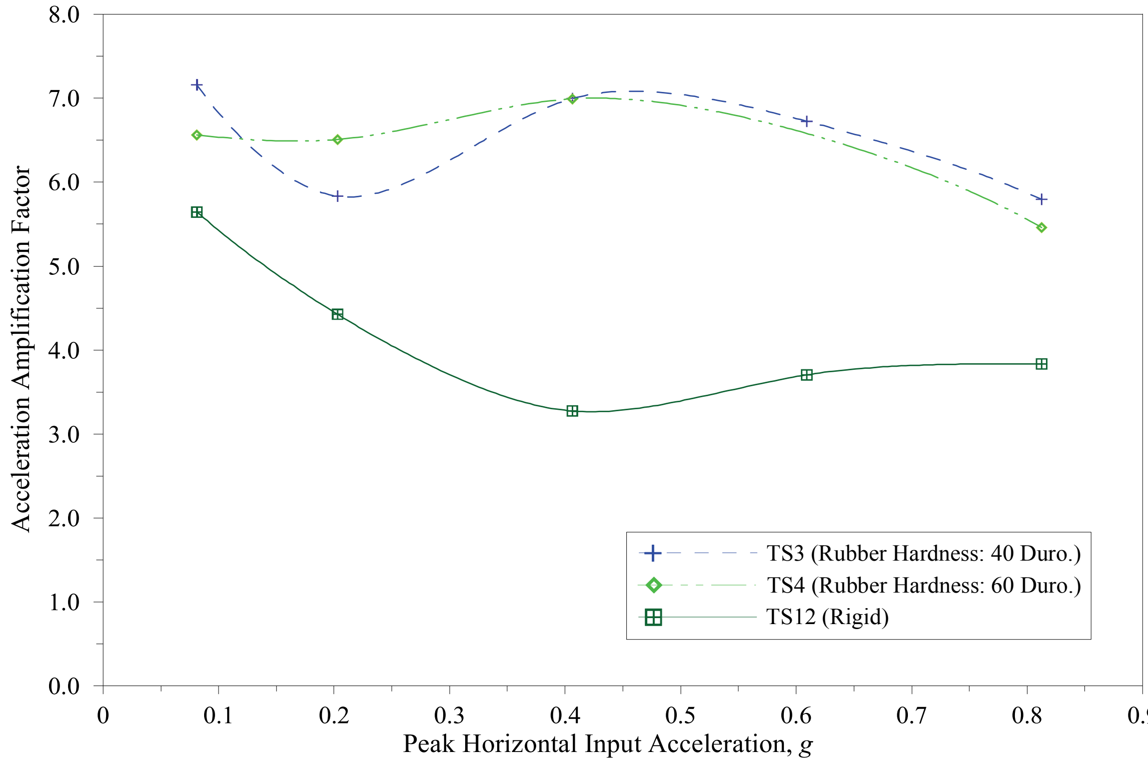

(a) Horizontal *AAF* on Top of Motor Vs. Peak Horizontal Input Acceleration

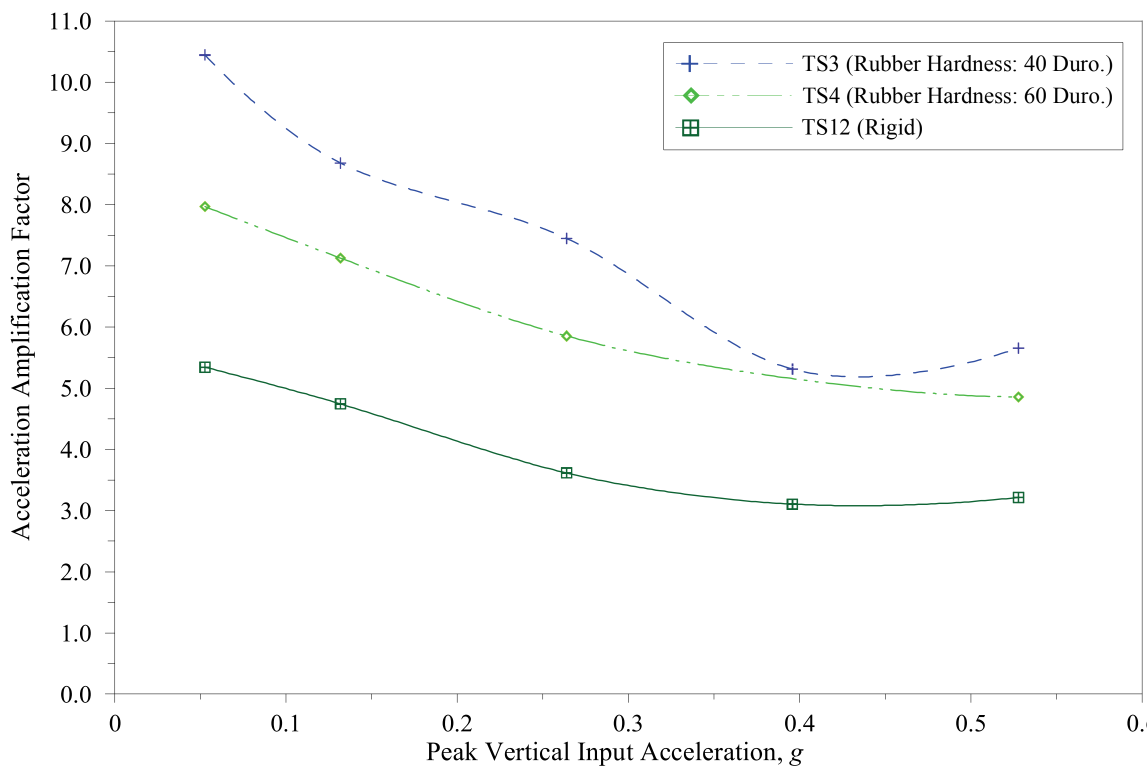

(b) Vertical *AAF* on Top of Motor Vs. Peak Vertical Input Acceleration

Figure 7-31 Effect of Variation of Rubber Snubber Hardness on *AAF* near Center of Mass of Test Specimen (on Top of Motor), Comparison of Results of Test Series 3 and 4

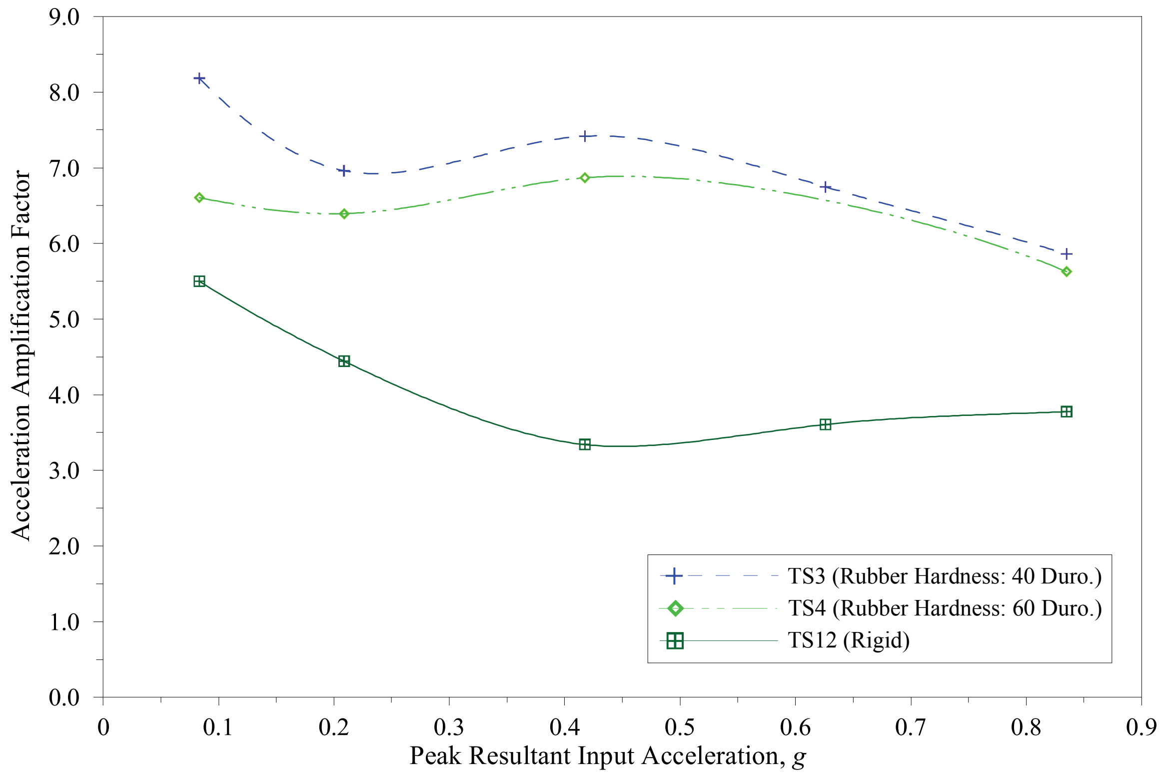

(c) Resultant *AAF* on Top of Motor Vs. Peak Resultant Input Acceleration

Figure 7-31 (cont'd) Effect of Variation of Rubber Snubber Hardness on *AAF* near Center of Mass of Test Specimen (on Top of Motor), Comparison of Results of Test Series 3 and 4

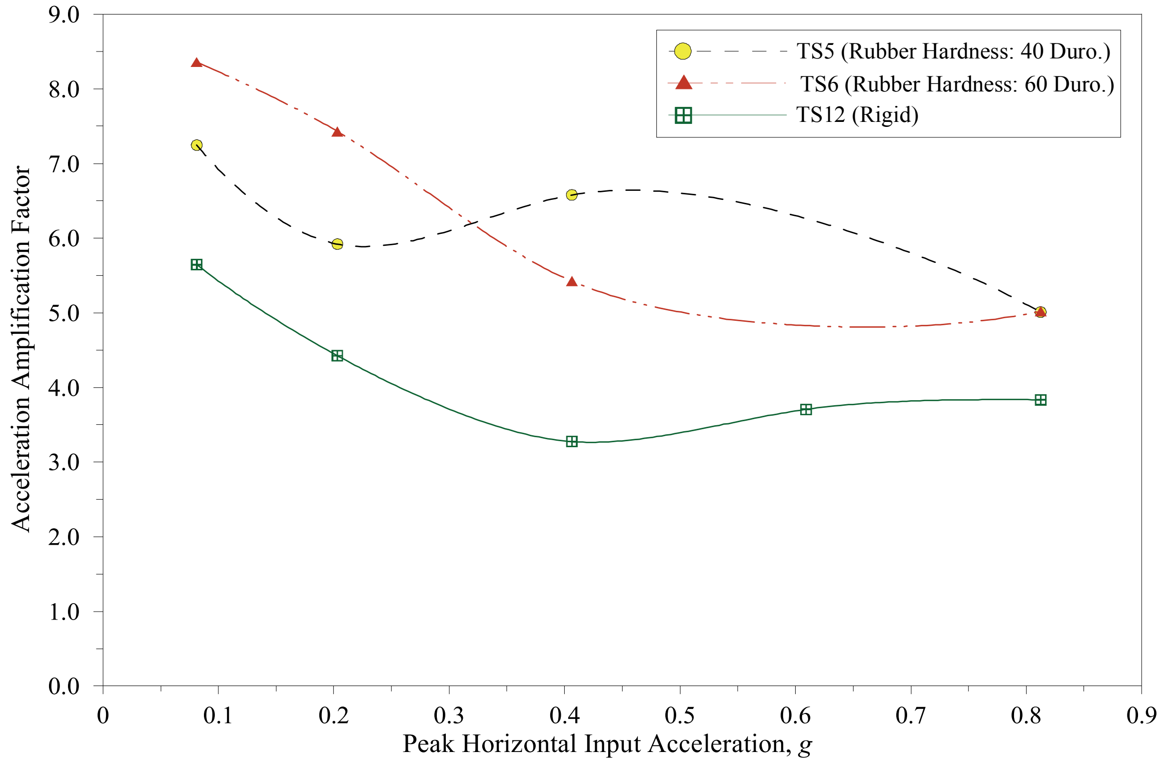

(a) Horizontal *AAF* on Top of Motor Vs. Peak Horizontal Input Acceleration

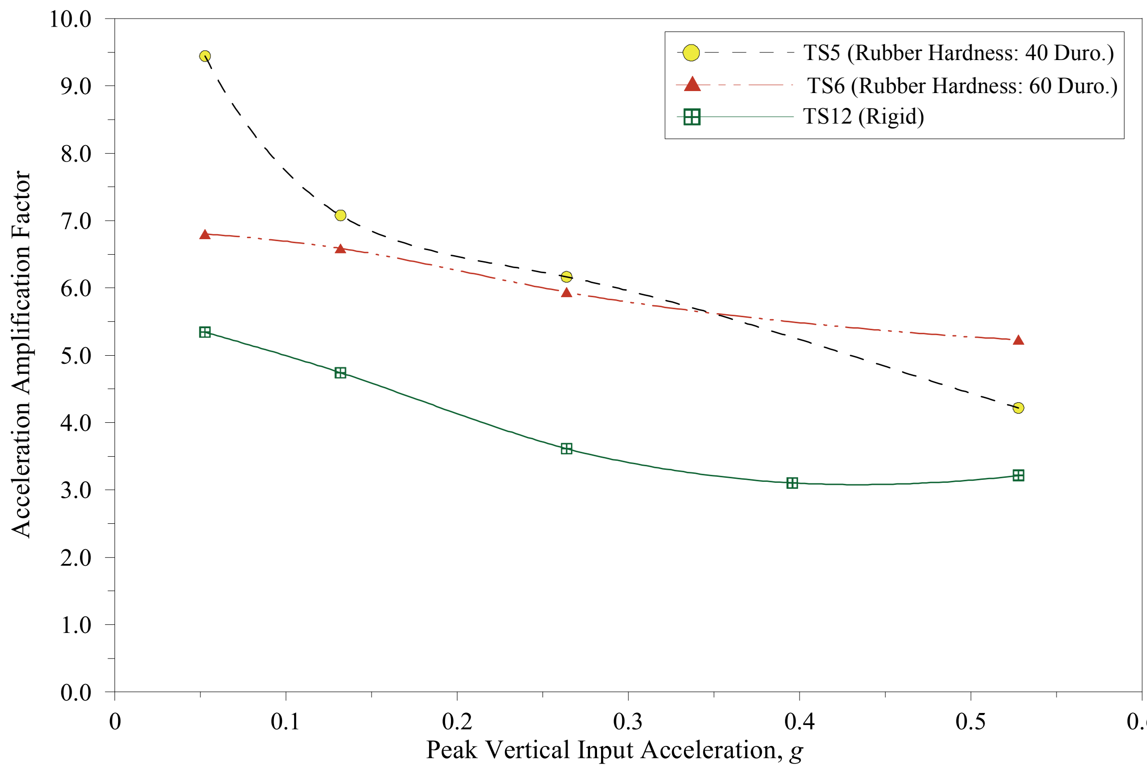

(b) Vertical *AAF* on Top of Motor Vs. Peak Vertical Input Acceleration

Figure 7-32 Effect of Variation of Rubber Snubber Hardness on *AAF* near Center of Mass of Test Specimen (on Top of Motor), Comparison of Results of Test Series 5 and 6

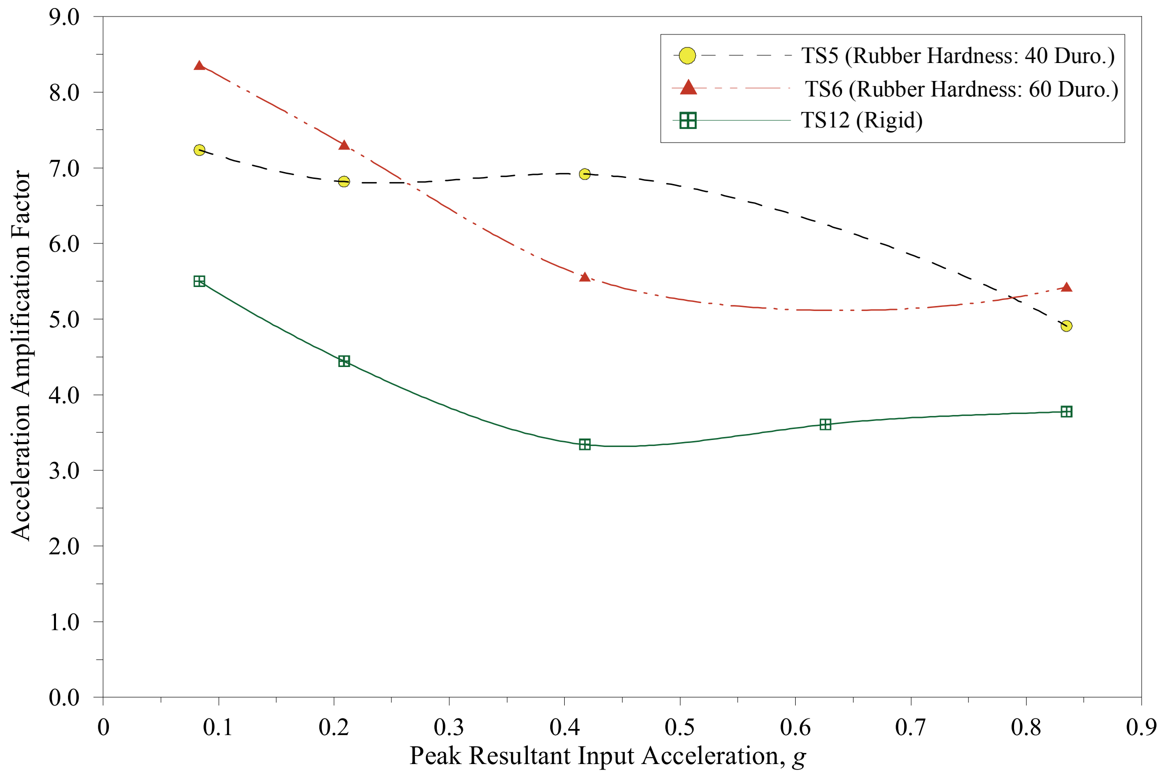

(c) Resultant *AAF* on Top of Motor Vs. Peak Resultant Input Acceleration

Figure 7-32 (cont'd) Effect of Variation of Rubber Snubber Hardness on *AAF* near Center of Mass of Test Specimen (on Top of Motor), Comparison of Results of Test Series 5 and 6

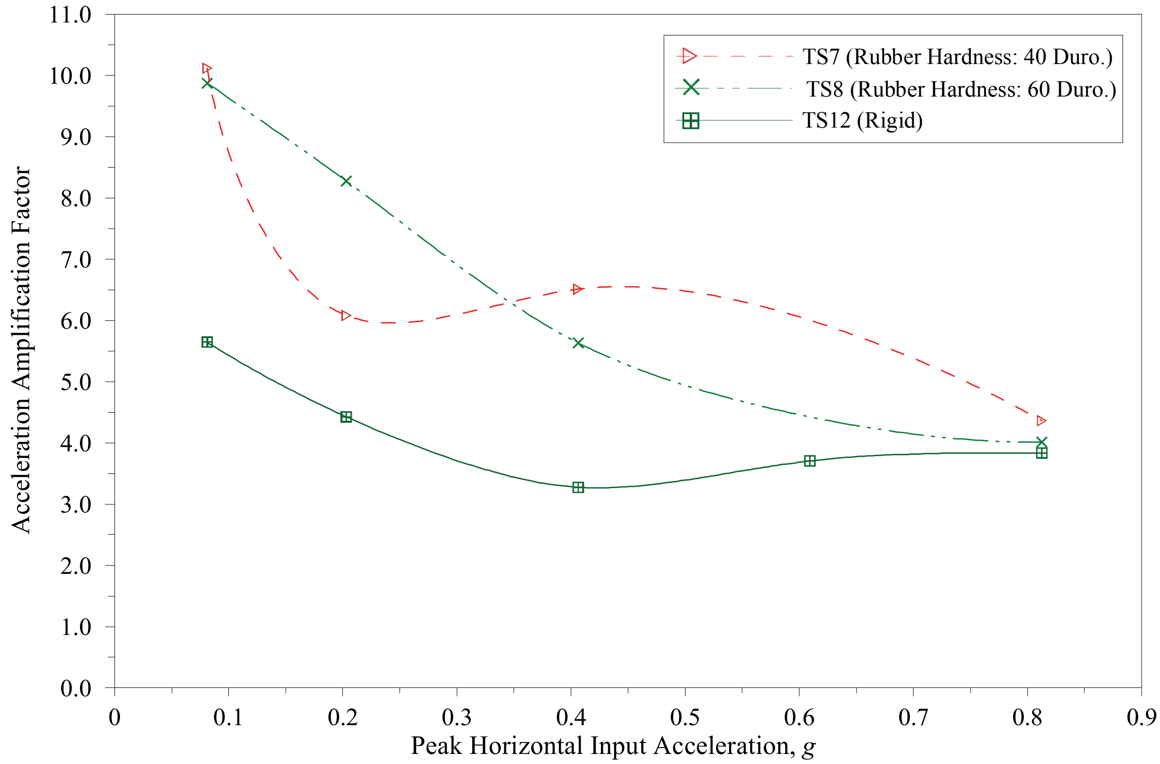

(a) Horizontal *AAF* on Top of Motor Vs. Peak Horizontal Input Acceleration

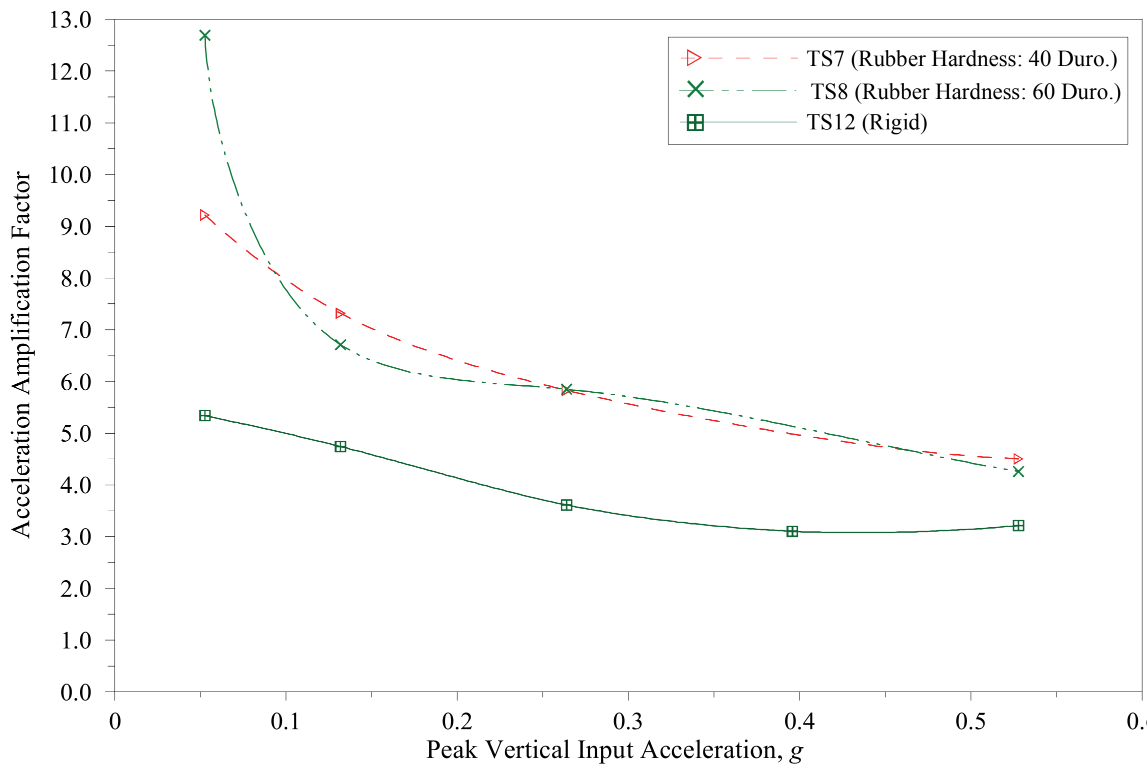

(b) Vertical *AAF* on Top of Motor Vs. Peak Vertical Input Acceleration

Figure 7-33 Effect of Variation of Rubber Snubber Hardness on *AAF* near Center of Mass of Test Specimen (on Top of Motor), Comparison of Results of Test Series 7 and 8

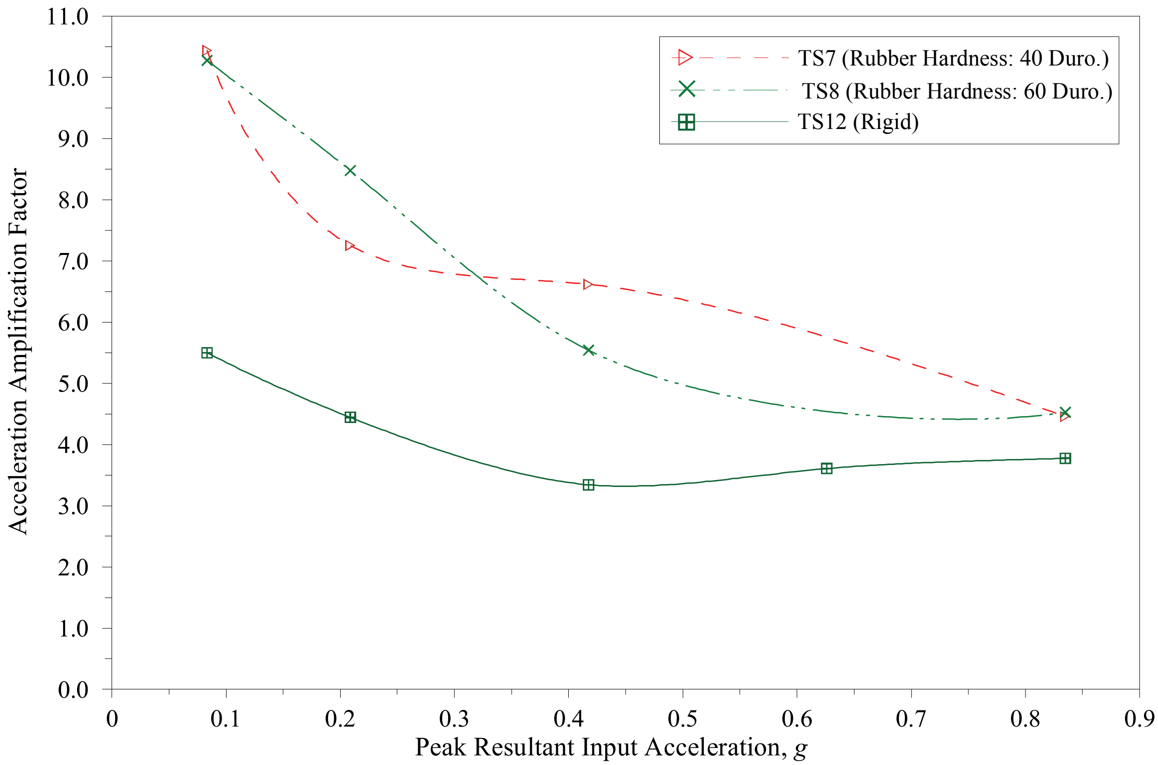

(c) Resultant *AAF* on Top of Motor Vs. Peak Resultant Input Acceleration

Figure 7-33 (cont'd) Effect of Variation of Rubber Snubber Hardness on *AAF* near Center of Mass of Test Specimen (on Top of Motor), Comparison of Results of Test Series 7 and 8

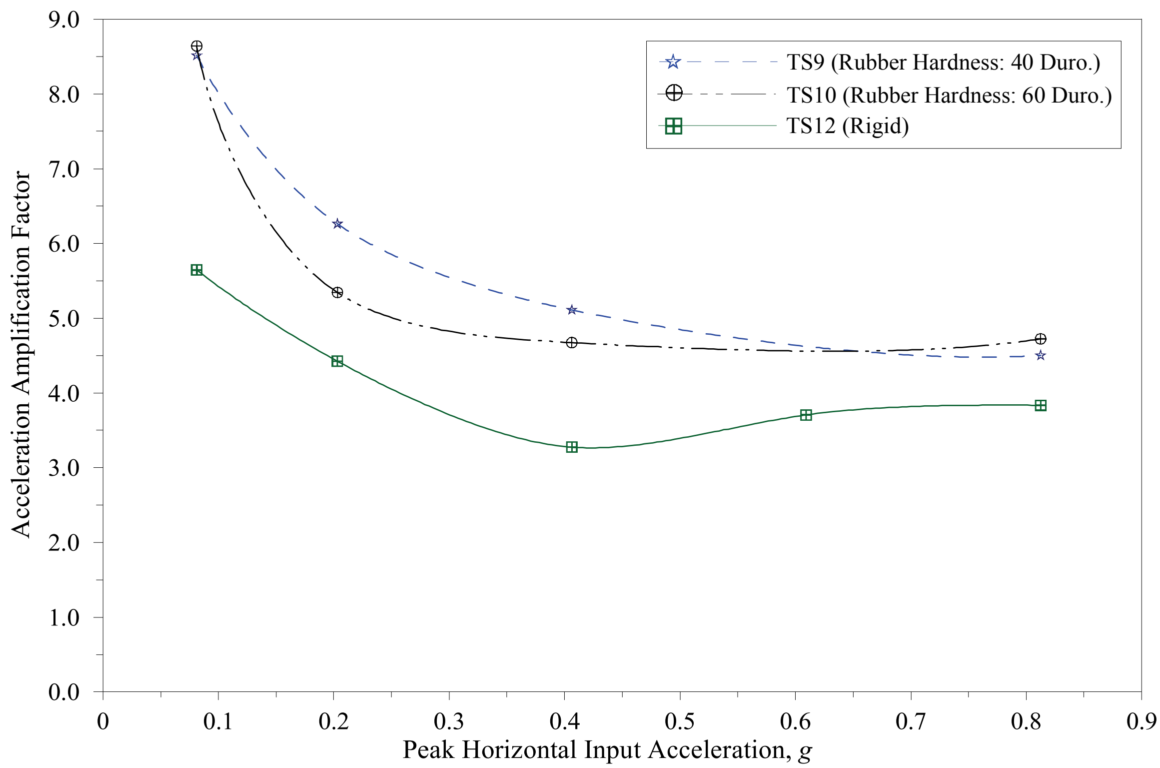

(a) Horizontal *AAF* on Top of Motor Vs. Peak Horizontal Input Acceleration

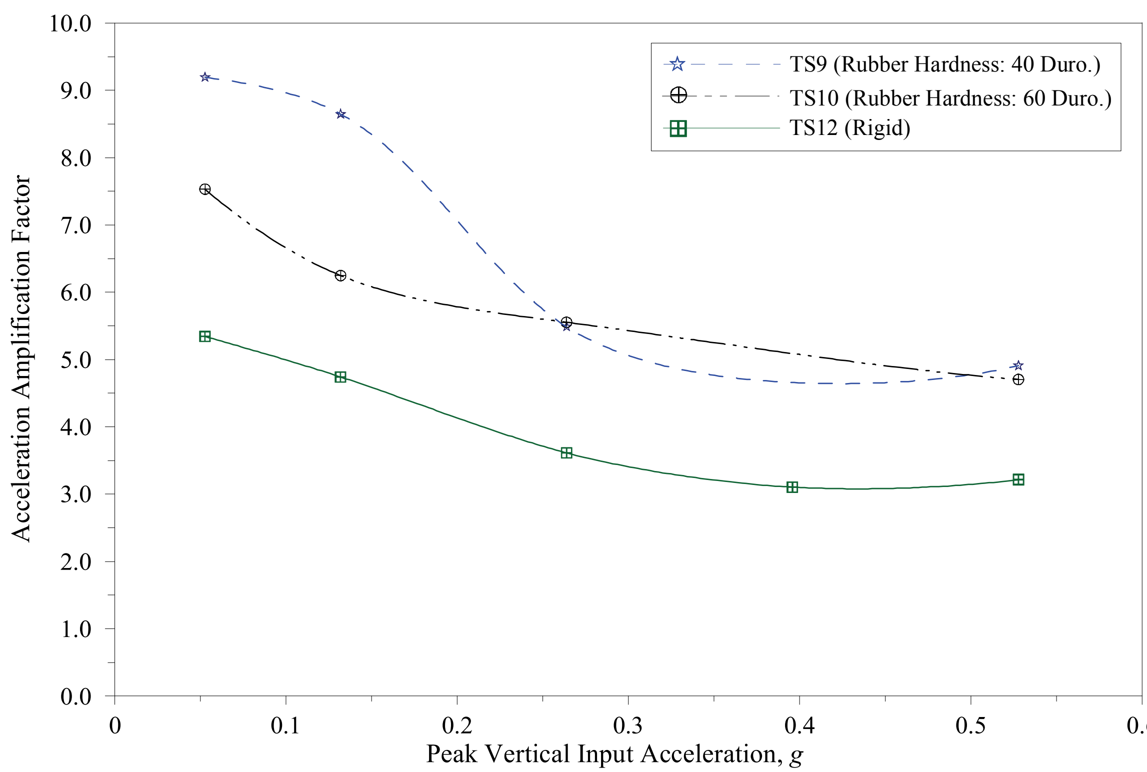

(b) Vertical *AAF* on Top of Motor Vs. Peak Vertical Input Acceleration

Figure 7-34 Effect of Variation of Rubber Snubber Hardness on *AAF* near Center of Mass of Test Specimen (on Top of Motor), Comparison of Results of Test Series 9 and 10

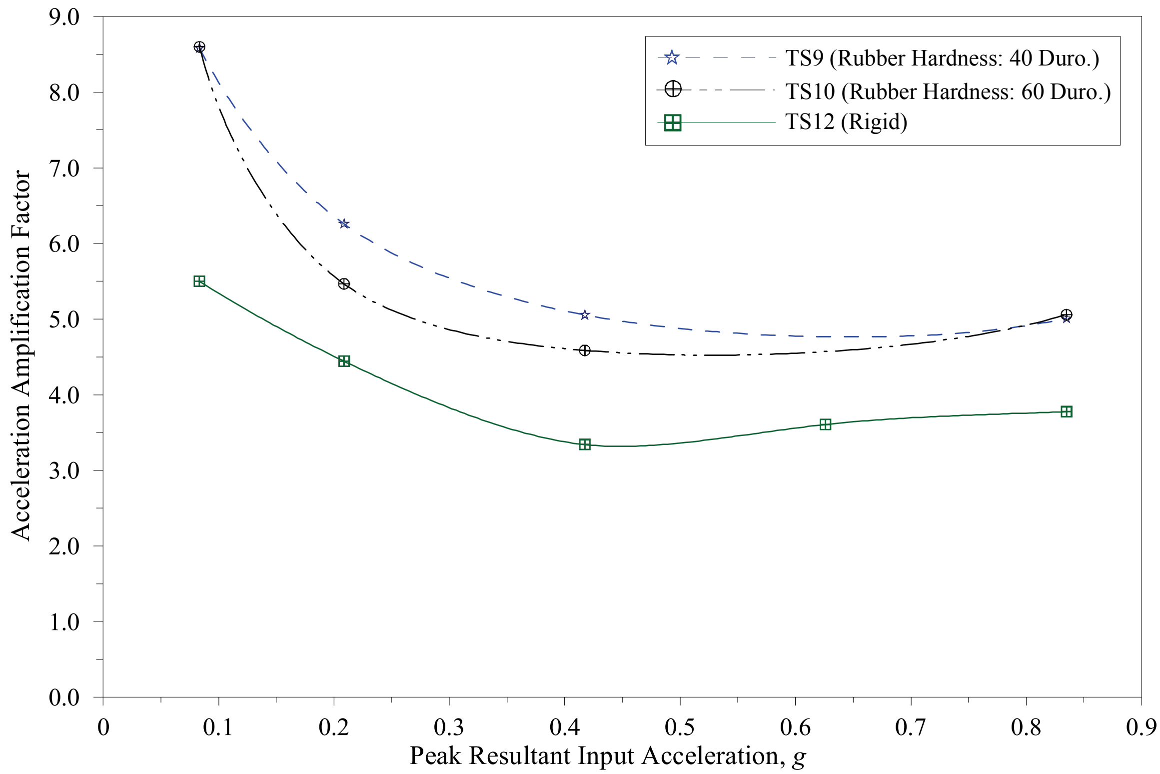

(c) Resultant *AAF* on Top of Motor Vs. Peak Resultant Input Acceleration

Figure 7-34 (cont'd) Effect of Variation of Rubber Snubber Hardness on *AAF* near Center of Mass of Test Specimen (on Top of Motor), Comparison of Results of Test Series 9 and 10

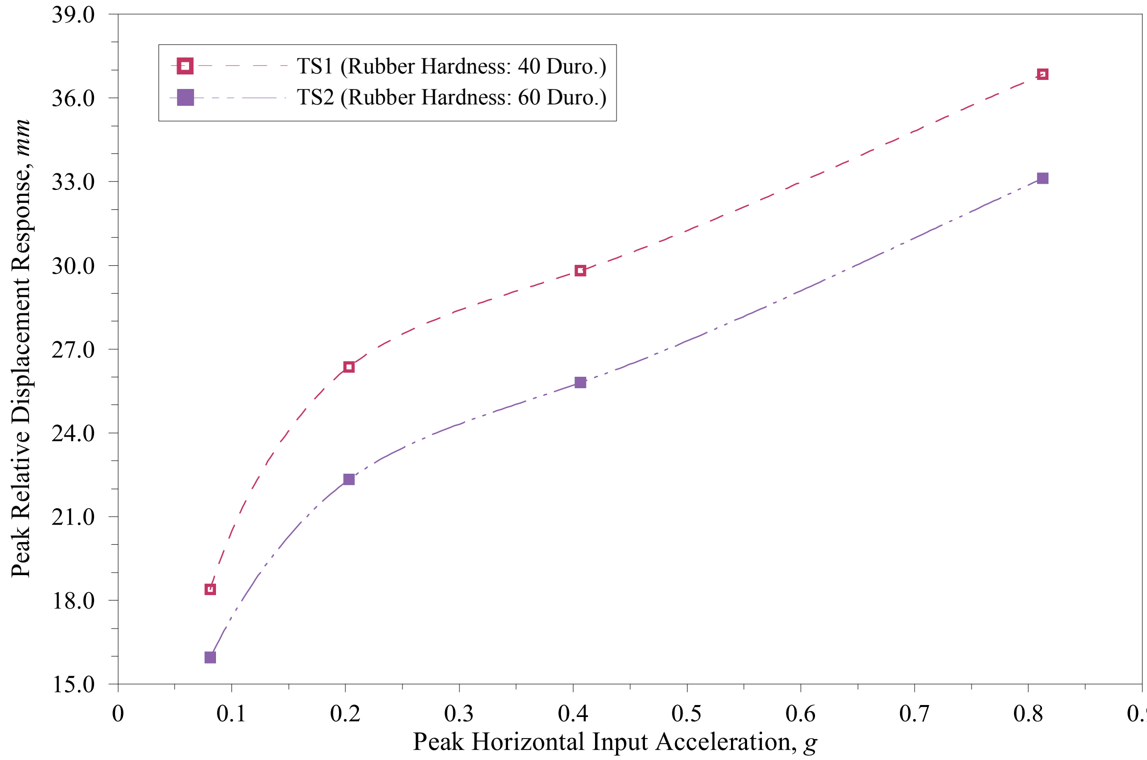

(a) Peak Horizontal Relative Displacement Response Vs. Peak Horizontal Input Acceleration

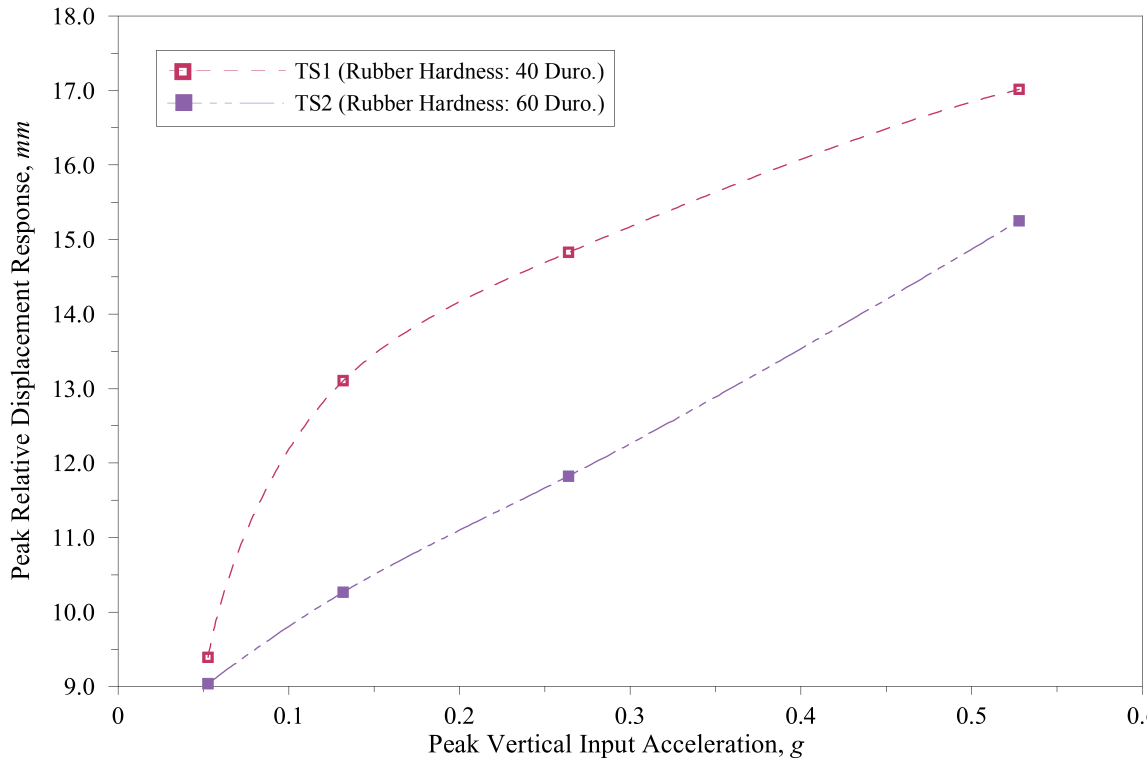

(b) Peak Vertical Relative Displacement Response Vs. Peak Vertical Input Acceleration

Figure 7-35 Effect of Variation of Rubber Snubber Hardness on Peak Relative Displacement Response at Top-South-East Corner of Test Specimen, Comparison of Results of Test Series 1 and 2

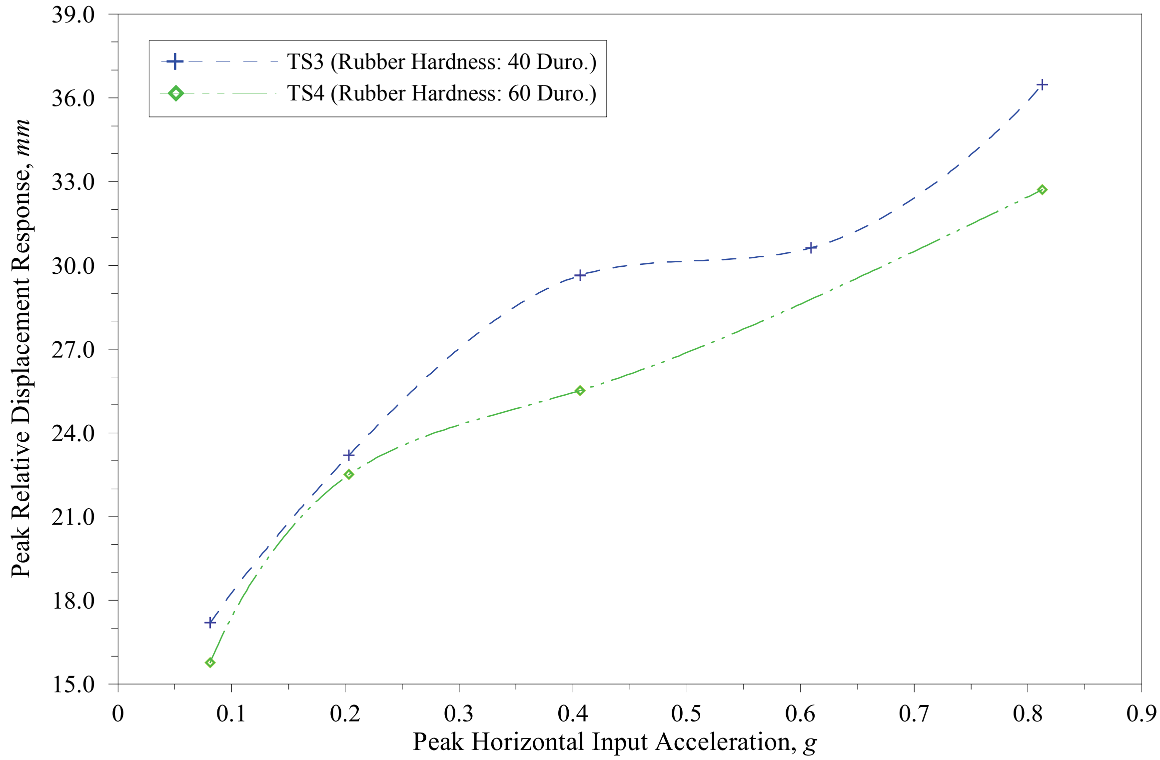

(a) Peak Horizontal Relative Displacement Response Vs. Peak Horizontal Input Acceleration

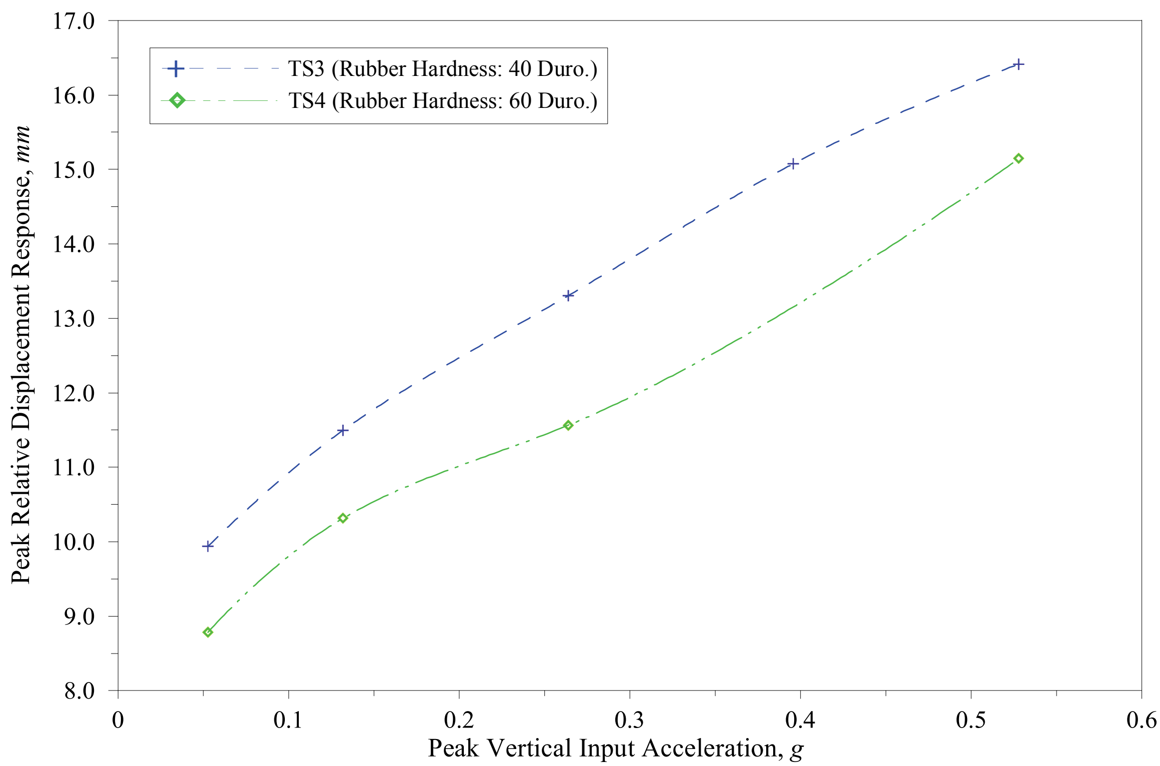

(b) Peak Vertical Relative Displacement Response Vs. Peak Vertical Input Acceleration

Figure 7-36 Effect of Variation of Rubber Snubber Hardness on Peak Relative Displacement Response at Top-South-East Corner of Test Specimen, Comparison of Results of Test Series 3 and 4

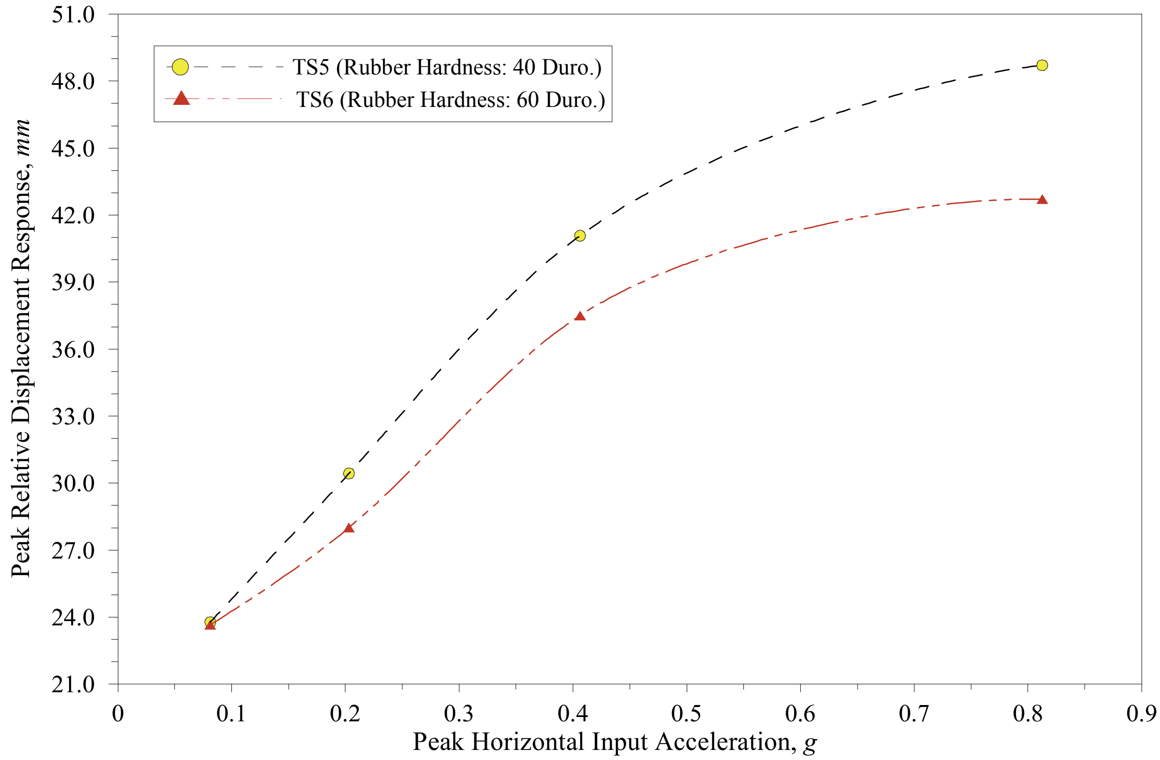

(a) Peak Horizontal Relative Displacement Response Vs. Peak Horizontal Input Acceleration

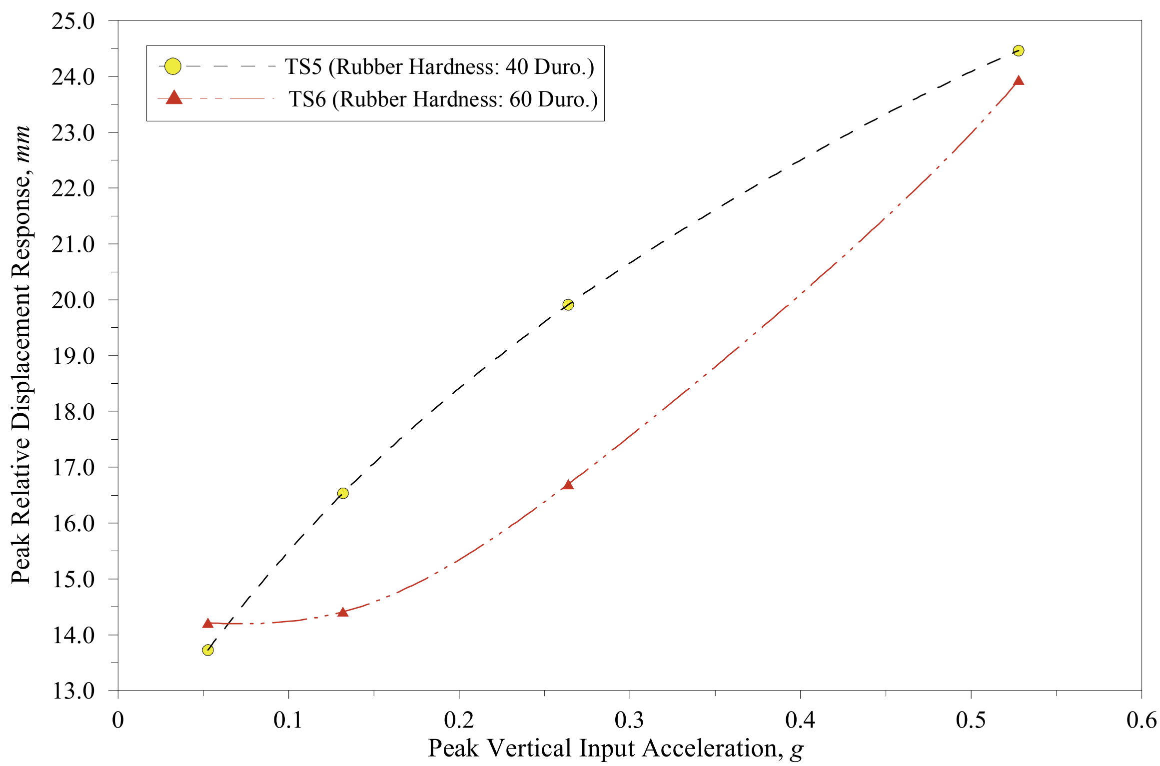

(b) Peak Vertical Relative Displacement Response Vs. Peak Vertical Input Acceleration

Figure 7-37 Effect of Variation of Rubber Snubber Hardness on Peak Relative Displacement Response at Top-South-East Corner of Test Specimen, Comparison of Results of Test Series 5 and 6

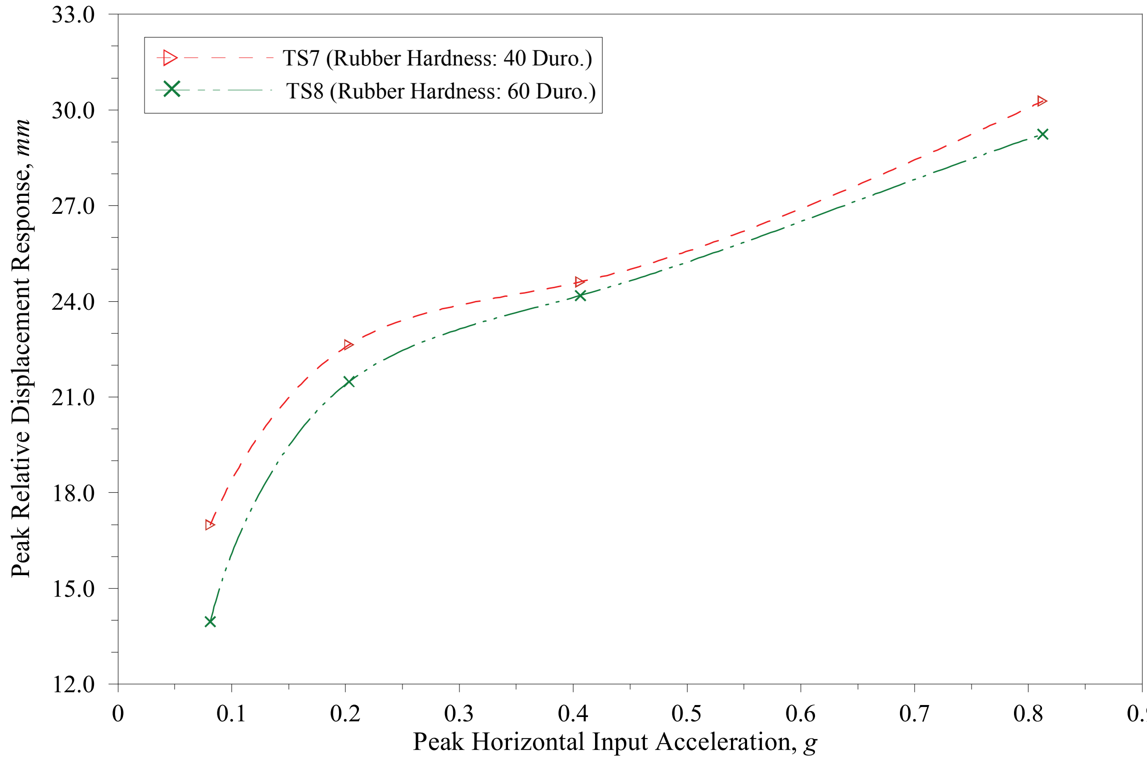

(a) Peak Horizontal Relative Displacement Response Vs. Peak Horizontal Input Acceleration

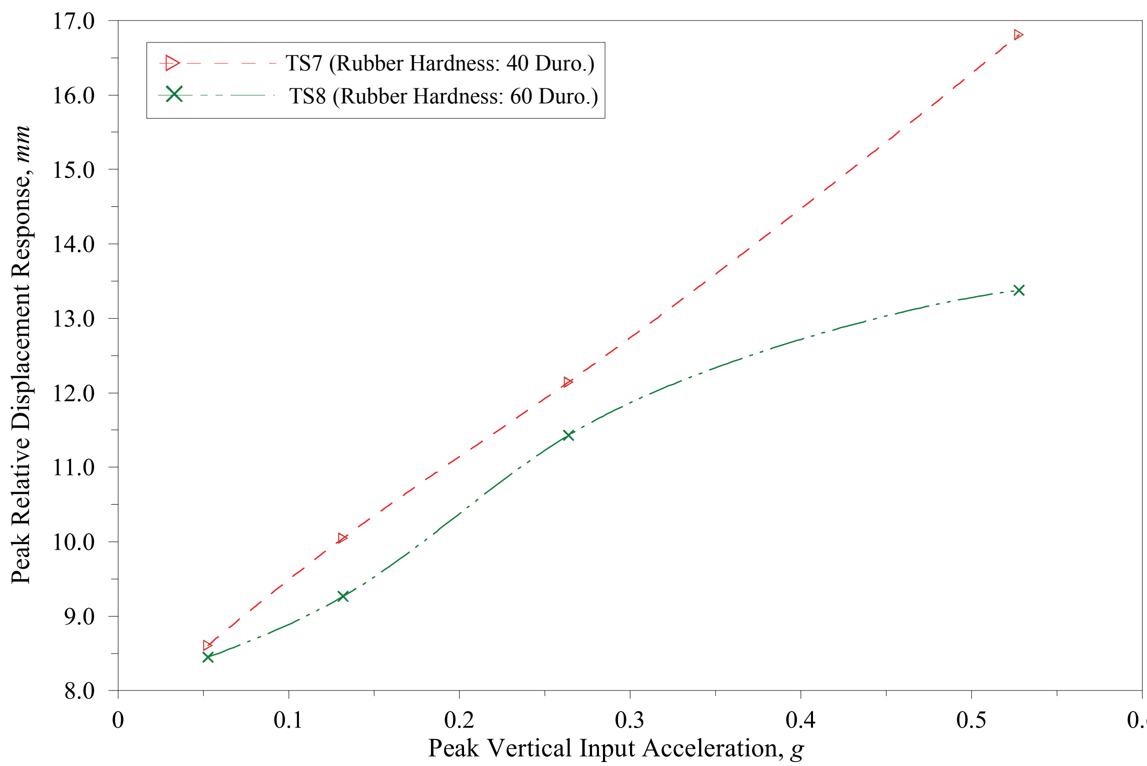

(b) Peak Vertical Relative Displacement Response Vs. Peak Vertical Input Acceleration

Figure 7-38 Effect of Variation of Rubber Snubber Hardness on Peak Relative Displacement Response at Top-South-East Corner of Test Specimen, Comparison of Results of Test Series 7 and 8

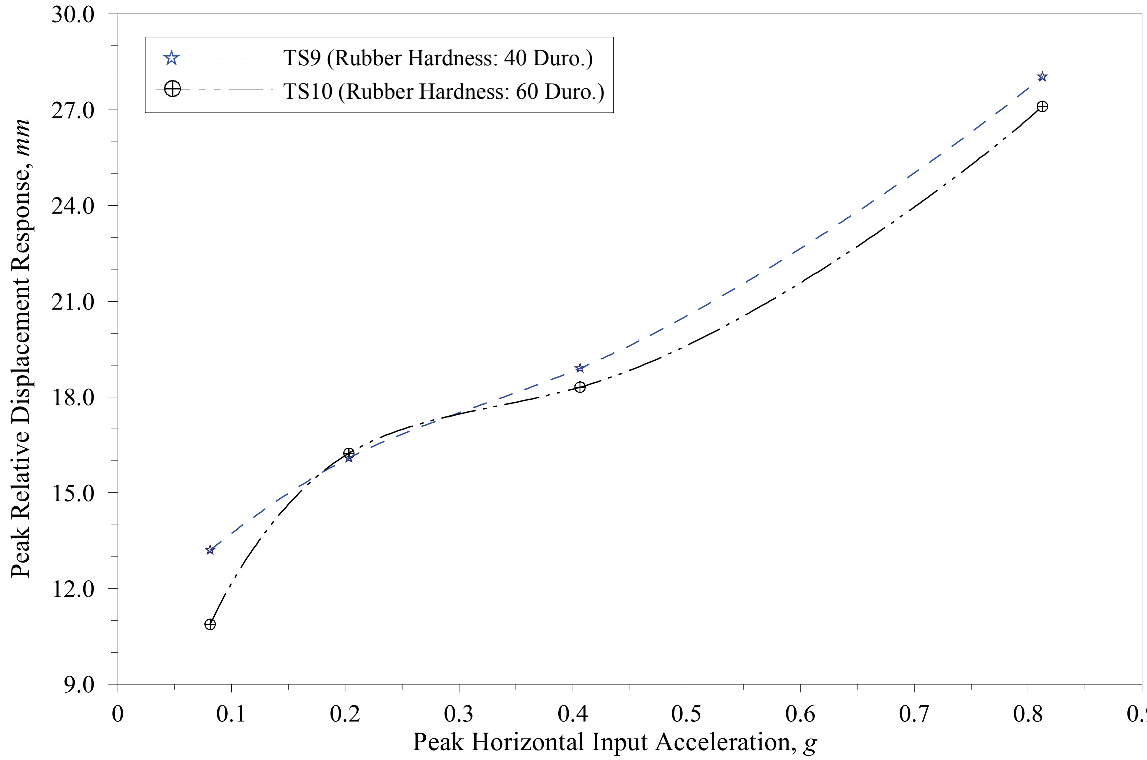

(a) Peak Horizontal Relative Displacement Response Vs. Peak Horizontal Input Acceleration

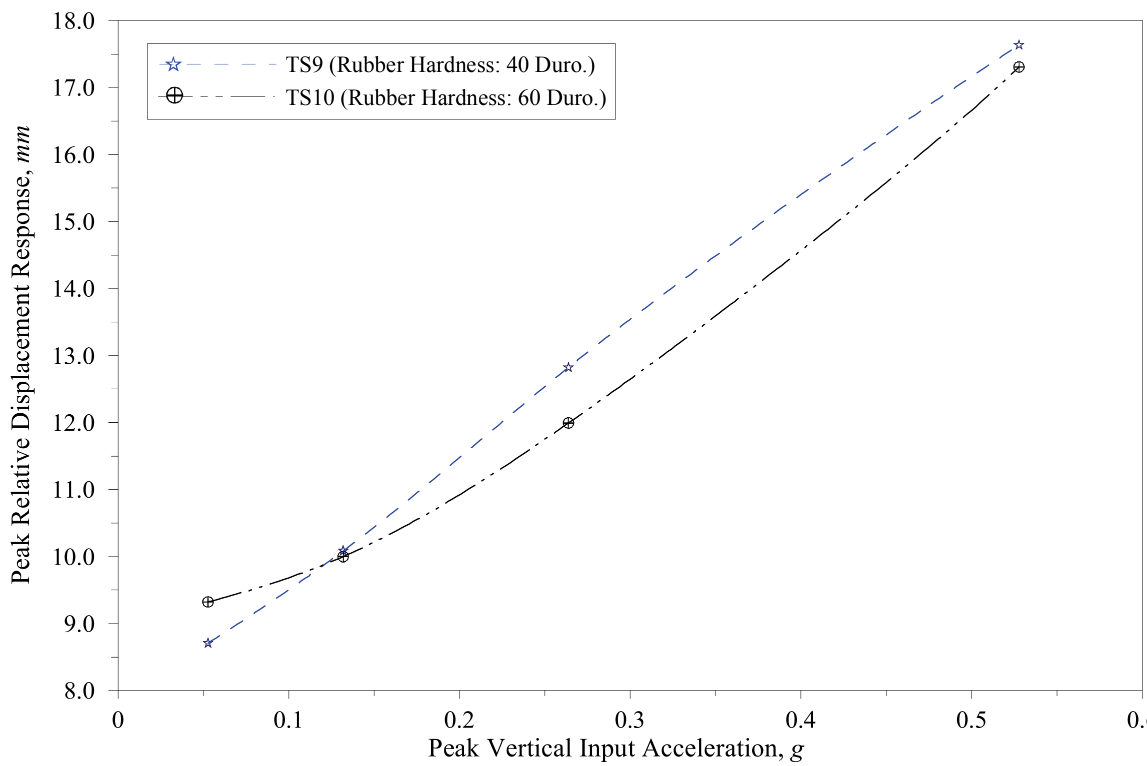

(b) Peak Vertical Relative Displacement Response Vs. Peak Vertical Input Acceleration

Figure 7-39 Effect of Variation of Rubber Snubber Hardness on Peak Relative Displacement Response at Top-South-East Corner of Test Specimen, Comparison of Results of Test Series 9 and 10

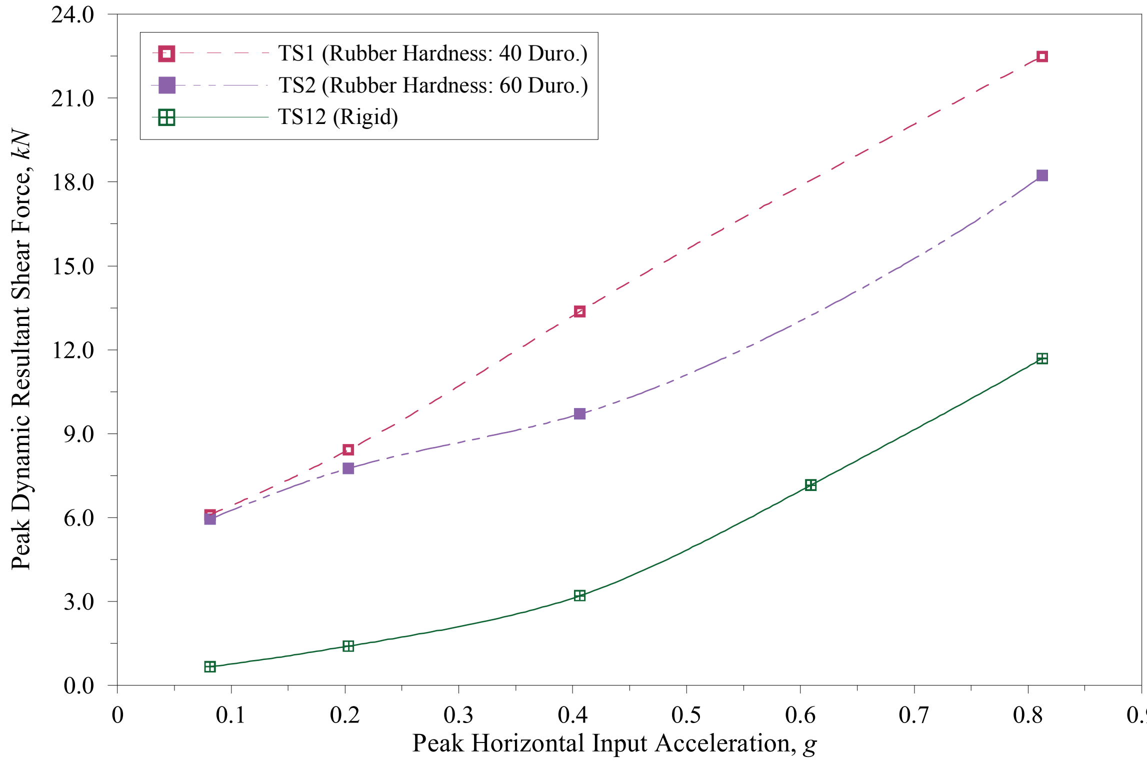

(a) Maximum Shear Force Induced into I/R Systems Vs. Peak Horizontal Input Acceleration

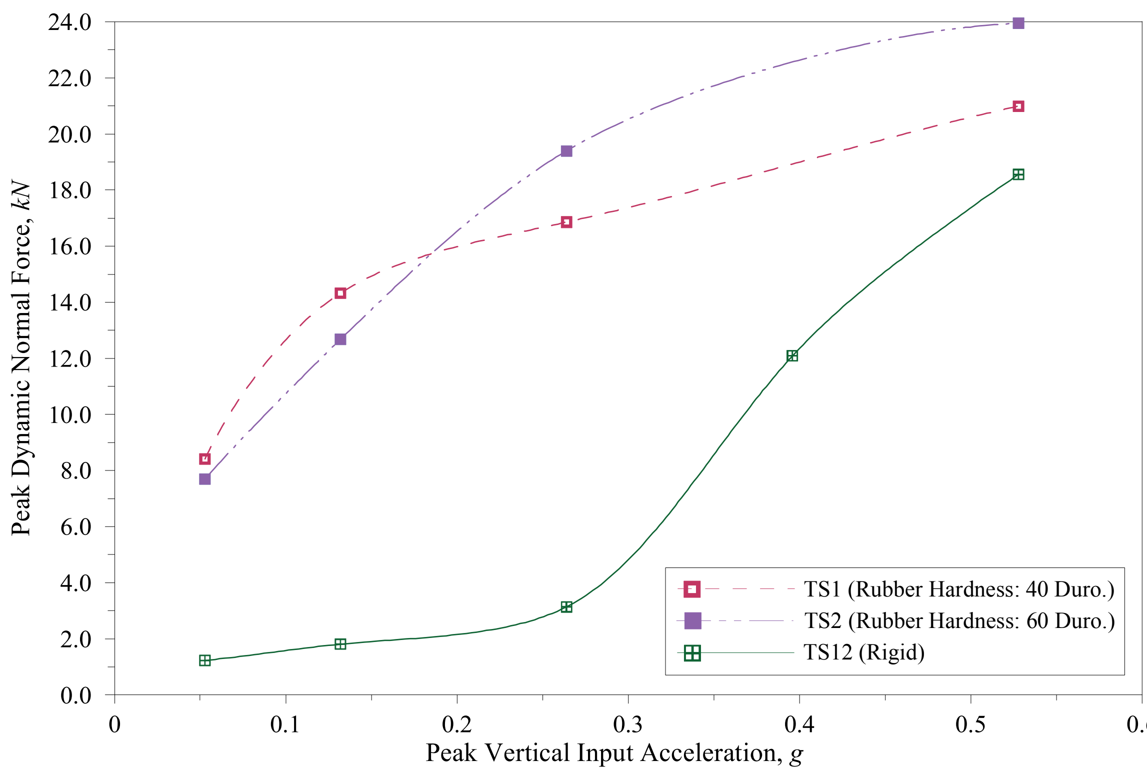

(b) Maximum Normal Force Induced into I/R Systems Vs. Peak Vertical Input Acceleration

Figure 7-40 Effect of Variation of Rubber Snubber Hardness on Peak Dynamic Forces Induced into I/R Systems, Comparison of Results of Test Series 1 and 2

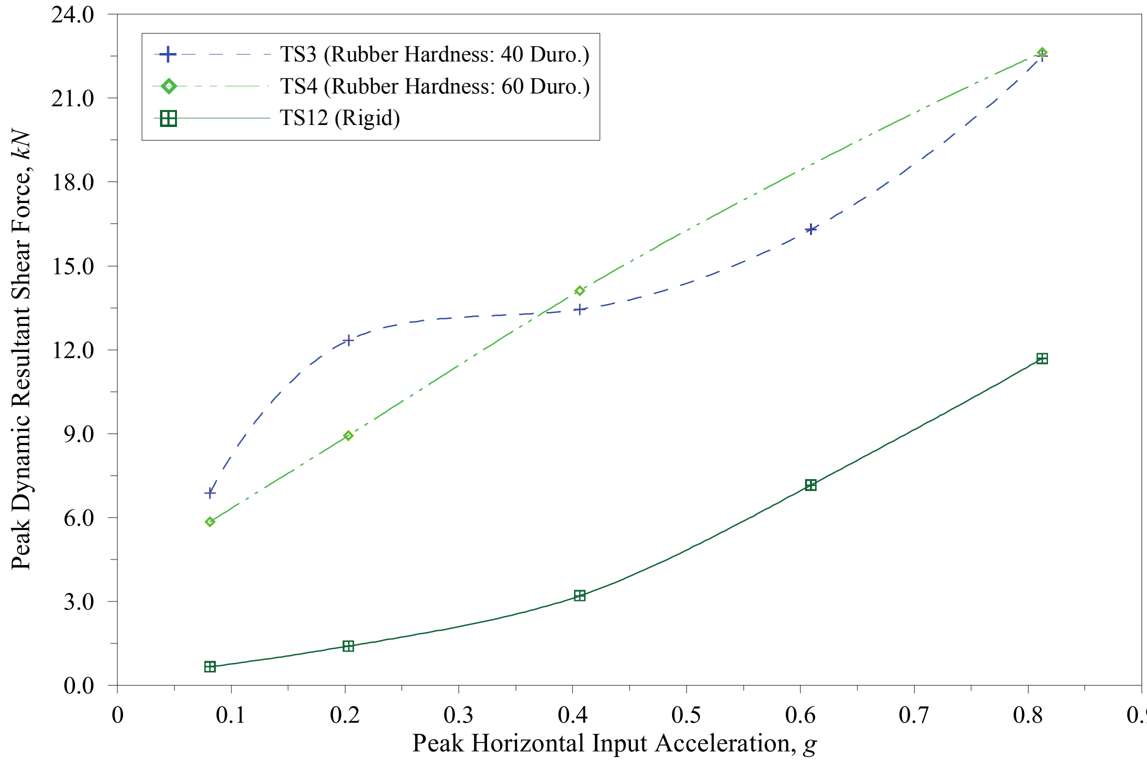

(a) Maximum Shear Force Induced into I/R Systems Vs. Peak Horizontal Input Acceleration

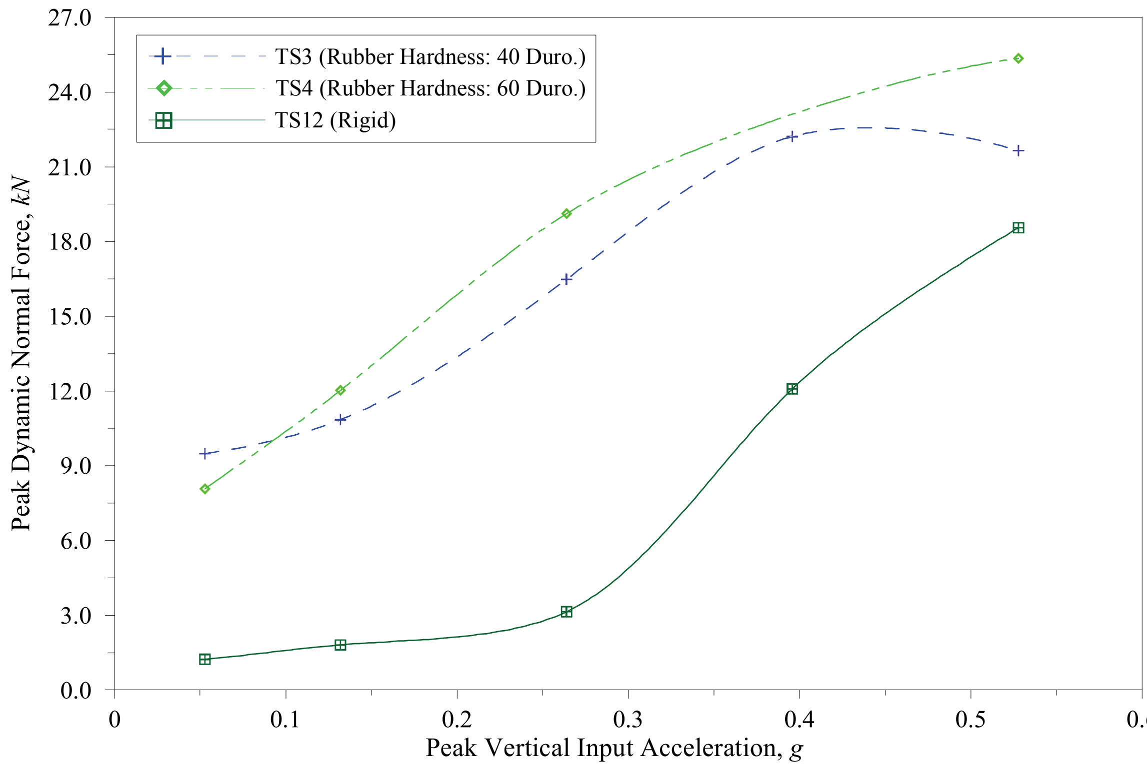

(b) Maximum Normal Force Induced into I/R Systems Vs. Peak Vertical Input Acceleration

Figure 7-41 Effect of Variation of Rubber Snubber Hardness on Peak Dynamic Forces Induced into I/R Systems, Comparison of Results of Test Series 3 and 4

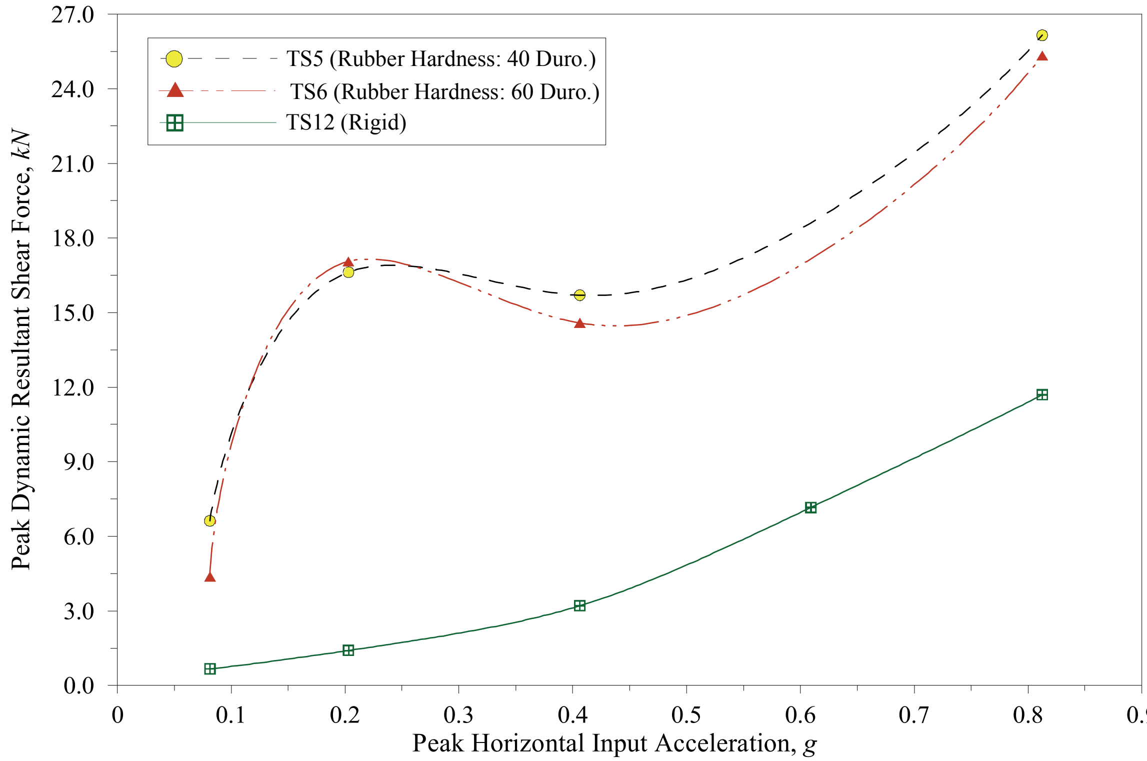

(a) Maximum Shear Force Induced into I/R Systems Vs. Peak Horizontal Input Acceleration

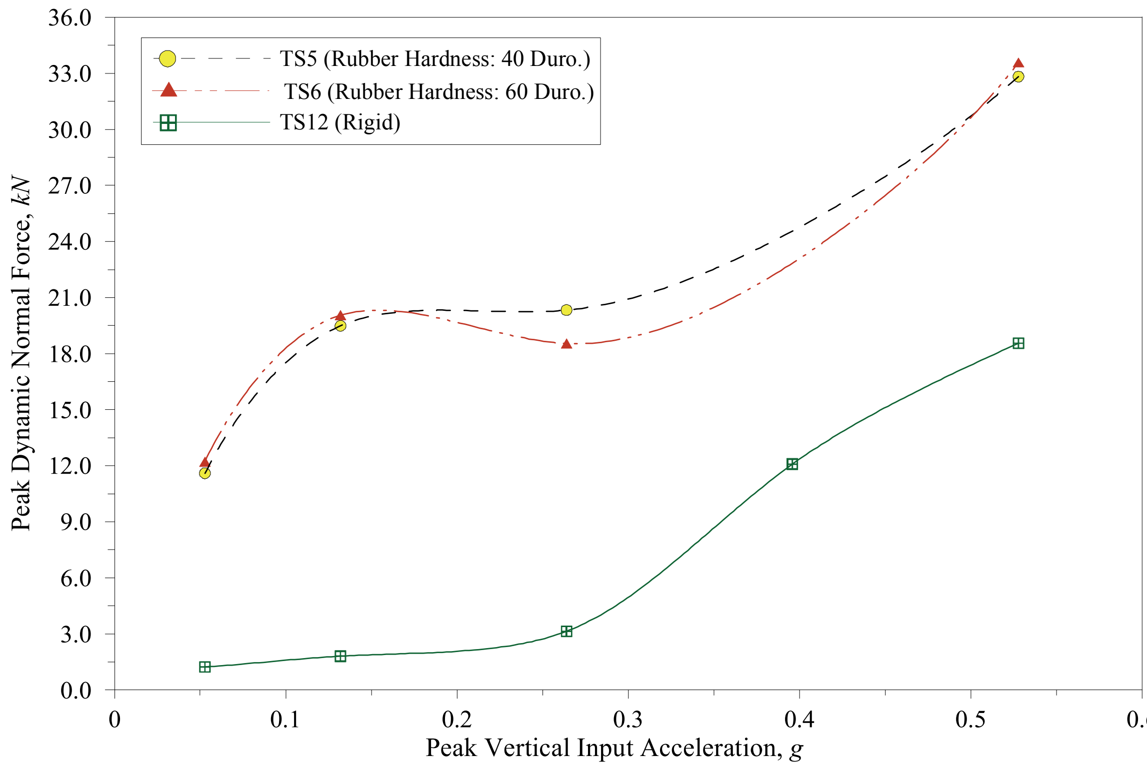

(b) Maximum Normal Force Induced into I/R Systems Vs. Peak Vertical Input Acceleration

Figure 7-42 Effect of Variation of Rubber Snubber Hardness on Peak Dynamic Forces Induced into I/R Systems, Comparison of Results of Test Series 5 and 6

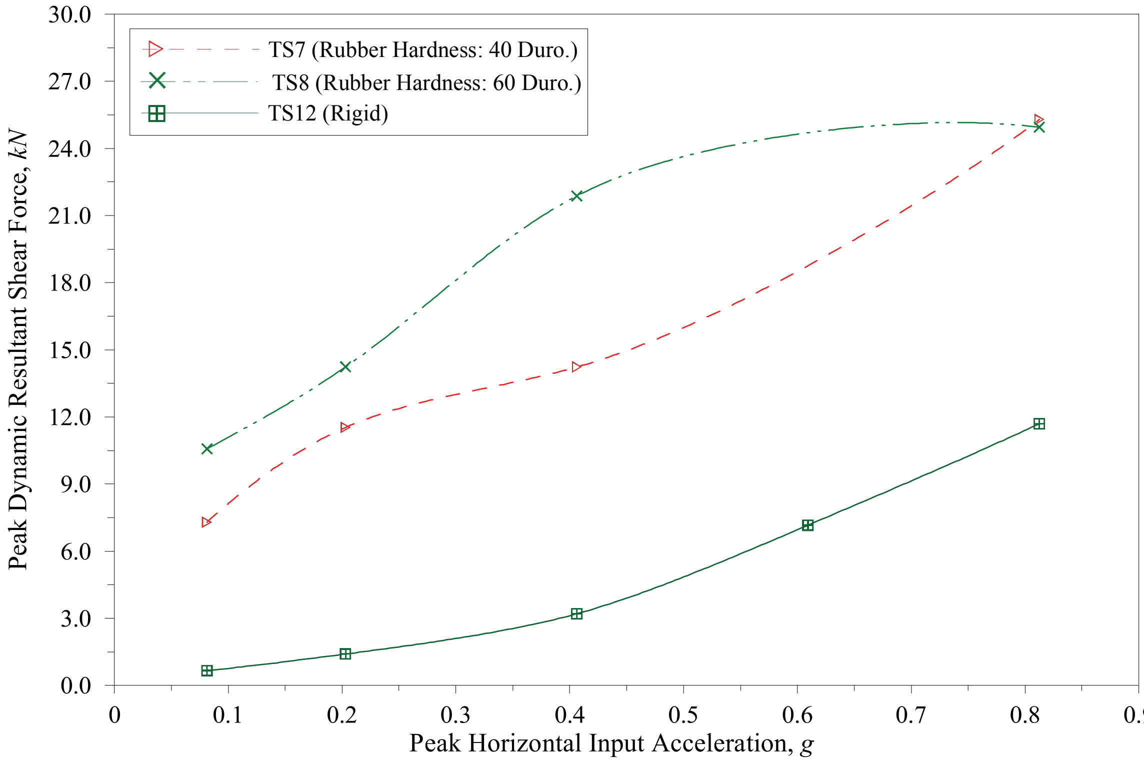

(a) Maximum Shear Force Induced into I/R Systems Vs. Peak Horizontal Input Acceleration

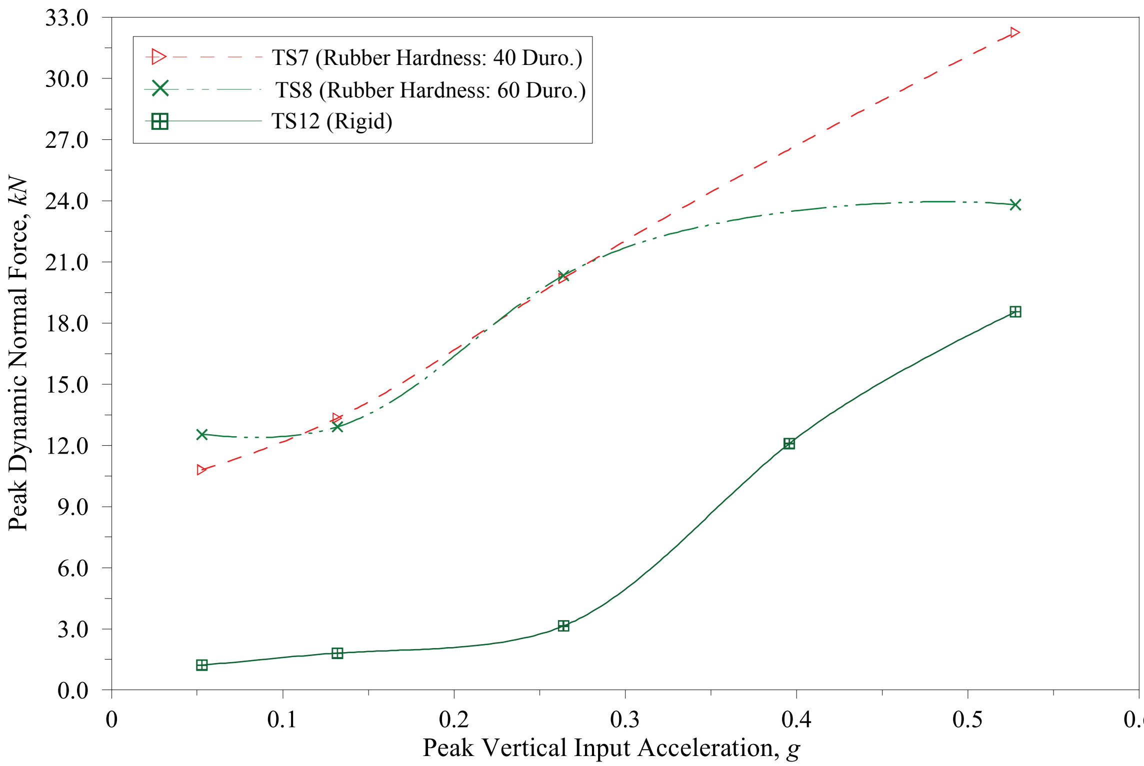

(b) Maximum Normal Force Induced into I/R Systems Vs. Peak Vertical Input Acceleration

Figure 7-43 Effect of Variation of Rubber Snubber Hardness on Peak Dynamic Forces Induced into I/R Systems, Comparison of Results of Test Series 7 and 8

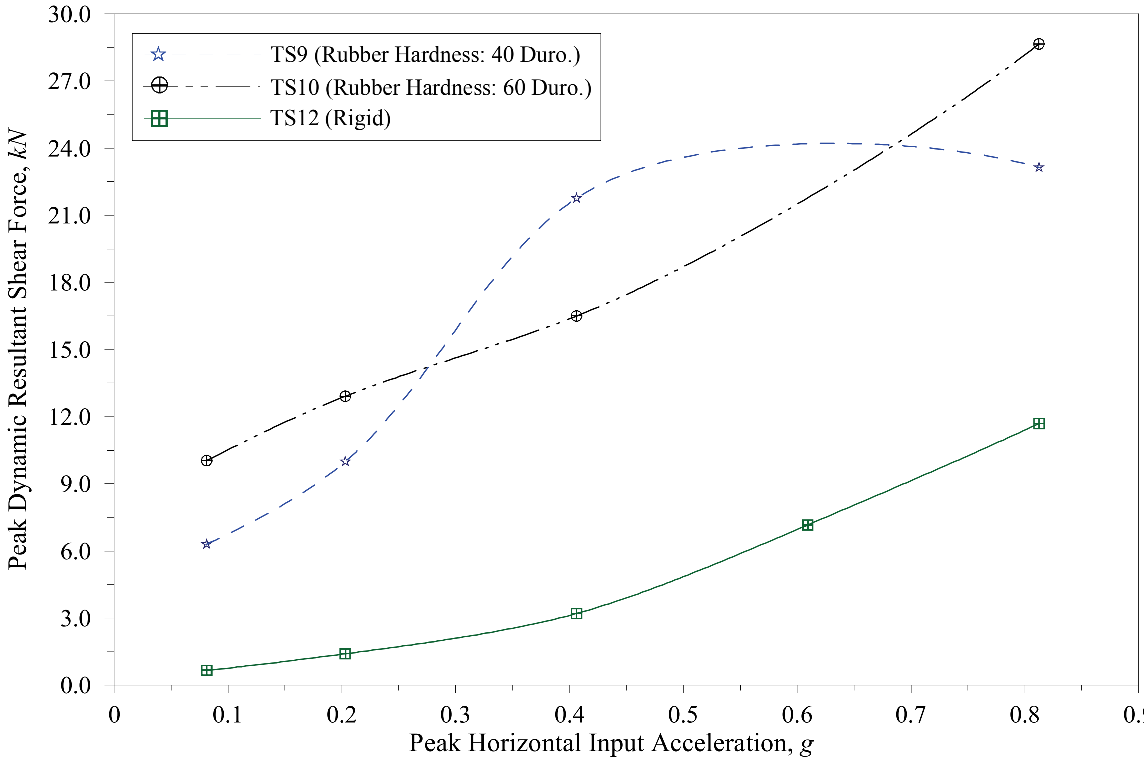

(a) Maximum Shear Force Induced into I/R Systems Vs. Peak Horizontal Input Acceleration

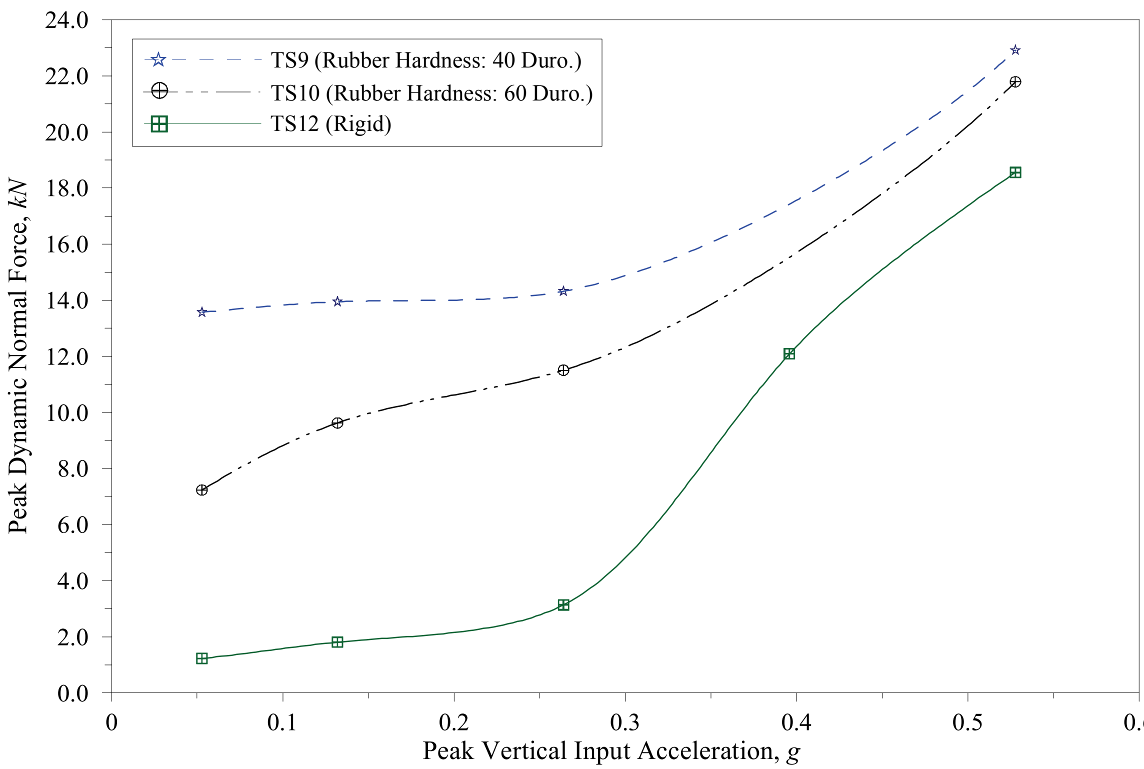

(b) Maximum Normal Force Induced into I/R Systems Vs. Peak Vertical Input Acceleration

Figure 7-44 Effect of Variation of Rubber Snubber Hardness on Peak Dynamic Forces Induced into I/R Systems, Comparison of Results of Test Series 9 and 10

7.4 Seismic Response of Damaged Test Specimen

In Section 6.2.2, it was described that during Seismic Test TS6-S4 the test specimen housing was damaged. After strengthening the test specimen housing (see Figure 6-3), the test with the full-scale input motion was repeated as Seismic Test TS6-S5. The selected peak response quantities of the test specimen during Seismic Tests TS6-S4 and TS6-S5 are compared in Table 7-16.

Table 7-16 Comparison of Selected Peak Response Quantities During Seismic Tests TS6-S4 and TS6-S5

Response Quantity	Direction	Test Name	
		TS6-S4*	TS6-S5**
Peak Acceleration Response on Top of Motor, *g*	Transverse	5.19	3.76
	Longitudinal	4.83	4.08
	Horizontal	5.43	4.08
	Vertical	3.07	2.76
	Resultant	6.24	4.53
Peak Acceleration Response on Test Specimen Housing, *g*	Transverse	6.20	4.45
	Longitudinal	3.46	3.30
Peak Relative Displacement Response at Top-South-East Corner of Test Specimen, *mm*	Transverse	41.8	40.8
	Longitudinal	33.7	30.9
	Horizontal	45.44	42.72
	Vertical	19.23	23.94
Peak Dynamic Forces Induced into I/R Systems, *kN*	Shear	27.75	25.33
	Normal	36.36	33.58

*. The test specimen housing was damaged during this seismic test
**. The test specimen housing was retrofitted before this seismic test (see Section 6.2.2)

The test results show that the damage of the connections between the base rail and modules during Seismic Test TS6-S4 resulted in a significant increase of the seismic responses of the test specimen and the dynamic forces induced into the I/R systems. The damaged test specimen housing experienced transverse acceleration larger than 6.0 *g*. The amplification of the response resulted from the damage to the housing was larger in the transverse direction than in the longitudinal direction.

7.5 Effect of Activation of Internal Isolation System on Seismic Response

During Test Series TS7 (Phase I), and TS12 (Phase II) of the experiments, the full-scale input motion tests were repeated after the isolation supports inside the fan module were activated. The selected peak response quantities during each pair of the seismic tests (Seismic Tests TS7-S4 and TS6-S5 with the isolated test specimen and Seismic Tests TS12-S5 and TS12-S6 with the rigidly mounted test specimen) are listed in Table 7-17.

Table 7-17 Comparison of Selected Peak Response Quantities with and without Activation of Internal Isolation Systems during Full-Scale Tests of Test Series TS7 and TS12

Response Quantity	Direction	Test Name			
		Phase I: Isolated Test Specimen		Phase II: Rigidly Mounted Test Specimen	
		TS7-S4*	TS7-S5**	TS12-S5*	TS6-S6**
Peak Acceleration Response on Top of Motor, *g*	Transverse	2.99	6.02	2.98	3.34
	Longitudinal	3.47	5.60	2.5	3.75
	Vertical	3.54	6.32	3.12	4.29
	Horizontal	2.38	3.83	1.70	2.44
	Resultant	3.72	7.39	3.15	4.29
Peak Acceleration Response on Test Specimen Housing, *g*	Transverse	4.28	4.05	2.52	2.10
	Longitudinal	2.62	2.41	1.24	1.15
Peak Relative Displacement Response Measured on South Face of Test Specimen, *mm*	Transverse	30.0	30.6	7.5	7.0
	Longitudinal	19.8	19.6	3.1	3.0
	Horizontal	30.3	30.9	7.7	7.1
	Vertical	16.8	16.7	2.4	2.3
Peak Dynamic Forces Induced into I/R Systems, *kN*	Shear	25.29	25.33	11.69	13.14
	Normal	32.26	26.44	18.55	13.7

*. Seismic test without internal isolation system
**. Seismic test with internal isolation system

The test results show that the activation of the internal isolation system supporting the motor and fan resulted in a significant increase of the acceleration response of the motor. However, the response of the test specimen housing and the dynamic forces induced into the I/R systems hardly changed (slightly decreased) after activation of the internal isolation system. The increase of the acceleration responses on top of the motor after activation of the internal isolation systems has been much larger in the test with the isolated test specimen than in the test with the rigidly mounted test specimen.

SECTION 8

CONCLUSIONS

The experimental research presented in this report is aimed at evaluating the seismic performance of an isolation/restraint (I/R) system supporting a relatively light mechanical equipment item. The I/R system considered in this study was typical of commercially available systems for seismic application. The mechanical equipment used as the test specimen was an Air-Handling Unit (AHU). The mass of the test specimen was 1971 *kg* (4345 *lb*). The experimental study included two phases of earthquake-simulator tests. During the first phase, the test specimen was supported by six I/R systems. The test plan of this phase of the experiments incorporated variations of the restraint component properties, and included 46 seismic tests. Each seismic test was preceded and followed by a pulse-type system-identification test. In order to establish the dynamic properties of the test specimen, and to compare the seismic responses of the isolated and rigidly mounted test specimen, the second phase of the experiments was conducted with the rigidly mounted test specimen. This phase included six seismic and seven system-identification tests. The main conclusions obtained from the system-identification and seismic tests conducted throughout the two phases of earthquake-simulator experiments are described in this section.

The results of the pulse-type system-identification tests showed that the first three natural frequencies of the isolated test specimen were 1.23, 1.55, and 2.06 *Hz*. These natural frequencies were significantly lower than the first (lowest) natural frequency of the rigidly mounted test specimen (9.6 *Hz*). Translations along the transverse, longitudinal, and vertical directions were the major component of the mode shapes established for the first three modes of the isolated test specimen. However, all of the first three modes of the isolated test specimen incorporated some rotational components. The mode shapes of the fourth, fifth, and sixth mode of the isolated test specimen involved more rotations. The mode shapes of the six modes of the isolated test specimen show that the total response of the isolated test specimen always involves some rotational movements. In other words, the test specimen would always engage the restraint components with both translational and rotational momentum.

Decay of responses of the isolated test specimen at the end of the seismic tests (free vibration without engagement of the restraint components) showed that the isolation component of the I/R system provided only less than three percents of the critical (equivalent) viscous damping ratio. The low damping capacity of the isolation component of the I/R system is in fact desirable from the vibration-isolation point of view.

Comparisons of similar responses of the isolated and rigidly mounted test specimen during the seismic tests confirmed that the restraint component of the I/R system limited the displacement responses of the isolated test specimen at the expense of significant amplified acceleration responses and large dynamic forces induced at the support locations (I/R systems).

During the seismic tests conducted with the different restraint component properties, the horizontal and vertical Acceleration Amplification Factor (*AAF*, defined as the ratio between the peak acceleration response measured on the test specimen and the peak input acceleration in a particular direction) near the center of mass of the test specimen varied in the range of 4.0 to 11.2 and 4.2 to 15.1, respectively. The variation ranges of the same response quantities for the rigidly mounted test specimen were 3.3 to 5.6 and 3.1 to 5.3, respectively.

The transverse and longitudinal *AAF* on the housing of the isolated test specimen during the seismic tests varied in the range of 3.4 to 13.4 and 2.8 to 7.3, respectively. The same response quantities for the rigidly mounted test specimen during the seismic tests varied in the range of 1.5 to 3.2 and 1.3 to 2.1, respectively.

Throughout the seismic tests of the first phase of the experiments, the transverse, longitudinal, and vertical *AAF* at the support locations of the isolated test specimen (on the top level of the I/R systems) varied in the range of 2.9 to 17.3, 2.7 to 9.5, and 4.2 to 27.0, respectively.

Throughout the seismic test, the following trends were observed in the variations the *AAF* near the center of mass, on the housing, and at the support locations of the test specimen:

1) The Horizontal *AAF* was usually smaller than the vertical *AAF*. The restraining mechanism in the horizontal direction, which incorporated a geometric nonlinearity by gradual expansion of the contact surface, was proven more successful in reducing the amplification of the acceleration responses.

2) Due to the rotational responses of the test specimen and the energy absorption by the test specimen housing and other components, the *AAF* was considerably larger at the support locations than near the center of mass or on the housing of the test specimen.

3) Comparison of the test results in this study and the results obtained in the previous study conducted with a heavy and rugged mechanical equipment item (Fathali and Filiatrault, 2007) confirmed that the amplification of acceleration response increases as the mass of the equipment decreases or its flexibility increases.

4) With the high input motion amplitude, the velocity (both translational and rotational) of the test specimen at the threshold of the engagement of the snubbers was more influenced by the input acceleration rather than by the restraint component properties. Therefore, as the test results showed, the sensitivity of the *AAF* to variations of the restraint component properties generally decreased with an increase of the input motion amplitude.

5) The acceleration responses of the test specimen increased with an increase of the input motion amplitude. However, the *AAF* usually decreased with an increase of the input motion amplitude. During most of the test series, the largest and smallest *AAF* was experienced during the test with the lowest and highest (full-scale) amplitude input motion, respectively.

The maximum horizontal and vertical acceleration responses measured near the center of mass of the isolated test specimen were 4.71 and 2.98 *g*, respectively. The similar response quantities for the rigidly mounted test specimen were 3.12 and 1.17 *g*, respectively. The maximum transverse and longitudinal acceleration responses on the housing of the isolated test specimen were 5.77 and 3.91 *g*, respectively. The similar response quantities for the rigidly mounted test specimen were 2.52 and 1.24 *g*, respectively.

Whereas the I/R systems were designed for a peak acceleration of 3.0 *g*, the peak transverse, longitudinal, and vertical acceleration responses measured at the support locations of the isolated test specimen during the seismic tests exceeded 7.6, 6.7, and 6.3 *g*, respectively.

During the seismic tests, the restraint components of the I/R systems designed for a 15 *kN* nominal static design capacity experienced dynamic shear and normal forces as large as 29 and 34 *kN*, respectively, and were not damaged. The dynamic forces induced into the I/R systems were considerably larger than the dynamic forces experienced at the support locations of the rigidly mounted equipment. The maximum shear and normal forces at the support locations of the rigidly mounted test specimen during the seismic tests were 12 and 19 *kN*, respectively.

The resultant shear and normal Force Amplification Factor (*FAF*, defined as the ratio between the maximum dynamic forces induced into the I/R systems and maximum dynamic forces experienced at the support locations of the rigidly mounted test specimen) varied in the range of 1.5 to 15.8 and 1.1 to 11.1, respectively. Both the resultant shear and normal *FAF* decreased with an increase of the input motion amplitude. During the tests with the full-scale input motion, the variation ranges of the resultant shear and normal *FAF* were limited to 1.5 to 2.5 and 1.1 to 2.0, respectively.

The peak dynamic forces induced into the I/R systems during the seismic tests showed that: 1) the maximum dynamic force was not necessarily induced into the I/R system that supported the largest tributary static mass; 2) the maximum dynamic force was not always induced in the direction along which the largest translational acceleration response was experienced near the center of mass of the test specimen, and 3) a reduction of the dynamic forces induced into the I/R systems resulting from changes in the restraint component properties could occur at the same time as an increase of the translational acceleration responses near the center of mass of the test specimen. These observations, which might contradict intuition, are justified when translational and rotational responses of the test specimen are considered together. In fact, a large portion of the dynamic forces induced into the I/R systems was attributed to the rotational responses of the test specimen. Even without translational response at the center of mass and only with rotations, significant dynamic forces could be induced into the I/R systems. Furthermore, due to the rotational and vertical responses of the test specimen, the dynamic mass supported by each I/R system could be significantly different form the tributary static mass. The I/R system that supported the maximum static mass would not necessarily support the maximum dynamic mass at the threshold of the engagement of the restraint component.

Because of rotational responses of the test specimen and compressibility of the rubber snubbers, the peak relative displacement responses during the seismic tests could be much larger than the gap size of the I/R systems. Whereas the largest gap size of the I/R systems during the experiments was 13 *mm,* peak relative displacement response as large as 46 *mm* was measured on the housing of the isolated test specimen. The test results showed that the relative displacement responses of the test specimen increased with an increase of the elevation from the support locations.

During the seismic tests with the isolated test specimen, increasing the gap size of the restraint component always resulted in larger displacement responses. However, effects of increasing the gap size on the acceleration response of the test specimen, and on the dynamic forces induced into the I/R systems were functions of the input motion amplitude. With the low-amplitude input motion, increasing the gap size could preclude the high-frequency and high-intensity engagements of the snubbers. Therefore, it resulted in lower acceleration responses and smaller dynamic forces. With the high-amplitude input motion, on the other hand, the large gap size allowed the test specimen to accelerate within a larger space and engage the snubbers with high momentum. The increased momentum of the test specimen resulted in excessive amplified acceleration responses and large dynamic forces induced into the I/R systems. The test specimen housing was damaged during the full-scale test of the test series with the largest gap size (13 *mm*). The peak transverse and longitudinal acceleration responses on the test specimen housing during the test that resulted in the damage, were as high as 6.20 and 3.46 *g*.

Increasing the thickness of the rubber snubbers in most of the seismic tests resulted in higher acceleration responses near the center of mass and larger displacement responses on the housing of the test specimen. However, in most of the seismic tests, increasing the rubber snubber thickness was successful in reducing the dynamic forces induced into the I/R systems. In fact, the reduction of the stiffness of the rubber snubbers by increasing their thickness allowed the test specimen to move and rock in a larger space, but at the same time, it resulted in reductions of the dynamic forces induced into the I/R systems.

In most of the seismic tests, reducing the hardness of the rubber snubbers from 60 to 40 *Duro* resulted in larger displacement responses. The effects of reducing the hardness of the rubber snubbers on the acceleration responses near the center of mass were functions of the input motion amplitude and thickness of the rubber snubber. In many tests, reducing the rubber hardness resulted in an increase of the acceleration responses near the center of mass. Despite of the increased displacement (on the housing) and acceleration responses (near the center of mass), still in some of the seismic tests reducing the rubber hardness resulted in reductions of the dynamic forces induced into the I/R systems. However, in some of the seismic tests, reducing the rubber hardness degraded the seismic performance of the I/R systems from all points of view as the acceleration response near the center of mass increased, the test specimen experienced larger displacements, and stronger dynamic forces were induced into the I/R systems.

The test results confirmed that the capability of the rubber snubber to reduce the dynamic forces was improved more by increasing the snubber stiffness than by reducing its hardness. Furthermore, it was observed that the effect of the snubber hardness on the seismic responses was overshadowed in presence of thick snubber or large gap size.

The test results showed that after activation of the internal vibration isolators (supporting the motor and fan inside the fan module) the acceleration responses on top of the motor significantly increased. However, other seismic responses of the test specimen were hardly affected by the activation of the internal vibration isolators. In addition, the test results showed that the amplification of the acceleration responses on top of the motor due to the activation of the internal vibration isolators was much larger for the isolated test specimen than for the rigidly mounted test specimen.

SECTION 9

GENERAL FINDINGS AND RECOMMENDATIONS ON SEISMIC PERFORMANCE OF I/R SYSTEMS

The general conclusions obtained from the earthquake-simulator experiments conducted with a relatively light and flexible equipment item (an air-handling unit) in the present study, and the conclusions previously obtained from similar experiments conducted with a relatively heavy and rugged mechanical equipment item (a centrifugal liquid chiller) are summarized as follows.

1) The seismic protection of vibration-isolated equipment by rubber snubbers is a displacement-control approach, which involves impact mechanisms. In general, impact is a crude control mechanism with poor energy-dissipation capability, which results in amplified acceleration responses and large dynamic forces. Similarly, the displacement-control of vibration-isolated equipment by rubber snubbers is achieved at the expense of amplified acceleration responses of the equipment and large dynamic forces induced into the snubbers. However, by proper selection of the snubber properties and without violation of the vibration-isolation requirements, it is possible to moderate the unwanted consequences of the impacts between the equipment and snubbers.

2) The response of a mechanical equipment item mounted on I/R systems to a seismic excitation is highly nonlinear. For a given seismic excitation, the peak seismic responses are functions of several parameters including, mass and mass moment of inertia of the equipment, flexibility of the equipment, eccentricities of the center of mass of the equipment , and the I/R system properties.

3) Effects of the restraint component properties on the equipment seismic responses are functions of the input motion amplitude. For instance, with low amplitude input motions, a large gape size might desirably allow the equipment to move within the air gaps without high-frequency and high-intensity engagements of the restraint components. However, with large-amplitude input motions, the large gap size might be seriously detrimental by allowing the equipment to accelerate in a larger space and engage the restraint components with high momentum.

4) Among the three properties of the restraint components, the gap size and the rubber snubber hardness has the most and the least influence on the seismic performance of the I/R systems, respectively. The first recommendation to improve the seismic performance of the I/R systems is to reduce the gap size. Particularly in the areas of high seismicity or wherever high amplitude input motions are expected (top levels of high-rise buildings), the gap size should be reduced to the minimum which satisfies the vibration-isolation requirements. Being conservative on the gap size to ensure the vibration-isolation efficiency seriously endangers the safety of the equipment, the I/R systems, and the lifelines connected to the equipment. Increasing the rubber snubber thickness is the second recommendation for the cases that small gap sizes violate the vibration-isolation requirements, and therefore, large gap sizes should be used. Reducing the hardness of the rubber snubber is not recommended since it slightly reduces the induced dynamic forces but at the same time increases displacement responses of the equipment and might also increase the acceleration responses of the equipment. In other words, reducing the dynamic forces (the main expected benefit of reducing the hardness of the rubber snubber) is achieved much more efficiently by increasing the rubber snubber thickness than by reducing its hardness. Moreover, when soft rubber snubber is used, it is better to increase the snubber thickness to delay/avoid the hardening (and snubber rupture) resulting from over-compression of the snubber during impacts.

5) Increasing the thickness and/or reducing the hardness of the rubber snubbers are the solutions to reduce the dynamic forces induced into the I/R systems. However, these solutions result in larger displacement of the equipment. The increased translation and rocking of the equipment could be damaging to the lifelines

connected to the equipment. Moreover, it might result in large acceleration responses at the points elevated from the support locations and damage the acceleration-sensitive components located at those points. Therefore, application of thick rubber (thicker than 0.25 in.) or soft rubber (40 *Duro*) might be necessary only for the I/R systems with strong potential dynamic forces such as I/R systems with the large gap size (larger than 0.25 in.).

6) The static approach to estimate the peak dynamic forces induced into the I/R systems is inaccurate because the mass supported by each I/R system is not constant during the seismic response, and, more importantly, because a large portion of the forces induced into the I/R systems is attributed to the rotational acceleration responses of the equipment. Contrary to what is predicted by the static approach, the maximum dynamic forces are not necessarily induced into the I/R system supporting the largest static tributary mass.

7) Due to the rotational responses of the equipment and compressibility of the rubber snubbers, the relative displacement responses at some points on the equipment can be much larger than the gap size of the I/R systems. The relative displacement response increases with an increase of any of the followings: the input motion amplitude, gap size, rubber snubber thickness, rubber snubber softness, or elevation from the support locations.

8) Higher acceleration-response amplifications should be expected for flexible and light mechanical equipment than for rugged and heavy mechanical equipment. Unfortunately, compared to heavy and rugged equipment items, light and flexible equipment items are usually more sensitive to acceleration. Therefore, the lower force-demands of I/R systems supporting light equipment should not lead to less attention in selecting the appropriate properties of the restraint components. Securing the I/R systems during an earthquake and keeping the equipment in place are important objectives but they do not fulfill the seismic protection of the equipment. The equipment should stay put but it also should be able to continue its normal operation after the earthquake.

9) Contrary to what might be expected by intuition, due to the rotational responses of the equipment, change of the restraint component properties in the horizontal or vertical direction could influence the equipment responses and the dynamic forces induced into the I/R systems in both horizontal and vertical directions.

10) Compared to restraining mechanisms with constant contact surface (such as a rubber washer pressing a rubber grommet), restraining mechanisms that incorporate geometric nonlinearity by gradual expansion of the contact surface (such as a cylindrical punch and a rubber tube) are certainly superior for protection of acceleration-sensitive mechanical equipment.

11) The restraining mechanism resulting from an impact between two steel objects induces very large dynamic forces and can be catastrophic. I/R systems should be designed to ensure that all restraining mechanisms incorporate resilient contact surfaces.

SECTION 10

REFERENCES

[1] American Society of Heating, Refrigerating, and Air-Conditioning Engineers (ASHRAE), (2003), ”Seismic and Wind Restraint Design”, 2003 ASHRAE Handbook: Heating, Ventilation, and Air-Conditioning Applications, Chapter 54, American Society of Heating, Refrigerating and Air-Conditioning Engineers, Atlanta, GA

[2] Ayres, J. M., and Phillips, R. J., (1998), “Water Damage in Hospitals Resulting from the Northridge Earthquake”, ASHRAE Transactions*,* 104(1B), 1286–1296

[3] Ayres, J. M., and Sun, T. Y., (1973), “Nonstructural Damage”, in San Fernando, California, Earthquake of February 9, 1971, US Department of Commerce, National Ocean and Atmospheric Administration, Vol. 1(B), 735–776

[4] Ayres, J. M., Sun, T. Y., and Brown, F. R., (1973), “Nonstructural Damage to Buildings”, in The Great Alaska Earthquake of 1964: Engineering, Division of Earth Sciences, National Research Council, National Academy of Sciences, Washington DC, 346–456

[5] Fathali, S., and Filiatrault, A., (2007), “Experimental Seismic-Performance Evaluation of Isolation/ Restraint Systems for Mechanical Equipment, Part I: Heavy Equipment Study”, Technical Report MCEER-07-0007, Multidisciplinary Center for Earthquake Engineering Research, University at Buffalo, State University of New York, Buffalo, NY

[6] Filiatrault, A., (2002), “Elements of Earthquake Engineering and Structural Dynamics”, 2nd Ed., Polytechnic International Press, Montreal, Canada

[7] Filiatrault, A., Christopoulos, C., and Stearns, C., (2002), “Guidelines, Specifications, and Seismic Performance Characterization of Nonstructural Building Components and Equipment”*,* Report PEER 2002/05, Pacific Earthquake Engineering Research Center, University of California, Berkeley

[8] Gates, W. E., and McGavin, G., (1998), “Lessons Learned from the 1994 Northridge Earthquake on the Vulnerability of Nonstructural Systems”, Proceedings of the Seminar on Seismic Design, Retrofit, and Performance of Nonstructural Components, ATC 29-1*,* San Francisco, CA, 93–106

[9] Gent A. N., (2001), “Engineering with Rubber, How to Design Rubber Components”, Hanser Publishers, Munich

[10] Harris C. M., and Crede C. E., (1961), “Shock and Vibration Handbook, Volume 2: Data Analysis, Testing, and Methods of Control”, McGraw Hill, NY

[11] International Code Council (ICC), (2003), “International Building Code”, International Code Council, Whittier, CA

[12] International Code Council-Evaluation Service Inc. (ICC-ES), (2004), “Acceptance Criteria for Seismic Qualification by Shake Table Testing of Nonstructural Components and Systems”, AC 156, Effective July 2004, ICC-ES Inc., International Code Council, Whittier, CA

[13] Iwan, W. D., (1978), “The Earthquake Design and Analysis of Equipment Isolation Systems, Earthquake Engineering and Structural Dynamics, 6, 523–534

[14] Kinetics Noise Control, (2004), “Estimating the Stiffness of Neoprene Isolators”, Technical Document T2.3.2, Kinetics Noise Control, Dublin, OH

[15] Kinetics Noise Control, (2007), < http://www.kineticsnoise.com >

[16] Lama P. J., (1994), “Effect of Seismic Input on Resiliently Mounted Mechanical Equipment”, Sound and Vibration, 28 (7), 20–26

[17] Lama, P. J., (1998), “Practical Guidelines for Seismic Retrofitting of HVAC Systems”, Proceedings of the Seminar on Seismic Design, Retrofit, and Performance of Nonstructural Components, ATC 29-1, San Francisco, CA, 445–454

[18] Lloyd R. J., (2003),” Case Studies of Anchorage Failures”, Proceedings of Seminar on Seismic Design, Performance, and Retrofit of Nonstructural Components in Critical Facilities, ATC-29-2, Newport Beach, CA, 189–200

[19] Mason Industries Inc., (2004), “A Discussion of, and Specification for, the Use of the Z-1011 Snubber and Computer Program for Isolated Equipment in Earthquake Zones”, SCS-100 Bulletin, Mason Industries Inc., Smithtown, NY

[20] Meisel, P. W., (2001), ”Static Modeling of Equipment Acted on by Seismic Forces”, ASHRAE Transactions, 107(1), 775–786

[21] Myrtle, R. C., Masri, S. F., Nigbor, R. L., and Caffrey, J. P., (2005), “Classification and Prioritization of Essential Systems in Hospitals under Extreme Events”, Earthquake Spectra, 21, 779–802

[22] Naeim, F., and Lobo, R., (1998), “Performance of Nonstructural Components during the January 17, 1994 Northridge Earthquake – Case Studies of Six Instrumented Multistory Buildings”, Proceedings of the Seminar on Seismic Design, Retrofit, and Performance of Nonstructural Components, ATC-29-1, San Francisco, CA, 107–119

[23] Reitherman, R., and Sabol, T., (1995), “Northridge Earthquake of January 17, 1994: Reconnaissance Report, Nonstructural Damage”, Earthquake Spectra, 11(Supplement C), 453–514

[24] Tauby, J. R., Lloyd, R., Nice, T., and Tünnissen, J., (1999), “A Practical Guide to Seismic Restraint”, American Society of Heating, Refrigerating, and Air-Conditioning Engineers, Atlanta, GA

[25] Trane Company, (2007), <http://www.trane.com>

[26] Wheeler, A. and Ganji, A. R., (2004), “Introduction to Engineering Experimentation”, Prentice Hall, Upper Saddle River, NJ

[27] Yao G.C. and Lien N., (1998), “Frequency Tuning for Spring-Supported Mechanical Components Protection”, Proceedings of Seminar on Seismic Design, Retrofit, and Performance of Nonstructural Components, San Francisco, California, January 22-23, ATC 29-1, 165–171

MCEER Technical Reports

MCEER publishes technical reports on a variety of subjects written by authors funded through MCEER. These reports are available from both MCEER Publications and the National Technical Information Service (NTIS). Requests for reports should be directed to MCEER Publications, MCEER, University at Buffalo, State University of New York, Red Jacket Quadrangle, Buffalo, New York 14261. Reports can also be requested through NTIS, 5285 Port Royal Road, Springfield, Virginia 22161. NTIS accession numbers are shown in parenthesis, if available.

NCEER-87-0001 "First-Year Program in Research, Education and Technology Transfer," 3/5/87, (PB88-134275, A04, MF-A01).

NCEER-87-0002 "Experimental Evaluation of Instantaneous Optimal Algorithms for Structural Control," by R.C. Lin, T.T. Soong and A.M. Reinhorn, 4/20/87, (PB88-134341, A04, MF-A01).

NCEER-87-0003 "Experimentation Using the Earthquake Simulation Facilities at University at Buffalo," by A.M. Reinhorn and R.L. Ketter, to be published.

NCEER-87-0004 "The System Characteristics and Performance of a Shaking Table," by J.S. Hwang, K.C. Chang and G.C. Lee, 6/1/87, (PB88-134259, A03, MF-A01). This report is available only through NTIS (see address given above).

NCEER-87-0005 "A Finite Element Formulation for Nonlinear Viscoplastic Material Using a Q Model," by O. Gyebi and G. Dasgupta, 11/2/87, (PB88-213764, A08, MF-A01).

NCEER-87-0006 "Symbolic Manipulation Program (SMP) - Algebraic Codes for Two and Three Dimensional Finite Element Formulations," by X. Lee and G. Dasgupta, 11/9/87, (PB88-218522, A05, MF-A01).

NCEER-87-0007 "Instantaneous Optimal Control Laws for Tall Buildings Under Seismic Excitations," by J.N. Yang, A. Akbarpour and P. Ghaemmaghami, 6/10/87, (PB88-134333, A06, MF-A01). This report is only available through NTIS (see address given above).

NCEER-87-0008 "IDARC: Inelastic Damage Analysis of Reinforced Concrete Frame - Shear-Wall Structures," by Y.J. Park, A.M. Reinhorn and S.K. Kunnath, 7/20/87, (PB88-134325, A09, MF-A01). This report is only available through NTIS (see address given above).

NCEER-87-0009 "Liquefaction Potential for New York State: A Preliminary Report on Sites in Manhattan and Buffalo," by M. Budhu, V. Vijayakumar, R.F. Giese and L. Baumgras, 8/31/87, (PB88-163704, A03, MF-A01). This report is available only through NTIS (see address given above).

NCEER-87-0010 "Vertical and Torsional Vibration of Foundations in Inhomogeneous Media," by A.S. Veletsos and K.W. Dotson, 6/1/87, (PB88-134291, A03, MF-A01). This report is only available through NTIS (see address given above).

NCEER-87-0011 "Seismic Probabilistic Risk Assessment and Seismic Margins Studies for Nuclear Power Plants," by Howard H.M. Hwang, 6/15/87, (PB88-134267, A03, MF-A01). This report is only available through NTIS (see address given above).

NCEER-87-0012 "Parametric Studies of Frequency Response of Secondary Systems Under Ground-Acceleration Excitations," by Y. Yong and Y.K. Lin, 6/10/87, (PB88-134309, A03, MF-A01). This report is only available through NTIS (see address given above).

NCEER-87-0013 "Frequency Response of Secondary Systems Under Seismic Excitation," by J.A. HoLung, J. Cai and Y.K. Lin, 7/31/87, (PB88-134317, A05, MF-A01). This report is only available through NTIS (see address given above).

NCEER-87-0014 "Modelling Earthquake Ground Motions in Seismically Active Regions Using Parametric Time Series Methods," by G.W. Ellis and A.S. Cakmak, 8/25/87, (PB88-134283, A08, MF-A01). This report is only available through NTIS (see address given above).

NCEER-87-0015 "Detection and Assessment of Seismic Structural Damage," by E. DiPasquale and A.S. Cakmak, 8/25/87, (PB88-163712, A05, MF-A01). This report is only available through NTIS (see address given above).

NCEER-87-0016 "Pipeline Experiment at Parkfield, California," by J. Isenberg and E. Richardson, 9/15/87, (PB88-163720, A03, MF-A01). This report is available only through NTIS (see address given above).

NCEER-87-0017 "Digital Simulation of Seismic Ground Motion," by M. Shinozuka, G. Deodatis and T. Harada, 8/31/87, (PB88-155197, A04, MF-A01). This report is available only through NTIS (see address given above).

NCEER-87-0018 "Practical Considerations for Structural Control: System Uncertainty, System Time Delay and Truncation of Small Control Forces," J.N. Yang and A. Akbarpour, 8/10/87, (PB88-163738, A08, MF-A01). This report is only available through NTIS (see address given above).

NCEER-87-0019 "Modal Analysis of Nonclassically Damped Structural Systems Using Canonical Transformation," by J.N. Yang, S. Sarkani and F.X. Long, 9/27/87, (PB88-187851, A04, MF-A01).

NCEER-87-0020 "A Nonstationary Solution in Random Vibration Theory," by J.R. Red-Horse and P.D. Spanos, 11/3/87, (PB88-163746, A03, MF-A01).

NCEER-87-0021 "Horizontal Impedances for Radially Inhomogeneous Viscoelastic Soil Layers," by A.S. Veletsos and K.W. Dotson, 10/15/87, (PB88-150859, A04, MF-A01).

NCEER-87-0022 "Seismic Damage Assessment of Reinforced Concrete Members," by Y.S. Chung, C. Meyer and M. Shinozuka, 10/9/87, (PB88-150867, A05, MF-A01). This report is available only through NTIS (see address given above).

NCEER-87-0023 "Active Structural Control in Civil Engineering," by T.T. Soong, 11/11/87, (PB88-187778, A03, MF-A01).

NCEER-87-0024 "Vertical and Torsional Impedances for Radially Inhomogeneous Viscoelastic Soil Layers," by K.W. Dotson and A.S. Veletsos, 12/87, (PB88-187786, A03, MF-A01).

NCEER-87-0025 "Proceedings from the Symposium on Seismic Hazards, Ground Motions, Soil-Liquefaction and Engineering Practice in Eastern North America," October 20-22, 1987, edited by K.H. Jacob, 12/87, (PB88-188115, A23, MF-A01). This report is available only through NTIS (see address given above).

NCEER-87-0026 "Report on the Whittier-Narrows, California, Earthquake of October 1, 1987," by J. Pantelic and A. Reinhorn, 11/87, (PB88-187752, A03, MF-A01). This report is available only through NTIS (see address given above).

NCEER-87-0027 "Design of a Modular Program for Transient Nonlinear Analysis of Large 3-D Building Structures," by S. Srivastav and J.F. Abel, 12/30/87, (PB88-187950, A05, MF-A01). This report is only available through NTIS (see address given above).

NCEER-87-0028 "Second-Year Program in Research, Education and Technology Transfer," 3/8/88, (PB88-219480, A04, MF-A01).

NCEER-88-0001 "Workshop on Seismic Computer Analysis and Design of Buildings With Interactive Graphics," by W. McGuire, J.F. Abel and C.H. Conley, 1/18/88, (PB88-187760, A03, MF-A01). This report is only available through NTIS (see address given above).

NCEER-88-0002 "Optimal Control of Nonlinear Flexible Structures," by J.N. Yang, F.X. Long and D. Wong, 1/22/88, (PB88-213772, A06, MF-A01).

NCEER-88-0003 "Substructuring Techniques in the Time Domain for Primary-Secondary Structural Systems," by G.D. Manolis and G. Juhn, 2/10/88, (PB88-213780, A04, MF-A01).

NCEER-88-0004 "Iterative Seismic Analysis of Primary-Secondary Systems," by A. Singhal, L.D. Lutes and P.D. Spanos, 2/23/88, (PB88-213798, A04, MF-A01).

NCEER-88-0005 "Stochastic Finite Element Expansion for Random Media," by P.D. Spanos and R. Ghanem, 3/14/88, (PB88-213806, A03, MF-A01).

NCEER-88-0006 "Combining Structural Optimization and Structural Control," by F.Y. Cheng and C.P. Pantelides, 1/10/88, (PB88-213814, A05, MF-A01).

NCEER-88-0007 "Seismic Performance Assessment of Code-Designed Structures," by H.H-M. Hwang, J-W. Jaw and H-J. Shau, 3/20/88, (PB88-219423, A04, MF-A01). This report is only available through NTIS (see address given above).

NCEER-88-0008 "Reliability Analysis of Code-Designed Structures Under Natural Hazards," by H.H-M. Hwang, H. Ushiba and M. Shinozuka, 2/29/88, (PB88-229471, A07, MF-A01). This report is only available through NTIS (see address given above).

NCEER-88-0009 "Seismic Fragility Analysis of Shear Wall Structures," by J-W Jaw and H.H-M. Hwang, 4/30/88, (PB89-102867, A04, MF-A01).

NCEER-88-0010 "Base Isolation of a Multi-Story Building Under a Harmonic Ground Motion - A Comparison of Performances of Various Systems," by F-G Fan, G. Ahmadi and I.G. Tadjbakhsh, 5/18/88, (PB89-122238, A06, MF-A01). This report is only available through NTIS (see address given above).

NCEER-88-0011 "Seismic Floor Response Spectra for a Combined System by Green's Functions," by F.M. Lavelle, L.A. Bergman and P.D. Spanos, 5/1/88, (PB89-102875, A03, MF-A01).

NCEER-88-0012 "A New Solution Technique for Randomly Excited Hysteretic Structures," by G.Q. Cai and Y.K. Lin, 5/16/88, (PB89-102883, A03, MF-A01).

NCEER-88-0013 "A Study of Radiation Damping and Soil-Structure Interaction Effects in the Centrifuge," by K. Weissman, supervised by J.H. Prevost, 5/24/88, (PB89-144703, A06, MF-A01).

NCEER-88-0014 "Parameter Identification and Implementation of a Kinematic Plasticity Model for Frictional Soils," by J.H. Prevost and D.V. Griffiths, to be published.

NCEER-88-0015 "Two- and Three- Dimensional Dynamic Finite Element Analyses of the Long Valley Dam," by D.V. Griffiths and J.H. Prevost, 6/17/88, (PB89-144711, A04, MF-A01).

NCEER-88-0016 "Damage Assessment of Reinforced Concrete Structures in Eastern United States," by A.M. Reinhorn, M.J. Seidel, S.K. Kunnath and Y.J. Park, 6/15/88, (PB89-122220, A04, MF-A01). This report is only available through NTIS (see address given above).

NCEER-88-0017 "Dynamic Compliance of Vertically Loaded Strip Foundations in Multilayered Viscoelastic Soils," by S. Ahmad and A.S.M. Israil, 6/17/88, (PB89-102891, A04, MF-A01).

NCEER-88-0018 "An Experimental Study of Seismic Structural Response With Added Viscoelastic Dampers," by R.C. Lin, Z. Liang, T.T. Soong and R.H. Zhang, 6/30/88, (PB89-122212, A05, MF-A01). This report is available only through NTIS (see address given above).

NCEER-88-0019 "Experimental Investigation of Primary - Secondary System Interaction," by G.D. Manolis, G. Juhn and A.M. Reinhorn, 5/27/88, (PB89-122204, A04, MF-A01).

NCEER-88-0020 "A Response Spectrum Approach For Analysis of Nonclassically Damped Structures," by J.N. Yang, S. Sarkani and F.X. Long, 4/22/88, (PB89-102909, A04, MF-A01).

NCEER-88-0021 "Seismic Interaction of Structures and Soils: Stochastic Approach," by A.S. Veletsos and A.M. Prasad, 7/21/88, (PB89-122196, A04, MF-A01). This report is only available through NTIS (see address given above).

NCEER-88-0022 "Identification of the Serviceability Limit State and Detection of Seismic Structural Damage," by E. DiPasquale and A.S. Cakmak, 6/15/88, (PB89-122188, A05, MF-A01). This report is available only through NTIS (see address given above).

NCEER-88-0023 "Multi-Hazard Risk Analysis: Case of a Simple Offshore Structure," by B.K. Bhartia and E.H. Vanmarcke, 7/21/88, (PB89-145213, A05, MF-A01).

NCEER-88-0024 "Automated Seismic Design of Reinforced Concrete Buildings," by Y.S. Chung, C. Meyer and M. Shinozuka, 7/5/88, (PB89-122170, A06, MF-A01). This report is available only through NTIS (see address given above).

NCEER-88-0025 "Experimental Study of Active Control of MDOF Structures Under Seismic Excitations," by L.L. Chung, R.C. Lin, T.T. Soong and A.M. Reinhorn, 7/10/88, (PB89-122600, A04, MF-A01).

NCEER-88-0026 "Earthquake Simulation Tests of a Low-Rise Metal Structure," by J.S. Hwang, K.C. Chang, G.C. Lee and R.L. Ketter, 8/1/88, (PB89-102917, A04, MF-A01).

NCEER-88-0027 "Systems Study of Urban Response and Reconstruction Due to Catastrophic Earthquakes," by F. Kozin and H.K. Zhou, 9/22/88, (PB90-162348, A04, MF-A01).

NCEER-88-0028 "Seismic Fragility Analysis of Plane Frame Structures," by H.H-M. Hwang and Y.K. Low, 7/31/88, (PB89-131445, A06, MF-A01).

NCEER-88-0029 "Response Analysis of Stochastic Structures," by A. Kardara, C. Bucher and M. Shinozuka, 9/22/88, (PB89-174429, A04, MF-A01).

NCEER-88-0030 "Nonnormal Accelerations Due to Yielding in a Primary Structure," by D.C.K. Chen and L.D. Lutes, 9/19/88, (PB89-131437, A04, MF-A01).

NCEER-88-0031 "Design Approaches for Soil-Structure Interaction," by A.S. Veletsos, A.M. Prasad and Y. Tang, 12/30/88, (PB89-174437, A03, MF-A01). This report is available only through NTIS (see address given above).

NCEER-88-0032 "A Re-evaluation of Design Spectra for Seismic Damage Control," by C.J. Turkstra and A.G. Tallin, 11/7/88, (PB89-145221, A05, MF-A01).

NCEER-88-0033 "The Behavior and Design of Noncontact Lap Splices Subjected to Repeated Inelastic Tensile Loading," by V.E. Sagan, P. Gergely and R.N. White, 12/8/88, (PB89-163737, A08, MF-A01).

NCEER-88-0034 "Seismic Response of Pile Foundations," by S.M. Mamoon, P.K. Banerjee and S. Ahmad, 11/1/88, (PB89-145239, A04, MF-A01).

NCEER-88-0035 "Modeling of R/C Building Structures With Flexible Floor Diaphragms (IDARC2)," by A.M. Reinhorn, S.K. Kunnath and N. Panahshahi, 9/7/88, (PB89-207153, A07, MF-A01).

NCEER-88-0036 "Solution of the Dam-Reservoir Interaction Problem Using a Combination of FEM, BEM with Particular Integrals, Modal Analysis, and Substructuring," by C-S. Tsai, G.C. Lee and R.L. Ketter, 12/31/88, (PB89-207146, A04, MF-A01).

NCEER-88-0037 "Optimal Placement of Actuators for Structural Control," by F.Y. Cheng and C.P. Pantelides, 8/15/88, (PB89-162846, A05, MF-A01).

NCEER-88-0038 "Teflon Bearings in Aseismic Base Isolation: Experimental Studies and Mathematical Modeling," by A. Mokha, M.C. Constantinou and A.M. Reinhorn, 12/5/88, (PB89-218457, A10, MF-A01). This report is available only through NTIS (see address given above).

NCEER-88-0039 "Seismic Behavior of Flat Slab High-Rise Buildings in the New York City Area," by P. Weidlinger and M. Ettouney, 10/15/88, (PB90-145681, A04, MF-A01).

NCEER-88-0040 "Evaluation of the Earthquake Resistance of Existing Buildings in New York City," by P. Weidlinger and M. Ettouney, 10/15/88, to be published.

NCEER-88-0041 "Small-Scale Modeling Techniques for Reinforced Concrete Structures Subjected to Seismic Loads," by W. Kim, A. El-Attar and R.N. White, 11/22/88, (PB89-189625, A05, MF-A01).

NCEER-88-0042 "Modeling Strong Ground Motion from Multiple Event Earthquakes," by G.W. Ellis and A.S. Cakmak, 10/15/88, (PB89-174445, A03, MF-A01).

NCEER-88-0043 "Nonstationary Models of Seismic Ground Acceleration," by M. Grigoriu, S.E. Ruiz and E. Rosenblueth, 7/15/88, (PB89-189617, A04, MF-A01).

NCEER-88-0044 "SARCF User's Guide: Seismic Analysis of Reinforced Concrete Frames," by Y.S. Chung, C. Meyer and M. Shinozuka, 11/9/88, (PB89-174452, A08, MF-A01).

NCEER-88-0045 "First Expert Panel Meeting on Disaster Research and Planning," edited by J. Pantelic and J. Stoyle, 9/15/88, (PB89-174460, A05, MF-A01).

NCEER-88-0046 "Preliminary Studies of the Effect of Degrading Infill Walls on the Nonlinear Seismic Response of Steel Frames," by C.Z. Chrysostomou, P. Gergely and J.F. Abel, 12/19/88, (PB89-208383, A05, MF-A01).

NCEER-88-0047 "Reinforced Concrete Frame Component Testing Facility - Design, Construction, Instrumentation and Operation," by S.P. Pessiki, C. Conley, T. Bond, P. Gergely and R.N. White, 12/16/88, (PB89-174478, A04, MF-A01).

NCEER-89-0001 "Effects of Protective Cushion and Soil Compliancy on the Response of Equipment Within a Seismically Excited Building," by J.A. HoLung, 2/16/89, (PB89-207179, A04, MF-A01).

NCEER-89-0002 "Statistical Evaluation of Response Modification Factors for Reinforced Concrete Structures," by H.H-M. Hwang and J-W. Jaw, 2/17/89, (PB89-207187, A05, MF-A01).

NCEER-89-0003 "Hysteretic Columns Under Random Excitation," by G-Q. Cai and Y.K. Lin, 1/9/89, (PB89-196513, A03, MF-A01).

NCEER-89-0004 "Experimental Study of `Elephant Foot Bulge' Instability of Thin-Walled Metal Tanks," by Z-H. Jia and R.L. Ketter, 2/22/89, (PB89-207195, A03, MF-A01).

NCEER-89-0005 "Experiment on Performance of Buried Pipelines Across San Andreas Fault," by J. Isenberg, E. Richardson and T.D. O'Rourke, 3/10/89, (PB89-218440, A04, MF-A01). This report is available only through NTIS (see address given above).

NCEER-89-0006 "A Knowledge-Based Approach to Structural Design of Earthquake-Resistant Buildings," by M. Subramani, P. Gergely, C.H. Conley, J.F. Abel and A.H. Zaghw, 1/15/89, (PB89-218465, A06, MF-A01).

NCEER-89-0007 "Liquefaction Hazards and Their Effects on Buried Pipelines," by T.D. O'Rourke and P.A. Lane, 2/1/89, (PB89-218481, A09, MF-A01).

NCEER-89-0008 "Fundamentals of System Identification in Structural Dynamics," by H. Imai, C-B. Yun, O. Maruyama and M. Shinozuka, 1/26/89, (PB89-207211, A04, MF-A01).

NCEER-89-0009 "Effects of the 1985 Michoacan Earthquake on Water Systems and Other Buried Lifelines in Mexico," by A.G. Ayala and M.J. O'Rourke, 3/8/89, (PB89-207229, A06, MF-A01).

NCEER-89-R010 "NCEER Bibliography of Earthquake Education Materials," by K.E.K. Ross, Second Revision, 9/1/89, (PB90-125352, A05, MF-A01). This report is replaced by NCEER-92-0018.

NCEER-89-0011 "Inelastic Three-Dimensional Response Analysis of Reinforced Concrete Building Structures (IDARC-3D), Part I - Modeling," by S.K. Kunnath and A.M. Reinhorn, 4/17/89, (PB90-114612, A07, MF-A01). This report is available only through NTIS (see address given above).

NCEER-89-0012 "Recommended Modifications to ATC-14," by C.D. Poland and J.O. Malley, 4/12/89, (PB90-108648, A15, MF-A01).

NCEER-89-0013 "Repair and Strengthening of Beam-to-Column Connections Subjected to Earthquake Loading," by M. Corazao and A.J. Durrani, 2/28/89, (PB90-109885, A06, MF-A01).

NCEER-89-0014 "Program EXKAL2 for Identification of Structural Dynamic Systems," by O. Maruyama, C-B. Yun, M. Hoshiya and M. Shinozuka, 5/19/89, (PB90-109877, A09, MF-A01).

NCEER-89-0015 "Response of Frames With Bolted Semi-Rigid Connections, Part I - Experimental Study and Analytical Predictions," by P.J. DiCorso, A.M. Reinhorn, J.R. Dickerson, J.B. Radziminski and W.L. Harper, 6/1/89, to be published.

NCEER-89-0016 "ARMA Monte Carlo Simulation in Probabilistic Structural Analysis," by P.D. Spanos and M.P. Mignolet, 7/10/89, (PB90-109893, A03, MF-A01).

NCEER-89-P017 "Preliminary Proceedings from the Conference on Disaster Preparedness - The Place of Earthquake Education in Our Schools," Edited by K.E.K. Ross, 6/23/89, (PB90-108606, A03, MF-A01).

NCEER-89-0017 "Proceedings from the Conference on Disaster Preparedness - The Place of Earthquake Education in Our Schools," Edited by K.E.K. Ross, 12/31/89, (PB90-207895, A012, MF-A02). This report is available only through NTIS (see address given above).

NCEER-89-0018 "Multidimensional Models of Hysteretic Material Behavior for Vibration Analysis of Shape Memory Energy Absorbing Devices, by E.J. Graesser and F.A. Cozzarelli, 6/7/89, (PB90-164146, A04, MF-A01).

NCEER-89-0019 "Nonlinear Dynamic Analysis of Three-Dimensional Base Isolated Structures (3D-BASIS)," by S. Nagarajaiah, A.M. Reinhorn and M.C. Constantinou, 8/3/89, (PB90-161936, A06, MF-A01). This report has been replaced by NCEER-93-0011.

NCEER-89-0020 "Structural Control Considering Time-Rate of Control Forces and Control Rate Constraints," by F.Y. Cheng and C.P. Pantelides, 8/3/89, (PB90-120445, A04, MF-A01).

NCEER-89-0021 "Subsurface Conditions of Memphis and Shelby County," by K.W. Ng, T-S. Chang and H-H.M. Hwang, 7/26/89, (PB90-120437, A03, MF-A01).

NCEER-89-0022 "Seismic Wave Propagation Effects on Straight Jointed Buried Pipelines," by K. Elhmadi and M.J. O'Rourke, 8/24/89, (PB90-162322, A10, MF-A02).

NCEER-89-0023 "Workshop on Serviceability Analysis of Water Delivery Systems," edited by M. Grigoriu, 3/6/89, (PB90-127424, A03, MF-A01).

NCEER-89-0024 "Shaking Table Study of a 1/5 Scale Steel Frame Composed of Tapered Members," by K.C. Chang, J.S. Hwang and G.C. Lee, 9/18/89, (PB90-160169, A04, MF-A01).

NCEER-89-0025 "DYNA1D: A Computer Program for Nonlinear Seismic Site Response Analysis - Technical Documentation," by Jean H. Prevost, 9/14/89, (PB90-161944, A07, MF-A01). This report is available only through NTIS (see address given above).

NCEER-89-0026 "1:4 Scale Model Studies of Active Tendon Systems and Active Mass Dampers for Aseismic Protection," by A.M. Reinhorn, T.T. Soong, R.C. Lin, Y.P. Yang, Y. Fukao, H. Abe and M. Nakai, 9/15/89, (PB90-173246, A10, MF-A02). This report is available only through NTIS (see address given above).

NCEER-89-0027 "Scattering of Waves by Inclusions in a Nonhomogeneous Elastic Half Space Solved by Boundary Element Methods," by P.K. Hadley, A. Askar and A.S. Cakmak, 6/15/89, (PB90-145699, A07, MF-A01).

NCEER-89-0028 "Statistical Evaluation of Deflection Amplification Factors for Reinforced Concrete Structures," by H.H.M. Hwang, J-W. Jaw and A.L. Ch'ng, 8/31/89, (PB90-164633, A05, MF-A01).

NCEER-89-0029 "Bedrock Accelerations in Memphis Area Due to Large New Madrid Earthquakes," by H.H.M. Hwang, C.H.S. Chen and G. Yu, 11/7/89, (PB90-162330, A04, MF-A01).

NCEER-89-0030 "Seismic Behavior and Response Sensitivity of Secondary Structural Systems," by Y.Q. Chen and T.T. Soong, 10/23/89, (PB90-164658, A08, MF-A01).

NCEER-89-0031 "Random Vibration and Reliability Analysis of Primary-Secondary Structural Systems," by Y. Ibrahim, M. Grigoriu and T.T. Soong, 11/10/89, (PB90-161951, A04, MF-A01).

NCEER-89-0032 "Proceedings from the Second U.S. - Japan Workshop on Liquefaction, Large Ground Deformation and Their Effects on Lifelines, September 26-29, 1989," Edited by T.D. O'Rourke and M. Hamada, 12/1/89, (PB90-209388, A22, MF-A03).

NCEER-89-0033 "Deterministic Model for Seismic Damage Evaluation of Reinforced Concrete Structures," by J.M. Bracci, A.M. Reinhorn, J.B. Mander and S.K. Kunnath, 9/27/89, (PB91-108803, A06, MF-A01).

NCEER-89-0034 "On the Relation Between Local and Global Damage Indices," by E. DiPasquale and A.S. Cakmak, 8/15/89, (PB90-173865, A05, MF-A01).

NCEER-89-0035 "Cyclic Undrained Behavior of Nonplastic and Low Plasticity Silts," by A.J. Walker and H.E. Stewart, 7/26/89, (PB90-183518, A10, MF-A01).

NCEER-89-0036 "Liquefaction Potential of Surficial Deposits in the City of Buffalo, New York," by M. Budhu, R. Giese and L. Baumgrass, 1/17/89, (PB90-208455, A04, MF-A01).

NCEER-89-0037 "A Deterministic Assessment of Effects of Ground Motion Incoherence," by A.S. Veletsos and Y. Tang, 7/15/89, (PB90-164294, A03, MF-A01).

NCEER-89-0038 "Workshop on Ground Motion Parameters for Seismic Hazard Mapping," July 17-18, 1989, edited by R.V. Whitman, 12/1/89, (PB90-173923, A04, MF-A01).

NCEER-89-0039 "Seismic Effects on Elevated Transit Lines of the New York City Transit Authority," by C.J. Costantino, C.A. Miller and E. Heymsfield, 12/26/89, (PB90-207887, A06, MF-A01).

NCEER-89-0040 "Centrifugal Modeling of Dynamic Soil-Structure Interaction," by K. Weissman, Supervised by J.H. Prevost, 5/10/89, (PB90-207879, A07, MF-A01).

NCEER-89-0041 "Linearized Identification of Buildings With Cores for Seismic Vulnerability Assessment," by I-K. Ho and A.E. Aktan, 11/1/89, (PB90-251943, A07, MF-A01).

NCEER-90-0001 "Geotechnical and Lifeline Aspects of the October 17, 1989 Loma Prieta Earthquake in San Francisco," by T.D. O'Rourke, H.E. Stewart, F.T. Blackburn and T.S. Dickerman, 1/90, (PB90-208596, A05, MF-A01).

NCEER-90-0002 "Nonnormal Secondary Response Due to Yielding in a Primary Structure," by D.C.K. Chen and L.D. Lutes, 2/28/90, (PB90-251976, A07, MF-A01).

NCEER-90-0003 "Earthquake Education Materials for Grades K-12," by K.E.K. Ross, 4/16/90, (PB91-251984, A05, MF-A05). This report has been replaced by NCEER-92-0018.

NCEER-90-0004 "Catalog of Strong Motion Stations in Eastern North America," by R.W. Busby, 4/3/90, (PB90-251984, A05, MF-A01).

NCEER-90-0005 "NCEER Strong-Motion Data Base: A User Manual for the GeoBase Release (Version 1.0 for the Sun3)," by P. Friberg and K. Jacob, 3/31/90 (PB90-258062, A04, MF-A01).

NCEER-90-0006 "Seismic Hazard Along a Crude Oil Pipeline in the Event of an 1811-1812 Type New Madrid Earthquake," by H.H.M. Hwang and C-H.S. Chen, 4/16/90, (PB90-258054, A04, MF-A01).

NCEER-90-0007 "Site-Specific Response Spectra for Memphis Sheahan Pumping Station," by H.H.M. Hwang and C.S. Lee, 5/15/90, (PB91-108811, A05, MF-A01).

NCEER-90-0008 "Pilot Study on Seismic Vulnerability of Crude Oil Transmission Systems," by T. Ariman, R. Dobry, M. Grigoriu, F. Kozin, M. O'Rourke, T. O'Rourke and M. Shinozuka, 5/25/90, (PB91-108837, A06, MF-A01).

NCEER-90-0009 "A Program to Generate Site Dependent Time Histories: EQGEN," by G.W. Ellis, M. Srinivasan and A.S. Cakmak, 1/30/90, (PB91-108829, A04, MF-A01).

NCEER-90-0010 "Active Isolation for Seismic Protection of Operating Rooms," by M.E. Talbott, Supervised by M. Shinozuka, 6/8/9, (PB91-110205, A05, MF-A01).

NCEER-90-0011 "Program LINEARID for Identification of Linear Structural Dynamic Systems," by C-B. Yun and M. Shinozuka, 6/25/90, (PB91-110312, A08, MF-A01).

NCEER-90-0012 "Two-Dimensional Two-Phase Elasto-Plastic Seismic Response of Earth Dams," by A.N. Yiagos, Supervised by J.H. Prevost, 6/20/90, (PB91-110197, A13, MF-A02).

NCEER-90-0013 "Secondary Systems in Base-Isolated Structures: Experimental Investigation, Stochastic Response and Stochastic Sensitivity," by G.D. Manolis, G. Juhn, M.C. Constantinou and A.M. Reinhorn, 7/1/90, (PB91-110320, A08, MF-A01).

NCEER-90-0014 "Seismic Behavior of Lightly-Reinforced Concrete Column and Beam-Column Joint Details," by S.P. Pessiki, C.H. Conley, P. Gergely and R.N. White, 8/22/90, (PB91-108795, A11, MF-A02).

NCEER-90-0015 "Two Hybrid Control Systems for Building Structures Under Strong Earthquakes," by J.N. Yang and A. Danielians, 6/29/90, (PB91-125393, A04, MF-A01).

NCEER-90-0016 "Instantaneous Optimal Control with Acceleration and Velocity Feedback," by J.N. Yang and Z. Li, 6/29/90, (PB91-125401, A03, MF-A01).

NCEER-90-0017 "Reconnaissance Report on the Northern Iran Earthquake of June 21, 1990," by M. Mehrain, 10/4/90, (PB91-125377, A03, MF-A01).

NCEER-90-0018 "Evaluation of Liquefaction Potential in Memphis and Shelby County," by T.S. Chang, P.S. Tang, C.S. Lee and H. Hwang, 8/10/90, (PB91-125427, A09, MF-A01).

NCEER-90-0019 "Experimental and Analytical Study of a Combined Sliding Disc Bearing and Helical Steel Spring Isolation System," by M.C. Constantinou, A.S. Mokha and A.M. Reinhorn, 10/4/90, (PB91-125385, A06, MF-A01). This report is available only through NTIS (see address given above).

NCEER-90-0020 "Experimental Study and Analytical Prediction of Earthquake Response of a Sliding Isolation System with a Spherical Surface," by A.S. Mokha, M.C. Constantinou and A.M. Reinhorn, 10/11/90, (PB91-125419, A05, MF-A01).

NCEER-90-0021 "Dynamic Interaction Factors for Floating Pile Groups," by G. Gazetas, K. Fan, A. Kaynia and E. Kausel, 9/10/90, (PB91-170381, A05, MF-A01).

NCEER-90-0022 "Evaluation of Seismic Damage Indices for Reinforced Concrete Structures," by S. Rodriguez-Gomez and A.S. Cakmak, 9/30/90, PB91-171322, A06, MF-A01).

NCEER-90-0023 "Study of Site Response at a Selected Memphis Site," by H. Desai, S. Ahmad, E.S. Gazetas and M.R. Oh, 10/11/90, (PB91-196857, A03, MF-A01).

NCEER-90-0024 "A User's Guide to Strongmo: Version 1.0 of NCEER's Strong-Motion Data Access Tool for PCs and Terminals," by P.A. Friberg and C.A.T. Susch, 11/15/90, (PB91-171272, A03, MF-A01).

NCEER-90-0025 "A Three-Dimensional Analytical Study of Spatial Variability of Seismic Ground Motions," by L-L. Hong and A.H.-S. Ang, 10/30/90, (PB91-170399, A09, MF-A01).

NCEER-90-0026 "MUMOID User's Guide - A Program for the Identification of Modal Parameters," by S. Rodriguez-Gomez and E. DiPasquale, 9/30/90, (PB91-171298, A04, MF-A01).

NCEER-90-0027 "SARCF-II User's Guide - Seismic Analysis of Reinforced Concrete Frames," by S. Rodriguez-Gomez, Y.S. Chung and C. Meyer, 9/30/90, (PB91-171280, A05, MF-A01).

NCEER-90-0028 "Viscous Dampers: Testing, Modeling and Application in Vibration and Seismic Isolation," by N. Makris and M.C. Constantinou, 12/20/90 (PB91-190561, A06, MF-A01).

NCEER-90-0029 "Soil Effects on Earthquake Ground Motions in the Memphis Area," by H. Hwang, C.S. Lee, K.W. Ng and T.S. Chang, 8/2/90, (PB91-190751, A05, MF-A01).

NCEER-91-0001 "Proceedings from the Third Japan-U.S. Workshop on Earthquake Resistant Design of Lifeline Facilities and Countermeasures for Soil Liquefaction, December 17-19, 1990," edited by T.D. O'Rourke and M. Hamada, 2/1/91, (PB91-179259, A99, MF-A04).

NCEER-91-0002 "Physical Space Solutions of Non-Proportionally Damped Systems," by M. Tong, Z. Liang and G.C. Lee, 1/15/91, (PB91-179242, A04, MF-A01).

NCEER-91-0003 "Seismic Response of Single Piles and Pile Groups," by K. Fan and G. Gazetas, 1/10/91, (PB92-174994, A04, MF-A01).

NCEER-91-0004 "Damping of Structures: Part 1 - Theory of Complex Damping," by Z. Liang and G. Lee, 10/10/91, (PB92-197235, A12, MF-A03).

NCEER-91-0005 "3D-BASIS - Nonlinear Dynamic Analysis of Three Dimensional Base Isolated Structures: Part II," by S. Nagarajaiah, A.M. Reinhorn and M.C. Constantinou, 2/28/91, (PB91-190553, A07, MF-A01). This report has been replaced by NCEER-93-0011.

NCEER-91-0006 "A Multidimensional Hysteretic Model for Plasticity Deforming Metals in Energy Absorbing Devices," by E.J. Graesser and F.A. Cozzarelli, 4/9/91, (PB92-108364, A04, MF-A01).

NCEER-91-0007 "A Framework for Customizable Knowledge-Based Expert Systems with an Application to a KBES for Evaluating the Seismic Resistance of Existing Buildings," by E.G. Ibarra-Anaya and S.J. Fenves, 4/9/91, (PB91-210930, A08, MF-A01).

NCEER-91-0008 "Nonlinear Analysis of Steel Frames with Semi-Rigid Connections Using the Capacity Spectrum Method," by G.G. Deierlein, S-H. Hsieh, Y-J. Shen and J.F. Abel, 7/2/91, (PB92-113828, A05, MF-A01).

NCEER-91-0009 "Earthquake Education Materials for Grades K-12," by K.E.K. Ross, 4/30/91, (PB91-212142, A06, MF-A01). This report has been replaced by NCEER-92-0018.

NCEER-91-0010 "Phase Wave Velocities and Displacement Phase Differences in a Harmonically Oscillating Pile," by N. Makris and G. Gazetas, 7/8/91, (PB92-108356, A04, MF-A01).

NCEER-91-0011 "Dynamic Characteristics of a Full-Size Five-Story Steel Structure and a 2/5 Scale Model," by K.C. Chang, G.C. Yao, G.C. Lee, D.S. Hao and Y.C. Yeh," 7/2/91, (PB93-116648, A06, MF-A02).

NCEER-91-0012 "Seismic Response of a 2/5 Scale Steel Structure with Added Viscoelastic Dampers," by K.C. Chang, T.T. Soong, S-T. Oh and M.L. Lai, 5/17/91, (PB92-110816, A05, MF-A01).

NCEER-91-0013 "Earthquake Response of Retaining Walls; Full-Scale Testing and Computational Modeling," by S. Alampalli and A-W.M. Elgamal, 6/20/91, to be published.

NCEER-91-0014 "3D-BASIS-M: Nonlinear Dynamic Analysis of Multiple Building Base Isolated Structures," by P.C. Tsopelas, S. Nagarajaiah, M.C. Constantinou and A.M. Reinhorn, 5/28/91, (PB92-113885, A09, MF-A02).

NCEER-91-0015 "Evaluation of SEAOC Design Requirements for Sliding Isolated Structures," by D. Theodossiou and M.C. Constantinou, 6/10/91, (PB92-114602, A11, MF-A03).

NCEER-91-0016 "Closed-Loop Modal Testing of a 27-Story Reinforced Concrete Flat Plate-Core Building," by H.R. Somaprasad, T. Toksoy, H. Yoshiyuki and A.E. Aktan, 7/15/91, (PB92-129980, A07, MF-A02).

NCEER-91-0017 "Shake Table Test of a 1/6 Scale Two-Story Lightly Reinforced Concrete Building," by A.G. El-Attar, R.N. White and P. Gergely, 2/28/91, (PB92-222447, A06, MF-A02).

NCEER-91-0018 "Shake Table Test of a 1/8 Scale Three-Story Lightly Reinforced Concrete Building," by A.G. El-Attar, R.N. White and P. Gergely, 2/28/91, (PB93-116630, A08, MF-A02).

NCEER-91-0019 "Transfer Functions for Rigid Rectangular Foundations," by A.S. Veletsos, A.M. Prasad and W.H. Wu, 7/31/91, to be published.

NCEER-91-0020 "Hybrid Control of Seismic-Excited Nonlinear and Inelastic Structural Systems," by J.N. Yang, Z. Li and A. Danielians, 8/1/91, (PB92-143171, A06, MF-A02).

NCEER-91-0021 "The NCEER-91 Earthquake Catalog: Improved Intensity-Based Magnitudes and Recurrence Relations for U.S. Earthquakes East of New Madrid," by L. Seeber and J.G. Armbruster, 8/28/91, (PB92-176742, A06, MF-A02).

NCEER-91-0022 "Proceedings from the Implementation of Earthquake Planning and Education in Schools: The Need for Change - The Roles of the Changemakers," by K.E.K. Ross and F. Winslow, 7/23/91, (PB92-129998, A12, MF-A03).

NCEER-91-0023 "A Study of Reliability-Based Criteria for Seismic Design of Reinforced Concrete Frame Buildings," by H.H.M. Hwang and H-M. Hsu, 8/10/91, (PB92-140235, A09, MF-A02).

NCEER-91-0024 "Experimental Verification of a Number of Structural System Identification Algorithms," by R.G. Ghanem, H. Gavin and M. Shinozuka, 9/18/91, (PB92-176577, A18, MF-A04).

NCEER-91-0025 "Probabilistic Evaluation of Liquefaction Potential," by H.H.M. Hwang and C.S. Lee," 11/25/91, (PB92-143429, A05, MF-A01).

NCEER-91-0026 "Instantaneous Optimal Control for Linear, Nonlinear and Hysteretic Structures - Stable Controllers," by J.N. Yang and Z. Li, 11/15/91, (PB92-163807, A04, MF-A01).

NCEER-91-0027 "Experimental and Theoretical Study of a Sliding Isolation System for Bridges," by M.C. Constantinou, A. Kartoum, A.M. Reinhorn and P. Bradford, 11/15/91, (PB92-176973, A10, MF-A03).

NCEER-92-0001 "Case Studies of Liquefaction and Lifeline Performance During Past Earthquakes, Volume 1: Japanese Case Studies," Edited by M. Hamada and T. O'Rourke, 2/17/92, (PB92-197243, A18, MF-A04).

NCEER-92-0002 "Case Studies of Liquefaction and Lifeline Performance During Past Earthquakes, Volume 2: United States Case Studies," Edited by T. O'Rourke and M. Hamada, 2/17/92, (PB92-197250, A20, MF-A04).

NCEER-92-0003 "Issues in Earthquake Education," Edited by K. Ross, 2/3/92, (PB92-222389, A07, MF-A02).

NCEER-92-0004 "Proceedings from the First U.S. - Japan Workshop on Earthquake Protective Systems for Bridges," Edited by I.G. Buckle, 2/4/92, (PB94-142239, A99, MF-A06).

NCEER-92-0005 "Seismic Ground Motion from a Haskell-Type Source in a Multiple-Layered Half-Space," A.P. Theoharis, G. Deodatis and M. Shinozuka, 1/2/92, to be published.

NCEER-92-0006 "Proceedings from the Site Effects Workshop," Edited by R. Whitman, 2/29/92, (PB92-197201, A04, MF-A01).

NCEER-92-0007 "Engineering Evaluation of Permanent Ground Deformations Due to Seismically-Induced Liquefaction," by M.H. Baziar, R. Dobry and A-W.M. Elgamal, 3/24/92, (PB92-222421, A13, MF-A03).

NCEER-92-0008 "A Procedure for the Seismic Evaluation of Buildings in the Central and Eastern United States," by C.D. Poland and J.O. Malley, 4/2/92, (PB92-222439, A20, MF-A04).

NCEER-92-0009 "Experimental and Analytical Study of a Hybrid Isolation System Using Friction Controllable Sliding Bearings," by M.Q. Feng, S. Fujii and M. Shinozuka, 5/15/92, (PB93-150282, A06, MF-A02).

NCEER-92-0010 "Seismic Resistance of Slab-Column Connections in Existing Non-Ductile Flat-Plate Buildings," by A.J. Durrani and Y. Du, 5/18/92, (PB93-116812, A06, MF-A02).

NCEER-92-0011 "The Hysteretic and Dynamic Behavior of Brick Masonry Walls Upgraded by Ferrocement Coatings Under Cyclic Loading and Strong Simulated Ground Motion," by H. Lee and S.P. Prawel, 5/11/92, to be published.

NCEER-92-0012 "Study of Wire Rope Systems for Seismic Protection of Equipment in Buildings," by G.F. Demetriades, M.C. Constantinou and A.M. Reinhorn, 5/20/92, (PB93-116655, A08, MF-A02).

NCEER-92-0013 "Shape Memory Structural Dampers: Material Properties, Design and Seismic Testing," by P.R. Witting and F.A. Cozzarelli, 5/26/92, (PB93-116663, A05, MF-A01).

NCEER-92-0014 "Longitudinal Permanent Ground Deformation Effects on Buried Continuous Pipelines," by M.J. O'Rourke, and C. Nordberg, 6/15/92, (PB93-116671, A08, MF-A02).

NCEER-92-0015 "A Simulation Method for Stationary Gaussian Random Functions Based on the Sampling Theorem," by M. Grigoriu and S. Balopoulou, 6/11/92, (PB93-127496, A05, MF-A01).

NCEER-92-0016 "Gravity-Load-Designed Reinforced Concrete Buildings: Seismic Evaluation of Existing Construction and Detailing Strategies for Improved Seismic Resistance," by G.W. Hoffmann, S.K. Kunnath, A.M. Reinhorn and J.B. Mander, 7/15/92, (PB94-142007, A08, MF-A02).

NCEER-92-0017 "Observations on Water System and Pipeline Performance in the Limón Area of Costa Rica Due to the April 22, 1991 Earthquake," by M. O'Rourke and D. Ballantyne, 6/30/92, (PB93-126811, A06, MF-A02).

NCEER-92-0018 "Fourth Edition of Earthquake Education Materials for Grades K-12," Edited by K.E.K. Ross, 8/10/92, (PB93-114023, A07, MF-A02).

NCEER-92-0019 "Proceedings from the Fourth Japan-U.S. Workshop on Earthquake Resistant Design of Lifeline Facilities and Countermeasures for Soil Liquefaction," Edited by M. Hamada and T.D. O'Rourke, 8/12/92, (PB93-163939, A99, MF-E11).

NCEER-92-0020 "Active Bracing System: A Full Scale Implementation of Active Control," by A.M. Reinhorn, T.T. Soong, R.C. Lin, M.A. Riley, Y.P. Wang, S. Aizawa and M. Higashino, 8/14/92, (PB93-127512, A06, MF-A02).

NCEER-92-0021 "Empirical Analysis of Horizontal Ground Displacement Generated by Liquefaction-Induced Lateral Spreads," by S.F. Bartlett and T.L. Youd, 8/17/92, (PB93-188241, A06, MF-A02).

NCEER-92-0022 "IDARC Version 3.0: Inelastic Damage Analysis of Reinforced Concrete Structures," by S.K. Kunnath, A.M. Reinhorn and R.F. Lobo, 8/31/92, (PB93-227502, A07, MF-A02).

NCEER-92-0023 "A Semi-Empirical Analysis of Strong-Motion Peaks in Terms of Seismic Source, Propagation Path and Local Site Conditions, by M. Kamiyama, M.J. O'Rourke and R. Flores-Berrones, 9/9/92, (PB93-150266, A08, MF-A02).

NCEER-92-0024 "Seismic Behavior of Reinforced Concrete Frame Structures with Nonductile Details, Part I: Summary of Experimental Findings of Full Scale Beam-Column Joint Tests," by A. Beres, R.N. White and P. Gergely, 9/30/92, (PB93-227783, A05, MF-A01).

NCEER-92-0025 "Experimental Results of Repaired and Retrofitted Beam-Column Joint Tests in Lightly Reinforced Concrete Frame Buildings," by A. Beres, S. El-Borgi, R.N. White and P. Gergely, 10/29/92, (PB93-227791, A05, MF-A01).

NCEER-92-0026 "A Generalization of Optimal Control Theory: Linear and Nonlinear Structures," by J.N. Yang, Z. Li and S. Vongchavalitkul, 11/2/92, (PB93-188621, A05, MF-A01).

NCEER-92-0027 "Seismic Resistance of Reinforced Concrete Frame Structures Designed Only for Gravity Loads: Part I - Design and Properties of a One-Third Scale Model Structure," by J.M. Bracci, A.M. Reinhorn and J.B. Mander, 12/1/92, (PB94-104502, A08, MF-A02).

NCEER-92-0028 "Seismic Resistance of Reinforced Concrete Frame Structures Designed Only for Gravity Loads: Part II - Experimental Performance of Subassemblages," by L.E. Aycardi, J.B. Mander and A.M. Reinhorn, 12/1/92, (PB94-104510, A08, MF-A02).

NCEER-92-0029 "Seismic Resistance of Reinforced Concrete Frame Structures Designed Only for Gravity Loads: Part III - Experimental Performance and Analytical Study of a Structural Model," by J.M. Bracci, A.M. Reinhorn and J.B. Mander, 12/1/92, (PB93-227528, A09, MF-A01).

NCEER-92-0030 "Evaluation of Seismic Retrofit of Reinforced Concrete Frame Structures: Part I - Experimental Performance of Retrofitted Subassemblages," by D. Choudhuri, J.B. Mander and A.M. Reinhorn, 12/8/92, (PB93-198307, A07, MF-A02).

NCEER-92-0031 "Evaluation of Seismic Retrofit of Reinforced Concrete Frame Structures: Part II - Experimental Performance and Analytical Study of a Retrofitted Structural Model," by J.M. Bracci, A.M. Reinhorn and J.B. Mander, 12/8/92, (PB93-198315, A09, MF-A03).

NCEER-92-0032 "Experimental and Analytical Investigation of Seismic Response of Structures with Supplemental Fluid Viscous Dampers," by M.C. Constantinou and M.D. Symans, 12/21/92, (PB93-191435, A10, MF-A03). This report is available only through NTIS (see address given above).

NCEER-92-0033 "Reconnaissance Report on the Cairo, Egypt Earthquake of October 12, 1992," by M. Khater, 12/23/92, (PB93-188621, A03, MF-A01).

NCEER-92-0034 "Low-Level Dynamic Characteristics of Four Tall Flat-Plate Buildings in New York City," by H. Gavin, S. Yuan, J. Grossman, E. Pekelis and K. Jacob, 12/28/92, (PB93-188217, A07, MF-A02).

NCEER-93-0001 "An Experimental Study on the Seismic Performance of Brick-Infilled Steel Frames With and Without Retrofit," by J.B. Mander, B. Nair, K. Wojtkowski and J. Ma, 1/29/93, (PB93-227510, A07, MF-A02).

NCEER-93-0002 "Social Accounting for Disaster Preparedness and Recovery Planning," by S. Cole, E. Pantoja and V. Razak, 2/22/93, (PB94-142114, A12, MF-A03).

NCEER-93-0003 "Assessment of 1991 NEHRP Provisions for Nonstructural Components and Recommended Revisions," by T.T. Soong, G. Chen, Z. Wu, R-H. Zhang and M. Grigoriu, 3/1/93, (PB93-188639, A06, MF-A02).

NCEER-93-0004 "Evaluation of Static and Response Spectrum Analysis Procedures of SEAOC/UBC for Seismic Isolated Structures," by C.W. Winters and M.C. Constantinou, 3/23/93, (PB93-198299, A10, MF-A03).

NCEER-93-0005 "Earthquakes in the Northeast - Are We Ignoring the Hazard? A Workshop on Earthquake Science and Safety for Educators," edited by K.E.K. Ross, 4/2/93, (PB94-103066, A09, MF-A02).

NCEER-93-0006 "Inelastic Response of Reinforced Concrete Structures with Viscoelastic Braces," by R.F. Lobo, J.M. Bracci, K.L. Shen, A.M. Reinhorn and T.T. Soong, 4/5/93, (PB93-227486, A05, MF-A02).

NCEER-93-0007 "Seismic Testing of Installation Methods for Computers and Data Processing Equipment," by K. Kosar, T.T. Soong, K.L. Shen, J.A. HoLung and Y.K. Lin, 4/12/93, (PB93-198299, A07, MF-A02).

NCEER-93-0008 "Retrofit of Reinforced Concrete Frames Using Added Dampers," by A. Reinhorn, M. Constantinou and C. Li, to be published.

NCEER-93-0009 "Seismic Behavior and Design Guidelines for Steel Frame Structures with Added Viscoelastic Dampers," by K.C. Chang, M.L. Lai, T.T. Soong, D.S. Hao and Y.C. Yeh, 5/1/93, (PB94-141959, A07, MF-A02).

NCEER-93-0010 "Seismic Performance of Shear-Critical Reinforced Concrete Bridge Piers," by J.B. Mander, S.M. Waheed, M.T.A. Chaudhary and S.S. Chen, 5/12/93, (PB93-227494, A08, MF-A02).

NCEER-93-0011 "3D-BASIS-TABS: Computer Program for Nonlinear Dynamic Analysis of Three Dimensional Base Isolated Structures," by S. Nagarajaiah, C. Li, A.M. Reinhorn and M.C. Constantinou, 8/2/93, (PB94-141819, A09, MF-A02).

NCEER-93-0012 "Effects of Hydrocarbon Spills from an Oil Pipeline Break on Ground Water," by O.J. Helweg and H.H.M. Hwang, 8/3/93, (PB94-141942, A06, MF-A02).

NCEER-93-0013 "Simplified Procedures for Seismic Design of Nonstructural Components and Assessment of Current Code Provisions," by M.P. Singh, L.E. Suarez, E.E. Matheu and G.O. Maldonado, 8/4/93, (PB94-141827, A09, MF-A02).

NCEER-93-0014 "An Energy Approach to Seismic Analysis and Design of Secondary Systems," by G. Chen and T.T. Soong, 8/6/93, (PB94-142767, A11, MF-A03).

NCEER-93-0015 "Proceedings from School Sites: Becoming Prepared for Earthquakes - Commemorating the Third Anniversary of the Loma Prieta Earthquake," Edited by F.E. Winslow and K.E.K. Ross, 8/16/93, (PB94-154275, A16, MF-A02).

NCEER-93-0016 "Reconnaissance Report of Damage to Historic Monuments in Cairo, Egypt Following the October 12, 1992 Dahshur Earthquake," by D. Sykora, D. Look, G. Croci, E. Karaesmen and E. Karaesmen, 8/19/93, (PB94-142221, A08, MF-A02).

NCEER-93-0017 "The Island of Guam Earthquake of August 8, 1993," by S.W. Swan and S.K. Harris, 9/30/93, (PB94-141843, A04, MF-A01).

NCEER-93-0018 "Engineering Aspects of the October 12, 1992 Egyptian Earthquake," by A.W. Elgamal, M. Amer, K. Adalier and A. Abul-Fadl, 10/7/93, (PB94-141983, A05, MF-A01).

NCEER-93-0019 "Development of an Earthquake Motion Simulator and its Application in Dynamic Centrifuge Testing," by I. Krstelj, Supervised by J.H. Prevost, 10/23/93, (PB94-181773, A-10, MF-A03).

NCEER-93-0020 "NCEER-Taisei Corporation Research Program on Sliding Seismic Isolation Systems for Bridges: Experimental and Analytical Study of a Friction Pendulum System (FPS)," by M.C. Constantinou, P. Tsopelas, Y-S. Kim and S. Okamoto, 11/1/93, (PB94-142775, A08, MF-A02).

NCEER-93-0021 "Finite Element Modeling of Elastomeric Seismic Isolation Bearings," by L.J. Billings, Supervised by R. Shepherd, 11/8/93, to be published.

NCEER-93-0022 "Seismic Vulnerability of Equipment in Critical Facilities: Life-Safety and Operational Consequences," by K. Porter, G.S. Johnson, M.M. Zadeh, C. Scawthorn and S. Eder, 11/24/93, (PB94-181765, A16, MF-A03).

NCEER-93-0023 "Hokkaido Nansei-oki, Japan Earthquake of July 12, 1993, by P.I. Yanev and C.R. Scawthorn, 12/23/93, (PB94-181500, A07, MF-A01).

NCEER-94-0001 "An Evaluation of Seismic Serviceability of Water Supply Networks with Application to the San Francisco Auxiliary Water Supply System," by I. Markov, Supervised by M. Grigoriu and T. O'Rourke, 1/21/94, (PB94-204013, A07, MF-A02).

NCEER-94-0002 "NCEER-Taisei Corporation Research Program on Sliding Seismic Isolation Systems for Bridges: Experimental and Analytical Study of Systems Consisting of Sliding Bearings, Rubber Restoring Force Devices and Fluid Dampers," Volumes I and II, by P. Tsopelas, S. Okamoto, M.C. Constantinou, D. Ozaki and S. Fujii, 2/4/94, (PB94-181740, A09, MF-A02 and PB94-181757, A12, MF-A03).

NCEER-94-0003 "A Markov Model for Local and Global Damage Indices in Seismic Analysis," by S. Rahman and M. Grigoriu, 2/18/94, (PB94-206000, A12, MF-A03).

NCEER-94-0004 "Proceedings from the NCEER Workshop on Seismic Response of Masonry Infills," edited by D.P. Abrams, 3/1/94, (PB94-180783, A07, MF-A02).

NCEER-94-0005 "The Northridge, California Earthquake of January 17, 1994: General Reconnaissance Report," edited by J.D. Goltz, 3/11/94, (PB94-193943, A10, MF-A03).

NCEER-94-0006 "Seismic Energy Based Fatigue Damage Analysis of Bridge Columns: Part I - Evaluation of Seismic Capacity," by G.A. Chang and J.B. Mander, 3/14/94, (PB94-219185, A11, MF-A03).

NCEER-94-0007 "Seismic Isolation of Multi-Story Frame Structures Using Spherical Sliding Isolation Systems," by T.M. Al-Hussaini, V.A. Zayas and M.C. Constantinou, 3/17/94, (PB94-193745, A09, MF-A02).

NCEER-94-0008 "The Northridge, California Earthquake of January 17, 1994: Performance of Highway Bridges," edited by I.G. Buckle, 3/24/94, (PB94-193851, A06, MF-A02).

NCEER-94-0009 "Proceedings of the Third U.S.-Japan Workshop on Earthquake Protective Systems for Bridges," edited by I.G. Buckle and I. Friedland, 3/31/94, (PB94-195815, A99, MF-A06).

NCEER-94-0010 "3D-BASIS-ME: Computer Program for Nonlinear Dynamic Analysis of Seismically Isolated Single and Multiple Structures and Liquid Storage Tanks," by P.C. Tsopelas, M.C. Constantinou and A.M. Reinhorn, 4/12/94, (PB94-204922, A09, MF-A02).

NCEER-94-0011 "The Northridge, California Earthquake of January 17, 1994: Performance of Gas Transmission Pipelines," by T.D. O'Rourke and M.C. Palmer, 5/16/94, (PB94-204989, A05, MF-A01).

NCEER-94-0012 "Feasibility Study of Replacement Procedures and Earthquake Performance Related to Gas Transmission Pipelines," by T.D. O'Rourke and M.C. Palmer, 5/25/94, (PB94-206638, A09, MF-A02).

NCEER-94-0013 "Seismic Energy Based Fatigue Damage Analysis of Bridge Columns: Part II - Evaluation of Seismic Demand," by G.A. Chang and J.B. Mander, 6/1/94, (PB95-18106, A08, MF-A02).

NCEER-94-0014 "NCEER-Taisei Corporation Research Program on Sliding Seismic Isolation Systems for Bridges: Experimental and Analytical Study of a System Consisting of Sliding Bearings and Fluid Restoring Force/Damping Devices," by P. Tsopelas and M.C. Constantinou, 6/13/94, (PB94-219144, A10, MF-A03).

NCEER-94-0015 "Generation of Hazard-Consistent Fragility Curves for Seismic Loss Estimation Studies," by H. Hwang and J-R. Huo, 6/14/94, (PB95-181996, A09, MF-A02).

NCEER-94-0016 "Seismic Study of Building Frames with Added Energy-Absorbing Devices," by W.S. Pong, C.S. Tsai and G.C. Lee, 6/20/94, (PB94-219136, A10, A03).

NCEER-94-0017 "Sliding Mode Control for Seismic-Excited Linear and Nonlinear Civil Engineering Structures," by J. Yang, J. Wu, A. Agrawal and Z. Li, 6/21/94, (PB95-138483, A06, MF-A02).

NCEER-94-0018 "3D-BASIS-TABS Version 2.0: Computer Program for Nonlinear Dynamic Analysis of Three Dimensional Base Isolated Structures," by A.M. Reinhorn, S. Nagarajaiah, M.C. Constantinou, P. Tsopelas and R. Li, 6/22/94, (PB95-182176, A08, MF-A02).

NCEER-94-0019 "Proceedings of the International Workshop on Civil Infrastructure Systems: Application of Intelligent Systems and Advanced Materials on Bridge Systems," Edited by G.C. Lee and K.C. Chang, 7/18/94, (PB95-252474, A20, MF-A04).

NCEER-94-0020 "Study of Seismic Isolation Systems for Computer Floors," by V. Lambrou and M.C. Constantinou, 7/19/94, (PB95-138533, A10, MF-A03).

NCEER-94-0021 "Proceedings of the U.S.-Italian Workshop on Guidelines for Seismic Evaluation and Rehabilitation of Unreinforced Masonry Buildings," Edited by D.P. Abrams and G.M. Calvi, 7/20/94, (PB95-138749, A13, MF-A03).

NCEER-94-0022 "NCEER-Taisei Corporation Research Program on Sliding Seismic Isolation Systems for Bridges: Experimental and Analytical Study of a System Consisting of Lubricated PTFE Sliding Bearings and Mild Steel Dampers," by P. Tsopelas and M.C. Constantinou, 7/22/94, (PB95-182184, A08, MF-A02).

NCEER-94-0023 "Development of Reliability-Based Design Criteria for Buildings Under Seismic Load," by Y.K. Wen, H. Hwang and M. Shinozuka, 8/1/94, (PB95-211934, A08, MF-A02).

NCEER-94-0024 "Experimental Verification of Acceleration Feedback Control Strategies for an Active Tendon System," by S.J. Dyke, B.F. Spencer, Jr., P. Quast, M.K. Sain, D.C. Kaspari, Jr. and T.T. Soong, 8/29/94, (PB95-212320, A05, MF-A01).

NCEER-94-0025 "Seismic Retrofitting Manual for Highway Bridges," Edited by I.G. Buckle and I.F. Friedland, published by the Federal Highway Administration (PB95-212676, A15, MF-A03).

NCEER-94-0026 "Proceedings from the Fifth U.S.-Japan Workshop on Earthquake Resistant Design of Lifeline Facilities and Countermeasures Against Soil Liquefaction," Edited by T.D. O'Rourke and M. Hamada, 11/7/94, (PB95-220802, A99, MF-E08).

NCEER-95-0001 "Experimental and Analytical Investigation of Seismic Retrofit of Structures with Supplemental Damping: Part 1 - Fluid Viscous Damping Devices," by A.M. Reinhorn, C. Li and M.C. Constantinou, 1/3/95, (PB95-266599, A09, MF-A02).

NCEER-95-0002 "Experimental and Analytical Study of Low-Cycle Fatigue Behavior of Semi-Rigid Top-And-Seat Angle Connections," by G. Pekcan, J.B. Mander and S.S. Chen, 1/5/95, (PB95-220042, A07, MF-A02).

NCEER-95-0003 "NCEER-ATC Joint Study on Fragility of Buildings," by T. Anagnos, C. Rojahn and A.S. Kiremidjian, 1/20/95, (PB95-220026, A06, MF-A02).

NCEER-95-0004 "Nonlinear Control Algorithms for Peak Response Reduction," by Z. Wu, T.T. Soong, V. Gattulli and R.C. Lin, 2/16/95, (PB95-220349, A05, MF-A01).

NCEER-95-0005 "Pipeline Replacement Feasibility Study: A Methodology for Minimizing Seismic and Corrosion Risks to Underground Natural Gas Pipelines," by R.T. Eguchi, H.A. Seligson and D.G. Honegger, 3/2/95, (PB95-252326, A06, MF-A02).

NCEER-95-0006 "Evaluation of Seismic Performance of an 11-Story Frame Building During the 1994 Northridge Earthquake," by F. Naeim, R. DiSulio, K. Benuska, A. Reinhorn and C. Li, to be published.

NCEER-95-0007 "Prioritization of Bridges for Seismic Retrofitting," by N. Basöz and A.S. Kiremidjian, 4/24/95, (PB95-252300, A08, MF-A02).

NCEER-95-0008 "Method for Developing Motion Damage Relationships for Reinforced Concrete Frames," by A. Singhal and A.S. Kiremidjian, 5/11/95, (PB95-266607, A06, MF-A02).

NCEER-95-0009 "Experimental and Analytical Investigation of Seismic Retrofit of Structures with Supplemental Damping: Part II - Friction Devices," by C. Li and A.M. Reinhorn, 7/6/95, (PB96-128087, A11, MF-A03).

NCEER-95-0010 "Experimental Performance and Analytical Study of a Non-Ductile Reinforced Concrete Frame Structure Retrofitted with Elastomeric Spring Dampers," by G. Pekcan, J.B. Mander and S.S. Chen, 7/14/95, (PB96-137161, A08, MF-A02).

NCEER-95-0011 "Development and Experimental Study of Semi-Active Fluid Damping Devices for Seismic Protection of Structures," by M.D. Symans and M.C. Constantinou, 8/3/95, (PB96-136940, A23, MF-A04).

NCEER-95-0012 "Real-Time Structural Parameter Modification (RSPM): Development of Innervated Structures," by Z. Liang, M. Tong and G.C. Lee, 4/11/95, (PB96-137153, A06, MF-A01).

NCEER-95-0013 "Experimental and Analytical Investigation of Seismic Retrofit of Structures with Supplemental Damping: Part III - Viscous Damping Walls," by A.M. Reinhorn and C. Li, 10/1/95, (PB96-176409, A11, MF-A03).

NCEER-95-0014 "Seismic Fragility Analysis of Equipment and Structures in a Memphis Electric Substation," by J-R. Huo and H.H.M. Hwang, 8/10/95, (PB96-128087, A09, MF-A02).

NCEER-95-0015 "The Hanshin-Awaji Earthquake of January 17, 1995: Performance of Lifelines," Edited by M. Shinozuka, 11/3/95, (PB96-176383, A15, MF-A03).

NCEER-95-0016 "Highway Culvert Performance During Earthquakes," by T.L. Youd and C.J. Beckman, available as NCEER-96-0015.

NCEER-95-0017 "The Hanshin-Awaji Earthquake of January 17, 1995: Performance of Highway Bridges," Edited by I.G. Buckle, 12/1/95, to be published.

NCEER-95-0018 "Modeling of Masonry Infill Panels for Structural Analysis," by A.M. Reinhorn, A. Madan, R.E. Valles, Y. Reichmann and J.B. Mander, 12/8/95, (PB97-110886, MF-A01, A06).

NCEER-95-0019 "Optimal Polynomial Control for Linear and Nonlinear Structures," by A.K. Agrawal and J.N. Yang, 12/11/95, (PB96-168737, A07, MF-A02).

NCEER-95-0020 "Retrofit of Non-Ductile Reinforced Concrete Frames Using Friction Dampers," by R.S. Rao, P. Gergely and R.N. White, 12/22/95, (PB97-133508, A10, MF-A02).

NCEER-95-0021 "Parametric Results for Seismic Response of Pile-Supported Bridge Bents," by G. Mylonakis, A. Nikolaou and G. Gazetas, 12/22/95, (PB97-100242, A12, MF-A03).

NCEER-95-0022 "Kinematic Bending Moments in Seismically Stressed Piles," by A. Nikolaou, G. Mylonakis and G. Gazetas, 12/23/95, (PB97-113914, MF-A03, A13).

NCEER-96-0001 "Dynamic Response of Unreinforced Masonry Buildings with Flexible Diaphragms," by A.C. Costley and D.P. Abrams," 10/10/96, (PB97-133573, MF-A03, A15).

NCEER-96-0002 "State of the Art Review: Foundations and Retaining Structures," by I. Po Lam, to be published.

NCEER-96-0003 "Ductility of Rectangular Reinforced Concrete Bridge Columns with Moderate Confinement," by N. Wehbe, M. Saiidi, D. Sanders and B. Douglas, 11/7/96, (PB97-133557, A06, MF-A02).

NCEER-96-0004 "Proceedings of the Long-Span Bridge Seismic Research Workshop," edited by I.G. Buckle and I.M. Friedland, to be published.

NCEER-96-0005 "Establish Representative Pier Types for Comprehensive Study: Eastern United States," by J. Kulicki and Z. Prucz, 5/28/96, (PB98-119217, A07, MF-A02).

NCEER-96-0006 "Establish Representative Pier Types for Comprehensive Study: Western United States," by R. Imbsen, R.A. Schamber and T.A. Osterkamp, 5/28/96, (PB98-118607, A07, MF-A02).

NCEER-96-0007 "Nonlinear Control Techniques for Dynamical Systems with Uncertain Parameters," by R.G. Ghanem and M.I. Bujakov, 5/27/96, (PB97-100259, A17, MF-A03).

NCEER-96-0008 "Seismic Evaluation of a 30-Year Old Non-Ductile Highway Bridge Pier and Its Retrofit," by J.B. Mander, B. Mahmoodzadegan, S. Bhadra and S.S. Chen, 5/31/96, (PB97-110902, MF-A03, A10).

NCEER-96-0009 "Seismic Performance of a Model Reinforced Concrete Bridge Pier Before and After Retrofit," by J.B. Mander, J.H. Kim and C.A. Ligozio, 5/31/96, (PB97-110910, MF-A02, A10).

NCEER-96-0010 "IDARC2D Version 4.0: A Computer Program for the Inelastic Damage Analysis of Buildings," by R.E. Valles, A.M. Reinhorn, S.K. Kunnath, C. Li and A. Madan, 6/3/96, (PB97-100234, A17, MF-A03).

NCEER-96-0011 "Estimation of the Economic Impact of Multiple Lifeline Disruption: Memphis Light, Gas and Water Division Case Study," by S.E. Chang, H.A. Seligson and R.T. Eguchi, 8/16/96, (PB97-133490, A11, MF-A03).

NCEER-96-0012 "Proceedings from the Sixth Japan-U.S. Workshop on Earthquake Resistant Design of Lifeline Facilities and Countermeasures Against Soil Liquefaction, Edited by M. Hamada and T. O'Rourke, 9/11/96, (PB97-133581, A99, MF-A06).

NCEER-96-0013 "Chemical Hazards, Mitigation and Preparedness in Areas of High Seismic Risk: A Methodology for Estimating the Risk of Post-Earthquake Hazardous Materials Release," by H.A. Seligson, R.T. Eguchi, K.J. Tierney and K. Richmond, 11/7/96, (PB97-133565, MF-A02, A08).

NCEER-96-0014 "Response of Steel Bridge Bearings to Reversed Cyclic Loading," by J.B. Mander, D-K. Kim, S.S. Chen and G.J. Premus, 11/13/96, (PB97-140735, A12, MF-A03).

NCEER-96-0015 "Highway Culvert Performance During Past Earthquakes," by T.L. Youd and C.J. Beckman, 11/25/96, (PB97-133532, A06, MF-A01).

NCEER-97-0001 "Evaluation, Prevention and Mitigation of Pounding Effects in Building Structures," by R.E. Valles and A.M. Reinhorn, 2/20/97, (PB97-159552, A14, MF-A03).

NCEER-97-0002 "Seismic Design Criteria for Bridges and Other Highway Structures," by C. Rojahn, R. Mayes, D.G. Anderson, J. Clark, J.H. Hom, R.V. Nutt and M.J. O'Rourke, 4/30/97, (PB97-194658, A06, MF-A03).

NCEER-97-0003 “Proceedings of the U.S.-Italian Workshop on Seismic Evaluation and Retrofit,” Edited by D.P. Abrams and G.M. Calvi, 3/19/97, (PB97-194666, A13, MF-A03).

NCEER-97-0004 "Investigation of Seismic Response of Buildings with Linear and Nonlinear Fluid Viscous Dampers," by A.A. Seleemah and M.C. Constantinou, 5/21/97, (PB98-109002, A15, MF-A03).

NCEER-97-0005 "Proceedings of the Workshop on Earthquake Engineering Frontiers in Transportation Facilities," edited by G.C. Lee and I.M. Friedland, 8/29/97, (PB98-128911, A25, MR-A04).

NCEER-97-0006 "Cumulative Seismic Damage of Reinforced Concrete Bridge Piers," by S.K. Kunnath, A. El-Bahy, A. Taylor and W. Stone, 9/2/97, (PB98-108814, A11, MF-A03).

NCEER-97-0007 "Structural Details to Accommodate Seismic Movements of Highway Bridges and Retaining Walls," by R.A. Imbsen, R.A. Schamber, E. Thorkildsen, A. Kartoum, B.T. Martin, T.N. Rosser and J.M. Kulicki, 9/3/97, (PB98-108996, A09, MF-A02).

NCEER-97-0008 "A Method for Earthquake Motion-Damage Relationships with Application to Reinforced Concrete Frames," by A. Singhal and A.S. Kiremidjian, 9/10/97, (PB98-108988, A13, MF-A03).

NCEER-97-0009 "Seismic Analysis and Design of Bridge Abutments Considering Sliding and Rotation," by K. Fishman and R. Richards, Jr., 9/15/97, (PB98-108897, A06, MF-A02).

NCEER-97-0010 "Proceedings of the FHWA/NCEER Workshop on the National Representation of Seismic Ground Motion for New and Existing Highway Facilities," edited by I.M. Friedland, M.S. Power and R.L. Mayes, 9/22/97, (PB98-128903, A21, MF-A04).

NCEER-97-0011 "Seismic Analysis for Design or Retrofit of Gravity Bridge Abutments," by K.L. Fishman, R. Richards, Jr. and R.C. Divito, 10/2/97, (PB98-128937, A08, MF-A02).

NCEER-97-0012 "Evaluation of Simplified Methods of Analysis for Yielding Structures," by P. Tsopelas, M.C. Constantinou, C.A. Kircher and A.S. Whittaker, 10/31/97, (PB98-128929, A10, MF-A03).

NCEER-97-0013 "Seismic Design of Bridge Columns Based on Control and Repairability of Damage," by C-T. Cheng and J.B. Mander, 12/8/97, (PB98-144249, A11, MF-A03).

NCEER-97-0014 "Seismic Resistance of Bridge Piers Based on Damage Avoidance Design," by J.B. Mander and C-T. Cheng, 12/10/97, (PB98-144223, A09, MF-A02).

NCEER-97-0015 “Seismic Response of Nominally Symmetric Systems with Strength Uncertainty,” by S. Balopoulou and M. Grigoriu, 12/23/97, (PB98-153422, A11, MF-A03).

NCEER-97-0016 “Evaluation of Seismic Retrofit Methods for Reinforced Concrete Bridge Columns,” by T.J. Wipf, F.W. Klaiber and F.M. Russo, 12/28/97, (PB98-144215, A12, MF-A03).

NCEER-97-0017 “Seismic Fragility of Existing Conventional Reinforced Concrete Highway Bridges,” by C.L. Mullen and A.S. Cakmak, 12/30/97, (PB98-153406, A08, MF-A02).

NCEER-97-0018 “Loss Asssessment of Memphis Buildings,” edited by D.P. Abrams and M. Shinozuka, 12/31/97, (PB98-144231, A13, MF-A03).

NCEER-97-0019 “Seismic Evaluation of Frames with Infill Walls Using Quasi-static Experiments,” by K.M. Mosalam, R.N. White and P. Gergely, 12/31/97, (PB98-153455, A07, MF-A02).

NCEER-97-0020 “Seismic Evaluation of Frames with Infill Walls Using Pseudo-dynamic Experiments,” by K.M. Mosalam, R.N. White and P. Gergely, 12/31/97, (PB98-153430, A07, MF-A02).

NCEER-97-0021 “Computational Strategies for Frames with Infill Walls: Discrete and Smeared Crack Analyses and Seismic Fragility,” by K.M. Mosalam, R.N. White and P. Gergely, 12/31/97, (PB98-153414, A10, MF-A02).

NCEER-97-0022 "Proceedings of the NCEER Workshop on Evaluation of Liquefaction Resistance of Soils," edited by T.L. Youd and I.M. Idriss, 12/31/97, (PB98-155617, A15, MF-A03).

MCEER-98-0001 "Extraction of Nonlinear Hysteretic Properties of Seismically Isolated Bridges from Quick-Release Field Tests," by Q. Chen, B.M. Douglas, E.M. Maragakis and I.G. Buckle, 5/26/98, (PB99-118838, A06, MF-A01).

MCEER-98-0002 "Methodologies for Evaluating the Importance of Highway Bridges," by A. Thomas, S. Eshenaur and J. Kulicki, 5/29/98, (PB99-118846, A10, MF-A02).

MCEER-98-0003 "Capacity Design of Bridge Piers and the Analysis of Overstrength," by J.B. Mander, A. Dutta and P. Goel, 6/1/98, (PB99-118853, A09, MF-A02).

MCEER-98-0004 "Evaluation of Bridge Damage Data from the Loma Prieta and Northridge, California Earthquakes," by N. Basoz and A. Kiremidjian, 6/2/98, (PB99-118861, A15, MF-A03).

MCEER-98-0005 "Screening Guide for Rapid Assessment of Liquefaction Hazard at Highway Bridge Sites," by T. L. Youd, 6/16/98, (PB99-118879, A06, not available on microfiche).

MCEER-98-0006 "Structural Steel and Steel/Concrete Interface Details for Bridges," by P. Ritchie, N. Kauhl and J. Kulicki, 7/13/98, (PB99-118945, A06, MF-A01).

MCEER-98-0007 "Capacity Design and Fatigue Analysis of Confined Concrete Columns," by A. Dutta and J.B. Mander, 7/14/98, (PB99-118960, A14, MF-A03).

MCEER-98-0008 "Proceedings of the Workshop on Performance Criteria for Telecommunication Services Under Earthquake Conditions," edited by A.J. Schiff, 7/15/98, (PB99-118952, A08, MF-A02).

MCEER-98-0009 "Fatigue Analysis of Unconfined Concrete Columns," by J.B. Mander, A. Dutta and J.H. Kim, 9/12/98, (PB99-123655, A10, MF-A02).

MCEER-98-0010 "Centrifuge Modeling of Cyclic Lateral Response of Pile-Cap Systems and Seat-Type Abutments in Dry Sands," by A.D. Gadre and R. Dobry, 10/2/98, (PB99-123606, A13, MF-A03).

MCEER-98-0011 "IDARC-BRIDGE: A Computational Platform for Seismic Damage Assessment of Bridge Structures," by A.M. Reinhorn, V. Simeonov, G. Mylonakis and Y. Reichman, 10/2/98, (PB99-162919, A15, MF-A03).

MCEER-98-0012 "Experimental Investigation of the Dynamic Response of Two Bridges Before and After Retrofitting with Elastomeric Bearings," by D.A. Wendichansky, S.S. Chen and J.B. Mander, 10/2/98, (PB99-162927, A15, MF-A03).

MCEER-98-0013 "Design Procedures for Hinge Restrainers and Hinge Sear Width for Multiple-Frame Bridges," by R. Des Roches and G.L. Fenves, 11/3/98, (PB99-140477, A13, MF-A03).

MCEER-98-0014 "Response Modification Factors for Seismically Isolated Bridges," by M.C. Constantinou and J.K. Quarshie, 11/3/98, (PB99-140485, A14, MF-A03).

MCEER-98-0015 "Proceedings of the U.S.-Italy Workshop on Seismic Protective Systems for Bridges," edited by I.M. Friedland and M.C. Constantinou, 11/3/98, (PB2000-101711, A22, MF-A04).

MCEER-98-0016 "Appropriate Seismic Reliability for Critical Equipment Systems: Recommendations Based on Regional Analysis of Financial and Life Loss," by K. Porter, C. Scawthorn, C. Taylor and N. Blais, 11/10/98, (PB99-157265, A08, MF-A02).

MCEER-98-0017 "Proceedings of the U.S. Japan Joint Seminar on Civil Infrastructure Systems Research," edited by M. Shinozuka and A. Rose, 11/12/98, (PB99-156713, A16, MF-A03).

MCEER-98-0018 "Modeling of Pile Footings and Drilled Shafts for Seismic Design," by I. PoLam, M. Kapuskar and D. Chaudhuri, 12/21/98, (PB99-157257, A09, MF-A02).

MCEER-99-0001 "Seismic Evaluation of a Masonry Infilled Reinforced Concrete Frame by Pseudodynamic Testing," by S.G. Buonopane and R.N. White, 2/16/99, (PB99-162851, A09, MF-A02).

MCEER-99-0002 "Response History Analysis of Structures with Seismic Isolation and Energy Dissipation Systems: Verification Examples for Program SAP2000," by J. Scheller and M.C. Constantinou, 2/22/99, (PB99-162869, A08, MF-A02).

MCEER-99-0003 "Experimental Study on the Seismic Design and Retrofit of Bridge Columns Including Axial Load Effects," by A. Dutta, T. Kokorina and J.B. Mander, 2/22/99, (PB99-162877, A09, MF-A02).

MCEER-99-0004 "Experimental Study of Bridge Elastomeric and Other Isolation and Energy Dissipation Systems with Emphasis on Uplift Prevention and High Velocity Near-source Seismic Excitation," by A. Kasalanati and M. C. Constantinou, 2/26/99, (PB99-162885, A12, MF-A03).

MCEER-99-0005 "Truss Modeling of Reinforced Concrete Shear-flexure Behavior," by J.H. Kim and J.B. Mander, 3/8/99, (PB99-163693, A12, MF-A03).

MCEER-99-0006 "Experimental Investigation and Computational Modeling of Seismic Response of a 1:4 Scale Model Steel Structure with a Load Balancing Supplemental Damping System," by G. Pekcan, J.B. Mander and S.S. Chen, 4/2/99, (PB99-162893, A11, MF-A03).

MCEER-99-0007 "Effect of Vertical Ground Motions on the Structural Response of Highway Bridges," by M.R. Button, C.J. Cronin and R.L. Mayes, 4/10/99, (PB2000-101411, A10, MF-A03).

MCEER-99-0008 "Seismic Reliability Assessment of Critical Facilities: A Handbook, Supporting Documentation, and Model Code Provisions," by G.S. Johnson, R.E. Sheppard, M.D. Quilici, S.J. Eder and C.R. Scawthorn, 4/12/99, (PB2000-101701, A18, MF-A04).

MCEER-99-0009 "Impact Assessment of Selected MCEER Highway Project Research on the Seismic Design of Highway Structures," by C. Rojahn, R. Mayes, D.G. Anderson, J.H. Clark, D'Appolonia Engineering, S. Gloyd and R.V. Nutt, 4/14/99, (PB99-162901, A10, MF-A02).

MCEER-99-0010 "Site Factors and Site Categories in Seismic Codes," by R. Dobry, R. Ramos and M.S. Power, 7/19/99, (PB2000-101705, A08, MF-A02).

MCEER-99-0011 "Restrainer Design Procedures for Multi-Span Simply-Supported Bridges," by M.J. Randall, M. Saiidi, E. Maragakis and T. Isakovic, 7/20/99, (PB2000-101702, A10, MF-A02).

MCEER-99-0012 "Property Modification Factors for Seismic Isolation Bearings," by M.C. Constantinou, P. Tsopelas, A. Kasalanati and E. Wolff, 7/20/99, (PB2000-103387, A11, MF-A03).

MCEER-99-0013 "Critical Seismic Issues for Existing Steel Bridges," by P. Ritchie, N. Kauhl and J. Kulicki, 7/20/99, (PB2000-101697, A09, MF-A02).

MCEER-99-0014 "Nonstructural Damage Database," by A. Kao, T.T. Soong and A. Vender, 7/24/99, (PB2000-101407, A06, MF-A01).

MCEER-99-0015 "Guide to Remedial Measures for Liquefaction Mitigation at Existing Highway Bridge Sites," by H.G. Cooke and J. K. Mitchell, 7/26/99, (PB2000-101703, A11, MF-A03).

MCEER-99-0016 "Proceedings of the MCEER Workshop on Ground Motion Methodologies for the Eastern United States," edited by N. Abrahamson and A. Becker, 8/11/99, (PB2000-103385, A07, MF-A02).

MCEER-99-0017 "Quindío, Colombia Earthquake of January 25, 1999: Reconnaissance Report," by A.P. Asfura and P.J. Flores, 10/4/99, (PB2000-106893, A06, MF-A01).

MCEER-99-0018 "Hysteretic Models for Cyclic Behavior of Deteriorating Inelastic Structures," by M.V. Sivaselvan and A.M. Reinhorn, 11/5/99, (PB2000-103386, A08, MF-A02).

MCEER-99-0019 "Proceedings of the 7th U.S.- Japan Workshop on Earthquake Resistant Design of Lifeline Facilities and Countermeasures Against Soil Liquefaction," edited by T.D. O'Rourke, J.P. Bardet and M. Hamada, 11/19/99, (PB2000-103354, A99, MF-A06).

MCEER-99-0020 "Development of Measurement Capability for Micro-Vibration Evaluations with Application to Chip Fabrication Facilities," by G.C. Lee, Z. Liang, J.W. Song, J.D. Shen and W.C. Liu, 12/1/99, (PB2000-105993, A08, MF-A02).

MCEER-99-0021 "Design and Retrofit Methodology for Building Structures with Supplemental Energy Dissipating Systems," by G. Pekcan, J.B. Mander and S.S. Chen, 12/31/99, (PB2000-105994, A11, MF-A03).

MCEER-00-0001 "The Marmara, Turkey Earthquake of August 17, 1999: Reconnaissance Report," edited by C. Scawthorn; with major contributions by M. Bruneau, R. Eguchi, T. Holzer, G. Johnson, J. Mander, J. Mitchell, W. Mitchell, A. Papageorgiou, C. Scaethorn, and G. Webb, 3/23/00, (PB2000-106200, A11, MF-A03).

MCEER-00-0002 "Proceedings of the MCEER Workshop for Seismic Hazard Mitigation of Health Care Facilities," edited by G.C. Lee, M. Ettouney, M. Grigoriu, J. Hauer and J. Nigg, 3/29/00, (PB2000-106892, A08, MF-A02).

MCEER-00-0003 "The Chi-Chi, Taiwan Earthquake of September 21, 1999: Reconnaissance Report," edited by G.C. Lee and C.H. Loh, with major contributions by G.C. Lee, M. Bruneau, I.G. Buckle, S.E. Chang, P.J. Flores, T.D. O'Rourke, M. Shinozuka, T.T. Soong, C-H. Loh, K-C. Chang, Z-J. Chen, J-S. Hwang, M-L. Lin, G-Y. Liu, K-C. Tsai, G.C. Yao and C-L. Yen, 4/30/00, (PB2001-100980, A10, MF-A02).

MCEER-00-0004 "Seismic Retrofit of End-Sway Frames of Steel Deck-Truss Bridges with a Supplemental Tendon System: Experimental and Analytical Investigation," by G. Pekcan, J.B. Mander and S.S. Chen, 7/1/00, (PB2001-100982, A10, MF-A02).

MCEER-00-0005 "Sliding Fragility of Unrestrained Equipment in Critical Facilities," by W.H. Chong and T.T. Soong, 7/5/00, (PB2001-100983, A08, MF-A02).

MCEER-00-0006 "Seismic Response of Reinforced Concrete Bridge Pier Walls in the Weak Direction," by N. Abo-Shadi, M. Saiidi and D. Sanders, 7/17/00, (PB2001-100981, A17, MF-A03).

MCEER-00-0007 "Low-Cycle Fatigue Behavior of Longitudinal Reinforcement in Reinforced Concrete Bridge Columns," by J. Brown and S.K. Kunnath, 7/23/00, (PB2001-104392, A08, MF-A02).

MCEER-00-0008 "Soil Structure Interaction of Bridges for Seismic Analysis," I. PoLam and H. Law, 9/25/00, (PB2001-105397, A08, MF-A02).

MCEER-00-0009 "Proceedings of the First MCEER Workshop on Mitigation of Earthquake Disaster by Advanced Technologies (MEDAT-1), edited by M. Shinozuka, D.J. Inman and T.D. O'Rourke, 11/10/00, (PB2001-105399, A14, MF-A03).

MCEER-00-0010 "Development and Evaluation of Simplified Procedures for Analysis and Design of Buildings with Passive Energy Dissipation Systems, Revision 01," by O.M. Ramirez, M.C. Constantinou, C.A. Kircher, A.S. Whittaker, M.W. Johnson, J.D. Gomez and C. Chrysostomou, 11/16/01, (PB2001-105523, A23, MF-A04).

MCEER-00-0011 "Dynamic Soil-Foundation-Structure Interaction Analyses of Large Caissons," by C-Y. Chang, C-M. Mok, Z-L. Wang, R. Settgast, F. Waggoner, M.A. Ketchum, H.M. Gonnermann and C-C. Chin, 12/30/00, (PB2001-104373, A07, MF-A02).

MCEER-00-0012 "Experimental Evaluation of Seismic Performance of Bridge Restrainers," by A.G. Vlassis, E.M. Maragakis and M. Saiid Saiidi, 12/30/00, (PB2001-104354, A09, MF-A02).

MCEER-00-0013 "Effect of Spatial Variation of Ground Motion on Highway Structures," by M. Shinozuka, V. Saxena and G. Deodatis, 12/31/00, (PB2001-108755, A13, MF-A03).

MCEER-00-0014 "A Risk-Based Methodology for Assessing the Seismic Performance of Highway Systems," by S.D. Werner, C.E. Taylor, J.E. Moore, II, J.S. Walton and S. Cho, 12/31/00, (PB2001-108756, A14, MF-A03).

MCEER-01-0001 "Experimental Investigation of P-Delta Effects to Collapse During Earthquakes," by D. Vian and M. Bruneau, 6/25/01, (PB2002-100534, A17, MF-A03).

MCEER-01-0002 "Proceedings of the Second MCEER Workshop on Mitigation of Earthquake Disaster by Advanced Technologies (MEDAT-2)," edited by M. Bruneau and D.J. Inman, 7/23/01, (PB2002-100434, A16, MF-A03).

MCEER-01-0003 "Sensitivity Analysis of Dynamic Systems Subjected to Seismic Loads," by C. Roth and M. Grigoriu, 9/18/01, (PB2003-100884, A12, MF-A03).

MCEER-01-0004 "Overcoming Obstacles to Implementing Earthquake Hazard Mitigation Policies: Stage 1 Report," by D.J. Alesch and W.J. Petak, 12/17/01, (PB2002-107949, A07, MF-A02).

MCEER-01-0005 "Updating Real-Time Earthquake Loss Estimates: Methods, Problems and Insights," by C.E. Taylor, S.E. Chang and R.T. Eguchi, 12/17/01, (PB2002-107948, A05, MF-A01).

MCEER-01-0006 "Experimental Investigation and Retrofit of Steel Pile Foundations and Pile Bents Under Cyclic Lateral Loadings," by A. Shama, J. Mander, B. Blabac and S. Chen, 12/31/01, (PB2002-107950, A13, MF-A03).

MCEER-02-0001 "Assessment of Performance of Bolu Viaduct in the 1999 Duzce Earthquake in Turkey" by P.C. Roussis, M.C. Constantinou, M. Erdik, E. Durukal and M. Dicleli, 5/8/02, (PB2003-100883, A08, MF-A02).

MCEER-02-0002 "Seismic Behavior of Rail Counterweight Systems of Elevators in Buildings," by M.P. Singh, Rildova and L.E. Suarez, 5/27/02. (PB2003-100882, A11, MF-A03).

MCEER-02-0003 "Development of Analysis and Design Procedures for Spread Footings," by G. Mylonakis, G. Gazetas, S. Nikolaou and A. Chauncey, 10/02/02, (PB2004-101636, A13, MF-A03, CD-A13).

MCEER-02-0004 "Bare-Earth Algorithms for Use with SAR and LIDAR Digital Elevation Models," by C.K. Huyck, R.T. Eguchi and B. Houshmand, 10/16/02, (PB2004-101637, A07, CD-A07).

MCEER-02-0005 "Review of Energy Dissipation of Compression Members in Concentrically Braced Frames," by K.Lee and M. Bruneau, 10/18/02, (PB2004-101638, A10, CD-A10).

MCEER-03-0001 "Experimental Investigation of Light-Gauge Steel Plate Shear Walls for the Seismic Retrofit of Buildings" by J. Berman and M. Bruneau, 5/2/03, (PB2004-101622, A10, MF-A03, CD-A10).

MCEER-03-0002 "Statistical Analysis of Fragility Curves," by M. Shinozuka, M.Q. Feng, H. Kim, T. Uzawa and T. Ueda, 6/16/03, (PB2004-101849, A09, CD-A09).

MCEER-03-0003 "Proceedings of the Eighth U.S.-Japan Workshop on Earthquake Resistant Design f Lifeline Facilities and Countermeasures Against Liquefaction," edited by M. Hamada, J.P. Bardet and T.D. O'Rourke, 6/30/03, (PB2004-104386, A99, CD-A99).

MCEER-03-0004 "Proceedings of the PRC-US Workshop on Seismic Analysis and Design of Special Bridges," edited by L.C. Fan and G.C. Lee, 7/15/03, (PB2004-104387, A14, CD-A14).

MCEER-03-0005 "Urban Disaster Recovery: A Framework and Simulation Model," by S.B. Miles and S.E. Chang, 7/25/03, (PB2004-104388, A07, CD-A07).

MCEER-03-0006 "Behavior of Underground Piping Joints Due to Static and Dynamic Loading," by R.D. Meis, M. Maragakis and R. Siddharthan, 11/17/03, (PB2005-102194, A13, MF-A03, CD-A00).

MCEER-03-0007 "Seismic Vulnerability of Timber Bridges and Timber Substructures," by A.A. Shama, J.B. Mander, I.M. Friedland and D.R. Allicock, 12/15/03.

MCEER-04-0001 "Experimental Study of Seismic Isolation Systems with Emphasis on Secondary System Response and Verification of Accuracy of Dynamic Response History Analysis Methods," by E. Wolff and M. Constantinou, 1/16/04 (PB2005-102195, A99, MF-E08, CD-A00).

MCEER-04-0002 "Tension, Compression and Cyclic Testing of Engineered Cementitious Composite Materials," by K. Kesner and S.L. Billington, 3/1/04, (PB2005-102196, A08, CD-A08).

MCEER-04-0003 "Cyclic Testing of Braces Laterally Restrained by Steel Studs to Enhance Performance During Earthquakes," by O.C. Celik, J.W. Berman and M. Bruneau, 3/16/04, (PB2005-102197, A13, MF-A03, CD-A00).

MCEER-04-0004 "Methodologies for Post Earthquake Building Damage Detection Using SAR and Optical Remote Sensing: Application to the August 17, 1999 Marmara, Turkey Earthquake," by C.K. Huyck, B.J. Adams, S. Cho, R.T. Eguchi, B. Mansouri and B. Houshmand, 6/15/04, (PB2005-104888, A10, CD-A00).

MCEER-04-0005 "Nonlinear Structural Analysis Towards Collapse Simulation: A Dynamical Systems Approach," by M.V. Sivaselvan and A.M. Reinhorn, 6/16/04, (PB2005-104889, A11, MF-A03, CD-A00).

MCEER-04-0006 "Proceedings of the Second PRC-US Workshop on Seismic Analysis and Design of Special Bridges," edited by G.C. Lee and L.C. Fan, 6/25/04, (PB2005-104890, A16, CD-A00).

MCEER-04-0007 "Seismic Vulnerability Evaluation of Axially Loaded Steel Built-up Laced Members," by K. Lee and M. Bruneau, 6/30/04, (PB2005-104891, A16, CD-A00).

MCEER-04-0008 "Evaluation of Accuracy of Simplified Methods of Analysis and Design of Buildings with Damping Systems for Near-Fault and for Soft-Soil Seismic Motions," by E.A. Pavlou and M.C. Constantinou, 8/16/04, (PB2005-104892, A08, MF-A02, CD-A00).

MCEER-04-0009 "Assessment of Geotechnical Issues in Acute Care Facilities in California," by M. Lew, T.D. O'Rourke, R. Dobry and M. Koch, 9/15/04, (PB2005-104893, A08, CD-A00).

MCEER-04-0010 "Scissor-Jack-Damper Energy Dissipation System," by A.N. Sigaher-Boyle and M.C. Constantinou, 12/1/04 (PB2005-108221).

MCEER-04-0011 "Seismic Retrofit of Bridge Steel Truss Piers Using a Controlled Rocking Approach," by M. Pollino and M. Bruneau, 12/20/04 (PB2006-105795).

MCEER-05-0001 "Experimental and Analytical Studies of Structures Seismically Isolated with an Uplift-Restraint Isolation System," by P.C. Roussis and M.C. Constantinou, 1/10/05 (PB2005-108222).

MCEER-05-0002 "A Versatile Experimentation Model for Study of Structures Near Collapse Applied to Seismic Evaluation of Irregular Structures," by D. Kusumastuti, A.M. Reinhorn and A. Rutenberg, 3/31/05 (PB2006-101523).

MCEER-05-0003 "Proceedings of the Third PRC-US Workshop on Seismic Analysis and Design of Special Bridges," edited by L.C. Fan and G.C. Lee, 4/20/05, (PB2006-105796).

MCEER-05-0004 "Approaches for the Seismic Retrofit of Braced Steel Bridge Piers and Proof-of-Concept Testing of an Eccentrically Braced Frame with Tubular Link," by J.W. Berman and M. Bruneau, 4/21/05 (PB2006-101524).

MCEER-05-0005 "Simulation of Strong Ground Motions for Seismic Fragility Evaluation of Nonstructural Components in Hospitals," by A. Wanitkorkul and A. Filiatrault, 5/26/05 (PB2006-500027).

MCEER-05-0006 "Seismic Safety in California Hospitals: Assessing an Attempt to Accelerate the Replacement or Seismic Retrofit of Older Hospital Facilities," by D.J. Alesch, L.A. Arendt and W.J. Petak, 6/6/05 (PB2006-105794).

MCEER-05-0007 "Development of Seismic Strengthening and Retrofit Strategies for Critical Facilities Using Engineered Cementitious Composite Materials," by K. Kesner and S.L. Billington, 8/29/05 (PB2006-111701).

MCEER-05-0008 "Experimental and Analytical Studies of Base Isolation Systems for Seismic Protection of Power Transformers," by N. Murota, M.Q. Feng and G-Y. Liu, 9/30/05 (PB2006-111702).

MCEER-05-0009 "3D-BASIS-ME-MB: Computer Program for Nonlinear Dynamic Analysis of Seismically Isolated Structures," by P.C. Tsopelas, P.C. Roussis, M.C. Constantinou, R. Buchanan and A.M. Reinhorn, 10/3/05 (PB2006-111703).

MCEER-05-0010 "Steel Plate Shear Walls for Seismic Design and Retrofit of Building Structures," by D. Vian and M. Bruneau, 12/15/05 (PB2006-111704).

MCEER-05-0011 "The Performance-Based Design Paradigm," by M.J. Astrella and A. Whittaker, 12/15/05 (PB2006-111705).

MCEER-06-0001 "Seismic Fragility of Suspended Ceiling Systems," H. Badillo-Almaraz, A.S. Whittaker, A.M. Reinhorn and G.P. Cimellaro, 2/4/06 (PB2006-111706).

MCEER-06-0002 "Multi-Dimensional Fragility of Structures," by G.P. Cimellaro, A.M. Reinhorn and M. Bruneau, 3/1/06 (PB2007-106974, A09, MF-A02, CD A00).

MCEER-06-0003 "Built-Up Shear Links as Energy Dissipators for Seismic Protection of Bridges," by P. Dusicka, A.M. Itani and I.G. Buckle, 3/15/06 (PB2006-111708).

MCEER-06-0004 "Analytical Investigation of the Structural Fuse Concept," by R.E. Vargas and M. Bruneau, 3/16/06 (PB2006-111709).

MCEER-06-0005 "Experimental Investigation of the Structural Fuse Concept," by R.E. Vargas and M. Bruneau, 3/17/06 (PB2006-111710).

MCEER-06-0006 "Further Development of Tubular Eccentrically Braced Frame Links for the Seismic Retrofit of Braced Steel Truss Bridge Piers," by J.W. Berman and M. Bruneau, 3/27/06 (PB2007-105147).

MCEER-06-0007 "REDARS Validation Report," by S. Cho, C.K. Huyck, S. Ghosh and R.T. Eguchi, 8/8/06 (PB2007-106983).

MCEER-06-0008 "Review of Current NDE Technologies for Post-Earthquake Assessment of Retrofitted Bridge Columns," by J.W. Song, Z. Liang and G.C. Lee, 8/21/06 06 (PB2007-106984).

MCEER-06-0009 "Liquefaction Remediation in Silty Soils Using Dynamic Compaction and Stone Columns," by S. Thevanayagam, G.R. Martin, R. Nashed, T. Shenthan, T. Kanagalingam and N. Ecemis, 8/28/06 06 (PB2007-106985).

MCEER-06-0010 "Conceptual Design and Experimental Investigation of Polymer Matrix Composite Infill Panels for Seismic Retrofitting," by W. Jung, M. Chiewanichakorn and A.J. Aref, 9/21/06 (PB2007-106986).

MCEER-06-0011 "A Study of the Coupled Horizontal-Vertical Behavior of Elastomeric and Lead-Rubber Seismic Isolation Bearings," by G.P. Warn and A.S. Whittaker, 9/22/06 (PB2007-108679).

MCEER-06-0012 "Proceedings of the Fourth PRC-US Workshop on Seismic Analysis and Design of Special Bridges: Advancing Bridge Technologies in Research, Design, Construction and Preservation," Edited by L.C. Fan, G.C. Lee and L. Ziang, 10/12/06 (PB2007-109042).

MCEER-06-0013 "Cyclic Response and Low Cycle Fatigue Characteristics of Plate Steels," by P. Dusicka, A.M. Itani and I.G. Buckle, 11/1/06 06 (PB2007-106987).

MCEER-06-0014 "Proceedings of the Second US-Taiwan Bridge Engineering Workshop," edited by W.P. Yen, J. Shen, J-Y. Chen and M. Wang, 11/15/06.

MCEER-06-0015 "User Manual and Technical Documentation for the REDARS^{TM} Import Wizard," by S. Cho, S. Ghosh, C.K. Huyck and S.D. Werner, 11/30/06 (PB2007-114766).

MCEER-06-0016 "Hazard Mitigation Strategy and Monitoring Technologies for Urban and Infrastructure Public Buildings: Proceedings of the China-US Workshops," edited by X.Y. Zhou, A.L. Zhang, G.C. Lee and M. Tong, 12/12/06.

MCEER-07-0001 "Static and Kinetic Coefficients of Friction for Rigid Blocks," by C. Kafali, S. Fathali, M. Grigoriu and A.S. Whittaker, 3/20/07 (PB2007-114767).

MCEER-07-0002 "Hazard Mitigation Investment Decision Making: Organizational Response to Legislative Mandate," by L.A. Arendt, D.J. Alesch and W.J. Petak, 4/9/07(PB2007-114768).

MCEER-07-0003 "Seismic Behavior of Bidirectional-Resistant Ductile End Diaphragms with Unbonded Braces in Straight or Skewed Steel Bridges," by O. Celik and M. Bruneau, 4/11/07.

MCEER-07-0004 "Modeling Pile Behavior in Large Pile Groups Under Lateral Loading," by A.M. Dodds and G.R. Martin, 4/16/07.

MCEER-07-0005 "Experimental Investigation of Blast Performance of Seismically Resistant Concrete-Filled Steel Tube Bridge Piers," by S. Fujikura, M. Bruneau and D. Lopez-Garcia, 4/20/07.

MCEER-07-0006 "Seismic Analysis of Conventional and Isolated Liquefied Natural Gas Tanks Using Mechanical Analogs," by I.P. Christovasilis and A.S. Whittaker, 5/1/07.

MCEER-07-0007 "Experimental Seismic Performance Evaluation of Isolation/Restraint Systems for Mechanical Equipment – Part 1: Heavy Equipment Study," by S. Fathali and A. Filiatrault, 6/6/07.

MCEER-07-0008 "Seismic Vulnerability of Timber Bridges and Timber Substructures," by A.A. Sharma, J.B. Mander, I.M. Friedland and D.R. Allicock, 6/7/07.

MCEER-07-0009 "Experimental and Analytical Study of the XY-Friction Pendulum (XY-FP) Bearing for Bridge Applications," by C.C. Marin-Artieda, A.S. Whittaker and M.C. Constantinou, 6/7/07.

MCEER-07-0010 "Proceedings of the PRC-US Earthquake Engineering Forum for Young Researchers," Edited by G.C. Lee and X.Z. Qi, 6/8/07.

MCEER-07-0011 "Design Recommendations for Perforated Steel Plate Shear Walls," by R. Purba and M. Bruneau, 6/18/07.

MCEER-07-0012 "Performance of Seismic Isolation Hardware Under Service and Seismic Loading," by M.C. Constantinou, A.S. Whittaker, Y. Kalpakidis, D.M. Fenz and G.P. Warn, 8/27/07.

MCEER-07-0013 "Experimental Evaluation of the Seismic Performance of Hospital Piping Subassemblies," by E.R. Goodwin, E. Maragakis and A.M. Itani, 9/4/07.

MCEER-07-0014 "A Simulation Model of Urban Disaster Recovery and Resilience: Implementation for the 1994 Northridge Earthquake," by S. Miles and S.E. Chang, 9/7/07.

MCEER-07-0015 "Statistical and Mechanistic Fragility Analysis of Concrete Bridges," by M. Shinozuka, S. Banerjee and S-H. Kim, 9/10/07.

MCEER-07-0016 "Three-Dimensional Modeling of Inelastic Buckling in Frame Structures," by M. Schachter and AM. Reinhorn, 9/13/07.

MCEER-07-0017 "Modeling of Seismic Wave Scattering on Pile Groups and Caissons," by I. Po Lam, H. Law and C.T. Yang, 9/17/07.

MCEER-07-0018 "Bridge Foundations: Modeling Large Pile Groups and Caissons for Seismic Design," by G.R. Martin (Coordinating Author), I. Po Lam and H. Law, 12/1/07.

MCEER-07-0019 "Principles and Performance of Roller Seismic Isolation Bearings for Highway Bridges," by G.C. Lee, Y.C. Ou, Z. Liang, T.C. Niu and J. Song, 12/10/07.

MCEER-07-0020 "Centrifuge Modeling of Permeability and Pinning Reinforcement Effects on Pile Response to Lateral Spreading," by L.L Gonzalez-Lagos, T. Abdoun and R. Dobry, 12/10/07.

MCEER-07-0021 "Damage to the Highway System from the Pisco, Perú Earthquake of August 15, 2007," by J.S. O'Connor, L. Mesa and M. Nykamp, 12/10/07.

MCEER-07-0022 "Experimental Seismic Performance Evaluation of Isolation/Restraint Systems for Mechanical Equipment – Part 2: Light Equipment Study," by S. Fathali and A. Filiatrault, 12/13/07.

MCEER
EARTHQUAKE ENGINEERING TO EXTREME EVENTS
University at Buffalo, The State University of New York
Red Jacket Quadrangle ▪ Buffalo, New York 14261
Phone: (716) 645-3391 ▪ Fax: (716) 645-3399
E-mail: *mceer@buffalo.edu* ▪ WWW Site *http://mceer.buffalo.edu*
University at Buffalo *The State University of New York*

ISSN 1520-295X